ÉCOLE CENTRALE LYON

N° d'ordre NNT: 2020LYSEC43

THÈSE de DOCTORAT DE L'UNIVERSITÉ DE LYON
opérée au sein de l'École Centrale de Lyon

École Doctorale N° 162
Mécanique Énergétique Génie Civil Acoustique

Spécialité de doctorat : Acoustique

Soutenue publiquement le 16/12/2020, par

Étienne Spieser

Adjoint-based jet noise propagation model for the acoustic potential

---

Devant le jury composé de

Bailly, Christophe	Professeur	École Centrale de Lyon - LMFA	Directeur de thèse
Balin, Nolwenn	Docteur	Airbus Operations	Examinatrice
Bodard, Guillaume	Docteur	Safran Aircraft Engines	Directeur de thèse
Juvé, Daniel	Professeur	École Centrale de Lyon - LMFA	Président du jury
Karabasov, Sergey	Professeur	Queen Mary University of London	Rapporteur
Legendre, César	Docteur	Free Field Technologies	Examinateur
Lele, Sanjiva	Professeur	Stanford University	Rapporteur

Résumé

La question de dissocier le champ acoustique du champ aérodynamique, étroitement liée à celle de la définition adéquate des sources de bruit, reste une question ouverte d'une grande importance pratique en aéroacoustique. En proposant une analogie acoustique construite sur le potentiel acoustique, cette étude veut contribuer à la construction d'un modèle de prédiction du bruit de jet, qui soit robuste et pragmatique pour des applications de l'industrie aéronautique. Le formalisme de l'adjoint utilisé dans le calcul de la propagation du son, recours au principe de réciprocité, et est réalisé indépendamment des sources de bruit. Ce formalisme est le seul capable de modéliser le rayonnement acoustique de l'air éjecté par un turboréacteur avec un coup raisonnable, lorsque cet écoulement est calculé par les équations de Navier-Stokes moyennées et n'est connu que de manière statistique.

Le modèle statistique du bruit de mélange turbulent de Tam et Auriault (1999) est le premier à recourir à une approche adjointe de ce type. Ce travail reformule pour le potentiel acoustique ce modèle emblématique, et compare le modèle de propagation proposé, basée sur l'équation de Pierce (1990), au modèle original utilisé par Tam et Auriault (1998). Un accord satisfaisant est trouvé entre les deux approches. Contrairement à la formulation de Tam et Auriault, l'équation d'onde pour l'acoustique potentielle conserve l'énergie acoustique et ainsi ne présente pas de couplage avec le mode entropique ou le hydrodynamique possiblement instable. De plus, la formulation proposée prend en compte l'effet de la présence des surfaces dans le calcul de la propagation acoustique. Le calcul de la solution réciproque par retournement d'écoulement représente une alternative plus intuitive et plus simple à mettre en oeuvre que la méthode de l'adjoint. Ce travail montre que cette approche simplifiée ne s'applique que pour des opérateurs auto-adjoints comme l'équation de Pierce retenue. Pour démontrer la viabilité opérationnelle de la méthode, la solution adjointe à l'équation de Pierce pour une configuration réaliste de turboréacteur a été calculée à l'aide du code commercial *Actran TM*. Des champ adjoints correspondant à une propagation en champ proche et en champ lointain sont présentés.

Dans le modèle considéré, le champ acoustique est linéaire, dérive d'un potentiel et se propage autour d'un écoulement moyen quelconque. La théorie peut être réécrite à l'aide du formalisme des rayons exacts (Foreman, 1989), et coïncide ainsi avec les cas limites de l'acoustique potentielle et de l'acoustique géométrique; soit avec les deux seuls cas pour lesquels l'acoustique peut être définie sans ambivalence. De surcroît, ce travail réécrit les équations d'Euler sous une forme originale et fournit une équation d'onde très générale sur la seule variable de la vitesse.

Abstract

The issue of properly distinguishing the acoustic field from the aerodynamic field, which is in close relation with that of the adequate definition of noise sources, remains an open question of great practical importance in aeroacoustics. By proposing an acoustic analogy built on the acoustic potential, this study intends to contribute to the construction of a prediction model for jet noise, that is robust and pragmatic with respect to the context of the aeronautical industry. The adjoint formalism used in the calculation of the sound propagation is based on the reciprocity principle, and is carried out independently of noise sources. This formalism is the only one capable of modelling the acoustic radiation of the air ejected by an aircraft engine, at a reasonable computational cost, when this flow is obtained by Reynolds averaged Navier-Stokes (RANS) equations and is only known statistically.

The statistical model of turbulent mixing noise of Tam and Auriault (1999) is the first to use an adjoint approach of this kind. This work reformulates this emblematic model for the acoustic potential, and compares the proposed model, based on the equation of Pierce (1990), with the original propagation model that Tam and Auriault (1998) used. A satisfactory agreement is found between the two approaches. Unlike in Tam and Auriault's formulation, the wave equation for the acoustic potential conserves the acoustic energy and therefore does not present any coupling with the entropic mode nor with the hydrodynamic mode, that is possibly unstable. The proposed formulation also takes into account the effect of the presence of surfaces in the calculation of acoustic propagation. The calculation of the reciprocal solution by flow reversal represents a more intuitive and easier to implement alternative to the adjoint method. This work shows that this simplified approach is applicable only for self-adjoint operators such as Pierce's wave equation that has been selected. To demonstrate the operational viability of the method, the adjoint solution to Pierce's equation for a realistic turbofan engine configuration is calculated using the commercial code *Actran TM*. Adjoint fields corresponding to near-field and far-field propagation are presented.

In the model considered, the linear acoustic field is obtained from a potential scalar function and propagates around an arbitrary mean flow. The theory can be rewritten using the exact ray formalism (Foreman, 1989), and thus coincides with the two limiting cases of potential acoustics and geometric acoustics, the only cases in which acoustics can be defined without ambivalence. Furthermore, Euler's equations are recast in an original form in this study and provides a very general wave equation based solely on the velocity variable.

À mes parents,

Remerciements

J'ai réalisé ce travail au sein du Laboratoire de Mécaniques des Fluides et d'Acoustique sur le campus de l'École Centrale de Lyon entre 2017 et 2020. J'ai évolué dans un cadre bon et stimulant, et j'ai réellement pris plaisir à effectuer mon doctorat. S'il ne me fallait garder qu'une chose de ces années, ce ne serait pas la tentative − plus ou moins réussie − de figer dans l'étreinte de l'encre et du papier quelque loi immuable de la nature, mais plutôt le souvenir de ma rencontre avec une communauté scientifique. La découverte que derrière l'esthétique de la physique et la fascination pour les équations, il y a des visages et il y a des noms. Qui sait bien la regarder, verra que l'histoire donne à la science une épaisseur humaine et de là, ses véritables lettres de noblesses. De cette rencontre aussi inattendue pour moi alors, qu'évidente pour celui qui lis ces lignes avec du recul, j'ai découvert, vivant, l'héritage légué par des générations de scientifiques. De la réception d'un héritage, naît le zèle et la reconnaissance, et c'est avec une profonde gratitude envers ceux qui m'ont précédés que j'écris ces lignes.

Je voudrais commencer par remercier Christophe Bailly, mon directeur de thèse, qui m'a introduit dans cet univers et qui le premier m'a fait confiance. Son soutien constant, son enthousiasme communicatif et son intérêt pour les traductions fidèles de Hermann von Helmholtz, ont rendu ces années des plus agréables. Si mon travail a quelque chose de pertinent, je le dois en grande partie à sa clairvoyance et à son fin sens de l'organisation, deux attributs de son excellence scientifique qui n'est plus à refaire. Je vois comme une chance pour le laboratoire d'avoir à sa tête quelqu'un avec son expérience et ses qualités humaines et je lui souhaite beaucoup de succès dans sa nouvelle fonction.

Je suis très reconnaissant envers messieurs Sergey Karabasov et Sanjiva Lele de m'avoir fait l'honneur d'examiner mon travail. Je voudrais les remercier l'un et l'autre pour leur investissement et les commentaires formulés dans leur rapport. Merci à Sergey Karabasov pour la sagacité des questions posées lors de ma soutenance de thèse.

Merci à Daniel Juvé qui a eu la bonté de montrer de l'intérêt pour mes travaux tout au long de ma thèse et d'avoir accepté de présider mon jury de soutenance. Ses remarques toujours judicieuses, nourries par une impressionnante connaissance de la littérature, m'ont grandement aidées à clarifier mon travail.

Merci à César Legendre pour l'aide très compétente apportée au fil de ma thèse ainsi que pour la minutie avec laquelle il a relu mon manuscrit. Sans sa bienveillance et sa pédagogie, jamais je n'aurai réussi à percer les secrets d'*Actran TM*. Merci également à l'équipe de *Free Field Technologies* pour m'avoir accueilli lors de mon séjour en Septembre 2019.

Je voudrais également exprimer ma reconnaissance envers Nolwenn Balin qui a accepté d'apporter son regard extérieur et expert en examinant mon travail. Merci pour ses encouragements.

Cette thèse a été co-encadrée par Guillaume Bodard dans le cadre d'un partenariat CIFRE financé par *Safran Aircraft Engines*. Je le remercie d'avoir assuré le suivi de ma thèse et d'avoir suggéré l'instigation de l'approche adjointe, sujet passionnant qui a donné cette thèse. Je lui souhaite un bon début dans ses nouvelles fonctions.

Il est d'usage de remercier nommément les compagnons de route de passage au LMFA, et je ne veux pas déroger à cette coutume. Mais avant cela, j'adresse mes remerciements aux membres permanents du laboratoire qui permettent et entretiennent une ambiance de travail conviviale. J'ai su l'apprécier tout particulièrement en cette période désoeuvrante de pandémie. Je veux rendre hommage ici au corps enseignant dont j'ai été témoin de l'investissement, phénoménal et inlassable. Merci au personnel du laboratoire pour l'application et la rigueur avec lesquelles ils réalisent leur travail, j'en ai été grandement impressionné. Merci à chacun et chacune d'entre vous. En écrivant ces lignes, je n'oublie pas non plus

Pierre Roland et Dominique Berthet, aujourd'hui retraités, qui ont contribué à la vie du laboratoire durant de nombreuses années.

Permettez-moi d'user d'une 'analogie acoustique' pour décrire le travail qui a été le mien : s'il est tout à fait possible pour un individu seul d'interpréter *Fratres*, ce morceau d'Arvo Pärt prend cependant une toute autre envergure lorsqu'il est interprété par un soliste dans un ensemble musical. De manière comparable, il me semble que rédiger une thèse est une entreprise solitaire dont la sonorité devient mélodie lorsque cet effort s'inscrit dans un ensemble. Tandis que chacun jouait sa partition bien à lui, le mouvement musical du pupitre était clairement reconnaissable, et j'ai osé à mon tour jouer quelques notes qui me sont propres. « La pluralité jaillit à chaque fois de l'unité, se justifie à partir d'elle et peut à tout moment être réintégrée en elle » écrivait Hans Urs von Balthasar… Je dois beaucoup aux membres du laboratoire, et du groupe acoustique en particulier qui m'ont accueilli et éduqué à une certaine forme de virtuosité. Je garderai vivante la mémoire de la mélodie entendue durant mon passage à Écully.

Ces années de thèse auraient été bien monotones sans mes collègues de la cohorte des doctorants, post-doctorants, stagiaires et assimilés. Au J12 et plus tard au H10 je fus le spect-acteur émerveillé d'un *multikultifest* permanent. Sans ordre particulier: Merci à Thomas Lechat dont l'apparente nonchalance cache mal la créativité bouillonnante. Merci à Yuanyuan Deng pour son fabuleux 'British accent' et son amitié, 后会有期! Merci à Georgios Bampanis *ο αδερφός μου με μια χρυσή καρδιά*. Merci à Yann Martelet, mon adjoint, seul à parler ma langue et qui m'a laissé sans voix en rencontrant CKWT. Merci à Simon Prigent pour son impressionnante méticulosité et pour la finesse de son humour anglais. Merci à "Nacho" (Ignacio Zurbano Fernandez) pour sa classe américaine et son grand coeur. Merci à Courtney Ford pour m'avoir fait goûter les meilleurs cookies de ma vie. Merci à Danny Lewis pour avoir rythmé nos pauses par sa bonne humeur, il ne lui manque que l'ananas pour parfaire sa sicilienne. Merci à Ariane Emmanuelli pour l'enthousiasme débordant qu'elle déploie dans ce qu'elle fait. Merci à Daher Diab et à Jean Al Am "ils fleuriront comme la vigne, ils seront renommés comme le vin du Liban" (Osée,14-8b). Merci à Igor Kurek une lumière parfois un peu diffuse, et un grand acousticien en devenir. Merci à Miguel Pestana et Justine Giez, les premiers doctorants autochtones rencontrés au milieu d'un champ de betterave. Merci à Élina Cros pour l'atmosphère chaleureuse qu'elle fait régner dans le bureau (jamais en dessous de $25\,^oC$). Merci à Alexis Jamois, jeune recrue prometteuse de l'équipage. Merci à l' imperturbable Léo Girier, en passe d'apporter des réponses aux questions que Leonhard Euler se posaient il y a 250 ans. Vivement sa soutenance ! Merci à Maroua Ben Nasr pour sa gentillesse. Merci à Vianney Masson, Marion Capuano, Paul Laffay, Mathias Nkoum, Han Meng, Simon Bouley, Yuta Ozawa, Sarah Cleve, David Lamidel, Damien Cabut, Raphaël Da Mota, et Maxime Joly. Спасибо à Gyuzel Yakhina, Maria Karzova et Petr Yuldashev. Merci aussi à Achraf Radi, Loic Berger, Javier Beltran. Yoyoyoo à Rafael Engelmann, deine Zeit bei uns bleibt voll guter Erringerungen für mich, herzlichen Dank. Jetzt bist du dran Bro. Merci à Bertrand Mercier, le Mac Gyver des lasers et un pilote de haut vol. Merci au roi Arthur Guibard, protecteur des lagopèdes et de nos intérêts au CDL. Merci à Gabriele Grasso, le Dante Alighieri de `pgfplots` avec qui il est toujours agréable de discuter. Merci au boxeur Mohcene Oulmi, qui bientôt arrivera à concurrencer la LES avec son *mode matching*. Merci au camarade Mathieu Varé, avec qui j'ai eu plaisir à partager de succulents pains aux raisins dans le mythique bus 55. Merci au chef Pierre Pineau, toujours prêt à échanger une bonne référence de la littérature contre un carreau de chocolat. Merci à Hugo Vincent, qui saura prendre soin de l'adjoint et le mener au zénith. Merci enfin à Antoni Ignasi Alomar Sitjes, qui ne ménage pas ses efforts et son temps pour les autres et dont les encouragements et les conseils me furent précieux.

En concluant cette liste de noms, riche pour moi de souvenirs, j'ai au coeur le visage de mes amis et de mes proches qui m'ont soutenu durant ma période sur Lyon. Ils sont nombreux et me sont très chers. J'ai pour eux également une gratitude que le temps ne pourra tarir. Les voir avancer et grandir a été, et continue d'être, pour moi un grand motif de joie et de fierté. J'adresse mes ultimes remerciements à ceux qui me portent et supportent depuis si longtemps, mon frère Samuel et ma soeur Marie-Laure, ainsi qu'à mes deux parents formidables à qui je dédie ce travail : je vous aime.

«En les regardant,
Son visage a jeté
Sur eux le vêtement de la beauté. »

St Jean de la Croix

Table of contents

Guide de lecture

Cette thèse s'articule en deux parties, une description succinte des chapitres les composant est donné ici.

Partie I:

Chapitre 1

Le cadre d'étude des analogies acoustiques est introduit, leur domaine de validité et leur intérêt sont exposés. Le son est décrit sous la forme d'une perturbation linéaire se propageant autour d'un écoulement porteur. La capacité qu'ont les analogies acoustiques à pouvoir caractériser les sources de bruit d'un jet est dépeinte sommairement. Le concept d'ondes d'instabilités est introduit, et des raisons pour ne pas chercher à décrire ces dernières sont avancées. Enfin, la structure de cette partie de la thèse est donnée.

Chapitre 2

L'équation d'onde d'Euler (en anglais "*Euler's wave equation*", abrégé en EWE) sous forme non homogène est déduite des équations de Navier-Stokes. Les analogies acoustiques établies à partir d'une linéarisation et d'une expansion autour d'un écoulement incompressible sont passées en revue et ces techniques sont appliquées à EWE. Un modèle aéroacoustique basé sur l'équation d'onde de Pierce (1990) est proposé. La métrique acoustique associée à cette équation d'onde est présentée, ainsi que son hamiltonien. Les rayons exacts de Foreman (1989) sont généralisés à un écoulement moyen quelconque, de sorte a être équivalente à l'équation de Pierce.

Chapitre 3

Le code maison de différence finie PROPA est présenté et validé pour la quatrième configuration du workshop d'aéroacoustique numérique. Le concept de noyau auto-adjoint est introduit et de nouvelles équations d'ondes stables sont proposées. Avec l'aide de PROPA, leur stabilité est testée et leur capacité à calculer avec précision la propagation du son se propageant autour d'un écoulement cisaillé est comparée.

Partie II:

Chapitre 1

Une introduction à la certification acoustique des avions et aux effets de l'installation des turboréacteurs met en évidence le besoin et l'enjeu pour les motoristes de développer un outil fiable de prédiction du bruit produit par le jet. Compte tenu de la complexité de la géométrie rencontrée dans les architectures d'avions modernes et les ressources de calcul disponibles, la densité spectrale de puissance nécessaire à la certification doit être déterminée à partir des solutions des équations de Navier-Stokes moyennées (RANS). Dans ce type de modélisation statistique, le champ acoustique rayonné par le jet est pris en compte avec une approche adjointe. L'organisation de la seconde partie de la thèse est ensuite précisée.

Chapitre 2

Un examen détaillé du modèle de bruit de mélange de Tam and Auriault (1999) est fourni ici. Un effort est fait pour recalculer à nouveau la formule de prédiction en mettant l'accent sur une utilisation rigoureuse

de la méthode de l'adjoint. En complément des travaux de Tam et Auriault, la corrélation de fonction de Green adjointe (1999, eq. (34)) est modélisée à l'aide d'une expansion de Taylor. La deuxième partie de ce chapitre est consacrée à l'application de ce modèle à une formulation basée sur l'équation de Pierce, et utilisant l'acoustique potentielle. Quelques remarques sur la manière de modéliser le bruit de choc large bande (en anglais, Broadband shock associated noise abrégé en BBSAN) de Morris and Miller (2010) avec le formalisme proposé sont données en perspective.

Chapitre 3
L'énoncé le plus général du principe de réciprocité est basé sur le formalisme de l'adjoint. Dans ce chapitre, une discussion approfondie sur la méthode de l'adjoint est menée, et le bénéfice que représente le recours à des opérateurs auto-adjoints pour résoudre le problème de la propagation acoustique est souligné. Tam and Auriault (1998) ont exposé comment une approche adjointe permet de prédire le bruit de sources stochastiques distribuées dans un écoulement complexe (Tam and Auriault, 1999). Une déclaration claire portant sur l'applicabilité du théorème de retournement d'écoulement (en anglais "*flow reversal theorem*", abrégé en FRT), et sur sa restriction aux équations d'ondes auto-adjointes est également donnée. À titre d'illustration, un cas de propagation acoustique autour d'un écoulement moyen cisaillé et stratifié est résolu pour les équations d'onde de Lilley et de Pierce. Les champs acoustiques obtenues par la méthode de l'adjoint sont ensuite comparés aux prédictions obtenues avec le FRT.

Chapitre 4
Cette section détaille comment *Actran TM*, solveur conçu pour résoudre l'équation de Möhring (1999), est transformé de sorte à pouvoir résoudre l'équation de Pierce (1990). Après avoir présenté l'équation de Möhring normalisée, telle que résolue par *Actran TM*, ses solutions sont comparées au code maison PROPA. Comme l'équation de Pierce est auto-adjointe, le problème adjoint résolu avec *Actran TM* recourt au FRT. Un template permettant le calcul de la fonction de Green adjointe pour un écoulement de jet bidimensionnel est fourni. En guise de démonstrateur, la solution acoustique réciproque pour une configuration réaliste de moteur d'avion à double flux présentant des effets de vol est calculée.

Conclusion

Ce travail porte sur la modélisation de la propagation du son émis par un jet turbulent à grande vitesse. Le cadre de travail est celui des analogies acoustiques et l'approche retenue principalement celle de la modélisation analytique. Sous cette hypothèse simplificatrice, le champ acoustique produit par l'écoulement aérodynamique ne rétroagit pas sur ce dernier, et les problèmes de la génération et de la propagation sonore peuvent être traitées de manière séparée.

L'objectif de la première partie de cette étude est de proposer une modélisation simplifiée précise et robuste de la propagation du son autour d'un écoulement de base. Pour garantir la robustesse de l'approche, une formulation basée sur l'utilisation du potentiel acoustique est proposée. Cette méthode conserve l'énergie acoustique. Ceci constitue un atout de la méthode, qui ainsi concorde avec les cas limites de la propagation du son autour d'un écoulement potentiel et de l'acoustique géométrique. Le modèle proposé coïncide avec les seules formulations de la littérature pour lesquels l'acoustique est définit sans ambiguïté. Que la conservation de l'énergie acoustique soit imposée, signifie également que les phénomènes de conversion de mode ne peuvent pas être traités par cette approche. Ceci représente également un désavantage de la méthodologie proposée, qui par construction, est incapable de décrire certains mécanismes de génération de bruit, comme les ondes d'instabilité ou le rayonnement acoustique d'un tourbillon cisaillé dans son

transport par l'écoulement. Cela paraît être un tribut nécessaire à payer pour garantir la conservation de l'énergie acoustique.

Pour aboutir à cette formulation, les équations d'Euler ont été reformulées en l'équation d'onde d'Euler (EWE). Sous l'hypothèse des gaz parfaits, une équation de fermeture des équations est établie, et il est montré que les équations d'Euler peuvent être reformulées à l'aide de seulement deux variables. La linéarisation d'EWE (LEWE) a permis d'obtenir une équation d'onde sur la vitesse fluctuante qui est équivalente aux équations d'Euler linéarisées pour peu que le mode entropique ne soit pas généré. Cela n'est pas très contraignant pour les équations d'Euler qui présupposent un écoulement adiabatique. LEWE est plus générale que l'équation de Lilley et al. (1972), l'équivalence des deux équations est vérifiée numériquement sur une configuration présentant une onde d'instabilité. Tirant profit de la propriété de conservation de l'énergie des opérateurs auto-adjoints (Möhring, 1999), plusieurs approximations stables de LEWE sont proposées. En optant pour une définition du potentiel acoustique basée sur un potentiel de moment plutôt qu'un potentiel de vitesse, une analogie acoustique est construite. L'opérateur de propagation ainsi formé correspond à l'équation d'onde de Pierce (1990), dont l'utilité pratique est grandement accrue par la donnée nouvelle d'un terme source. C'est en optant pour cette définition du potentiel acoustique que l'équivalence de l'acoustique potentielle et du formalisme des rayons exacts (Foreman, 1989) a pu être établie. Le choix en faveur de cette convention originale pour le potentiel acoustique s'en trouve conforté. Le champ acoustique calculé par l'équation de Pierce est comparé à d'autres opérateurs de propagation stables sur un cas test, et son accord avec la solution de référence est trouvé satisfaisant. Alors que l'équation de Pierce et l'équation de Phillips (1960) possèdent le même opérateur d'onde, il est apparu que leurs prédictions diffèrent grandement. La grande importance d'un choix judicieux de la variable acoustique est par-là soulignée. Pour l'opérateur d'onde de Phillips-Pierce, la preuve n'a pas été établie que ce soit la définition de l'acoustique potentielle retenue ici qui offre la meilleure approximation du champ acoustique. D'autres définitions du potentiel acoustique, comme par exemple l'enthalpie fluctuante (Howe, 1975a), pourraient être envisagées dans de futures études. Grâce au développement du code PROPA, la stabilité des opérateurs de propagation a pu être validée. La précision des différentes formulations a été comparée sur un cas test, qui en raison des limites du code PROPA, s'étend sur un domaine de calcul restreint. Une étude comparative plus poussée pourrait avoir recours à un environnement de développement plus sophistiqué comme par exemple FreeFEM.

La seconde partie de ce travail illustre comment l'analogie acoustique formée à partir de l'équation de Pierce permet de reformuler avantageusement les modèles de bruit de jet existants. L'application visée est la prédiction du bruit rayonné par le jet d'un moteur d'avion installé sous la voilure. Devant la complexité de l'écoulement s'échappant d'un tel turboréacteur, seule une description statistique de l'écoulement est envisageable, et les méthodes usuelles pour simuler la propagation acoustique sont rendues inopérantes. La méthode de l'adjoint, initialement introduite par Lagrange (1761) et reformulée pour le bruit de jet par Tam and Auriault (1998), surmonte astucieusement cette difficulté en recourant au principe de réciprocité. Cette étude récapitule et reformalise cette méthode, puis la compare à la technique concurrente et plus intuitive du retournement d'écoulement. Ces deux techniques, la méthode de l'adjoint et le retournement d'écoulement, sont appliquées à l'équation de Pierce et à l'équation de Lilley. Alors que la méthode de l'adjoint est toujours exacte, le retournement d'écoulement ne s'applique qu'à des équations auto-adjointes comme celle de Pierce. L'utilisation de l'équation de Pierce possède donc dans ce contexte plusieurs avantages majeurs. Comme le retournement d'écoulement ne nécessite pas le développement de conditions aux limites anti-causales, la résolution numérique du champ adjoint à l'équation de Pierce s'en

trouve simplifiée, et des outils numériques déjà existants peuvent être employés à cette fin. Par ailleurs, l'équation de Pierce est scalaire et possède une expression très simple, de sorte que le coût de calcul associé à sa résolution soit minimal. Ceci constitue un avantage indéniable dans la résolution de problèmes à grand nombre de degré de liberté. Enfin, son caractère auto-adjoint garantit la stabilité du problème de propagation. Ceci semble avoir été la pierre d'achoppement empêchant jusqu'à présent une utilisation plus répandue de la résolution numérique des équations adjointes. En effet l'équation de Lilley et les équations d'Euler linéarisées utilisées jusqu'à présent dans les formulations adjointes (Tam and Auriault, 1998) décrivent le mode d'instabilité et des méthodes analytiques approchées du type WKBJ ont été privilégiées à une résolution numérique (Goldstein, 2003).

De sorte à démontrer la viabilité de l'utilisation de l'analogie de Pierce pour reformuler les modèles de bruit de jet, le modèle de bruit de mélange turbulent de Tam and Auriault (1999) a été réécrit pour l'acoustique potentielle. Une méthodologie pour transposer d'autres sources de bruit comme le BBSAN a été donnée, et les travaux futurs devront en éprouver la pertinence. Pour indiquer une manière possible de mettre oeuvre la méthode, qui soit compatible aux exigences de l'industrie aéronautique, une stratégie de calcul basée sur le logiciel commercial *Actran TM* a été proposée. Une géométrie réaliste de turboréacteur a été considéré comme démonstrateur et différents champs adjoints ont pu être calculés en champ proche et lointain en des temps compatibles avec les exigences industrielles. Des travaux futurs devront s'attacher à mettre en oeuvre l'ensemble de la chaine de prédiction, allant du calcul de la solution RANS jusqu'au spectre de bruit, et à la valider. Des écarts ont été observés entre la solution de l'équation de Pierce calculée avec PROPA et celle obtenue à l'aide d'*Actran TM*, bien que faibles, leurs origines doit être comprises et des correctifs apportés. La présence des surfaces dans la propagation acoustique peut être pris en compte par la méthode de l'adjoint telle que formulée ici, ceci représente une amélioration par rapport à la formulation originale de Tam and Auriault (1998), et demande à être mis en oeuvre et validé en pratique. Lorsque la propagation ne peut être résolue analytiquement, cette méthode est la seule qui puisse décrire le champ acoustique de sources de bruit uniquement connues de manière statistiques. La méthode de l'adjoint est générale et permet de traiter toute sortes de sources de bruit. Un unique calcul de champ adjoint pourrait ainsi être utilisé pour déterminer la propagation acoustique de l'ensemble des sources de bruit d'un turboréacteur. Cette technique traite la propagation sonore indépendamment des mécanismes de génération de bruit, et les champs adjoints permettent de caractériser complètement un milieu de propagation. En un sens, quant au découplage opéré, la méthode de l'adjoint apparaît comme un prolongement logique des analogies acoustiques.

Synopsis of the thesis

This thesis is structured in two parts, a brief overview of the chapters composing them is given here.

Part I:

Chapter 1

An introduction to the framework of acoustic analogies is provided, their purpose and limitations are outlined. The description of sound seen as a linear perturbation propagating over a base flow is presented. The capability of acoustic analogies to track some representative sound sources of a jet is briefly sketched. The concept of instability waves is depicted, and reasons not to account for them with a linear operator, are given. Finally, the organisation of this part of the thesis is given.

Chapter 2

Euler's wave equation (EWE) in non-homogeneous form is derived from the Navier-Stokes equations. Acoustic analogies based on linearisation and expansion about an incompressible flow are reviewed and applied to EWE. An aeroacoustic model based on the wave equation of Pierce (1990) is proposed. The acoustic metric associated to Pierce's wave equation is exhibited, as well as its Hamiltonian, and the exact rays (Foreman, 1989) are generalised to a medium with steady flow.

Chapter 3

The in-house finite difference code PROPA is presented and validated on the fourth CAA workshop case. The concept of self-adjoint kernel is introduced and some new stable wave equations are derived. With help of PROPA, their stability is tested, and their ability to accurately compute sound propagation on a sheared flow is compared.

Part II:

Chapter 1

An introduction to aircraft noise certification and turbofan engine installation effects highlights the need and the stakes for engine manufacturer to develop a reliable jet noise prediction tool. Given the complexity of the geometry encountered in modern aircraft architectures and the available computational capacities, the power spectral density of interest in the certification process needs to be computed from RANS solutions. In such statistical modellings, the noise radiated from jets is accounted for with an adjoint approach. The layout of the second part of the thesis is finally given.

Chapter 2

A detailed review on the mixing noise model of Tam and Auriault (1999) is provided here. Effort is given to properly derive the prediction formula anew with a focus on a rigorous use of the adjoint technique. Additionnaly to Tam and Auriault's work, adjoint Green's function correlation (1999, eq. (34)) is modelled using a Taylor expansion. The second part of this chapter is devoted to apply this technique to a potential acoustics formulation based on Pierce's equation. Some remarks on how to model the broadband shock

associated noise (BBSAN) as done by Morris and Miller (2010) within the present framework are given as a perspective.

Chapter 3

The most general statement for reciprocity principle is based upon the adjoint formalism. In this chapter, a comprehensive description of the adjoint approach is proposed and the benefit of using self-adjoint wave equations to solve acoustic propagation problems is highlighted. Tam and Auriault (1998) presented how an adjoint approach can be built to predict the noise of distributed stochastic sources in a complex environment (Tam and Auriault, 1999). A clear statement is also provided about the application of the flow reversal theorem (FRT), and its restriction to self-adjoint wave equations. As an illustration, sound propagation is computed numerically over a sheared and stratified mean flow for Lilley's and Pierce's wave equations. Acoustic solutions obtained with the adjoint approach are then compared to predictions obtained with the FRT.

Chapter 4

This section details how *Actran TM*, designed to solve Möhring's equation (1999), is turned into a solver for Pierce's equation (1990). After presenting the normalised Möhring equation solved by *Actran TM*, the accuracy of the solver is compared with respect to the in-house code PROPA. Because Pierce's equation is self-adjoint, the adjoint problem is solved with help of *Actran TM* using the FRT. A template enabling the computation of adjoint Green's function for a bidimensional jet flow is provided. As a proof of concept, the reciprocal acoustic solution for a realistic dual-stream aircraft engine with flight effects is presented.

Introduction

In his final contribution to acoustics, Euler (1767) gazed with wonder at the science he significantly contributed to. "*The most sublime research that Geometrist have undertaken nowadays with success*, he wrote, *is unarguably in all respect that of sound propagation. Because a given perturbation of air is dealt, this research has been all the more difficult, for among all those that were concerned with the movement of different bodies, none was found successful in describing the movement of air; so that this area of Mechanics was hitherto entirely unknown.*" The then pioneering developments in acoustics were indeed tremendous. He continues further on, "*When I investigated this topic for the first time, my main concern was to determine the speed at which a tremor is transmitted through the air; but now I will endeavour to detail all the particularities that may occur in the perturbation of air, and also the way they are altered in their propagation. This research is all the more interesting, that it is from there that all the variations that we observe in the sounds result.*" As a matter of fact, Euler's equations which describe the conservation of momentum in fluids (1757) was the stepping stone on which all later developments of sound propagation would be based. From this theory it was henceforth possible to account for the vibration of air and trace their propagation. Moreover, thanks to the joint developments of functional analysis, in which Lagrange played a foreground role, similarities in the motion of a vibrating string and the vibrations of air were found. From this analogy, an early-stage picture of waves invisibly travelling in air could be drawn, and propagation effects like echoes, could be explained (Hascher and Papadopoulos, 2015). Lagrange, in close collaboration with Euler, meticulously analysed the three-dimensional propagation of acoustic waves in air. Lagrange (1761, §18) proposed a model of spherical wave fronts for which he was the first to compute a solution using a variational statement and adjoint functions. By browsing through the literature, one is struck by the modernity and the accuracy of the conceptual framework these great scientists mastered. These concepts gave keys to grasp most of the propagation problems in acoustics. Consider for instance the acoustic wave fronts emitted from a self-sustained oscillating supersonic jet as depicted in figure 1; they clearly appear as spherical, while the reflectors visible on the photography left side corners generate what Euler would have called echoes.

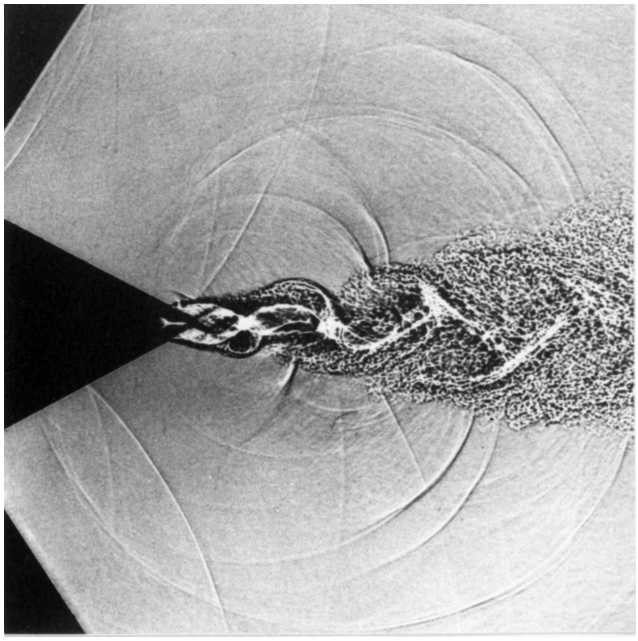

Figure 1: Shadowgraph of a planar under-expanded screeching supersonic jet of air taken by Poldervaart, Vink and Wijnands (1969) of the technological university of Eindhoven, and reprinted in Hirschberg (2009). For more details see Hirschberg et al. (2018) and the *Youtube* chanel of Avraham Hirschberg.

This golden age of acoustics is prior to French revolution, can only be compared with the breakthroughs of the second half of the twentieth century. Indeed, although Euler successfully addresses acoustic propagation back in (1767), it is only in (1952) that Lighthill introduced the framework to apprehend the flow-noise generation mechanisms. Neglecting the effect of viscosity, and using standard notations; Lighthill (1952) recast Euler's equations with the help of the continuity equation into the following equivalent formula,

$$\frac{\partial^2 \rho}{\partial t^2} - a^2 \Delta \rho = \nabla \cdot \nabla \cdot (\rho \boldsymbol{u} \otimes \boldsymbol{u}) + \Delta p - a^2 \Delta \rho \tag{1}$$

where ρ is the density, $\boldsymbol{u}$ is the velocity, p is the pressure and a is the speed of sound. On the left-hand side the d'Alembertian operator, that Euler and his peers used to evaluate for the fluid particle displacement, is retrieved for the density. The right-hand side furnishes a source term for the wave equation that brought about the recent craze for acoustic studies. For the first time indeed, the amount of energy converted from the fluid motion into acoustics could be quantified by integrating this equation. There is also an exact parallel between the equations of the fluid dynamics and the wave equation; from there an acoustic analogy for the noise generation mechanisms in fluids is derived. Interpreting Lighthill's equation, Powell (1964) showed that the mechanisms of energy conversion are substantial only in the region of space were vortices are distorted. This would correspond, in figure 1, to the mixing region of the jet, which is dominated by aerodynamical phenomena and governed by Euler's non-linear equations. Out of this domain, the source term vanishes, and the perturbations in the fluid obeys the simpler linear acoustic equation. Such a split of the space between aerodynamic and acoustic driven regions is characteristic of the aeroacoustic approach, and intuitively distinguishes sound generation from its propagation. Yet, to achieve acoustic predictions with Lighthill's formula, a variable decomposition is furthermore required in order to dissociate the source term from the acoustic variable. This split is intricate and tedious in the source region, because there exists no general and unambiguous way to define acoustic perturbations: as a matter of fact, acoustics is a manner for energy to propagate without transporting matter and its definition becomes equivocal when it is superimposed on arbitrary flows. Only when the ratio of the fluid vorticity by the acoustic frequency (Legendre, 2014, eq. (6.25)) tends toward zero, is acoustics properly defined (Michalke, 1965). It seems therefore hollow to seek a general definition for acoustic energy in arbitrary moving media (McIntyre, 1981). It must be recognized, that the conceptual framework of aeroacoustics raises in itself unresolved practical and fundamental questions.

Despite this gray area, acoustic analogies have proved themselves to be a powerful tool to predict and describe how flow induces noise. Aeronautics has been the primary field of application for this theory; it was developed to identify the sound generation mechanisms in jets exhausting from turbofan engines and made noise reduction possible (Lighthill, 1962, §5). This acoustic analogy moreover successfully predicted a remarkable scaling law for the acoustic power radiated from jets. While an increasing demand for quieter aircraft steadily challenged the emerging aeroacoustic community, the prodigious development in available computational resources significantly heighten the scope of the studies. Better understanding of the noise generation mechanisms has been achieved with high-fidelity numerical techniques (Lele and Nichols, 2014; Brès and Lele, 2019). Besides that, acoustic analogies were used combined with timely statistical simulations of the flow, to carry out jet noise predictions. During the manufacturing processes of aircraft engines, timely and accurate prediction tools are indeed required to further reduce jet noise. In this view, there is a need for jet noise statistical modelling to properly assess the refraction effects encountered in the jets as well as the effects on the acoustic propagation of the turbofan installation under the plane wing. For such jet noise statistical modelling, acoustic propagation effects can naturally be accounted for

from an adjoint perspective (Lagrange, 1761; Tam and Auriault, 1998), and the use of the adjoint method to this end is now standard.

Objective of the work

This work is concerned with the propagation of acoustic waves superimposed on a flow in application to statistical jet noise modelling. In the context of acoustic analogies, this study deliberately adopts a pragmatic stance and aims at proposing a consistent and robust approximate framework to compute sound propagation. A formulation based on the acoustic potential is given and the widespread jet mixing noise model of Tam and Auriault (1999) is demonstratively recast within this scope. Encouraging results in the description of propagation effects have been obtained with the adjoint method in previous studies. A further objective of this study is to propose a throughout discussion on the application of this method in an industrial environment and to come with a concrete solution enhancing the state of the art jet noise prediction capabilities.

Outline of the manuscript

This thesis is made of two autonomous parts.

The first part details a theoretical framework to describe sound generation and propagation. The issue of noise prediction with an acoustic analogy is first introduced (Chapter 1). The equations of fluid mechanics are then recast into a creative wave equation for the fluid velocity, referred to as Euler's wave equation. After linearisation, a Helmholtz decomposition of the fluctuating momentum is found to deliver the wave equation of Pierce (1990), and a source term for the latter equation is proposed. The equivalence of Pierce's equation with the exact rays (Foreman, 1989) framework is finally demonstrated (Chapter 2). The problematic of achieving acoustic propagation on a sheared flow without to trigger instability waves is addressed. Following Möhring (1999), some original stable self-adjoint wave equations are proposed. The sound propagation for the latter equations are compared with an in-house code on a benchmark problem (Chapter 3).

The second part focuses on the modelling of noise radiated from jets, and is applied to the context of aeronautical industry. It is illustrated how the acoustic analogy based on Pierce's wave equation can advantageously be applied to account for jet noise propagation effects. The stake of statistical jet noise prediction is first introduced (Chapter 1). The standard mixing noise prediction formula of Tam and Auriault (1999) is thoroughly presented and recast for the acoustic potential (Chapter 2). The adjoint method, introduced in aeroacoustics by Tam and Auriault (1998), is presented and used as a rigorous mean to assess propagation effects. The method is compared to the flow reversal theorem, that is its intuitive alternative (Chapter 3). An additional step to prove the viability of the approach is achieved by using the commercial software *Actran TM* to compute the solution to Pierce's adjoint equation. A computation carried out for a realistic turbofan engine serves as a proof of concept (Chapter 4).

ÉCLAIRCISSEMENS PLUS DÉTAILLÉS SUR LA GÉNÉRATION ET LA PROPAGATION DU SON, ET SUR LA FORMATION DE L'ECHO,

PAR M. EULER.

1.

La plus ſublime recherche que les *Géometres* ayent entrepriſe de nos jours avec ſuccès, eſt ſans contredit à tous égards celle de la propagation du ſon. Comme il y eſt queſtion d'une certaine agitation de l'air, cette recherche a été d'autant plus difficile, que parmi toutes celles qu'on a faites ſur le mouvement de différens corps, il ne s'en trouve pas une ſeule, où l'on ait réuſſi à ſoumettre au calcul le mouvement de l'air: de ſorte que cette partie de la Mécanique a été juſqu'ici entierement inconnue. Car on n'y ſauroit rapporter le peu de choſe qu'on a fait ſur le mouvement des corps pouſſés par la force d'un air comprimé; puiſqu'on n'y a conſidéré que la ſeule force de l'air, ſans examiner le mouvement dont les différentes particules de l'air ſont agitées entr'elles. Ainſi on ne ſavoit encore abſolument rien des différens mouvemens dont une maſſe d'air eſt ſuſceptible.

2. Outre cette difficulté, on en a rencontré encore une autre auſſi grande de la part de l'Analyſe: quelque perfectionnée que paroiſſe déjà cette ſcience par les ſoins des plus grands Géometres, elle n'étoit pas encore ſuffiſante pour entreprendre cette recherche; il falloit quaſi ouvrir une carriere tout à fait nouvelle, où il s'agit d'étendre l'Analyſe à des fonctions de deux ou pluſieurs variables, pendant que preſque toutes les découvertes des Géometres ont été bornées à des fonctions d'une ſeule variable. Il falloit donc s'appliquer à une branche tout à fait

fait nouvelle de l'Analyſe des infinis, dont même les premiers élémens n'étoient preſque pas encore développés. De là on ne ſera pas ſurpris ſi cette nouvelle Analyſe rencontre de grandes contradictions, même de la part des plus grands Géometres; quand on ſe rappelle à combien de contradictions le calcul différentiel a été expoſé dans ſa premiere naiſſance.

3. Quoique j'aye déjà traité ce ſujet en quelques Mémoires après le célebre M. de la Grange, à qui on eſt redevable de cette importante découverte, tant la nouveauté que l'importance mérite bien toute l'attention, & des recherches ultérieures ne manqueront pas de nous fournir encore de plus grands éclairciſſemens. Lorsque je traitai cette matiere pour la premiere fois, je me ſuis attaché principalement à déterminer la viteſſe dont un tremouſſement eſt tranſmis par l'air; mais à préſent je tacherai de développer toutes les particularités qui peuvent avoir lieu dans les agitations de l'air, & la maniere dont elles ſont altérées dans leur propagation. Cette recherche eſt d'autant plus intéreſſante, que c'eſt de là que réſultent toutes les variétés que nous obſervons dans les ſons. Mais, ayant déjà fait voir que la propagation ſe fait à peu près de la même maniere dans le plein air que dans un tuyau, je bornerai mes recherches préſentes à des tuyaux, & même également larges par toute leur étendue: il n'importe preſque rien ſi ces tuyaux ſont droits ou courbés d'une maniere quelconque, puiſque les phénomenes du ſon n'en ſouffrent aucun changement.

43. Mais on comprend aiſément, que tout ce que je viens de développer, ne regarde qu'un cas trés particulier, & qu'on ſe tromperoit bien groſſierement, ſi l'on vouloit aſſigner à tous les échos

échos cette même origine. Je n'ai conſidéré que des tuyaux également larges par toute leur étendue; ce qui eſt ſans doute un cas très particulier, auquel les bornes de l'Analyſe m'ont attaché, vu qu'il eſt encore impoſſible de définir le mouvement de l'air dans les tuyaux, dont la largeur varie d'une maniere quelconque. Cependant on avouera que ce cas, quelque particulier qu'il ſoit, nous a fourni des éclairciſſemens très importans tant ſur la génération & propagation du ſon, que ſur la formation des *échos:* d'où nous pourrons puiſer des idées beaucoup plus juſtes qu'on n'en a eu juſqu'ici. Mais, comme cette recherche eſt fondée ſur une branche tout à fait nouvelle de l'Analyſe, elle doit principalement exciter tous les Géometres à la cultiver; puisque c'eſt de là qu'on peut attendre les plus importantes découvertes, qui ſont entierement inacceſſibles à l'Analyſe ordinaire, & parmi leſquelles il faut ſurtout compter celles où le mouvement de l'air entre en conſidération.

44. Donc, ſi nous poſſédons encore à peine les premiers principes pour connoitre le mouvement de l'air, & ſi tout ce que nous en ſavons ſe réduit à certaines eſpeces de tuyaux; combien ſommes-nous encore éloignés de déterminer toutes les modifications que le ſon reçoit dans des cavités quelconques? La cavité de la bouche humaine nous en fournit un exemple frappant, dont nous ne connoiſſons que fort en gros l'effet dans la formation de la voix: ne ſachant preſque rien de la maniere dont les articulations & autres modifications ſont opérées. Mais il n'y a aucun doute que, s'il nous étoit poſſible de pénétrer dans ces myſteres, nous découvririons auſſi dans la figure de la bouche un vrai chef-d'oeuvre de la ſouveraine ſageſſe, qui ſurpaſſe infiniment tout ce que le plus ſublime Géometre eſt capable d'imaginer. C'eſt ainſi que partout le Créateur a mis l'empreinte de ſon infinie ſageſſe, même dans les choſes qui en paroiſſent le moins ſuſceptibles.

The beginning and ending of the last of Euler's (1767) many studies that he contributed on sound propagation. He had derived the basic equations of fluid mechanics a decade earlier (1757). The almost 20 year long controversy in which he opposed d'Alembert on the existence of discontinuous solutions to the wave equation was solved, paving the way to the concept of a wave. In the meanwhile, the repeated canon shot experiences had sown doubts on Newton's isothermal estimate of the speed of sound, and Lagrange (1761) solved the wave propagation problem with his adjoint approach.

Part I

Acoustic analogy based on the acoustic potential

1 Basic features of acoustic analogies

Summary:
Introduction to the framework of acoustic analogies is provided, their purpose and limitations are outlined. The description of sound seen as a linear perturbation propagating over a base flow is presented. The capability of acoustic analogies to track some representative sound sources of a jet is briefly sketched. The concept of instability waves is depicted, and reasons not to account for them with a linear operator, are given. Finally, the organisation of this part of the thesis is given.

1.1 Introductory discussion

On its early stage, aeroacoustics has been introduced by Lighthill (1952) as the study of sound generated aerodynamically. The original idea was to build a theoretical framework to describe the physical process at play in the production of flow induced noise. Lighthill sought to estimate the amount of energy converted from the fluid motion into acoustics. He succeeded in his endeavour by skilfully rearranging Euler's equations,

$$\begin{cases} \dfrac{\partial \rho}{\partial t} + \nabla \cdot (\rho \boldsymbol{u}) = 0 \\ \dfrac{\partial \rho \boldsymbol{u}}{\partial t} + \nabla \cdot (\rho \boldsymbol{u} \otimes \boldsymbol{u}) + \nabla p = \boldsymbol{0} \\ \dfrac{\partial p}{\partial t} + \nabla \cdot (p \boldsymbol{u}) + (\gamma - 1) p \nabla \cdot \boldsymbol{u} = 0 \end{cases} \tag{1.1}$$

into a non-homogeneous wave equation for the fluid density ρ,

$$\frac{\partial^2 \rho}{\partial t^2} - a^2 \Delta \rho = \nabla \cdot \nabla \cdot \boldsymbol{T} \tag{1.2}$$

Thereby an exact analogy between the density ρ of any real flow, and the acoustic fluctuations produced by a quadrupole source $\nabla \cdot \nabla \cdot \boldsymbol{T}$ propagating in an idealised medium at rest, with constant sound speed a, was derived. Lighthill's stress tensor $\boldsymbol{T} = \rho \boldsymbol{u} \otimes \boldsymbol{u} + (p - a^2 \rho) \boldsymbol{I}$ is the wave equation source, $\boldsymbol{u}$ refers to the flow velocity, p corresponds to the pressure field and $\boldsymbol{I}$ is the identity tensor. For simplicity, the effect of viscosity is discarded. The double divergence of the Lighthill tensor $\boldsymbol{T}$ is tagged as quadrupole sound source. These spatial derivatives confer the latter source a directive nature that resembles a four-leaf clover which leaves may be twisted. Powell (1964, §5) gave insight into the physical mechanisms at play in the formation of quadrupole sound sources, and this concept is an important construct in jet noise modelling (Ribner, 1969). Lighthill selected the fluid density ρ, as the appropriate dependence variable to model jet noise (1982). However its definition is implicitly given in his analogy. Hence, for his theory

to be operable, sound propagation needs to be addressed in a two step procedure, independently from its generation. In practice, noise sources are first identified, the propagation of sound over a quiescent base flow is addressed subsequently. Acoustic analogies describe a one-way energy conversion from the fluid kinetic energy to sound, and the back-reaction of acoustics on the base flow (Maestrello et al., 1981) is not account for. Therefore configuration for which acoustic feedback mechanisms are crucial, like screeching supersonic jets or noise from cavities, cannot be tackled with such an approach.

Ffowcs Williams and Hawkings (1969) and Möhring et al. (1969) have independently shown that, different equivalent distributions of sound sources consistently describe the same acoustic field. And in fact, plenty of acoustic analogies have continuously been proposed over the years[1], highlighting thereby considerable efforts to find the most appropriate framework to address flow noise. This built-in non-uniqueness of acoustic analogies has been pointed out by Tam (2001, 2002) as a fundamental obstacle to ever succeed in identifying the correct sound sources. An additional hardship comes from the intricate distinction between the acoustic field and the non-acoustic part of the flow (Morfey, 1971; Fedorchenko, 2000). Indeed, acoustic analogies assume it is possible to associate to a unsteady turbulent flow a corresponding quiescent flow, which contains all the representative sound-producing features of the flow. At low Mach number, the flow incompressible part is such a quiescent base flow (Ribner, 1962), but in general it is too crude to restrict the silent base flow to its solenoidal part (Fedorchenko, 1997).

Noise generation mechanisms are inextricably coupled (Chu and Kovásznay, 1958), so is also the propagation of sound (Doak, 1954; Golubev and Atassi, 1998), with this in mind, some authors explicitly introduced the concept of acoustic-vortical-entropy waves to depict the manner energy propagates in a moving fluid (Campos and Serrão, 2013). The proper and non-ambivalent separation of acoustics from the base flow is thus undeniably jeopardized (McIntyre, 1981). Such a bold undertaking was not, of course, Lighthill's intent when he derived his acoustic analogy. He was well aware of how complex it is to define turbulent noise sources. In (1952) he explained the ambition and purpose of his new methodology: "*The problem's utility may be questioned on the grounds that we never know a fluctuating fluid flow very accurately, and that therefore the sound produced in a given process could only be estimated very roughly. Indeed, one could hardly expect, even with the great advances in knowledge of turbulent flow which have lately been made, that such a theory could be used with confidence to predict acoustic intensities within a factor of much less than 10. But, on the other hand, one could certainly make no confident estimate even within a factor of 1000 on existing knowledge*". Searching for a pragmatic basements for acoustic analogies is a commendable initiative (Goldstein, 2002, 2003, 2005b); but in order not to pursue a pipe-dream, the method constitutive limitations need to be borne in mind. In proposing his generalised acoustic analogy, Goldstein (2003) summarised several techniques stemming from the literature, that are individually defined for different base flows. For steady mean flows of Reynolds averaged Navier-Stokes (RANS) solutions, a Reynolds or a Favre decomposition adequately models acoustic fluctuations. If a solenoidal unsteady base flow is given, then an expansion about incompressible flow (Ribner, 1962; Hardin and Pope, 1994) may be applied. If a general radiating flow simulation is available, a modal non-radiating decomposition of the flow (Taira et al., 2017) may be considered. Yet in practice, the amplitude of acoustic fluctuations are often small with respect to the incompressible fluctuations and the complete flow solution may conveniently be included in the definition of the sound source without prejudice to the computed sound

[1]Among which (Phillips, 1960; Ribner, 1962; Powell, 1964; Lilley et al., 1972; Howe, 1975a; Goldstein, 1978; Hardin and Pope, 1994; Doak, 1998; Starobinski and Aurégan, 1998; Möhring, 1999; Shen and Sørensen, 1999a; Ewert and Schröder, 2003; Goldstein, 2003; Gabard et al., 2004b; Perez Bergliaffa et al., 2004; Seo and Moon, 2006; Posson and Peake, 2013; Kaltenbacher et al., 2015).

(Ribner, 1962; Bogey et al., 2002). Notice that hybrid methodologies (Goldstein, 2006; Bodard et al., 2009; Semiletov and Karabasov, 2018) may also be conceived.

1.2 Linear acoustic perturbations superimposed over a base flow

At the inception of aeroacoustics, the directivity of jet noise was solely explained by the Doppler amplification factor associated with the movement of sound sources (Lighthill, 1952, 1954). The predominant role of the flow in the refraction of acoustic waves was recognised soon after. Gottlieb (1959) predicted, that such sound propagation over flow heterogeneities, would create a 'zone of silence' close to the jet axis in the flow downward direction[2]. Such a quiet region resulting from flow velocity gradients was verified experimentally by Atvars et al. (1965). Grande (1965) illustrated, with measurements performed on a nitrogen jet, that the temperature gradients may also create impressive acoustic refraction. Since, it is acknowledged that the flow significantly alters sound radiation (Ribner, 1996). This influence of the medium non-uniformities is referred to as acoustic propagation effects and include amongst others, flow refraction, scattering by turbulence, atmospheric dissipation, reflection and absorbency at solid boundaries, as well as scattering at surface edges.

Again, the clear distinction between propagation effects and sound generation mechanism is tedious. Tam (2001) argues this point as follow, "*if the complete wave propagation terms are kept, the assertion of the Acoustic Analogy argument would end up with only viscous terms as the noise source terms. This is definitely erroneous. Thus the so-called noise source terms of the Acoustic Analogy are, in many instances, propagation terms wrongly classified as noise sources.*" As a matter of fact, in the most general case, acoustic propagation is coupled and non-linear, and sound propagation cannot be addressed separately from its generation. This is not the simplified perspective underpinning the acoustic analogies, for which only a one-way coupling from the flow dynamics to acoustics is considered. What is more, non-linear propagation effects may exist in configuration without acoustic feed-back mechanisms (Petitjean et al., 2006), but they are often irrelevant to a first approximation.

To account for acoustic propagation effects in jets, it is convenient to model acoustics as a linear perturbation superimposed over a steady base flow (Schubert, 1972a,b). Very often, the steady base flow is modelled as the time-averaged part of the flow. If the mean flow variables are indexed with a zero, and in absence of coupling with the acoustic field, they simply verify Euler's equations (1.1),

$$\begin{cases} \rho_0 \nabla \cdot \boldsymbol{u}_0 + \boldsymbol{u}_0 \cdot \nabla \rho_0 = 0 \\ \rho_0 (\nabla \boldsymbol{u}_0) \cdot \boldsymbol{u}_0 + \nabla p_0 = \boldsymbol{0} \\ \boldsymbol{u}_0 \cdot \nabla p_0 + \gamma p_0 (\nabla \cdot \boldsymbol{u}_0) = 0 \end{cases} \tag{1.3}$$

where γ corresponds to the fluid adiabatic index. It is also useful[3] to define a_0 the mean speed of sound for an idealised gas with $a_0 = \sqrt{\gamma p_0 / \rho_0}$. The equations governing linear acoustic propagation are then obtained with a Reynolds decomposition of the flow variables, such that, $\rho = \rho_0 + \rho'$, $\boldsymbol{u} = \boldsymbol{u}_0 + \boldsymbol{u'}$ and $p = p_0 + p'$. The fluctuating variable are denoted here with a prime and have zero mean value. By

[2]This concept was readily introduced in the study of atmospheric sound propagation, e.g. (Galbrun, 1931) and (Blokhintzev, 1956, §II.9). The current terminology of 'cone of silence' was in use soon after, in reference maybe to the 1960s television series 'Get Smart'.

[3]Note that these relations can be rearranged to retrieve the isentropy conservation for the mean flow $\vec{u}_0 \cdot (\nabla p_0 - a_0^2 \nabla \rho_0) = 0$ and in $\frac{\vec{u}_0 \cdot \nabla (a_0^2)}{1-\gamma} = a_0^2 \nabla \cdot \vec{u}_0 = \vec{u}_0 \cdot (\nabla \vec{u}_0) \cdot \vec{u}_0$ so to highlight that the speed of sound is conserved along streamlines for an incompressible mean flow.

subtracting the steady state solution described by equations (1.3), the linearised Euler's equations are obtained,

$$\begin{cases} \dfrac{\mathrm{D}\rho'}{\mathrm{D}t} + \nabla\cdot(\rho_0\boldsymbol{u'}) + \rho'\nabla\cdot\boldsymbol{u}_0 = S_{\rho'} \\ \dfrac{\mathrm{D}\rho_0\boldsymbol{u'}}{\mathrm{D}t} + \rho_0\boldsymbol{u'}\nabla\cdot\boldsymbol{u}_0 + (\nabla\boldsymbol{u}_0)\cdot(\rho_0\boldsymbol{u'}) + \nabla p' - \rho'\dfrac{\nabla p_0}{\rho_0} = \boldsymbol{S}_{\rho_0\boldsymbol{u'}} \\ \dfrac{\mathrm{D}p'}{\mathrm{D}t} + \boldsymbol{u'}\cdot(\nabla p_0 - a_0^2\nabla\rho_0) + a_0^2\nabla\cdot(\rho_0\boldsymbol{u'}) + \gamma p'\nabla\cdot\boldsymbol{u}_0 = S_{p'} \end{cases} \tag{1.4}$$

where $\mathrm{D}/\mathrm{D}t = \partial/\partial t + \boldsymbol{u}_0\cdot\nabla$ is the material derivative along the mean flow. The second order interaction terms are stored in the right hand side (RHS) of equations (1.4). They express as,

$$\begin{cases} S_{\rho'} \equiv -\nabla\cdot(\rho'\boldsymbol{u'}) \\ \boldsymbol{S}_{\rho_0\boldsymbol{u'}} \equiv -(\nabla\boldsymbol{u'})\cdot(\rho_0\boldsymbol{u'}) + \rho'\nabla p'/\rho_0 \\ S_{p'} \equiv -\boldsymbol{u'}\cdot\nabla p' - \gamma p'\nabla\cdot\boldsymbol{u'} \end{cases} \tag{1.5}$$

From such a variable decomposition and rearrangement of the equations, what we may refer as inviscid sound sources naturally appear. Even though every possible propagation effects are accounted for in the linear operator as suggested by Tam (2001), inviscid sound sources may be defined. Figure 1.1 illustrates this with a two-dimensional harmonic solution of equations (1.4). The fluctuating pressure p' obtained

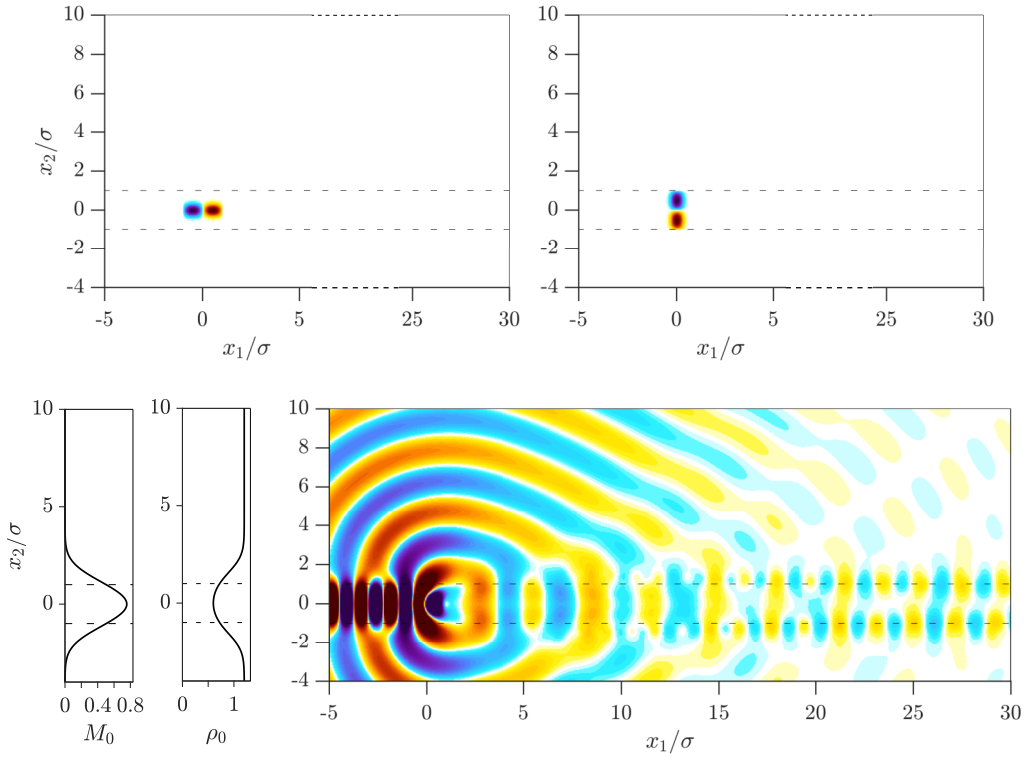

Figure 1.1: Quadrupole source $\boldsymbol{S}_{\rho_0\boldsymbol{u'}}$ forcing the direct problem $S_{\rho_0 u_1'}$ (top-left), and $S_{\rho_0 u_2'}$ (top-right). Mach number M_0 and density ρ_0 profiles of the parallel mean flow considered (bottom-left), and pressure field p' solution of Lilley's equation and computed with PROPA, see §3.1, for $St_{2\sigma} = 0.60$ (bottom-right). Dashed lines represent the position of maximal shearing ($x_2/\sigma = 1$).

for a parallel sheared and heated flow, as considered for the fourth computational aeroacoustic workshop

(Dahl, 2004), is presented, and qualitatively represents the acoustic propagation encountered in jets for such an idealised sound source. The forcing term $\boldsymbol{S}_{\rho_0 \boldsymbol{u}'}$ is defined so to mimic a quadrupole distribution and is adapted from in (Gréverie and Bailly, 1998, eq. (4)), with $\alpha = 1/(2\sigma)^2$. The modulation in the cosine is replaced by $\alpha/4$. $S_{\rho'} = 0$, and $S_{p'} = 0$. The predominant effect of the mean flow on the acoustic propagation is observed, and the quadrupole radiation pattern is hardly recognisable in figure 1.1. A quieter region downward of the jet is observed (Gottlieb, 1959), while high amplitude fluctuations are trapped by the flow upstream of the source.

Note that the remark of Tam (2001) transcripted previously is a fundamental one. For equations (1.4) not to be coupled with second-order perturbations, and to enable a linear explicit resolution of the equations, the non-linear terms need in practice to be defined as source terms. But, the choice of keeping all linear terms in left hand side (LHS) of equations (1.4), and thereby consider them as acoustic propagation terms rather than sources, is arbitrary. In fact, the link between first-order terms and propagation effect, and between second-order terms and sound sources is the result of a half-century progresses in aeroacoustics. To form his acoustic analogy, Lighthill (1952) built up a d'Alembertian's operator from the equations of fluid motion. Thereby he repelled all remaining terms in the RHS as possible sound source. Because noise generating flows are not medium at rest for which acoustic propagation can be described with a d'Alembertian's wave equation, many RHS terms of Lighthill's analogy compensate for the source motion and do not account for noise generation mechanisms. The aeroacoustic community made thus continuous effort (Phillips, 1960; Lilley et al., 1972; Bogey et al., 2002; Goldstein, 2003) to properly build a linear equation that most representatively depicts propagation effects, in order to account for all sound propagation mechanisms in the LHS. If in Lighthill's equation, all possible sound sources are stored in the RHS; with an acoustic analogy like equations (1.4), then all possible propagation effects are cast in the LHS.

A noticeable drawback of these reformulations lies in the fact, that these linearised set of fluid equations are not any more genuine wave equations. In fact, unlike classical second order wave equations, e.g. (Lighthill, 1952; Phillips, 1960; Möhring, 1999), all energetic modes are now described with equations (1.4). This has thoroughly been discussed by Chu and Kovásznay (1958), and can be illustrated using a Helmholtz decomposition of the quadrupole sound source $\boldsymbol{S}_{\rho_0 \boldsymbol{u}'}$ used to compute the pressure fluctuations p' of figure 1.1. Figure 1.2 and figure 1.3 represent the fluctuating pressure p' produced by the potential part of $\boldsymbol{S}_{\rho_0 \boldsymbol{u}'}$ shown in figure 1.1, and its solenoidal part respectively. Because the propagation problem is linear, the sum of the fluctuations of p' of figure 1.2 and figure 1.3 corresponds to the solution figure 1.1, computed for the full quadrupole source. The solution computed for the source solenoidal part appears to be mostly non-radiating; most of the fluctuating pressure perturbations p' are simply convected along the mean flow. Oppositely, such convection phenomena cannot be observed for the fluctuating field associated with the potential source given in figure 1.2. This solution corresponds to the acoustic mode generated by the quadrupole source, for which a cone of silence is clearly identifiable. The other solution figure 1.3 is slightly radiating in the jet downward region. These sound waves correspond to indirect acoustic fluctuations which are created by the movement and shearing of the solenoidal sources. This solenoidal contribution to the quadrupole source is otherwise essentially silent. A coupling mechanisms is at stake transforming the vortical fluctuations into acoustics. As a consequence, with a formulation like equations (1.4), not all sound sources are cast in the RHS.

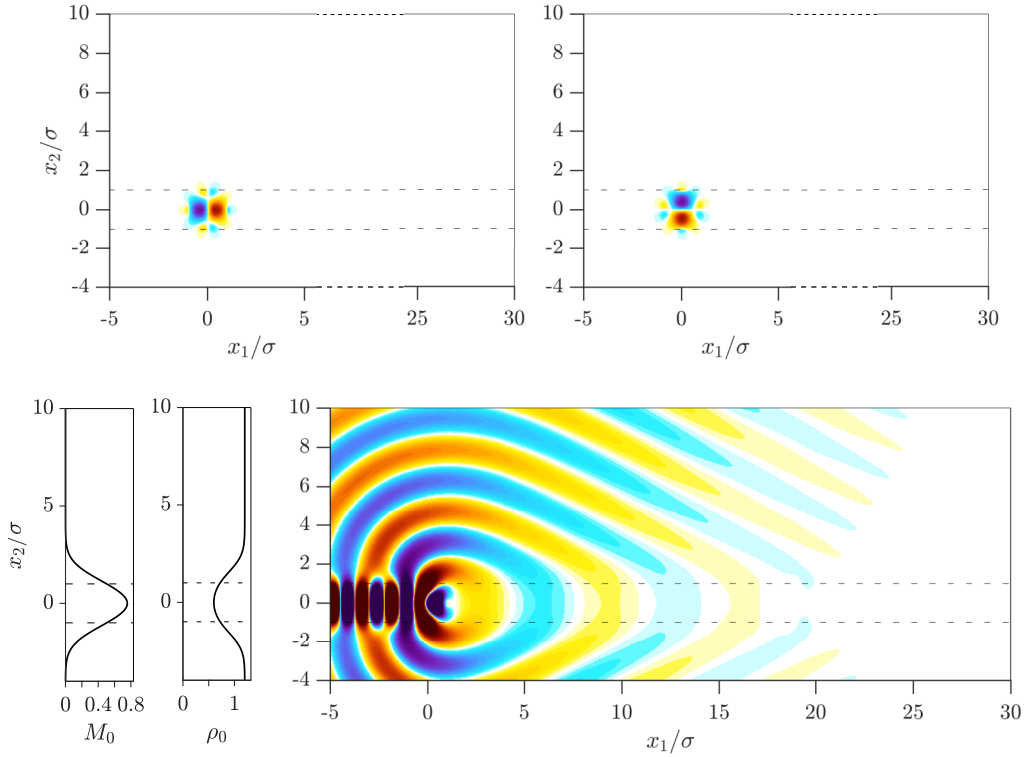

Figure 1.2: Potential part of the quadrupole sound source $\boldsymbol{S}_{\rho_0 \boldsymbol{u}'}$ shown in figure 1.1 (top). Mach number M_0 and density ρ_0 profiles of the parallel mean flow considered (bottom-left), and corresponding pressure field p' (bottom-right). Dashed lines represent the position of maximal shearing ($x_2/\sigma = 1$).

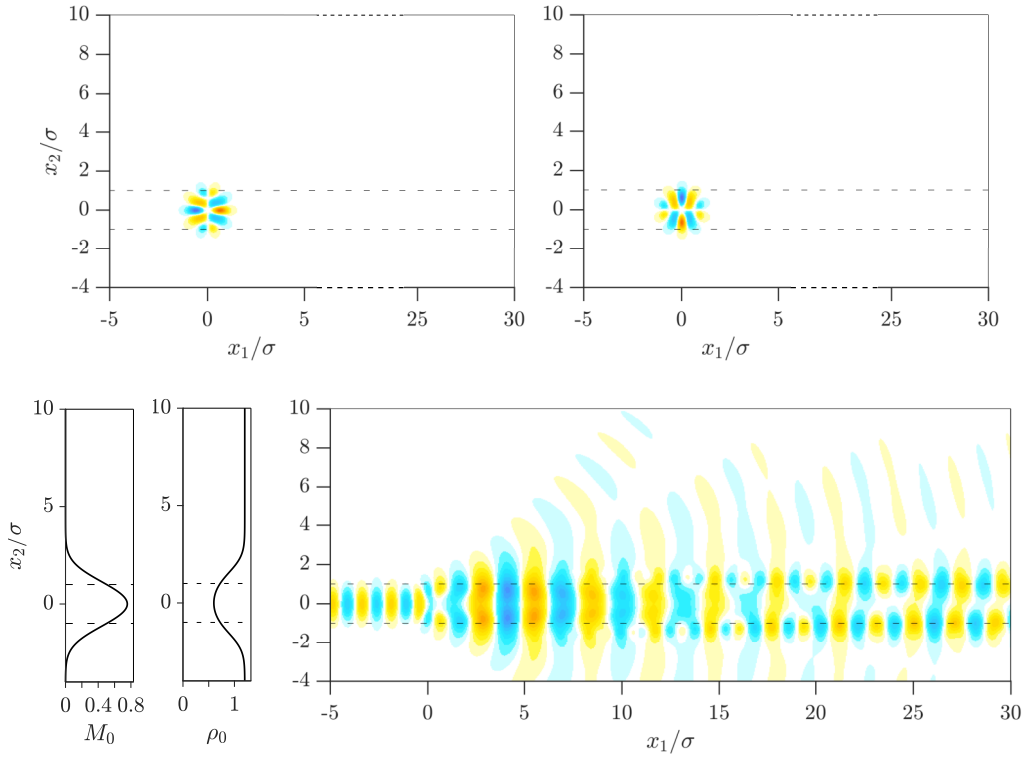

Figure 1.3: Solenoidal part of the quadrupole sound source $\boldsymbol{S}_{\rho_0 \boldsymbol{u}'}$ shown in figure 1.1 (top). Mach number M_0 and density ρ_0 profiles of the parallel mean flow considered (bottom-left), and corresponding pressure field p' (bottom-right). Dashed lines represent the position of maximal shearing ($x_2/\sigma = 1$).

1.3 Instability waves as a source of sound

For many applications, the divergence of the Reynolds tensor $\nabla\cdot(\rho_0\boldsymbol{u}\otimes\boldsymbol{u})$ appearing in Euler's momentum equation is the dominant source of aerodynamic noise (Lighthill, 1952, eq. (7)). In the previous acoustic analogy example, sounds propagates over a steady base flow, given by equations (1.3), and acoustic perturbations are linearly superimposed on the latter. This is described by equations (1.4). Some insight on the noise generation mechanisms is given here by analysing more in depth the Reynolds decomposition $\boldsymbol{u}=\boldsymbol{u}_0+\boldsymbol{u'}$ of $\nabla\cdot(\rho_0\boldsymbol{u}\otimes\boldsymbol{u})$. Following Ribner's theory of dilatation (1962), it is assumed here that the part of the flow dynamics that produces sound is at leading order purely solenoidal, i.e. $\nabla\cdot\boldsymbol{u}_0=\nabla\cdot\boldsymbol{u'}=0$. In the linearised framework, the amplitude of the perturbations are small with respect to those of the mean flow dynamics, let $\varepsilon=|\boldsymbol{u'}|/|\boldsymbol{u}_0|$ measure this velocity magnitude gap. Furthermore, let λ and L be the typical length scales of the flow structures associated to $\boldsymbol{u'}$ and $\boldsymbol{u}_0$ respectively. $\delta=\lambda/L$ quantifies this scale separation and is not necessary small. The order of magnitude of the different term appearing in the Reynolds decomposition is then,

$$\nabla\cdot(\rho_0\boldsymbol{u}\otimes\boldsymbol{u})=\underbrace{\rho_0(\nabla\boldsymbol{u}_0)\cdot\boldsymbol{u}_0}_{\sim O(\delta/\varepsilon)}+\underbrace{(\nabla\rho_0\boldsymbol{u'})\cdot\boldsymbol{u}_0}_{\sim O(1)}+\underbrace{(\nabla\boldsymbol{u}_0)\cdot(\rho_0\boldsymbol{u'})}_{\sim O(\delta)}+\underbrace{\nabla\cdot(\rho_0\boldsymbol{u'}\otimes\boldsymbol{u'})}_{\sim O(\varepsilon)} \tag{1.6}$$

The first term in $O(\delta/\varepsilon)$ is possibly large, but it can be discarded since it describes the dynamics of the steady flow and vanishes for an isobar mean flow. The second term $(\nabla\rho_0\boldsymbol{u'})\cdot\boldsymbol{u}_0$ describes the convection of the fluctuating momentum $\rho_0\boldsymbol{u'}$. If $\delta\ll 1$, the vortical structures are simply convected along $\boldsymbol{u}_0$ without deformation and hence are silent, otherwise they radiate noise. The two other terms correspond to the distortion of vortices by the mean flow shear and interactions of the vortices amongst themselves. These two last sources of flow noise have been extensively addressed by Ribner (1964, 1969, 1981) who referred to them as shear-noise and self-noise. Even though they are linear and quadratic with respect to $\boldsymbol{u'}$, they appear to have comparable order of magnitude for small vortices when $\delta\sim\epsilon$, that is in the acoustic high frequency limit. Yet as in the equations (1.4), they are usually not stow away in the same member of the acoustic analogy. Indeed, since the contribution of Lilley et al. (1972), the term responsible for shear-noise is often tagged as a propagation term, while self-noise is undoubtedly a 'real' sound source. Ribner (1969) gave evidences that shear-noise dominated the jet noise spectra in the low frequency range, while self-noise was predominant for higher acoustic frequencies. His result is reproduced in figure 1.4. In meticulously analysing all possible quadrupole correlations, Ribner (1969) proved that shear-noise was

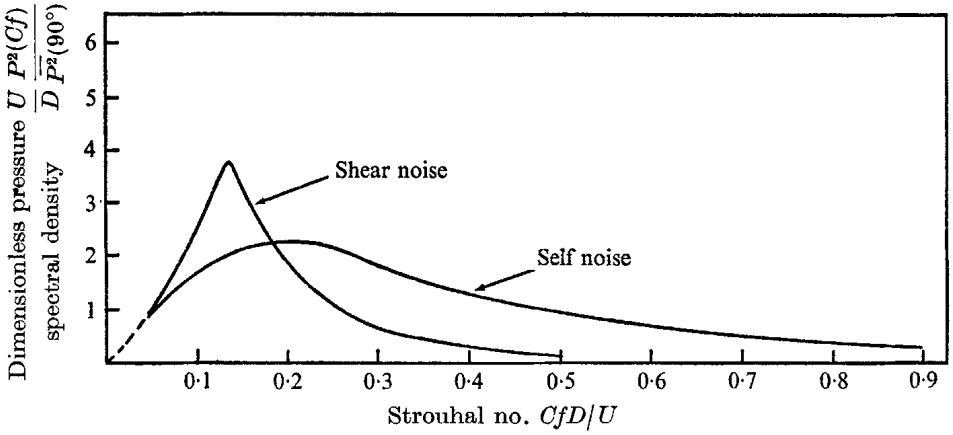

Figure 1.4: Jet noise two-components spectrum prediction by Ribner (1969), experimentally calibrated.

very directive while self-noise radiation was more omnidirectional. Figure 1.5 qualitatively illustrates how these two sources of sound contribute to the jet directivity spectra. From figure 1.5, self-noise is the dominant sound source in a direction perpendicular to the jet axis while shear-noise mainly contributes in the jet downward region. The existence of two self-similar spectra in jet noise have been evidenced

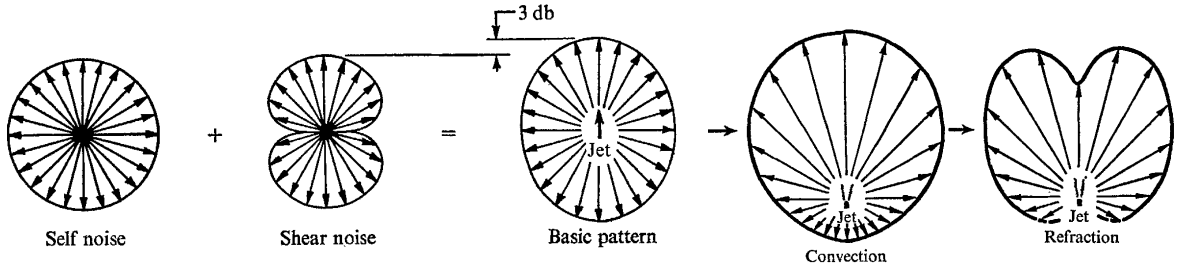

Figure 1.5: Jet noise directivity explained by the combination of shear-noise, self-noise and propagation effects, figure adapted from (Ribner, 1969).

experimentally by Tam et al. (1996) for supersonic jet noise. These contributions to jet mixing noise are referred in these authors' study as stemming from the fine-scale structures of turbulence (self-noise) and from the large-scales (shear-noise). These authors argued that this two-components model transposes to subsonic jet noise as well (Tam et al., 1996, §5). Notice that the concepts of self-noise and shear-noise are constructs of the acoustic analogy framework, while fine-scales and large-scales draw their existence on experimental evidences. Even though these notions are not perfectly alike, this must be considered as an achievement of the acoustic analogies to have predicted the existence of the two component spectrum of jet noise.

In a famous contribution, reviewed in §2.1 of this work, Tam and Auriault (1999) proposed an acoustic description for the fine-scale mixing process for which they modelled the contribution of the turbulence self-noise $\nabla \cdot (\rho_0 \boldsymbol{u'} \otimes \boldsymbol{u'})$ with a potential sound source ∇q_s. This description for fine-scale turbulence mixing does not favour any spatial direction, complies with the idealised isotropic pattern of self-noise radiation as depicted by Ribner in figure 1.5, but also with measurements performed on jet turbulence at sufficient large distance from the nozzle lip lines (Fleury et al., 2008). Considering the Helmholtz decomposition of the quadrupole sound source $\boldsymbol{S}_{\rho_0 \boldsymbol{u'}}$ and their corresponding acoustic solutions, it can be alleged that the acoustic field stemming from the quadrupole potential part in figure 1.2 may fairly well represent the radiation of turbulence self-noise, while the radiation of the quadrupole solenoidal part of figure 1.3 rather qualitatively corresponds to shear-noise radiation. Indeed, if the shear-noise term $(\nabla \boldsymbol{u}_0) \cdot (\rho_0 \boldsymbol{u'})$ is dropped from the the linearised equations (1.4), this solenoidal term radiates almost[4] no more sound and is quietly convected by the mean flow. The corresponding solution for the fluctuating pressure p' is presented in figure 1.6, where the simplified formulation of Bogey et al. (2002, eq. (B3)) for a parallel mean flow was used for this calculation. In turn, the term responsible for shear-noise in the linearised equations converts solenoidal fluctuations into acoustics, acknowledging the general statement: "*vortex dynamics makes noise*". This may be one of the shear-noise generation principle.

Tam et al. (1996) also referred in their work to the noise of large turbulent structures as instability waves. The latter correspond to the sound radiated from a Kelvin-Helmholtz flow instability. This is another way to create shear-noise. This noise generation process is described by the linearised equations written for an inviscid fluid and takes place for a moderate low frequency range of flow disturbances (Michalke, 1965;

[4]The residual radiation may be due to the definition of the solenoidal sound source that does not respect $\delta \ll 1$ strictly.

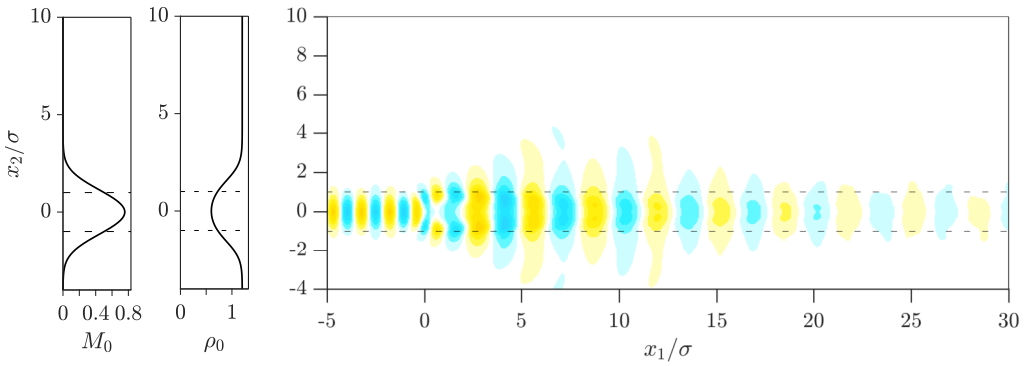

Figure 1.6: Mach number M_0 and density ρ_0 profiles of the parallel mean flow considered (left), and the pressure field p' solved with the stabilised Lilley's equation (Bogey et al., 2002, eq. (B3)). The solenoidal part of $\boldsymbol{S}_{\rho_0 \boldsymbol{u}'}$ that is presented in figure 1.3 is used as sound source. This fluctuating pressure field p' corresponds to the solution of the linearised equation for which the shear-noise term $(\nabla \boldsymbol{u}_0) \cdot (\rho_0 \boldsymbol{u}')$ is discarded (right). Dashed lines represent the position of maximal shearing ($x_2/\sigma = 1$).

Moore, 1977; Morris, 1981; Bailly and Comte-Bellot, 2015, §1.5). This is a selective process for which some frequencies of perturbations are damped and other amplified, with a model similar to equations (1.4) it is furthermore linear so that the perturbation growth rate is irrespective from the perturbation amplitude. Figure 1.7 (left) presents the acoustic solution to the linearised Euler's solution computed by Ewert (2007) for a jet with a stochastic reconstruction of the fine-scale mixing noise source of Tam and Auriault (1999). While for such a stochastic model, $\varepsilon \ll 1$ and $\delta \ll 1$, and the hypothesis of the linearised framework are initially fulfilled; the instability wave growths unreasonably and faults the hypothesis of small amplitudes. This is because the non-linear saturation is not accounted for in the acoustic propagation. If the mean flow gradients are removed from the acoustic solution, as for the computation presented in figure 1.6, this instability wave completely disappears from the computed solution, see figure 1.7 (right), and a fairly isotropic sound radiation, characteristic of the fine-scale mixing noise, is obtained.

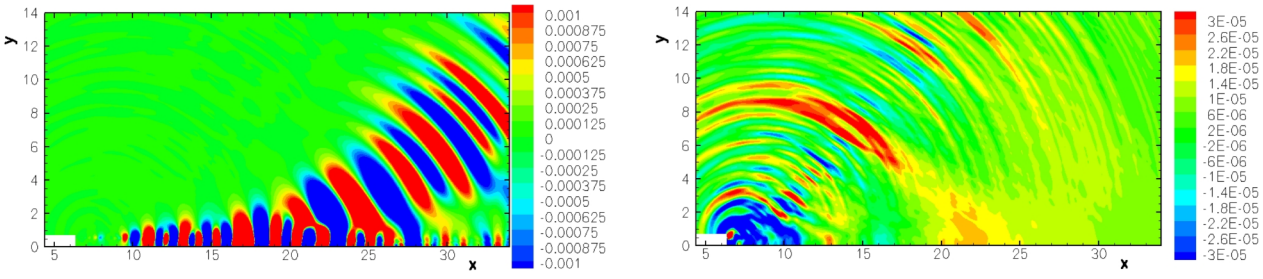

Figure 1.7: Jet noise computation with a stochastic reconstruction of Tam and Auriault's mixing noise model by Ewert (2007). Acoustic propagation is computed over a steady base flow with the linearised Euler's equations (left), the acoustic field is solved with linearised equations for which the mean flow gradients are neglected (right).

Previous paragraphs illustrate, how an acoustic analogy with a simple Reynolds decomposition is successful to describe some relevant features of jet noise, such as its directivity, its radiated acoustic energy spectrum and some noise generation mechanisms. Two sound sources of subsonic jets are identified. The first one originates from the interaction of the mean flow shear $\nabla \boldsymbol{u}_0$ with the fluctuating momentum of the vortices $\rho_0 \boldsymbol{u}'$. Whereas the second one describes the effect of the small eddies $\rho_0 \boldsymbol{u}'$ that are sheared by equally small

vortices $\nabla \boldsymbol{u'}$. These are definitely two limit process of a continuous spectrum of possible interactions. As a result of linearisation, the non-linear contributions of the intermediate scales of turbulence is wiped out. This is a serious limitation to the linearised modelling framework of jet noise, and may explain the failure of this simplified description to quantitatively predict the noise of the large scale turbulent structures. Mohseni et al. (2002) compared the radiation of the large scales as computed with a direct numerical simulation of the flow against the instability waves computed with a acoustic analogy methodology relying on a Reynolds decomposition of the flow. A qualitative good agreement was found for the directivity, but apart for the azimuthal order and the amplitude of the most amplified frequency, these authors concluded that a linear description essentially fails in quantitatively predicting the radiation of instability waves.

Summarily put, even though instability waves intrinsically result from convection phenomena, it appears safer not to account for them in the linear operator of the acoustic analogy. This is for two main reasons. First, it would appear that linearised Euler's equations are inoperative to properly model the generation of instability waves. Essential non-linear mechanisms are indeed at stake. Secondly, in a linearised framework their growth are unbounded, and instability waves are likely to become overwhelming and corrupt the acoustic solution. With a pragmatic stance, for the acoustic analogy methodology to be robust, the linear operator accounting for the propagation needs to be stable. It is argued that the term responsible for the instability waves must be dislodged from the acoustic propagation operator and be dealt as a sound source. As such, this noise mechanisms can be addressed with a large scale non-linear unsteady flow solver (Goldstein, 2006; Bodard et al., 2009; Semiletov and Karabasov, 2018) or modelled analytically relying on a stochastic flow solution (Bailly et al., 1996).

This part of the thesis is concerned with the description of acoustic waves propagating in a moving fluid. Chapter 2 begins by reformulating Euler's equations in an original form from which a very general wave equation on fluctuating velocity is drawn up. A pragmatic stance is adopted, and this study wants to contribute to the construction of a robust and practically oriented solution to achieve acoustic predictions. With this in mind, a formulation based on the acoustic potential is chosen and an acoustic analogy based on the equation of Pierce (1990) is introduced in paragraph §2.5. To obtain this equation, an unusual expression of the acoustic potential is chosen. Section §2.7 shows how with this convention, the formalism of the acoustic rays can be found in a way that is not approximate. The in-house code that has been developed in this thesis is briefly presented in chapter 3; it is then used to validate the stability of the wave equations proposed and to give an appreciation of their accuracy.

2 Constitutive equations of aeroacoustics

Summary: Euler's wave equation (EWE) in non-homogeneous form is derived from the Navier-Stokes equations. Acoustic analogies based on linearisation and expansion about an incompressible flow are reviewed and applied to EWE. An aeroacoustic model based on the wave equation of Pierce (1990) is proposed. The acoustic metric associated to Pierce's wave equation is exhibited, as well as its Hamiltonian, and the exact rays of Foreman (1989) are generalised to a medium with steady flow.

2.1 Equations of fluid motion

The Navier-Stokes equations are governing the dynamics of viscous flows. This set of equations is constituted by the mass, the momentum and the energy conservation equations which reads in non-homogeneous form as follow,

$$\begin{cases} \dfrac{\partial \rho}{\partial t} + \nabla \cdot (\rho \boldsymbol{u}) = \dot{m} \\ \dfrac{\partial \rho \boldsymbol{u}}{\partial t} + \nabla \cdot (\rho \boldsymbol{u} \otimes \boldsymbol{u}) + \nabla p = \nabla \cdot \Sigma + \boldsymbol{f} + \dot{m} \boldsymbol{u} \\ \dfrac{\partial \rho e_t}{\partial t} + \nabla \cdot (\rho e_t \boldsymbol{u}) + \nabla \cdot (p \boldsymbol{u}) = \nabla \cdot (\Sigma \cdot \boldsymbol{u}) - \nabla \cdot \boldsymbol{q} + \dot{\theta} + \boldsymbol{f} \cdot \boldsymbol{u} + \dot{m} e_t \end{cases} \tag{2.1}$$

The states variables $\boldsymbol{u}$, ρ, p are the fluid velocity, its density and the thermodynamic pressure. Σ corresponds to the (symmetric) shear stress tensor and $\boldsymbol{q}$ is the heat flux defined by Fourier's law as $\boldsymbol{q} = -\lambda \nabla T$, where $\lambda \equiv \lambda(T)$ is the heat conductivity and T the fluid temperature. $e_t = e + \boldsymbol{u}^2/2$ is the specific total energy, where e is the fluid internal energy as defined by Gibbs' formula $\delta e = T\ \delta s - p\ \delta \left(1/\rho\right)$ with s the fluid entropy and where the δ refer to total derivatives. Additionally, some hypothetical source terms for mass $\dot{m}$, heat $\dot{\theta}$ or driven by an external force $\boldsymbol{f}$ are introduced (Chu and Kovásznay, 1958), (Delfs, 2016, §2.2). Defining additionally the material derivative $\mathrm{D}/\mathrm{D}t = \partial/\partial t + \boldsymbol{u} \cdot \nabla$ the constitutive equations of fluid mechanics can be recast into,

$$\begin{cases} \dfrac{\mathrm{D}\rho}{\mathrm{D}t} + \rho \nabla \cdot \boldsymbol{u} = \dot{m} \\ \rho \dfrac{\mathrm{D}\boldsymbol{u}}{\mathrm{D}t} + \nabla p = \nabla \cdot \Sigma + \boldsymbol{f} \\ \rho \dfrac{\mathrm{D}e}{\mathrm{D}t} + p \nabla \cdot \boldsymbol{u} = \mathrm{tr}(\Sigma \cdot \nabla \boldsymbol{u}) - \nabla \cdot \boldsymbol{q} + \dot{\theta} \end{cases} \tag{2.2}$$

Using Gibbs' formula, the equation for entropy is computed from the previous equations,

$$\rho T \frac{\mathrm{D}s}{\mathrm{D}t} = \mathrm{tr}(\Sigma \cdot \nabla \boldsymbol{u}) - \nabla \cdot \boldsymbol{q} + \dot{\theta} - \frac{p}{\rho}\dot{m} \tag{2.3}$$

To close the system of equations a relation between the state variables is required. The fluid is therefore particularised here to obey the perfect gas law, that is $p = \rho r T$, where r denotes the specific gas constant. The internal energy of a perfect gas solely depends on its temperature, $\mathrm{d}e = C_v \mathrm{d}T$, so does its enthalpy $\mathrm{d}h = C_p \mathrm{d}T$, where C_p and C_v are the specific heat capacity for constant pressure and volume respectively. The isentropic constant γ is such as $\gamma = C_p/C_v$, from the definition of enthalpy $h = e + p/\rho$, Mayer's relation is then retrieved $C_p - C_v = r$, and thus $C_p = \gamma r/(\gamma - 1)$ and $C_v = r/(\gamma - 1)$. Expressing Gibbs' relation in terms of variations of density, pressure and entropy delivers,

$$\delta p - \frac{\gamma p}{\rho}\delta\rho = (\gamma - 1)\rho T \delta s \tag{2.4}$$

The speed of sound a is defined as the characteristic velocity measuring the variation of pressure associated with an isentropic change of the density,

$$a = \sqrt{\left(\frac{\partial p}{\partial \rho}\right)_s} \tag{2.5}$$

hence, $a^2 = \gamma p/\rho = \gamma r T$. The state equation for a perfect gas enables by now the closure of the system, offering a further reformulation of the energy equation,

$$\frac{\mathrm{D}p}{\mathrm{D}t} + \gamma p \nabla \cdot \boldsymbol{u} = (\gamma - 1)\mathrm{tr}(\Sigma \cdot \nabla \boldsymbol{u}) - (\gamma - 1)\nabla \cdot \boldsymbol{q} + (\gamma - 1)\dot{\theta} + rT\dot{m} \tag{2.6}$$

2.1.1 Euler's wave equation (EWE)

Beside these concise expressions describing the fluid dynamics, the governing equations may be written in some other elegant forms. For instance subtracting the gradient of the energy equation from the material derivative of the momentum equation and dividing the obtained expression by the density offers,

$$\boxed{\frac{\mathrm{D}^2\boldsymbol{u}}{\mathrm{D}t^2} + (\nabla \boldsymbol{u})^T \cdot \frac{\mathrm{D}\boldsymbol{u}}{\mathrm{D}t} + (\gamma - 1)(\nabla \cdot \boldsymbol{u})\frac{\mathrm{D}\boldsymbol{u}}{\mathrm{D}t} - a^2 \nabla(\nabla \cdot \boldsymbol{u}) = \mathbb{S}_1} \tag{2.7}$$

where $\mathbb{S}_1$ expresses as,

$$\begin{aligned} \mathbb{S}_1 = \; & \frac{\gamma - 1}{\rho}\left[\nabla\left(\nabla \cdot \boldsymbol{q} - \dot{\theta} - \mathrm{tr}(\Sigma \cdot \nabla \boldsymbol{u})\right) + (\nabla \cdot \boldsymbol{u})\left(\boldsymbol{f} + \nabla \cdot \Sigma\right)\right] + \frac{\mathrm{D}(\boldsymbol{f} + \nabla \cdot \Sigma)}{\mathrm{D}t} \\ & + \frac{(\nabla \boldsymbol{u})^T}{\rho} \cdot (\boldsymbol{f} + \nabla \cdot \Sigma) - rT\nabla\left(\frac{\dot{m}}{\rho}\right) \end{aligned} \tag{2.8}$$

Equation (2.7) for the velocity $\boldsymbol{u}$ possesses a skeleton which resembles a wave operator and is referred in the present study as Euler's wave equation (EWE). Indeed, in absence of viscous contributions and heat conduction phenomena, this equation becomes homogeneous and equivalent to Euler's equations. It is the exact generalisation of Powell's analogy, that Powell (1964, eq. (49)) has derived for a low Mach number quasi-incompressible flow. Some similitude of EWE with (Chapman, 2000, § 4.2) can also be found. Interestingly, a closure for Euler's wave equation can be obtained in combining the continuity and

energy equations to derive a transport equation for the sound speed a,

$$\boxed{\frac{\mathrm{D}a}{\mathrm{D}t} + \frac{\gamma - 1}{2} a \nabla \cdot \boldsymbol{u} = \mathbb{S}_2} \tag{2.9}$$

where $\mathbb{S}_2$ is independent of the mass injection $\dot{m}$ and writes,

$$\mathbb{S}_2 = \frac{\gamma - 1}{2p} \left[\mathrm{tr}(\Sigma \cdot \nabla \boldsymbol{u}) - \nabla \cdot \boldsymbol{q} + \dot{\theta} \right] \tag{2.10}$$

Whenever viscous effects of the fluid may be neglected, e.g. far from solid boundaries for high Reynolds number flows, and when thermal conduction plays no role, thus in the framework of Euler's equations; then the above boxed equations (2.7) and (2.9), in their homogeneous form, fully describe perfect gases dynamics. As a consequence if the fluid can be modelled as an inviscid and adiabatic ideal gas, then the flow velocity $\boldsymbol{u}$ and the sound speed a (or temperature T) are sufficient to fully characterise the flow state.

In their homogeneous form, Euler's wave equation together with the transport equation for the speed of sound form a system of quasi-linear partial differential equations. That is a second order system which possesses two unknowns $\boldsymbol{u}$ and a, that represent in total $n + 1$ scalar unknowns, where n corresponds to the dimension of $\boldsymbol{u}$. For such a non-linear wave equation no standard classification into hyperbolic, parabolic, elliptic problem is possible. Even when the linearised and parallel flow simplification of EWE is considered, which is presented in this script equation (2.18), the problem is described by a set of second order partial differential equation with n unknowns, and a classification of the linear operator is not feasible, for dimensions greater than one. To obtain some insight in the structure of the flow solution, an analysis of Euler's equations is presented in appendix D. It is observed that an additional variable, like the entropy s, is required to close Euler's equations when recast with the flow velocity $\boldsymbol{u}$ and speed of sound a.

2.2 Linearisation of Euler's wave equation (LEWE)

In chapter 1, §1.2 some noise source term for Euler's equations are given. They consist in second order interaction terms yielded from the linearisation of the fluid governing equations. The linearised equation of the fluid were found also to adequately model sound propagation. A similar procedure is considered here to deduce from EWE sound sources as well as a corresponding linear operator for sound propagation. It is possible to directly linearise EWE from equations (2.7), but for this specific problem, it is simpler to form again the corresponding wave equation from the linearised Euler's equations (LEE). In what follows, the linearisation is performed over an unsteady base flow that obeys,

$$\begin{cases} \mathrm{D}_{\boldsymbol{u}_0}(\rho_0) + \rho_0(\nabla \cdot \boldsymbol{u}_0) = 0 \\ \rho_0 \mathrm{D}_{\boldsymbol{u}_0}(\boldsymbol{u}_0) + \nabla p_0 = \boldsymbol{0} \\ \mathrm{D}_{\boldsymbol{u}_0}(p_0) + \gamma p_0(\nabla \cdot \boldsymbol{u}_0) = 0 \end{cases} \tag{2.11}$$

The material derivative along the base flow is introduced, $\mathrm{D}_{\boldsymbol{u}_0} = \partial/\partial t + \boldsymbol{u}_0 \cdot \nabla$. From here, the primes are omitted in superscript to refer to fluctuating quantities. The linearised Euler's equations are recalled

hereafter for some generic source term $(S_\rho, \boldsymbol{S_u}, S_p)$ as,

$$\begin{cases} \mathrm{D}_{\boldsymbol{u}_0}(\rho) + \nabla\cdot(\rho_0\boldsymbol{u}) + (\nabla\cdot\boldsymbol{u}_0)\rho = S_\rho \\ \mathrm{D}_{\boldsymbol{u}_0}(\boldsymbol{u}) + (\nabla\boldsymbol{u}_0)\cdot\boldsymbol{u} + \dfrac{\nabla p}{\rho_0} - \dfrac{\nabla p_0}{\rho_0^2}\rho = \boldsymbol{S_u} \\ \mathrm{D}_{\boldsymbol{u}_0}(p) + \nabla p_0\cdot\boldsymbol{u} + \gamma p_0(\nabla\cdot\boldsymbol{u}) + \gamma(\nabla\cdot\boldsymbol{u}_0)p = S_p \end{cases} \tag{2.12}$$

This reformulation of the LEE does not present any technical difficulty, it is however lengthy and the key steps for the derivation are given in appendix C.1. The linearised Euler's wave equation (LEWE) is eventually obtained as,

$$\begin{aligned} &D^2_{\boldsymbol{u}_0}(\boldsymbol{u}) + \mathrm{D}_{\boldsymbol{u}_0}((\nabla\boldsymbol{u}_0)\cdot\boldsymbol{u}) + (\nabla\boldsymbol{u}_0)^T\cdot\mathrm{D}_{\boldsymbol{u}_0}(\boldsymbol{u}) + (\nabla\boldsymbol{u}_0)^T\cdot(\nabla\boldsymbol{u}_0)\cdot\boldsymbol{u} - a_0^2\nabla(\nabla\cdot\boldsymbol{u}) \\ &+(\gamma-1)\mathrm{D}_{\boldsymbol{u}_0}(\boldsymbol{u}_0)(\nabla\cdot\boldsymbol{u}) + \nabla\left(\mathrm{D}_{\boldsymbol{u}_0}(\boldsymbol{u}_0)\right)\cdot\boldsymbol{u} + (\nabla\boldsymbol{u})^T\cdot\mathrm{D}_{\boldsymbol{u}_0}(\boldsymbol{u}_0) \\ &+(\gamma-1)(\nabla\cdot\boldsymbol{u}_0)\left[\mathrm{D}_{\boldsymbol{u}_0}(\boldsymbol{u}) + (\nabla\boldsymbol{u}_0)\cdot\boldsymbol{u}\right] + a_0^2\nabla(\nabla\cdot\boldsymbol{u}_0)\left[\frac{\rho}{\rho_0} - \frac{p}{p_0}\right] \\ &= \mathrm{D}_{\boldsymbol{u}_0}(\boldsymbol{S_u}) + (\nabla\boldsymbol{u}_0)^T\cdot\boldsymbol{S_u} + (\gamma-1)(\nabla\cdot\boldsymbol{u}_0)\boldsymbol{S_u} - \frac{\nabla S_p}{\rho_0} - \frac{\mathrm{D}_{\boldsymbol{u}_0}(\boldsymbol{u}_0)}{\rho_0}S_\rho \end{aligned} \tag{2.13}$$

This wave equation is very general and apart from the term $\left(\rho/\rho_0 - p/p_0\right)$, it is function of the fluctuating velocity $\boldsymbol{u}$ only. This odd term corresponds to fluctuations of the speed of sound a, in fact,

$$a^2 = \frac{\gamma p}{\rho_0} - \frac{\gamma p_0\rho}{\rho_0^2} = a_0^2\left(\frac{p}{p_0} - \frac{\rho}{\rho_0}\right) \tag{2.14}$$

It can be expressed alternatively with help of equations (2.12). Then, using Gibbs' relation (2.4), it is claimed that this term measures entropy s variations, since,

$$\underbrace{\mathrm{D}_{\boldsymbol{u}_0}(p) - a_0^2\mathrm{D}_{\boldsymbol{u}_0}(\rho)}_{=\frac{(\gamma-1)p_0}{r}\mathrm{D}_{\boldsymbol{u}_0}(s)} = \underbrace{\left(a_0^2\nabla\rho_0 - \nabla p_0\right)}_{=\frac{(1-\gamma)p_0}{r}\nabla s_0}\cdot\boldsymbol{u} + \gamma p_0(\nabla\cdot\boldsymbol{u}_0)\left(\frac{\rho}{\rho_0} - \frac{p}{p_0}\right) + \mathrm{D}_{\boldsymbol{u}_0}(S_p) - a_0^2\mathrm{D}_{\boldsymbol{u}_0}(S_\rho) \tag{2.15}$$

From the linearisation of the entropy transport equation (2.3), for an inviscid and adiabatic fluid,

$$\mathrm{D}_{\boldsymbol{u}_0}(s) + \boldsymbol{u}\cdot\nabla s_0 = 0 \tag{2.16}$$

and,

$$\gamma p_0(\nabla\cdot\boldsymbol{u}_0)\left(\frac{\rho}{\rho_0} - \frac{p}{p_0}\right) = a_0^2\mathrm{D}_{\boldsymbol{u}_0}(S_\rho) - \mathrm{D}_{\boldsymbol{u}_0}(S_p) \tag{2.17}$$

Thus, in configurations for which no entropy source is present, i.e. $\mathrm{D}_{\boldsymbol{u}_0}(S_p) = a_0^2\mathrm{D}_{\boldsymbol{u}_0}(S_\rho)$, and as long solely acoustic propagation is concerned; the term $\nabla(\nabla\cdot\boldsymbol{u}_0)\left(\rho/\rho_0 - p/p_0\right)$ can reasonably be dropped. For Euler's equations are adiabatic, it is seen that the entropy mode decouples from the acoustic mode and the vorticity mode. A genuine wave equation for the fluctuating velocity $\boldsymbol{u}$ is thereby obtained. The so obtained linearised Euler's wave equation (LEWE) is very general, and represents an interesting cheaper alternative to the LEE[1], that may possibly be solved with a finite-element method (Peyret and Elias,

[1]Note that a similar wave equation for the fluctuating velocity $\boldsymbol{u}$ was derived by Blokhintzev (1946, eq. (9)) for an heterogeneous medium at rest. Similarities between the LEWE and the wave equations written for the particle displacements

2001). In many applications however, simplifications for incompressible base flows ($\nabla \cdot \boldsymbol{u}_0) = 0$ or parallel base flows $\mathrm{D}_{\boldsymbol{u}_0}(\boldsymbol{u}_0) = \boldsymbol{0}$ are handy. For parallel base flows, LEWE conveniently simplifies into,

$$\boxed{\begin{aligned} &D^2_{\boldsymbol{u}_0}(\boldsymbol{u}) + \left[(\nabla \boldsymbol{u}_0) + (\nabla \boldsymbol{u}_0)^T\right] \cdot \mathrm{D}_{\boldsymbol{u}_0}(\boldsymbol{u}) + (\nabla \boldsymbol{u}_0)^T \cdot (\nabla \boldsymbol{u}_0) \cdot \boldsymbol{u} - a_0^2 \nabla(\nabla \cdot \boldsymbol{u}) \\ &= \mathrm{D}_{\boldsymbol{u}_0}(\boldsymbol{S_u}) + (\nabla \boldsymbol{u}_0)^T \cdot \boldsymbol{S_u} - \frac{\nabla S_p}{\rho_0} \end{aligned}} \tag{2.18}$$

This simplification of LEWE is equivalent to Lilley's equation (1972). This is illustrated on a numerical test in §3.2.

Sound source

While Bogey et al. (2002) proposed a source for the linearised Euler's equation through a comparison with Lilley's equation sound source; Goldstein (2003) gave a more general expression for the source term accounting for all possible second order non-linear interactions. The general forcing term of the LEWE may similarly be given in relationship with the LEE source terms $(S_\rho, \boldsymbol{S_u}, S_p)$,

$$\mathbb{S} = \mathrm{D}_{\boldsymbol{u}_0}(\boldsymbol{S_u}) + (\nabla \boldsymbol{u}_0)^T \cdot \boldsymbol{S_u} + (\gamma - 1)(\nabla \cdot \boldsymbol{u}_0)\boldsymbol{S_u} - \frac{\nabla S_p}{\rho_0} + \frac{\nabla p_0}{\rho_0^2} S_\rho \tag{2.19}$$

These interaction terms for the LEE are given in equations (1.5) and are recalled hereafter,

$$\begin{cases} S_\rho \equiv -\nabla \cdot (\rho \boldsymbol{u}) \\ \boldsymbol{S_u} \equiv -\nabla \cdot (\boldsymbol{u} \otimes \boldsymbol{u}) + \boldsymbol{u}(\nabla \cdot \boldsymbol{u}) + \rho \nabla p / \rho_0^2 \\ S_p \equiv -\boldsymbol{u} \cdot \nabla p - \gamma p \nabla \cdot \boldsymbol{u} \end{cases} \tag{2.20}$$

The right hand side $\mathbb{S}$ of the LEWE given by equations (2.19) and (2.20) is a forcing term for the wave equation, but also accounts for non-linearities that may be encountered in the propagation of sound. Typically when an instability wave occurs, the velocity fluctuations $\boldsymbol{u}$ may become secular and contributions from $\mathbb{S}$ caps its growth. This continuous effect of $\mathbb{S}$ in the propagation is lost in a two-step acoustic analogy perspective. Therefore it should a posteriori be guaranteed, that the generated acoustic field does not heavily alter the initial distribution of $\mathbb{S}$. If the discrepancies between the initial and a posteriori evaluation of $\mathbb{S}$ are too significant, meaningful propagation effects are not acknowledged, and the linearised framework must be questioned.

Figure 2.1 presents the acoustic solution obtained by Bogey et al. (2002) within such a linearised framework. A direct Navier-Stokes (DNS) simulation of two corotating and merging vortices is investigated. The departure from the base flow of the computed unsteady simulation is used to inform the source term. The Linearised equations were found to reproduce very accurately the reference DNS solution.

(Galbrun, 1931; Biot and Tolstoy, 1957; Godin, 1997; Shnip, 1999) may also be found.

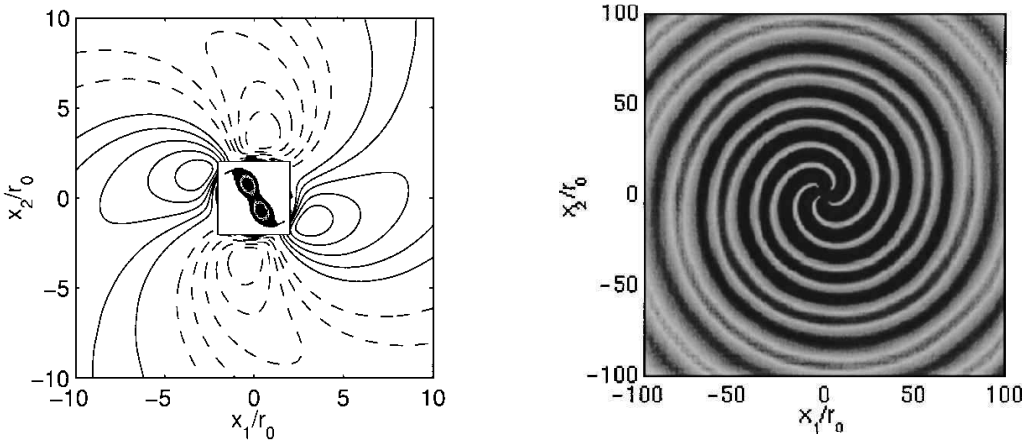

Figure 2.1: Snapshot of the near vorticity field and the fluid dilatation generated by two corotating vortices computed with the Navier-Stokes equations, where the rotation Mach number is $M_r \approx 1.1$ (left). The fluid dilatation is rebuilt with the linearised Euler's equations with the Reynolds stress tensor taken as the source of sound (right). The linearised solution proved to match the reference DNS solution perfectly in the study of Bogey et al. (2002).

2.3 Expansion about an incompressible flow (EIF)

The expansion about an incompressible flow (EIF) is an alternative methodology to model noise generation and propagation, and is briefly reviewed here. As a preliminary comment, notice that in previous approach the acoustic field is sought as a linear deviation from a base flow, and that therefore the equations describing the base flow dynamics are self-contained. No contribution stemming from the base flow forces the acoustic equations, and only second order perturbations may be defined as valid sound sources. A direct linearisation of the equations of fluid motion is consequently inappropriate to apprehend how the unsteadiness of large flow structures, as encountered in low Reynolds number flows, will generate sound.

The basic principle of the EIF was introduced by Ribner (1962), and consists in considering the flow essential sound producing part as solenoidal. In the literature, many authors[2] have contributed to model acoustic sources as departing from an incompressible base flow. Acoustics is correspondingly investigated as a perturbation computed from an expansion about an incompressible flow. To define the base flow relevant for an EIF analysis, an incompressible Navier-Stokes solver is used. Solely the momentum equation and the incompressibility condition are solved. The pressure field of the base flow p_0 is computed a posteriori with Poisson's equation, and is thus not solution of the fluid compressible equations (C.1). This mismatch of the base flow pressure p_0 with the compressible equations is used to provide source terms for the aeroacoustic perturbation equations. Seo and Moon (2006) gave perhaps the most completed version of acoustic perturbation equations obtained with such an EIF technique. Neglecting the effort induced by

[2]Notably (Powell, 1964; Yates, 1978; Klainerman and Majda, 1982; Hardin and Pope, 1994; Shen and Sørensen, 1999b,a; Slimon et al., 2000; Gabard et al., 2004a; Seo and Moon, 2006; Munz et al., 2007; Moon et al., 2010; Khalighi et al., 2010; Kaltenbacher et al., 2015).

viscosity and the heat conduction terms, the linearised perturbed compressible equations (LPCE) write,

$$\begin{cases} \mathrm{D}_{\boldsymbol{u}_0}(\rho) + \rho_0(\nabla \cdot \boldsymbol{u}) = 0 \\ \dfrac{\partial \boldsymbol{u}}{\partial t} + \nabla\left(\boldsymbol{u}_0 \cdot \boldsymbol{u}\right) + \dfrac{\nabla p}{\rho_0} = -(\nabla \times \boldsymbol{u}_0) \times \boldsymbol{u} - (\nabla \times \boldsymbol{u}) \times \boldsymbol{u}_0 - \dfrac{\rho}{\rho_0} D_{\boldsymbol{u}_0}(\boldsymbol{u}_0) \equiv \boldsymbol{S}_{\boldsymbol{u},LPCE} \\ \mathrm{D}_{\boldsymbol{u}_0}(p) + \gamma p_0(\nabla \cdot \boldsymbol{u}) + \boldsymbol{u} \cdot \nabla p_0 = -D_{\boldsymbol{u}_0}(p_0) \equiv S_{p,LPCE} \end{cases} \tag{2.21}$$

As for Euler's wave equation, this set of equations can be combined to derive a wave equation for the fluctuating velocity $\boldsymbol{u}$. For completeness this reformulation of LPCE is given here,

$$\begin{aligned} &\frac{\partial^2 \boldsymbol{u}}{\partial t^2} + \frac{\partial}{\partial t}\left[(\nabla \boldsymbol{u}) + (\nabla \boldsymbol{u})^T\right] \cdot \boldsymbol{u}_0 + 2(\nabla \boldsymbol{u}_0)^T \cdot \frac{\partial \boldsymbol{u}}{\partial t} + \nabla\left[\boldsymbol{u}_0 \cdot \nabla(\boldsymbol{u}_0 \cdot \boldsymbol{u})\right] - a_0^2 \nabla(\nabla \cdot \boldsymbol{u}) \\ &+\gamma \mathrm{D}_{\boldsymbol{u}_0}(\boldsymbol{u}_0)(\nabla \cdot \boldsymbol{u}) - \frac{\nabla(\boldsymbol{u} \cdot \nabla p_0)}{\rho_0} = \mathrm{D}_{\boldsymbol{u}_0}(\boldsymbol{S}_{\boldsymbol{u},LPCE}) + (\nabla \boldsymbol{u}_0)^T \cdot \boldsymbol{S}_{\boldsymbol{u},LPCE} - \frac{\nabla S_{p,LPCE}}{\rho_0} \end{aligned} \tag{2.22}$$

Sound source

Because the base flow is supposed incompressible for these perturbation equations, this method applies in the low Mach number limit, for which the principal sound source is $S_{p,LPCE}$ (Klainerman and Majda, 1982). In comparable configurations, this formulation presents a computational advantage over Lighthill's analogy, this is most easily seen if the low Mach number limit of equations (2.21) is considered, see (Seo and Moon, 2006, eq. (17)), and the analogy of Ribner (1962) retrieved,

$$\frac{\partial^2 p}{\partial t^2} - a^2 \Delta p = -\frac{\partial^2 p_0}{\partial t^2} \tag{2.23}$$

where (Ribner, 1962, eq. (2.5)) noticed, that the incompressible pressure p_0 obeys Poisson's equation,

$$\Delta p_0 = -\nabla \cdot \nabla \cdot (\rho_0 \boldsymbol{u} \otimes \boldsymbol{u}) \tag{2.24}$$

Thus in the low Mach number limit for an adiabatic flow, Ribner's analogy equation (2.23), describes the same sound generation mechanisms as in Lighthill's analogy, equation (1.2). Observe that the principal sound source for this analogy, consists in a double time derivative, that is numerically easier to process than the double divergence of Lighthill's tensor, even if the source domain is thereby stretched. This is illustrated by Prax et al. (2008), who moreover pointed out that Ribner's source definition filters out the source term of the vorticity mode. It is important to note, that the separation between the two coupled energetic modes is operable within the EIF framework because of the existence of discrepancies in the time scales. As a matter of fact, with the low Mach number assumption, the characteristic time of evolution of the flow is small, with respect to the acoustic one. For this reason, it is expected EIF fails to accurately describe the acoustics of high Mach number flows.

An illustration for an acoustic field solution of an EIF is provided in figure 2.2. The perturbed acoustic field computed with the LPCE for a elliptic spinning patch of vorticity is presented. A very satisfactory match of the acoustic solution and the corresponding analytical solution is found by Seo and Moon (2006).

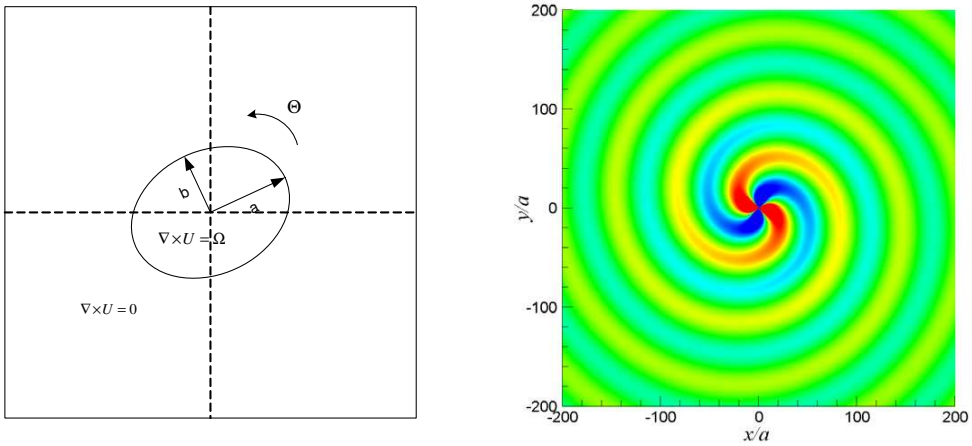

Figure 2.2: Sketch of the Kirchhoff vortex (rigid body rotation of a vortex patch) considered by Seo and Moon (2006) for which an analytical solution for the acoustic field exist (left). Instantaneous pressure field computed with the linearised perturbed compressible equations (right). The Mach number based on the rotating speed considered, is $M_\theta = 0.1$. A perfect match with the reference solution was obtained by these authors.

2.4 Choice of the aeroacoustic model

In spite of the efforts of Goldstein (2003) and others, there is still no satisfactory unified theory encompassing acoustic analogies obtained by linearisation and with an EIF. Second order perturbations may be included within an EIF, yet thereby a risk exists of double-counting sound sources. The major differences between acoustic analogies based on linearisation and those defined as an expansion about an incompressible flow are summarised:

- While in the first formulation, acoustics is inherently linear, non-linear acoustic propagation can be addressed with the second approach. With a linear propagation operator, unbounded exponentially growing solutions may arise and corrupt the acoustic solution.
- In the second strategy sound sources are defined from the base flow unsteadiness, and this method is adapted to track sound stemming from large flow structures as well as noise from fluid-structure interactions. Within the first methodology on the contrary, sound is produced by the non-linear interactions of fluctuating quantities only, and this techniques is appropriate to account for turbulent mixing noise, but inoperable to describe the sound generated by large flow structures.
- Expansion about an incompressible flow is valid over all possible Reynolds number, yet its relevance is questionable for high Mach flow, for which the computation costs become comparable to direct aeroacoustic numerical simulations. This remark on computational expense applies also for acoustic analogies based on linearisation. However for the latter statistical description of the noise sources may be used together with affordable steady flow computations and are readily used to achieve high Mach number supersonic jet noise predictions (Morris, 2012).
- EIF presumes a low Mach number flow for which the incompressible Navier-Stokes satisfactorily describes the non-acoustic contribution of the fluid. At moderate/high Mach number, the time scale separation on which the method relies vanishes, and the EIF foundations crumbles. For its part, linearisation is based on an amplitude separation in which the fluctuations are deemed small

with respect to typical base flow magnitudes. This theory collapses when overwhelming instability waves or resonance phenomena occur.

The present study is concerned with the noise modelling of jets with both, high Mach number, and high Reynolds number. As discussed in §1 of part II of this work, turbulent mixing noise plays a foreground role in such configurations and for the reasons detailed above, acoustic analogies based on linearisation are found more suitable. With regard to the complexity of the flow dynamics encountered in high speed jets, detailed unsteady simulations of the flow are unaffordable, and the sound sources must be modelled semi-empirically. To guarantee the robustness of the method, the exponentially growing solutions of the linear propagation problem must be withdrawn. Different strategies to achieve stable sound propagation are reviewed in chapter 3, and some original stable operators are also presented. In the aeroacoustic model proposed, stability is ensured with an acoustic preserving formulation. The conservation of acoustic energy is achieved thanks to an acoustic potential description.

2.5 Acoustic analogies for the acoustic potential

The paramount concepts in fluid mechanics of velocity potentials and stream functions have been introduced by Lagrange (Anderson Jr., 1997, chap. 3), and the tools to model acoustic potential sound propagation are very ancient. Already in (1781) as a member of Berlin's academy of sciences, did this franco-sardinian citizen derive a linearised wave equation for the acoustic potential. This equation was derived later anew by Helmholtz (1860). Their wave equation for the acoustic potential is acoustic preserving (Campos, 1988; Möhring, 1999), meaning that their relations solely describe acoustics, and conserve the energy. The acoustic potential framework guarantees a robust, yet arbitrary[3], decoupling of acoustic fluctuations from the incompressible flow dynamics (Helmholtz, 1858; Schoder et al., 2020). Such formulations based on the acoustic potential are common to address sound propagation (Blokhintzev, 1946; Crighton and Leppington, 1970; Pierce, 1990; Eversman, 2001; Möhring, 2001), because they deliver physically consistent simplifications to a given problem. But, even though some models for the source terms have been proposed (Marsh Jr., 1950; Yates, 1978; Goldstein, 1978; Ewert and Schröder, 2003; Perez Bergliaffa et al., 2004), the use of the potential acoustic has remained limited in aeroacoustics (Kaltenbacher et al., 2013). It is only recently[4], that Kaltenbacher et al. (2015) proposed a model suitable for computational aeroacoustics based on an EIF formulation. Note that this model is in close similitude with the contribution of Yates (1978). Encouraging results have been obtained with this methodology (Tautz et al., 2018), nevertheless its use is restricted to low Mach number flows, due to the inherent limitations of the EIF method. In this section, an acoustic analogy for the acoustic potential is presented. To be adapted to the investigation of the noise of high speed jets, it is obtained from the linearisation of the governing equations rather than from an EIF. To simplify the derivations, the base flow is supposed steady and parallel, and the corresponding simplification of LEWE, equation (2.18), is used as a starting point.

[3]Notice that another decoupling of acoustics from the flow dynamics is achieved in considering the Bernoulli constant B as the appropriate dependent variable for acoustics. The Bernoulli constant B, corresponding also to the stagnation enthalpy, is closely related with an acoustic potential formulation. In region without sound sources, Crocco's equation (Möhring, 1999, eq. (2)) delivers $\partial \boldsymbol{u}\ \partial t = -\nabla B$ and the velocity $\boldsymbol{u}$ is curl-free. This wave equation found more application in aeroacoustics than original potential acoustic formulations $\boldsymbol{u} = \nabla\psi$, because sound sources were proposed for the latter and acoustic analogies available (Howe, 1975a; Möhring, 1979).

[4]Surprisingly enough, whoever reviews Helmholtz's and Lagrange's contributions remarks, that these authors mentioned source terms for their equations. Giving a volume force ∇Q acting on the fluid and deriving from a potential Q, Helmholtz (1860, eq. (2)) wrote $\partial^2\psi/\partial t^2 - a^2\Delta\psi = \partial Q/\partial t$, while Lagrange (1781, §23) derived $\partial^2\psi/\partial t^2 - k\Delta\psi = \boldsymbol{u}\cdot\nabla Q$. The sum of these two sound sources with $Q = -p_0$ delivers a term that closely resembles to the one computed within an EIF framework.

2.5.1 Definition of the acoustic potential

Before detailing the analogy proposed, a preliminary remark will motivate the choice for this work of an unusual definition for the acoustic potential. Recall first, that prior to his wave equation[5], Helmholtz (1858) proposed an ingenious decomposition for the fluid velocity $\boldsymbol{u}$ into a potential part ψ and a solenoidal part $\boldsymbol{A}$,

$$\boldsymbol{u} = \nabla\psi + \nabla \times \boldsymbol{A} \tag{2.25}$$

It is well established that in presence of mean flow vorticity ($\nabla \times \boldsymbol{u}_0$), velocity fluctuations $\boldsymbol{u}$ do not remain potential (Yates, 1978; Pierce, 1990). Nevertheless, according to this definition of the acoustic potential and for an isobar mean flow at rest, spatial variations of the speed of sound a_0 are also giving rise to solenoidal fluctuations ($\nabla \times \boldsymbol{u}$). This is seen for an initial vorticity-free distribution of fluctuating velocity $\boldsymbol{u}$, by taking the curl of the wave equation,

$$\frac{\partial^2 \boldsymbol{u}}{\partial t^2} - a_0^2 \nabla(\nabla \cdot \boldsymbol{u}) = \boldsymbol{0} \tag{2.26}$$

which delivers,

$$\frac{\partial^2 (\nabla \times \nabla \times \boldsymbol{A})}{\partial t^2} = (\nabla a_0^2) \times \nabla(\Delta\psi) \neq \boldsymbol{0} \tag{2.27}$$

Consequently, fluctuations of the acoustic potential $\boldsymbol{u} = \nabla\psi$ propagating in an isobar media at rest are not guaranteed to remain potential. Pierce (1990) has shown that different definition for the acoustic potential are legitimate, and in what follows a Helmholtz decomposition based on the fluctuating momentum $\rho_0\boldsymbol{u}$ is chosen, such that,

$$\rho_0\boldsymbol{u} = \nabla\phi + \nabla \times \boldsymbol{B} \tag{2.28}$$

By multiplying equation (2.26) by ρ_0, and taking its curl for an isobar medium, then for an initial vorticity-free distribution of momentum fluctuations $\rho_0\boldsymbol{u}$,

$$\frac{\partial^2 (\nabla \times \nabla \times \boldsymbol{B})}{\partial t^2} = \nabla \times \nabla \left(\nabla \cdot \left(a_0^2 \nabla\phi \right) \right) = \boldsymbol{0} \tag{2.29}$$

Thus it is ensured that potential fluctuations $\rho_0\boldsymbol{u} = \nabla\phi$ remain potential for an isobar medium at rest. For a uniform mean density ρ_0, both definitions overlap, and they are expected to describe equivalently the effect of flow shearing on acoustic propagation. The constraint that the mean flow be isobar is not very stringent for jet flows, and in order to adequately model acoustic refraction caused by speed of sound a_0 heterogeneities the acoustic potential definition of equation (2.28), is preferred over the historical one.

2.5.2 Wave equations for the acoustic potential

From this Helmholtz decomposition of the fluctuating momentum $\rho_0\boldsymbol{u}$, a wave equation is sought for the acoustic potential ϕ alone. Possible couplings with the vorticity mode are discarded, and it is assumed that the momentum fluctuations are purely acoustical, i.e. $\rho_0\boldsymbol{u} = \nabla\phi$. Within this scope, it is possible to reformulate the linearised Euler's wave equation for the acoustic potential, taken as the dependent variable for acoustics. This is demonstrated in appendix §C.2 for a base flow that is steady and parallel.

[5] And prior to the alternative decomposition of Clebsch (1859), which uniqueness is not ensured (Lamb, 1879, §167).

The so obtained wave equation is referred to as LEWE-AP, and writes,

$$\begin{aligned}&\nabla\left[D^2_{\boldsymbol{u}_0}(\phi)-\nabla\cdot\left(a_0^2\nabla\phi\right)\right]+(\nabla\times\boldsymbol{u}_0)\times\left[\nabla\left(D_{\boldsymbol{u}_0}(\phi)\right)-\left[(\nabla\boldsymbol{u}_0)+(\nabla\boldsymbol{u}_0)^T\right]\cdot\nabla\phi\right]\\&=\mathrm{D}_{\boldsymbol{u}_0}(\rho_0\boldsymbol{S_u})+(\nabla\boldsymbol{u}_0)^T\cdot(\rho_0\boldsymbol{S_u})-\nabla S_p\end{aligned}\tag{2.30}$$

Considering the second order interaction terms from the LEE, equations (2.20), sound sources for LEWE-AP may be defined, and thereby an acoustic analogy for the acoustic potential. This acoustic analogy is obtained by linearisation, therefore it is by nature different from the EIF formulation proposed by Kaltenbacher et al. (2015), and its validity extends over the Mach numbers. It is seen from LEWE-AP that the wave equation of Pierce (1990, eq. (27)), does not consist in a high frequency approximation of acoustics, but it accurately describes acoustic propagation for isobar potential flows. What is more, if the momentum sound source $\rho_0\boldsymbol{S_u}$ can satisfactorily be represented by its potential part S_m, such that $\rho_0\boldsymbol{S_u}\approx\nabla S_m$, then whenever the effect of the mean flow vorticity $(\nabla\times\boldsymbol{u}_0)$ on the acoustic propagation can be neglected a handy acoustic analogy can be built from Pierce's equation,

$$D^2_{\boldsymbol{u}_0}(\phi)-\nabla\cdot\left(a_0^2\nabla\phi\right)=D_{\boldsymbol{u}_0}(S_m)-S_p\tag{2.31}$$

where from equations (2.20), the sound source of Pierce's equation is derived as,

$$\begin{cases}\Delta S_m=\nabla\cdot(\rho_0\boldsymbol{S_u})=-\nabla\cdot\nabla\cdot(\rho_0\boldsymbol{u}\otimes\boldsymbol{u})+\nabla\cdot\left(\boldsymbol{u}\nabla\cdot(\rho_0\boldsymbol{u})\right)+\nabla\cdot\left(\rho\nabla p/\rho_0\right)\\S_p=-\boldsymbol{u}\cdot\nabla p-\gamma p\nabla\cdot\boldsymbol{u}\end{cases}\tag{2.32}$$

Whenever the Reynolds stress tensor is the principal source of sound, S_m is solution of Poisson's equation,

$$\Delta S_m=-\nabla\cdot\nabla\cdot(\rho_0\boldsymbol{u}\otimes\boldsymbol{u})\tag{2.33}$$

which is very reminiscent of the sound source defined in Ribner's theory of dilatation, equation (2.24). Thus, in the low Mach number limit, $S_m=-p_0$ and the analogy of Kaltenbacher et al. (2015, eq. (11)) is retrieved exactly. At high Mach number, $\Delta p_0\neq\nabla\cdot\nabla\cdot(\rho_0\boldsymbol{u}\otimes\boldsymbol{u})$ and equation (2.33), needs to be solved explicitly. An analogous filtering of the momentum source has been proposed for the acoustic perturbation equations (Ewert and Schröder, 2003), and some commercial software like *Actran* (Free Field Technologies, 2018b, §33.5.4) are able to perform this processing on turbulent flows. This split is to be viewed in parallel with the discussion on the energetic modes of a fluid presented in §1.2, where it is illustrated that the potential part of the momentum sound source rather corresponds to an acoustic source, while its incompressible part is responsible for the vorticity mode. With a second order wave equation, as in equation (2.31), only acoustic fluctuations can be computed, and as a matter of consistency and well-possessedness, a sound source filtering should be considered for this wave equation. Note that this remark applies for any acoustic operator that aims at computing solely the acoustic mode. All mode conversion mechanisms being discarded, neither instability waves nor noise generated by the inhomogeneous convection of turbulent structures can be modelled with Pierce's acoustic analogy. This must be seen as a necessary tribute to pay to build an acoustic preserving wave equation. From equation (2.30), it appears that this source filtering is not necessary for LEWE-AP. It is argued, in the following, that this acoustic analogy is ill-posed, and that Pierce's wave equation must be preferred over LEWE-AP.

Leaving aside the issue of the source filtering, equations (2.30) and (2.31) correspond to two modelling limits for which the mean flow vorticity is fully accounted for in the wave operator or entirely discarded. It is clear that, for a potential mean flow, Pierce's equation and LEWE-AP equivalently and exactly describe the sound propagation. Apart from this specific case, an inconsistency appears when potential perturbations $\rho_0 \boldsymbol{u} = \nabla\phi$ are considered superimposed on a vortical mean flow. Two strategies may be conceived: 1/ Take into account the mean flow vorticity and endorse the ill-possessedness encountered when forcing the momentum fluctuations to remain potential, or, 2/ Neglect the effect of the mean flow vorticity on sound propagation, and mistakenly consider a wave equation valid for a potential mean flow in the applications. Motivation to prefer the second approach are mentioned:

- **If the vorticity mode is discarded, coupling mechanisms should be discarded accordingly**. When considering LEWE-AP mode conversion from acoustics to vorticity is discarded. However the coupling terms are still present in the wave equation and are erroneously lined up with propagation terms. When assuming the mean flow is parallel and the momentum fluctuations are purely potential $\rho_0 \boldsymbol{u} = \nabla\phi$, Euler's momentum equation, equation (2.12), can be recast in,

$$\nabla(\mathrm{D}_{\boldsymbol{u}_0}(\phi) + p) = \rho_0 \boldsymbol{S}_{\boldsymbol{u}} - (\nabla \times \boldsymbol{u}_0) \times \nabla\phi \tag{2.34}$$

  where the term $(\nabla \times \boldsymbol{u}_0) \times \nabla\phi$ describes the coupling mechanisms from acoustics to the vorticity. This has been thoroughly been addressed by Yates (1978, §II.C) and is supported by the contribution of Perez Bergliaffa et al. (2004, eq. (41) & (42)). In these contributions this term is stowed as a source of vorticity, and as such, it should be discarded from a purely acoustic equation. For not being removed, this contribution undoubtedly alters the ability of LEWE-AP to correctly describe sound propagation.

- **Most of potential acoustic operators of the literature do not consider the effect of the mean flow vorticity in the propagation**. The LPCE, presented equations (2.21), the acoustic perturbation equations (Ewert and Schröder, 2003), but also the wave equations built for the fluctuating enthalpy (Howe, 1975a; Möhring, 1999), can be considered as genuine potential acoustic operators. In absence of sources, it is straightforward to show that these equations lead to curl-free velocity fluctuations $\boldsymbol{u}$. From the homogeneous momentum equations of LPCE, equations (2.21), it comes,

$$\rho_0^2 \frac{\partial \nabla \times \boldsymbol{u}}{\partial t} = \nabla\rho_0 \times \nabla p \approx \boldsymbol{0} \qquad \text{, and} \qquad \boldsymbol{u} = \nabla\psi \tag{2.35}$$

  In the LPCE, terms expressing the mean flow vorticity are moved from the linear operator to the source $\boldsymbol{S}_{\boldsymbol{u},LPCE}$ as given in equations (2.21). This can be observed for the other acoustic models as well (Ewert and Schröder, 2003, eq. (76) & (78)), (Howe, 1975a, eq. (4.14)) and (Möhring, 1999, eq. (6) & (7)). For a constant density ρ_0 and a parallel mean flow, the homogeneous LPCE equations (2.21), may be recast in the convected wave equation,

$$\mathrm{D}^2_{\boldsymbol{u}_0}(\psi) - a_0^2 \Delta\psi = 0 \tag{2.36}$$

  Such that, the LPCE, and these linear operators do only consider the potential flow contribution of the actual flow in the acoustic propagation.

- **Attempts to consider the mean flow vorticity in acoustic potential propagation led to awkward acoustic predictions**. Efforts to include the effect of the flow vorticity in acous-

tic potential wave equations are seldom. Notable contributions have been made in this scope by Legendre et al. (2018), who compared different formulations that include the effect of the flow mean vorticity in the propagation (Legendre, 2014). When compared on a sheared flow configuration, encouraging results have been obtained for acoustic wavelengths λ that are small with respect to the flow characteristic length scale L. In the low frequency limit of acoustics, when λ/L is large, the wave equations that account for the flow vorticity diverged from the reference solution. Some computations are performed for LEWE-AP with the in-house code PROPA and presented in §3.3. Unreasonable acoustic field have been obtained, that are found much less accurate to represent the acoustic field than Pierce's equation. On parallel flow configurations, the implementation of LEWE-AP in PROPA has been validated with an alternative implementation of the LEE for which $\rho_0 \boldsymbol{u} = \nabla\phi$, that delivered identical inconsistent solutions.

- **Sound generation is at leading order a potential flow phenomenon**. This can qualitatively be understood from following reasoning. From Kelvin's minimum energy theorem, potential motions correspond to the flow realisation that satisfies given boundary conditions with a minimal energy expense. Yet, whenever a fluid motion cannot be contra-balanced by a reciprocal incompressible fluid movement, compressibility waves are generated to match the prescribed incompressible flow boundary conditions. This outing of Stokes' incompressible regime is accomplished with the creation of acoustic potential fluctuations that provide, for a minimum energy cost, a suitable solution that respects the imposed boundary conditions. Key idea for this interpretation is given in Lighthill's (1952) justification of the acoustic analogy, where he suggested that the sound sources correspond to '*the minute fraction in momentum flux which is not balanced by a local reciprocating motion*'. To this authors' interpretation of Lighthill's thoughts, if the momentum fluxes are caused by the kinetic motion of turbulent flows, sound generation however consists essentially in a potential flow mechanism. Mentioning the work of Stokes, Lighthill (1952, §2) provides a synthesis for the energy conversion at play: '*In brief the physical explanation is that any forcing motion on a scale comparable with the wave-length is balanced partly by a local reciprocal motion, or standing wave, and partly by compressions and rarefactions of the air whose effects is propagated outwards. The larger the wave-length in comparison with the scale of the forcing motion, the more completely can the motion be fully reciprocated by the local standing wave.*' What is more, with the multipolar expansion of the sound sources, vortices appear to emit sound as vibrating spheres that can accurately be described from an acoustic potential perspective (Ehrenfried, 2004, §5).

- **Sound propagation solely depends on the local mean flow characteristics $\boldsymbol{u}_0 \pm a_0$**. If acoustic propagation is described solely with a potential flow wave equation, it seems that some propagation effects are omitted. A more accurate acoustic preserving linear operator, that fully accounts for the mean flow gradients, may be sought. This is not necessarily correct. From the comparison of Pierce's operator, equation (2.31), with d'Alembert's equation a similar structure is found. Yet, in reformulating the one-dimensional convected d'Alembert operator as,

$$\left(\frac{\partial}{\partial t} + u_0\frac{\partial}{\partial x}\right)^2 - a_0^2\frac{\partial^2}{\partial x^2} = \left(\frac{\partial}{\partial t} + (u_0 + a_0)\frac{\partial}{\partial x}\right)\left(\frac{\partial}{\partial t} + (u_0 - a_0)\frac{\partial}{\partial x}\right) \tag{2.37}$$

it is seen, that this operator transports the variable of state along the x-axis at the characteristic speeds $u_0 + a_0$ and $u_0 - a_0$. Remark that the decomposition presented in equation (2.37), is valid for arbitrary u_0 irrespectively of the spatial variations $\partial u_0/\partial x$. Section § 2.7 illustrates how Pierce's

equation may be split in similar characteristic equations. Hence, while Pierce's equation is exact for a potential mean flow, it accounts in the sound propagation for all variations of the mean flow, whether they are potential or not. Since Riemann's (1860) work on characteristics, it is known that the characteristic writing of a problem are not, in any way, asymptotic simplifications (Lappas et al., 1999). This method may address coupled non-linear problems as-well. It is argued that the simplifications made in proposing Pierce's equation as a generally valid wave operator, are consequences of considering a linear propagation that is acoustic preserving. Section § 2.7 illustrates in particular that this does not correspond to a high frequency limit of acoustics.

2.6 Acoustic energy conserved by Pierce's equation

The analysis that led to propose Pierce's wave equation assumed the base flow be steady and parallel. This is because a more general expression for LEWE-AP could not be proposed. In the derivations of Blokhintzev (1946, §II) however, the base flow is supposed steady, homentropic and potential. Appendix §C.3 recalls his derivation using modern notations, and proposes a compressible generalisation of Pierce's wave equation. Let Pierce's wave equation be tagged with $\mathcal{L}_0(\phi)$, then it expresses as,

$$\mathcal{L}_0(\phi) = \mathrm{D}^2_{\boldsymbol{u}_0}(\phi) - \nabla\cdot(a_0^2\nabla\phi) + (\nabla\cdot\boldsymbol{u}_0)\mathrm{D}_{\boldsymbol{u}_0}(\phi) \tag{2.38}$$

and if the generic forcing term q is introduced,

$$\mathcal{L}_0(\phi) = q \tag{2.39}$$

This compressible flow wave equation for the acoustic potential serves as a starting point for the derivations hereafter.

2.6.1 Conservation of the acoustic energy

In this paragraph, relying on the work of Möhring (1999, §2.4), the acoustic energy conserved by Pierce's equation is computed. This author frequently insisted on the asset of using self-adjoint formulations (Möhring, 1979; Möhring et al., 1983; Möhring, 1999, 2001) such as Pierce's wave equation. A reason for this, is that from their self-adjointness property, a variational principle

$$\delta\mathbb{L} = 0 \tag{2.40}$$

exist, from which the equation can be derived. As a corollary, the acoustic energy conservation in the acoustic propagation is ensured. A possible Lagrangian $\mathbb{L}$ associated with equation (2.39) is,

$$\mathbb{L} = \frac{1}{2} < \phi, \mathcal{L}_0(\phi) > - < \phi, q > \tag{2.41}$$

since,

$$\delta\mathbb{L} = \frac{1}{2} < \delta\phi, \mathcal{L}_0(\phi) > + \frac{1}{2} < \phi, \mathcal{L}_0(\delta\phi) > - < \delta\phi, q > = < \delta\phi, \mathcal{L}_0(\phi) - q > \tag{2.42}$$

Integrating by parts equation (2.41) and discarding the boundary terms, one simply obtains,

$$\mathbb{L} = \int\int \Lambda \,\mathrm{d}t\,\mathrm{d}\boldsymbol{x} \quad \text{with} \quad \Lambda = \frac{1}{2}\left[-\left(\mathrm{D}_{\boldsymbol{u}_0}(\phi)\right)^2 + a_0^2(\nabla\phi)^2\right] - q\phi \tag{2.43}$$

where Λ corresponds to the Lagrangian density. If Euler-Lagrange's equation was used,

$$\frac{\partial \Lambda}{\partial \phi} = \nabla \cdot \left(\frac{\partial \Lambda}{\partial (\nabla \phi)} \right) + \frac{\partial}{\partial t} \left(\frac{\partial \Lambda}{\partial (\partial \phi / \partial t)} \right) \tag{2.44}$$

then equation (2.39) would have been retrieved (recall that in Euler-Lagrange's equation, variations of ϕ, $\partial\phi/\partial t$ and $\nabla\phi$ are deemed unrelated). Thus, to compute the acoustic energy associated with Pierce's wave equation, another conservation formula must be considered. Introducing the Hamiltonian $\mathcal{H}$ from a Legendre transformation of the Lagrangian Λ,

$$\mathcal{H} = \frac{\partial \phi}{\partial t} \frac{\partial \Lambda}{\partial (\partial \phi / \partial t)} - \Lambda \tag{2.45}$$

the acoustic energy conservation formula is deduced from the relation,

$$\frac{\partial \mathcal{H}}{\partial t} + \nabla \cdot \mathbf{\Pi} = 0 \tag{2.46}$$

where,

$$\mathbf{\Pi} = \frac{\partial \Lambda}{\partial (\nabla \phi)} \frac{\partial \phi}{\partial t} \tag{2.47}$$

is the energy flux associated to the energy density formed by the Hamiltonian $\mathcal{H}$. From equation (2.43), these quantity can be evaluated for Pierce's equation by noting that,

$$\frac{\partial \Lambda}{\partial (\partial \phi / \partial t)} = -\mathrm{D}_{\boldsymbol{u}_0}(\phi) \quad \text{and} \quad \frac{\partial \Lambda}{\partial (\nabla \phi)} = a_0^2 \nabla \phi - \mathrm{D}_{\boldsymbol{u}_0}(\phi) \boldsymbol{u}_0 \tag{2.48}$$

Then if the acoustic fluctuations are accurately described with an acoustic potential, i.e. $p = -\mathrm{D}_{\boldsymbol{u}_0}(\phi)$ and $\rho_0 \boldsymbol{u} = \nabla \phi$, then the acoustic energy density $\mathcal{H}$ and fluxes express as,

$$\begin{aligned} \mathcal{H} &= -\frac{p^2}{2} - \rho_0 (\boldsymbol{u}_0 \cdot \boldsymbol{u}) p - \gamma p_0 \rho_0 \frac{\boldsymbol{u} \cdot \boldsymbol{u}}{2} + q\phi \\ \mathbf{\Pi} &= -(p + \rho_0 \boldsymbol{u}_0 \cdot \boldsymbol{u})(\gamma p_0 \boldsymbol{u} + \boldsymbol{u}_0 p) \end{aligned} \tag{2.49}$$

Apart from the production term $\partial(q\phi)/\partial t$ that is here not particularised, equations (2.46) and (2.49) correspond to the generalised acoustic energy equation of Morfey (1971, eq. (22-24)). Note that similar conservation equations for the acoustic energy have merely been derived in the literature considering the Lagrangian (Whitham, 1965; Bretherton and Garrett, 1968; Hayes, 1970a; Campos, 1988).

2.6.2 Conservation of the acoustic intensity

The Hamiltonian conservation formula, given in equation (2.46), is deduced from the divergence free property of the four dimensional stress energy tensor $\boldsymbol{T}$ (alias energy momentum tensor) (Landau and Lifshitz, 1951, §32),

$$\dot{\nabla} \cdot \boldsymbol{T} = \mathbf{0} \tag{2.50}$$

where $\dot{\nabla} = (\partial/\partial t\ ,\ \nabla)^T$ corresponds to the four-vector differentiation and the stress-energy tensor expresses as,

$$\boldsymbol{T} = \dot{\nabla}\phi \otimes \frac{\partial \Lambda}{\partial(\dot{\nabla}\phi)} - \boldsymbol{I}\,\Lambda = \begin{pmatrix} \dfrac{\partial \phi}{\partial t}\dfrac{\partial \Lambda}{\partial(\partial\phi/\partial t)} - \Lambda & \dfrac{\partial \phi}{\partial t}\dfrac{\partial \Lambda}{\partial(\nabla\phi)} \\ \nabla\phi\,\dfrac{\partial \Lambda}{\partial(\partial\phi/\partial t)} & \nabla\phi \otimes \dfrac{\partial \Lambda}{\partial \nabla\phi} - \boldsymbol{I}\,\Lambda \end{pmatrix} \tag{2.51}$$

where $\boldsymbol{I}$ is the identity matrix (which dimension adapts to the context). In fact, the acoustic energy equation of Morfey (1971), that is equivalent to equation (2.46), only corresponds to the first relation that can be deduced from equation (2.50)[6], and an additional conservation relation for the acoustic field may be derived,

$$\frac{\partial}{\partial t}\left(\nabla\phi\,\frac{\partial \Lambda}{\partial(\partial\phi/\partial t)}\right) + \nabla\cdot\left(\nabla\phi \otimes \frac{\partial \Lambda}{\partial \nabla\phi} - \boldsymbol{I}\,\Lambda\right) = \boldsymbol{0} \tag{2.52}$$

where for Pierce's wave equation, and in the acoustic potential framework,

$$\begin{aligned} \nabla\phi\,\frac{\partial \Lambda}{\partial(\partial\phi/\partial t)} &= -\mathrm{D}_{\boldsymbol{u}_0}(\phi)\nabla\phi \\ &= \rho_0 p \boldsymbol{u} \end{aligned} \tag{2.53}$$

and,

$$\begin{aligned} \nabla\phi \otimes \frac{\partial \Lambda}{\partial \nabla\phi} - \boldsymbol{I}\,\Lambda &= -\nabla\phi \otimes \left[\mathrm{D}_{\boldsymbol{u}_0}(\phi)\boldsymbol{u}_0 + a_0^2\nabla\phi\right] - \left(\frac{1}{2}\left[-\left(\mathrm{D}_{\boldsymbol{u}_0}(\phi)\right)^2 + a_0^2(\nabla\phi)^2\right] - q\phi\right)\boldsymbol{I} \\ &= \rho_0\boldsymbol{u} \otimes \left[p\boldsymbol{u}_0 - \gamma p_0 \boldsymbol{u}\right] + \left(\frac{p^2}{2} - \gamma p_0 \rho_0 \frac{\boldsymbol{u}\cdot\boldsymbol{u}}{2} + q\phi\right)\boldsymbol{I} \end{aligned} \tag{2.54}$$

which delivers, after simplification by ρ_0, a conservation law for the acoustic intensity,

$$\mathrm{D}_{\boldsymbol{u}_0}(p\boldsymbol{u}) + \nabla\cdot(a_0^2\rho_0\boldsymbol{u})\boldsymbol{u} - \nabla(a_0^2)\rho_0\frac{\boldsymbol{u}\cdot\boldsymbol{u}}{2} + \frac{\nabla(p^2)}{2\rho_0} + \frac{\nabla(q\phi)}{\rho_0} = \boldsymbol{0} \tag{2.55}$$

Conservation law for the acoustic intensity are less common than acoustic energy conservation laws, and a correspondence for this equation was not found by this author in the literature. This conservation equation may find some application in sound source identification (Fernandez-Grande et al., 2012; Fernandez-Grande and Jacobsen, 2014), all the more than acoustic intensity is measurable in experiments.

2.7 Exact ray theoretical formulation of Pierce's equation

If acoustics has a wavy nature, its propagation can be modelled by ray tracing similarly as in optics. This is illustrated in figure 2.4. While the solving of the wave equations in an eulerian paradigm requires a mesh, ray acoustics is lagrangian by essence, and one understands why this method is also referred to as geometrical acoustics. It is well acknowledged that in the high frequency limit of acoustics, any wave equation simplifies to the geometrical acoustics formulation (Candel, 1972; Goldstein, 1982; Pierce, 1990; Wundrow and Khavaran, 2004). This section puts forward the existence of a one-to-one equivalence between Pierce's wave equation and the ray acoustics framework. Motivation for this analysis is to gain insight in the energy conservation of Pierce's equation (Hayes, 1970a,b; Candel, 1975). Blokhintzev

[6]Using vector calculus, equation (2.50) may be redraft into, $\dot{\nabla}\cdot\boldsymbol{T} = \dot{\nabla}\cdot\left(\dfrac{\partial\Lambda}{\partial(\dot{\nabla}\phi)}\right)\dot{\nabla}\phi + \dot{\nabla}\dot{\nabla}\phi\cdot\left(\dfrac{\partial\Lambda}{\partial(\dot{\nabla}\phi)}\right) - \dot{\nabla}\Lambda = \boldsymbol{0}$.

(1946, §III) first introduced geometrical acoustics, by drawing on the preexisting optical theory. In his dissertation, Gainville (2008, §2.3.1) distinguishes three ways to settle the ray acoustics formulation: 1/ a geometric approach based on the notion of wavefront (Pierce, 1981), 2/ a method based on the characteristics method (Candel, 1977), and 3/ a method based on Hamiltonian formalism (Bertschinger, 1999). The first two methods use a serial development to arrive at the ray equations, and thus only the method based on analytical mechanics may lead to the equivalence between the two methods.

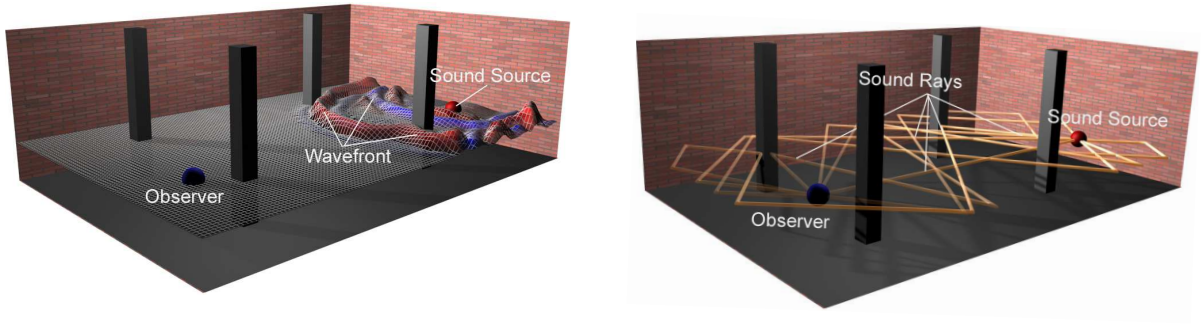

Figure 2.3: Illustration of the wave-based eulerian approach (left), and the ray-based lagrangian approach (right). Both methods find application in real time auralisation for video games (Röber et al., 2007).

Some strong connections between geometrical acoustics and acoustic potential wave equations have already been obtained. This has been achieved by relying on an analogy between sound waves and gravity waves. In relativistic mechanics, the concept that a light beam propagates in a straight line in a curved space-time is common; similarly in acoustics, sound rays are deemed to propagate straightly in a space curved by the presence of heterogeneities in the speed of sound a_0 and in the mean flow $\boldsymbol{u}_0$ (Unruh, 1981; Stone, 2000; Perez Bergliaffa et al., 2004; Barcelo et al., 2011). These authors have exhibited the metrics associated with potential acoustics to describe this curvature, and proposed a derivation for ray theory. However, these demonstrations have two shortcomings; 1/ they lead to a dimensionally inconsistent result from depending on the mean density of the fluid ρ_0 (Barcelo et al., 2011, §2.6), (Stone, 2000, §III), and 2/, the Hamiltonian proposed has inhomogeneous units (Stone, 2000, eq. (A10)). While the expression of the Hamiltonian does not comply with the expression proposed here, the equations in the course of Rienstra and Hirschberg (2004) are homogeneous. These authors end up with the ray tracing equation at the price of simplifying hypotheses. Because Pierce's wave equation is taken as a starting point, these two mentioned locks can be lifted. And it seems presently possible to show the equivalence between acoustic rays and acoustic potential waves. This section is organised as follows. The metric associated with the equation of potential acoustics is first calculated, from the latter and without any further approximation, the Hamiltonian is determined, the equation of acoustic rays are then presented. A parallel with exact rays of Foreman (1989) is finally given.

2.7.1 Metric corresponding to Pierce's wave equation

The metric is computed following Barcelo et al. (2011, §2.3). To this purpose, recast Pierce's equation (2.38) into the matrix expression,

$$\left(\begin{array}{cc} \dfrac{\partial}{\partial t} & \nabla\cdot \end{array} \right) \cdot \left\{ \left(\begin{array}{cc} 1 & \boldsymbol{u}_0{}^T \\ \boldsymbol{u}_0 & \boldsymbol{u}_0 \otimes \boldsymbol{u}_0 - a_0^2 \boldsymbol{I} \end{array} \right) \cdot \left(\begin{array}{c} \dfrac{\partial \phi}{\partial t} \\ \nabla \phi \end{array} \right) \right\} = 0 \tag{2.56}$$

Let $f^{\mu\nu}$ be the $d+1$ order tensor appearing in previous equation, where $d = 1, 2$ or 3 corresponds to the dimension of the physical configuration dealt, and where the Greek variables μ, ν refer to space-time coordinates and range from 0 to d, with $0 \equiv t$. If mute variables are implicitly summed, then Pierce's compressible equation (2.38) can be recast in the concise writing,

$$\partial_\mu(f^{\mu\nu}\,\partial_\nu\phi) = 0 \tag{2.57}$$

In a curved space-time, the inverse metric $g^{\mu\nu}$ of d'Alembert's equation is given by,

$$\frac{1}{\sqrt{-g}}\partial_\mu(\sqrt{-g}\;g^{\mu\nu}\partial_\nu\phi) = 0 \tag{2.58}$$

where $g \equiv det(g_{\mu\nu})$ and $g_{\mu\nu} = (g^{\mu\nu})^{-1}$ is the metric in related to the problem. A direct identification of the terms, leads to $f^{\mu\nu} = \sqrt{-g}\;g^{\mu\nu}$. By property of the inverse $det(g^{\mu\nu}) = g^{-1}$, then $det(f^{\mu\nu}) = \sqrt{-g}^{d+1}g^{-1}$. And by squaring this expression, $det(f^{\mu\nu})^2 = (-g)^{d-1}$. The direct computation of $det(f^{\mu\nu})$ delivers $det(f^{\mu\nu}) = -a_0^{2d}$, and thereby the determinant g of the metric, as well as the metric inverse $g^{\mu\nu}$ are within reach,

$$g = -a_0^{\frac{4d}{d-1}} \qquad\qquad g^{\mu\nu} = a_0^{\frac{-2d}{d-1}}\begin{pmatrix} 1 & \boldsymbol{u}_0{}^T \\ \\ \boldsymbol{u}_0 & \boldsymbol{u}_0\otimes\boldsymbol{u}_0 - a_0^2\boldsymbol{I} \end{pmatrix} \tag{2.59}$$

Note that the metric g is here independent of the mean density ρ_0 and is more in line with the intuition with respect to previous studies (Stone, 2000, §III). This gives an additional motivation to consider ϕ instead of ψ as the most suitable acoustic potential variable, where $\nabla\phi = \rho_0\boldsymbol{u}$ and $\nabla\psi = \boldsymbol{u}$. However, it is deplorable that the formulation is ill-posed for one-dimensional configurations, i.e. with $d = 1$. This is a fact acknowledged by the literature (Barcelo et al., 2011, §2.7.2). In the end, the acoustic metric expresses as,

$$g_{\mu\nu} = a_0^{\frac{2}{d-1}}\begin{pmatrix} a_0^2 - u_0^2 & \boldsymbol{u}_0{}^T \\ \\ \boldsymbol{u}_0 & -\boldsymbol{I} \end{pmatrix} \tag{2.60}$$

The terminology of metric is motivated, because it is precisely $g_{\mu\nu}$ that enables to measure the geodesic $S = \int \mathrm{d}s$ covered by an acoustic ray. Owing on Fermat's principle (Voronovich and Godin, 2003), the actual ray is precisely the ray that minimise this distance S. The infinitesimal length $\mathrm{d}s$ of an acoustic ray path is given by the expression,

$$\mathrm{d}s^2 = g_{\mu\nu}\mathrm{d}x^\mu\mathrm{d}x^\nu \equiv a_0^{\frac{2}{d-1}}\begin{pmatrix}\mathrm{d}t & \mathrm{d}\boldsymbol{x}\end{pmatrix}\cdot\begin{pmatrix} a_0^2 - u_0^2 & \boldsymbol{u}_0{}^T \\ \\ \boldsymbol{u}_0 & -\boldsymbol{I} \end{pmatrix}\cdot\begin{pmatrix}\mathrm{d}t \\ \\ \mathrm{d}\boldsymbol{x}\end{pmatrix} \tag{2.61}$$

Note that when the eigenvalues of $g_{\mu\nu}$ are positive, the matrix metric defines a scalar product and a norm. By defining $\mathrm{d}\tilde{\boldsymbol{x}}$ as an infinitesimal element of space-time, then the acoustic route that should be minimal $\mathrm{d}s$, writes, $\mathrm{d}s^2 = <\mathrm{d}\tilde{\boldsymbol{x}}, \mathrm{d}\tilde{\boldsymbol{x}}>_g = ||\mathrm{d}\tilde{\boldsymbol{x}}||_g^2$. Thus after calculations,

$$\mathrm{d}s^2 = a_0^{\frac{2}{d-1}}\left[a_0^2\mathrm{d}t^2 - (\mathrm{d}\boldsymbol{x} - \boldsymbol{u}_0\mathrm{d}t)^2\right] \tag{2.62}$$

It can be fairly straightly be observed , that this relation for $\mathrm{d}s$ is consistent with the kinematic equation of acoustics. For Fermat's principle to be fulfilled, indeed, $\mathrm{d}s = 0$ and $a_0\mathrm{d}t = |\mathrm{d}\boldsymbol{x} - \boldsymbol{u}_0\mathrm{d}t|$. There exists

therefore a unit vector $\boldsymbol{n}$, such that,

$$\frac{\mathrm{d}\boldsymbol{x}}{\mathrm{d}t} = a_0\boldsymbol{n} + \boldsymbol{u}_0 \tag{2.63}$$

Later derivations will show that $\boldsymbol{n} = \boldsymbol{k}/|\boldsymbol{k}|$, and corresponds to the wavenumber $\boldsymbol{k}$ unit vector. In next paragraph, drawing heavily on the lecture notes of Bertschinger (1999), it is shown how the Hamiltonian formalisms offers a systematic method to deliver the equations of ray tracing.

2.7.2 Acoustic rays as solution of the Hamilton-Jacobi equations

It is usual in analytical mechanics to introduce $\tilde{\boldsymbol{x}} = (t, \boldsymbol{x})^T$ as the position vector in the space-time frame, and, the four-vector $\boldsymbol{p} = (\omega, -\boldsymbol{k})^T$, which is chosen here in order to fulfil the convention $\boldsymbol{p}\cdot\tilde{\boldsymbol{x}} = \omega t - \boldsymbol{k}\cdot\boldsymbol{x}$. Let τ describe a parametrisation of the trajectory in this generalised framework. If the metric $g_{\mu\nu}$ is known, the Hamiltonian $H_2(\boldsymbol{p}, \tilde{\boldsymbol{x}}, \tau)$ may be computed by the relation,

$$H_2(\boldsymbol{p}, \tilde{\boldsymbol{x}}, \tau) = \frac{1}{2}g^{\mu\nu}p_\mu p_\nu = \frac{1}{2}g_{\mu\nu}\frac{\mathrm{d}x^\mu}{\mathrm{d}\tau}\frac{\mathrm{d}x^\nu}{\mathrm{d}\tau} \quad \text{, with} \quad p_\mu = g_{\mu\nu}\frac{\mathrm{d}x^\nu}{\mathrm{d}\tau} \tag{2.64}$$

When applied to the acoustic metric computed previously, the Hamiltonian $H_2(\boldsymbol{p}, \tilde{\boldsymbol{x}}, \tau)$ becomes,

$$H_2(\boldsymbol{p}, \tilde{\boldsymbol{x}}, \tau) = \frac{1}{2}\left((\omega - \boldsymbol{k}\cdot\boldsymbol{u}_0)^2 - a_0^2|\boldsymbol{k}|^2\right) \tag{2.65}$$

This equation of the Hamiltonian can identically be found in the literature, see (Stone, 2000, eq. (A9)) and (Revalor, 2007, eq. (C.5)), note the striking resemblance with the Lagrangian derived in equation (2.43). Please note additionally, that different equally valid expressions of the Hamiltonian may lead to the same equations of motion. Trajectories in space-time are governed by the Hamilton-Jacobi equations,

$$\frac{\mathrm{d}x^\mu}{\mathrm{d}\tau} = \frac{\partial H_2}{\partial p_\mu} \quad , \quad \frac{\mathrm{d}p_\mu}{\mathrm{d}\tau} = -\frac{\partial H_2}{\partial x^\mu} \tag{2.66}$$

The link between this formalism and ray acoustics is recurrent (Landau and Lifshitz, 1959; Candel, 1977; Stone, 2000; Virieux et al., 2004). Yet the details on the evaluation of the Hamilton-Jacobi equations which lead to geometrical acoustics are seldom available. Referring to Bertschinger (1999), when the Hamiltonian is computed from a metric, the equations (2.66) deliver $2 \times 4 = 8$ set of equations that are parametrised by τ. Meanwhile, what is of interest in geometrical acoustics are the following $2 \times 3 = 6$ equations, that are parametrised by the physical time t,

$$\frac{\mathrm{d}x^i}{\mathrm{d}t} = \frac{\partial H}{\partial k_i} \quad , \quad \frac{\mathrm{d}k_i}{\mathrm{d}t} = -\frac{\partial H}{\partial x^i} \tag{2.67}$$

This change in the parametrisation, that consist in considering the physical three-dimensional space instead of the four-dimensional space-time, is not straightforward. It is not possible in general to choose $\tau = t$. This is precisely what was missed in previous studies (Stone, 2000; Barcelo et al., 2011; Rienstra and Hirschberg, 2004). The expression of the Hamiltonian $H(\boldsymbol{k}, \boldsymbol{x}, t)$, parametrised by the time t, may be deduced from $H_2(\boldsymbol{p}, \tilde{\boldsymbol{x}}, \tau)$ by the following formula (Bertschinger, 1999),

$$H(\boldsymbol{k}, \boldsymbol{x}, t) = \frac{g^{0i}k_i}{g^{00}} + \sqrt{\frac{g^{ij}k_ik_j - 2H_2(\boldsymbol{p}, \tilde{\boldsymbol{x}}, \tau)}{-g^{00}} + \left(\frac{g^{0i}k_i}{g^{00}}\right)^2} \tag{2.68}$$

And as a result, the Hamiltonian for acoustics expresses in a physical space as,

$$\boxed{H(\boldsymbol{k},\boldsymbol{x},t) = \boldsymbol{u}_0\cdot\boldsymbol{k} + |\omega - \boldsymbol{u}_0\cdot\boldsymbol{k}|} \tag{2.69}$$

The here above absolute value $|.|$ is of meaning, it will make it possible to recover the acoustic characteristics. Note that the metric computed form Blokhintzev's acoustic potential wave equation (Barcelo et al., 2011, §2.3), would deliver the same Hamiltonian. This is because the transformation given in equation (2.68) involves a normalised metric.

2.7.3 Energy conservation and dispersion relation for the acoustic potential

For the geometrical acoustics framework to be completed, the energy conservation law and the dispersion relation must be established. This two equations of ray tracing are derived from Pierce's wave equation,

$$\frac{\mathrm{D}^2\phi}{\mathrm{D}t^2} - \nabla\cdot(a_0^2\nabla\phi) + (\nabla\cdot\boldsymbol{u}_0)\frac{\mathrm{D}\phi}{\mathrm{D}t} = 0 \tag{2.70}$$

for which the phase and the amplitude A of the solution ϕ are sought separately, by setting,

$$\phi = Ae^{i(\boldsymbol{k}\cdot\boldsymbol{x}-\omega t)} \tag{2.71}$$

For the dispersion relation $\omega \equiv \omega(\boldsymbol{k})$ to be obtained, ω and $\boldsymbol{k}$ are supposed constant with respect to time and space. In inserting this particular solution into Pierce's wave equation, following relation is deduced,

$$-(-\omega+\boldsymbol{u}_0\cdot\boldsymbol{k})^2A^2 + a_0^2|\boldsymbol{k}|^2A^2 + A\nabla\cdot\left[\left(\boldsymbol{u}_0\otimes\boldsymbol{u}_0 - a_0^2\boldsymbol{I}\right)\cdot\nabla A\right] + i\nabla\cdot\left[\left(\boldsymbol{u}_0(-\omega+\boldsymbol{u}_0\cdot\boldsymbol{k}) - a_0^2\boldsymbol{k}\right)A^2\right] = 0 \tag{2.72}$$

The real part of this equation corresponds to the dispersion relation,

$$\boxed{(-\omega+\boldsymbol{u}_0\cdot\boldsymbol{k})^2 - a_0^2|\boldsymbol{k}|^2 = \frac{\nabla\cdot\left[\left(\boldsymbol{u}_0\otimes\boldsymbol{u}_0 - a_0^2\boldsymbol{I}\right)\cdot\nabla A\right]}{A}} \tag{2.73}$$

And the imaginary part of equation (2.72) guarantees the acoustic energy conservation,

$$\boxed{\nabla\cdot\left(\left[\left(\boldsymbol{u}_0\otimes\boldsymbol{u}_0 - a_0^2\boldsymbol{I}\right)\cdot\boldsymbol{k} - \omega\boldsymbol{u}_0\right]A^2\right) = 0} \tag{2.74}$$

2.7.4 Asymptotic equations of geometrical acoustics

It is instructive to remark that a different dispersion relation can be obtained from the conservation of the Hamiltonian $H_2(\boldsymbol{p},\tilde{\boldsymbol{x}},\tau)$ along the ray trajectory. That the Hamiltonian $H_2(\boldsymbol{p},\tilde{\boldsymbol{x}},\tau)$ conserves along its trajectory can be deduced from a composite derivation with respect to the parametrisation τ,

$$\frac{\mathrm{d}H_2(\boldsymbol{p},\tilde{\boldsymbol{x}},\tau)}{\mathrm{d}\tau} = \frac{\partial H_2}{\partial\boldsymbol{p}}\cdot\frac{\mathrm{d}\boldsymbol{p}}{\mathrm{d}\tau} + \frac{\partial H_2}{\partial\tilde{\boldsymbol{x}}}\cdot\frac{\mathrm{d}\tilde{\boldsymbol{x}}}{\mathrm{d}\tau} + \frac{\partial H_2}{\partial\tau} \tag{2.75}$$

From the expression of $H_2(\boldsymbol{p},\tilde{\boldsymbol{x}},\tau)$ given in equation (2.65), it is seen that this Hamiltonian does not explicitly depend on τ; the last term of previous expression is therefore null. From the equations of Hamilton-Jacobi given in (2.66), the two first terms compensate and finally $\mathrm{d}H_2(\boldsymbol{p},\tilde{\boldsymbol{x}},\tau)/\mathrm{d}\tau = 0$. This

conservation along the ray path defined by the parameter τ delivers,

$$(-\omega + \boldsymbol{u}_0 \cdot \boldsymbol{k})^2 - a_0^2 |\boldsymbol{k}|^2 = 0 \tag{2.76}$$

which corresponds to the classical dispersion relation of ray acoustics (Landau and Lifshitz, 1959, eq. (68.1)) (Candel, 1977, app. A). In fact, this dispersion relation corresponds to an acoustic high frequency limit simplification of equation (2.73), such that (Foreman, 1989),

$$\omega^2 \gg a_0^2 \frac{\Delta A}{A} \tag{2.77}$$

That the Hamiltonian conservation equation delivers solely an asymptotic conservation law is understandable, to the extent that equation (2.76) is solely valid along the ray trajectory parametrised by τ. In that respect, a ray trajectory corresponds to an infinitely thin tube rather than a cone. Within such a tube, the acoustic energy is constant, and the energy conservation equation decouples from the equations of ray tracing, so that the amplitude A of the rays may be computed a posteriori (Virieux et al., 2004).

The ray equations are summarised hereafter in the acoustic high frequency limit. Beforehand, it is noted that the Hamiltonian, equation (2.69), consistently delivers the two characteristics of acoustics.

- for $\omega - \boldsymbol{u}_0 \cdot \boldsymbol{k} > 0$ then $\dfrac{\partial \omega}{\partial \boldsymbol{k}} = \boldsymbol{u}_0 + a_0 \dfrac{\boldsymbol{k}}{|\boldsymbol{k}|}$ and $H = \omega = \boldsymbol{k} \cdot \boldsymbol{u}_0 + a_0 |\boldsymbol{k}|$
- for $\omega - \boldsymbol{u}_0 \cdot \boldsymbol{k} < 0$ then $\dfrac{\partial \omega}{\partial \boldsymbol{k}} = \boldsymbol{u}_0 - a_0 \dfrac{\boldsymbol{k}}{|\boldsymbol{k}|}$ and $H = 2(\boldsymbol{u}_0 \cdot \boldsymbol{k}) - \omega = \boldsymbol{k} \cdot \boldsymbol{u}_0 + a_0 |\boldsymbol{k}|$

In this asymptotic framework, it is observed that the Hamiltonian has identical value on the two characteristic branches, yet it only corresponds to $H = \omega$ along the $+$ characteristic. Thus, the frequently encountered expression for ray tracing, i.e. $d\boldsymbol{x}/dt = \partial\omega/\partial\boldsymbol{k}$ and $d\boldsymbol{k}/dt = -\nabla\omega$ (Landau and Lifshitz, 1959, eq. (67.4)), can only account for one direction of propagation. The high frequency simplification of geometrical acoustics is given by,

$$\begin{cases} H(\boldsymbol{k}, \boldsymbol{x}, t) = \boldsymbol{k} \cdot \boldsymbol{u}_0 + a_0 |\boldsymbol{k}| & \text{Hamiltonian} \\ \left.\begin{aligned} \dfrac{d\boldsymbol{x}}{dt} &= \dfrac{\partial H}{\partial \boldsymbol{k}} \\ \dfrac{d\boldsymbol{k}}{dt} &= -\nabla H \end{aligned}\right\} & \text{Hamilton-Jacobi equations} \\ \omega = \boldsymbol{u}_0 \cdot \boldsymbol{k} \pm a_0 |\boldsymbol{k}| & \text{dispersion relation} \end{cases} \tag{2.78}$$

The energy conservation equation given in (2.74) can be recast with the asymptotic dispersion relation, and in particularising the trajectory laws, it comes to,

$$\begin{cases} \dfrac{d\boldsymbol{x}}{dt} = \boldsymbol{u}_0 + a_0 \dfrac{\boldsymbol{k}}{|\boldsymbol{k}|} \\ \dfrac{d\boldsymbol{k}}{dt} = -(\nabla \boldsymbol{u}_0)^T \cdot \boldsymbol{k} - |\boldsymbol{k}| \nabla a_0 \\ \nabla \cdot \left(a_0 \boldsymbol{u}_g |\boldsymbol{k}| A^2 \right) = 0 \end{cases} \tag{2.79}$$

where the group velocity $\boldsymbol{u}_g$ is computed as,

$$\boldsymbol{u}_g = \frac{\partial \omega}{\partial \boldsymbol{k}} = \boldsymbol{u}_0 \pm a_0 \frac{\boldsymbol{k}}{|\boldsymbol{k}|} \tag{2.80}$$

2.7.5 Generalisation of Foreman's exact rays

To solve the ray tracing equations, three unknowns must be determined, namely the ray trajectory $\boldsymbol{x}$, its wave number $\boldsymbol{k}$ and the acoustic field amplitude A. With help of equation (2.71), the acoustic potential ϕ may be recomputed, and subsequently all other fields of interest. The equations for $\boldsymbol{x}$ and $\boldsymbol{k}$ are coupled because $a_0 \equiv a_0(\boldsymbol{x})$ and $\boldsymbol{u}_0 \equiv \boldsymbol{u}_0(\boldsymbol{x})$. From the asymptotic ray equations (2.79), it is seen that the energy conservation equation decouples from the trajectory equations; and A may be computed a posteriori. This decoupling is legitimate as long as equation (2.77) is fulfilled. A detailed account of the specific regimes of linear wave motion that may invalid this condition is given by Berry (1980). From equation (2.77), it is clear that the large acoustic wavelength limit (wave dislocation) is such a configuration for which the equations are coupled. In the asymptotic case of geometrical acoustics, focal surfaces for the acoustic wavefronts may appear (caustics), which create sharp variations of the wave amplitude A, and may also fault equation (2.77). Figure 2.4 illustrates the phenomenon of caustics, that is recognisable by the focusing and crossing of acoustic rays. The asymptotic ray theory is compared to the reference Eulerian wave equation solution. In the asymptotic theory, acoustic rays are supposed independent each from another, and their merging occurring in caustics can consequently not be described. No physical relevance should thus be given to the ray paths that exit the caustics (Foreman, 1989). Moreover in the reference acoustic solution presented in figure 2.4, a blurring of the wavefront is visible that indicates that the media is dispersive. Such a frequency dependant behaviour of the wave motion cannot neither be accounted for with an asymptotic ray theory.

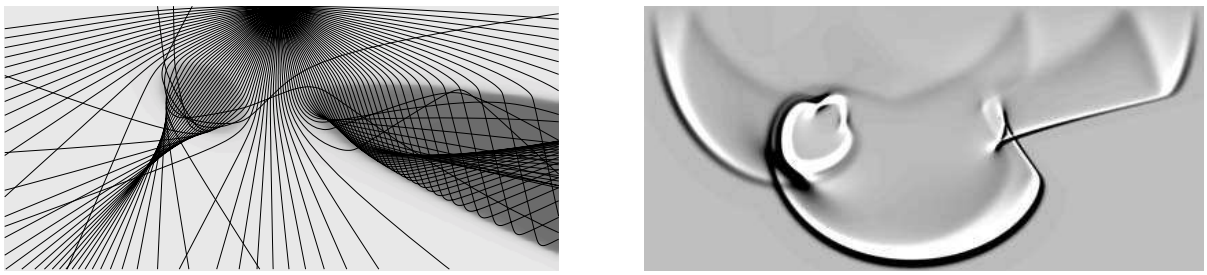

Figure 2.4: Acoustic refraction caused by heterogeneities in the sound speed a_0 (Engquist and Runborg, 2003). Acoustic rays are computed in the short wavelength limit and are displayed superimposed on the index of refraction map (left). Helmholtz's wave equation is solved for this configuration giving an accurate description of the caustics and the wave dispersion phenomena (right).

In the 1990s, a ray frequency-dependant formulation of the wave equation (Zhu, 1988; Foreman, 1989; Biondi, 1992) has been proposed. Some variations of this theory exist (Floyd, 1990), and the exact ray formulation of Foreman (1989) serves as reference for the present discussion. This formulation is an exact recast of the wave equation that is uniformly valid over the acoustic frequency range. The wavefront amplitude A is coupled with the equation of ray trajectory, this is seen in the table 2.1, where the dispersion relation obtained by Foreman for the classical wave equation, and the dispersion relation for Pierce's equation are compared. These two approaches are mutually consistent. Some major differences are noted by Foreman (1989) between exact rays and the classical asymptotic geometrical acoustic theory.

	classical equation	Pierce's equation
wave operator	$\dfrac{\partial^2\phi}{\partial t^2} - a_0^2\Delta\phi = 0$	$D^2_{\boldsymbol{u}_0}(\phi) - \nabla\cdot(a_0^2\nabla\phi) + (\nabla\cdot\boldsymbol{u}_0)D_{\boldsymbol{u}_0}(\phi) = 0$
dispersion relation	$\omega^2 - a_0^2\lvert\boldsymbol{k}\rvert^2 = \dfrac{a_0^2\Delta A}{A}$	$(-\omega+\boldsymbol{u}_0\boldsymbol{k})^2 - a_0^2\lvert\boldsymbol{k}\rvert^2 = \dfrac{\nabla\cdot\left[(\boldsymbol{u}_0\otimes\boldsymbol{u}_0 - a_0^2\boldsymbol{I})\cdot\nabla A\right]}{A}$

Table 2.1: The exact ray formalism of Foreman (1989) is compared with the present reformulation of Pierce's equation. Relying on $\phi = A\exp\big(i(\boldsymbol{k}\cdot\boldsymbol{x}-\omega t)\big)$, the dispersion relation is computed.

In particular, Foreman's acoustic exact rays do not cross. As a consequence, multipath do not exist in this framework, meaning that there exist only a unique eigenray from a source to an observation point. This eigenray is moreover always defined, and the observer may be located in the shadow zone of the asymptotic theory, which is entirely mapped by Foreman's exact rays. An illustration of exact ray tracing is provided figure 2.5.

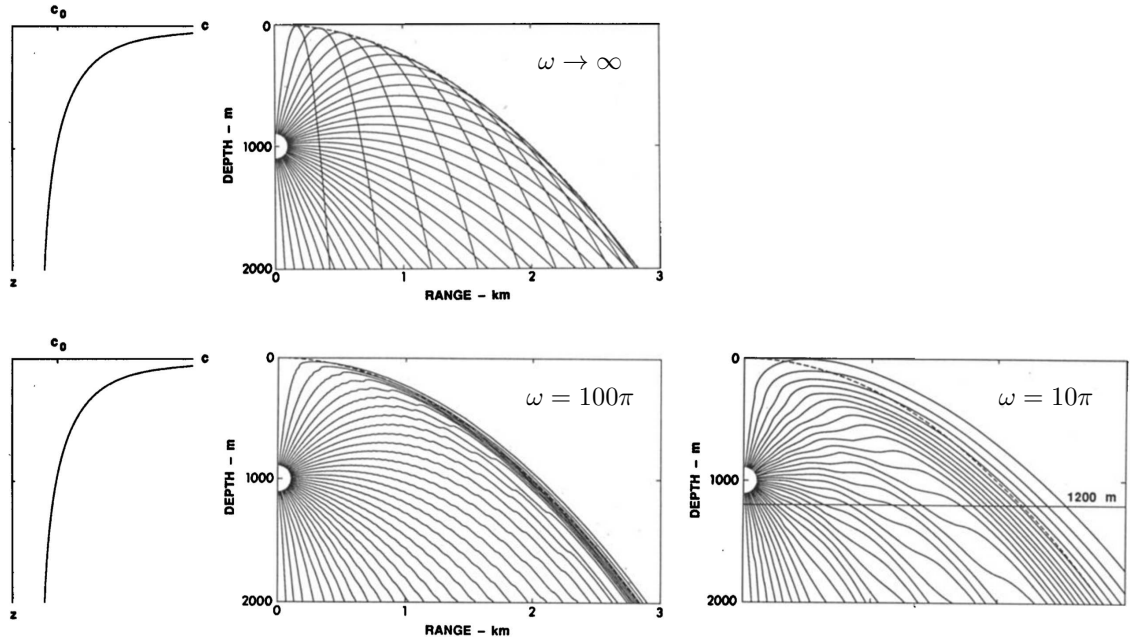

Figure 2.5: Ray tracing computed by geometrical acoustics in the short wavelength limit (top) is compared with exact rays (bottom). The media heterogeneity in sound speed a_0 is modelled with a Kormilitsin profile (Foreman, 1989). Exact rays do never cross, are frequency-dependant, and penetrate the shadow zone of the asymptotic theory.

Consistently with Foreman (1989), a theoretical formulation in terms of exact rays may be given for Pierce's wave equation (2.38). The acoustic Hamiltonian, equation (2.69) $H(\boldsymbol{k},\boldsymbol{x},t)$, may be recast with help of the dispersion relation $\omega \equiv \omega(\boldsymbol{k}, A)$, equation (2.73), to form,

$$H(\boldsymbol{k},\boldsymbol{x},t) = \boldsymbol{u}_0\cdot\boldsymbol{k} + \sqrt{\frac{\nabla\cdot\left[(\boldsymbol{u}_0\otimes\boldsymbol{u}_0 - a_0^2\boldsymbol{I})\cdot\nabla A\right]}{A} + a_0^2\lvert\boldsymbol{k}\rvert^2} \tag{2.81}$$

This expression for the Hamiltonian is valid in both characteristic directions. The Hamilton-Jacobi

equations can then be re-expressed to deliver an exact reformulation of Pierce's wave equation,

$$\begin{cases} \dfrac{\partial \boldsymbol{x}}{\partial t} = \boldsymbol{u}_0 + \dfrac{a_0^2 \boldsymbol{k}}{\sqrt{\dfrac{\nabla \cdot \left[(\boldsymbol{u}_0 \otimes \boldsymbol{u}_0 - a_0^2 \boldsymbol{I}) \cdot \nabla A \right]}{A} + a_0^2 |\boldsymbol{k}|^2}} \\ \dfrac{\partial \boldsymbol{k}}{\partial t} = -(\nabla \boldsymbol{u}_0)^T \cdot \boldsymbol{k} + \dfrac{-|\boldsymbol{k}|^2 \nabla (a_0^2) - \nabla \left(\dfrac{\nabla \cdot \left[(\boldsymbol{u}_0 \otimes \boldsymbol{u}_0 - a_0^2 \boldsymbol{I}) \cdot \nabla A \right]}{A} \right)}{2\sqrt{\dfrac{\nabla \cdot \left[(\boldsymbol{u}_0 \otimes \boldsymbol{u}_0 - a_0^2 \boldsymbol{I}) \cdot \nabla A \right]}{A} + a_0^2 |\boldsymbol{k}|^2}} \\ \nabla \cdot \left[a_0^2 A^2 \boldsymbol{k} \pm \boldsymbol{u}_0 A^2 \sqrt{\dfrac{\nabla \cdot \left[(\boldsymbol{u}_0 \otimes \boldsymbol{u}_0 - a_0^2 \boldsymbol{I}) \cdot \nabla A \right]}{A} + a_0^2 |\boldsymbol{k}|^2} \right] = 0 \end{cases} \tag{2.82}$$

This set of equations is coupled and its implementation may be cumbersome if no simplification is made (Biondi, 1992). This ray reformulation of Pierce's equation is expected to possess identical properties to the exact rays of Foreman (1989). In addition to the conservation law of self-adjoint operators that has been highlighted by Möhring (1999, §2.4), some alternative and perhaps more fundamental energy conservation equation may be derived from the trajectory equations and the geodesic framework used here (Ray and Reid, 1979; Bertschinger, 2002). To conclude, note that this entire discussion is based on the metric of Pierce's equation, the latter being solely computed from its linear operator. Thus, identical conclusions would have been obtained with the wave equation of Phillips (1960) that relies on the same wave operator. Because the range of validity for Pierce's equation is wider than the one of Phillips, it is expected that the energy conservation laws corresponding to Pierce's equation are more general. To confirm this assertion, future work will need to retrieve a conservation law that is based on the thermodynamic state variable, so to enable a comparison with other acoustic energy conservation law (Cantrell and Hart, 1964; Garrett, 1967; Hayes, 1968; Morfey, 1971; Andrews and McIntyre, 1978; Campos, 1988). A general acoustic framework that is consistent with the acoustic potential formulation, and simultaneously with asymptotic ray acoustics is provided with Pierce's equation. Only for these two configurations is acoustics decoupled from the other energetic modes, and is sound propagation unequivocally defined. While this is an arbitrary, Pierce's wave equation offers a pragmatic stance to model sound propagation that is robust and energy conserving.

3 Stable computation of sound propagation in a sheared flow

Summary: The in-house finite difference code PROPA is presented and validated on the fourth CAA workshop case. The concept of self-adjoint-kernel is introduced and some new stable wave equations are derived. With help of PROPA, their stability is tested, and their ability to accurately compute sound propagation on a sheared flow is compared.

3.1 Solving of acoustic equations in the frequency domain

The issue of achieving a reliable and stable acoustic propagation has been often stressed in previous paragraphs, and some new acoustic operators have been proposed. In the present chapter, some additional creative stable wave equations are proposed. For more insight, the stability property of these wave equations must be challenged and the accuracy of their acoustic prediction characterised. This is the purpose of PROPA, a malleable in-house finite difference code that is developed for this sake, and is presented hereafter. Adjoint linear operators are also implemented in PROPA, so that this code proved to be crucial in the discussion on the adjoint-based noise prediction technique of chapter 3 from part II. The code aims at tackling free-field acoustic propagation problems for arbitrary sound source and mean flow definitions in two-dimensions or in axisymmetric configurations.

The computed acoustic solution is discretised over a simple regular and uniform grid with help of finite differences. With this technique, the derivative f' of a field f at a current point x_i is computed from the knowledge of the values at neighbouring points. The differentiation relation may be obtained from a Taylor series expansion, as for the following simple three-points stencil approximation,

$$f'(x_i) = \frac{f(x_i + h) - f(x_i - h)}{2} + O(h^2) \tag{3.1}$$

The accuracy of the method increases when the grid spacing h decreases. Since this differentiation technique summons the points nearby the current point x_i, one-sided approximations must be conceived for points close to the frontier edges. Such a treatment for a second order $O(h^2)$, three-points stencil expresses as (Fornberg, 1988),

$$f'(x_i) = \frac{-3f(x_i) + 4f(x_i + h) - f(x_i + 2h)}{2} + O(h^2) \tag{3.2}$$

The wider the stencils, the more room for optimisation it exists, and numerous finite difference schemes

have been proposed (Fornberg, 1988; Tam and Webb, 1993; Bogey and Bailly, 2004; Berland et al., 2007). PROPA is written in the frequency domain, in a *Matlab* environment, and uses a direct inversion method relying on the UMFPACK solver (Davis, 2004), which is *Matlab*'s direct inversion multithreaded algorithm for sparse unsymmetric system. UMFPACK corresponds to one of the many algorithms that the generic 'backslash' operation may invoke. To implement finite differences in the frequency domain, a system matrix for the acoustic equation must be built. Figure 3.1 illustrates differentiation matrices for a column vector of $N = 15$ elements that are obtained for different stencil width. The derivative of any fifteen-elements array is straightforwardly computed by its multiplication with the differentiation matrix.

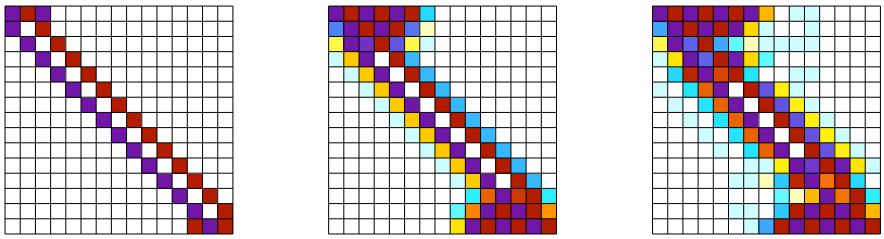

Figure 3.1: Differentiation matrices for a vector of $N = 15$ elements. The approximation of the derivative are based on three-points, seven-points and eleven-points stencils (from left to right). Non-centred schemes are used closed to the domain borders. Colours are indicative, and illustrate that higher order approximations are corrections of lower order ones.

To address a two-dimensional structured computational domain of, say, (`Nx1`, `Nx2`) elements with this technique, the two-dimensional array may be concatenated into a one-dimensional (`Nx1`$\times$`Nx2`, 1) array. The corresponding differentiation matrix `diff_x1` and `diff_x2` in the `x1` and `x2` direction, can then simply be obtained with a Kronecker product,

```
diff_x1 = kron(eye(Nx2),stencil_pattern(Nx1))/dx1
diff_x2 = kron(eye(Nx1),stencil_pattern(Nx2))/dx2
```

where `stencil_pattern(`N`)` is the elementary stencil pattern for an array of size N as given in figure 3.1. `eye(`N`)` is the diagonal matrix of size N, `dx1` and `dx2` are the regular grid spacing in the `x1` and `x2` directions. As an illustration, figure 3.2 presents the system matrix corresponding to the two-dimensional linearised Euler's equations at rest without mean flow gradients. This system operator is obtained by a left-side factorisation of the derivatives and apply on the state vector $(\rho,\ \rho_0 u_1,\ \rho_0 u_2,\ p)^T$, for a square domain of `Nx1` $=$ `Nx2` $= 15$ elements. The system matrix is consequently of size 900×900 ($4 \times 15 \times 15 = 900$) and is very sparse. A trade-off between the matrix system sparsity (RAM requirements) and the accuracy of the numerical method (grid refinement) is to be found. This has not been investigated in the present study, and, the eleven-points stencils of Bogey and Bailly (2004), and Berland et al. (2007) are used as reference in PROPA, as shown in figure 3.2. As an indication, the computations presented in chapter 3 of part II are obtained on a regular mesh composed of 800×450 elements including 50 cells-thick PML layers. Each run required approximatively 50 GB of RAM on a 16 core Dell T7810 computer of 64 GB (CPU: Xeon E5-2609v4) with the version R2016b of *Matlab*.

To simulate free-field radiating conditions, a perfectly matched layer (PML) reformulation of the derivative is used. This choice is motivated by the simplicity of implementation of PML in the frequency domain, their effectiveness, and robustness. The basic idea is to associate in the surrounding of the numerical domain a sponge layer with modified physical properties that renders the numerical solution evanescent. This method as been introduced by Berenger (1994) to simulate free-field propagation of electromagnetic

$$
\begin{aligned}
-i\omega\rho + \frac{\partial \rho_0 u_1}{\partial x_1} + \frac{\partial \rho_0 u_2}{\partial x_2} &\longrightarrow \\
-i\omega\rho_0 u_1 + \frac{\partial p}{\partial x_1} &\longrightarrow \\
-i\omega\rho_0 u_2 + \frac{\partial p}{\partial x_2} &\longrightarrow \\
-i\omega p + a_0^2 \frac{\partial \rho_0 u_1}{\partial x_1} + a_0^2 \frac{\partial \rho_0 u_2}{\partial x_2} &\longrightarrow
\end{aligned}
$$

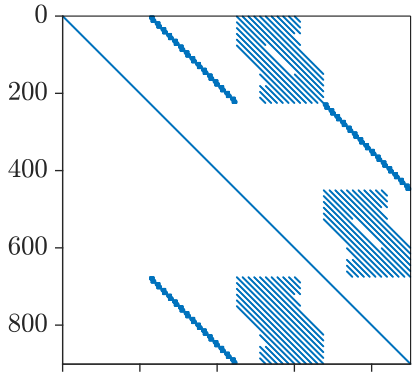

Figure 3.2: Linearised equations for a medium at rest, and the corresponding system matrix for a square domain of 15×15 elements. Non-zeros elements of the system are shown with *Matlab*'s `spy()` function.

waves, and is by now very popular in the fluid mechanics community (Hu, 2008). Introductory lectures on this topic (Johnson, 2010) may easily be found. Rao and Morris (2006) derived PML for the pulsation ω, yet some preliminary investigations with PROPA (not presented) have shown that their formulation may alter in some case the solution inside the domain, and the classical definition based on a modification of the wavenumber k is preferred. At a point $\boldsymbol{x}$ located in the PML sponge layer, the derivatives along x_i are modified by the addition of an absorption coefficient Γ, such that,

$$
\frac{\partial}{\partial x_i} \rightarrow \frac{1}{1 + i\ \Gamma(\boldsymbol{x})} \frac{\partial}{\partial x_i} \tag{3.3}
$$

To avoid an abrupt change in the media impedance and the onset of spurious reflections, the absorption coefficient Γ is defined in PROPA to follow a cubic evolution in the directions normal to the frontier edge. The sponge layer width and the amplitude of the damping are defined by trial and error so to avoid visible PML reflections and in a way so that in the extremity of the sponge layer, the signal is damped by at least 10 orders of magnitude. Hu (2005) highlighted that in presence of flow gradients in the sponge layer, some categories of waves may destabilise the PML. This feature is likely to be a characteristic of the implementation of the method in the time domain, since it has not been observed with PROPA. No special treatment of the mean flow defined in the PML zones has thus been considered for the computations presented in this study.

To conclude this descriptive section of the in-house code PROPA developed, the colourmap used for the plotting of the data is given in figure 3.3. To make fluctuations easily traceable, it is centred around zero with the central value coloured in white. The *Matlab* code to create the colourbar is also provided.

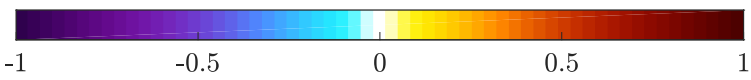

Figure 3.3: Colourmap used to visualise the solutions computed with PROPA.

```
levels = 59;
m_vec = linspace(0,1,levels)';
sigma_white = 0.022; % controls the sharpness of the transition fom yellow to blue
sigma_color = 0.15; % controls the amount of purple and the fading from yellow to blue
fpos = 1/5;

```

```
red_line = heaviside(1/3-m_vec).*(0.3+0.7*3*m_vec) ...
    + heaviside(m_vec-1/3) - heaviside(m_vec-1/2) ...
    + heaviside(m_vec-1/2).*exp(-(m_vec-1/2).^2/(2*sigma_white^2) ) ...
    + 0.45*heaviside(1-fpos-m_vec).*exp(-(m_vec-1+fpos).^2/(2*sigma_color^2) ) ...
    + 0.45*heaviside(m_vec-1+fpos).*exp(-(m_vec-1+fpos).^2/(2*sigma_color^2) );
green_line = heaviside(1/2-m_vec).*exp(-(m_vec-1/2).^2/(2*sigma_color^2) ) ...
    + heaviside(m_vec-1/2).*exp(-(m_vec-1/2).^2/(2*sigma_color^2) );
blue_line = heaviside(1/2-m_vec).*exp(-(m_vec-1/2).^2/(2*sigma_white^2) ) ...
    + heaviside(m_vec-1/2) - heaviside(m_vec-2/3) ...
    + heaviside(m_vec-2/3).*(1 + 3*0.7*(2/3-m_vec));

wave_map = flipud([red_line,green_line,blue_line]);
wave_map = min(wave_map,1); % to ensure, no value greater than one is specified
% figure, rgbplot(wave_map)
% figure, pcolor(peaks), colormap(wave_map)
```

3.2 Stable acoustic propagation

3.2.1 Computation of the instability wave

Several acoustic equations are implemented in PROPA, many of which have no reference solution against which the code could be validated. An enhanced and precise validation of the in-house code seems out of reach. Only for Pierce's equation could the implementation verified with help of the commercial software *Actran TM*, for more details see chapter 4 of part II. In this section, the fourth computational aeroacoustic (CAA) workshop is presented, and serves as a validation for Lilley's equation and for the linearised Euler's wave equation (LEWE). In a second step, this configuration for which mode coupling occurs is used to verify that the stable wave equations proposed truly are stable.

The category four of the fourth CAA workshop (Dahl, 2004) considers the mode coupling occurring by an acoustic source set in a two-dimension heated Gaussian jet flow profile. The source is broadband, given by $S_p = A\exp\left(-\alpha_1 x_1^2 - \alpha_2 x_2^2\right)$ and pulses at a frequency of $f = 76\,\mathrm{Hz}$. This corresponds to a Strouhal number of $St_{2\sigma} = 2\sigma f/u_j \approx 0.073$, and following value for the source are taken, $A = 10^{-3}\,\mathrm{kg.m^{-1}.s^{-3}}$, $\alpha_1 = 0.04\log(2)\,\mathrm{m}^{-2}$ and $\alpha_2 = 0.32\log(2)\,\mathrm{m}^{-2}$. The mean velocity profile follows a Gaussian evolution in the transverse direction according to,

$$\frac{u_{0,1}(x_2)}{u_j} = \exp\left(-\frac{x_2^2}{2\sigma^2}\right) \tag{3.4}$$

where $\boldsymbol{x} = (x_1, x_2)$, $u_j = M_j a_j$, $a_j = \sqrt{\gamma R T_j}$ and $\sigma = \sqrt{0.845\cdot\log(2)}\,\mathrm{m}$ is its standard deviation. To model a high-speed and heated jet flow, the following values are taken: $M_j = 0.756$, $T_j = 600\,\mathrm{K}$, $T_\infty = 300\,\mathrm{K}$, $\gamma = 1.4$ and $R = 287\,\mathrm{m^2{\cdot}s^{-2}{\cdot}K^{-1}}$. Considering $\rho_j = \gamma p_0/a_j^2$ and $p_0 = 103330\,\mathrm{Pa}$, the mean density $\rho_0(x_2)$ is defined with Crocco-Busemann's law by,

$$\frac{\rho_j}{\rho_0(x_2)} = \frac{T_\infty}{T_j} - \left(\frac{T_\infty}{T_j} - 1\right)\frac{u_{0,1}(x_2)}{u_j} + \frac{\gamma-1}{2}M_j^2\frac{u_{0,1}(x_2)}{u_j}\left(1 - \frac{u_{0,1}(x_2)}{u_j}\right) \tag{3.5}$$

The stability analysis of this mean flow profile has been performed and the spatial growth rate of the Kelvin-Helmholtz instability wave is given in Bailly and Bogey (2003, fig. 1). Analytical solutions of the radiated acoustic field have been calculated by Agarwal et al. (2004) along $x_2 = 15\,\mathrm{m}$ and $x_2 = 50\,\mathrm{m}$

(with normalisation, this corresponds to $x_2/\sigma \approx 13.6$, $x_2/\sigma \approx 45.3$).

A symmetry boundary condition is used in PROPA to reduce the cost of the numerical simulation. The solution to Lilley's equation is computed over two regular grids, a fine mesh that consists in 800×450 elements (including a 75 elements wide layer of PML) and a coarse mesh composed of 170×100 elements (including a 20 elements wide layer of PML). The grid spacing ($\mathrm{d}x_1/\sigma$, $\mathrm{d}x_2/\sigma$) is of $(0.313, 0.153)$ for the fine mesh and $(1.765, 0.8)$ for the coarse mesh. The real part of the pressure field computed on these two grids is presented in figure 3.4. While the acoustic solution is consistently predicted on both mesh,

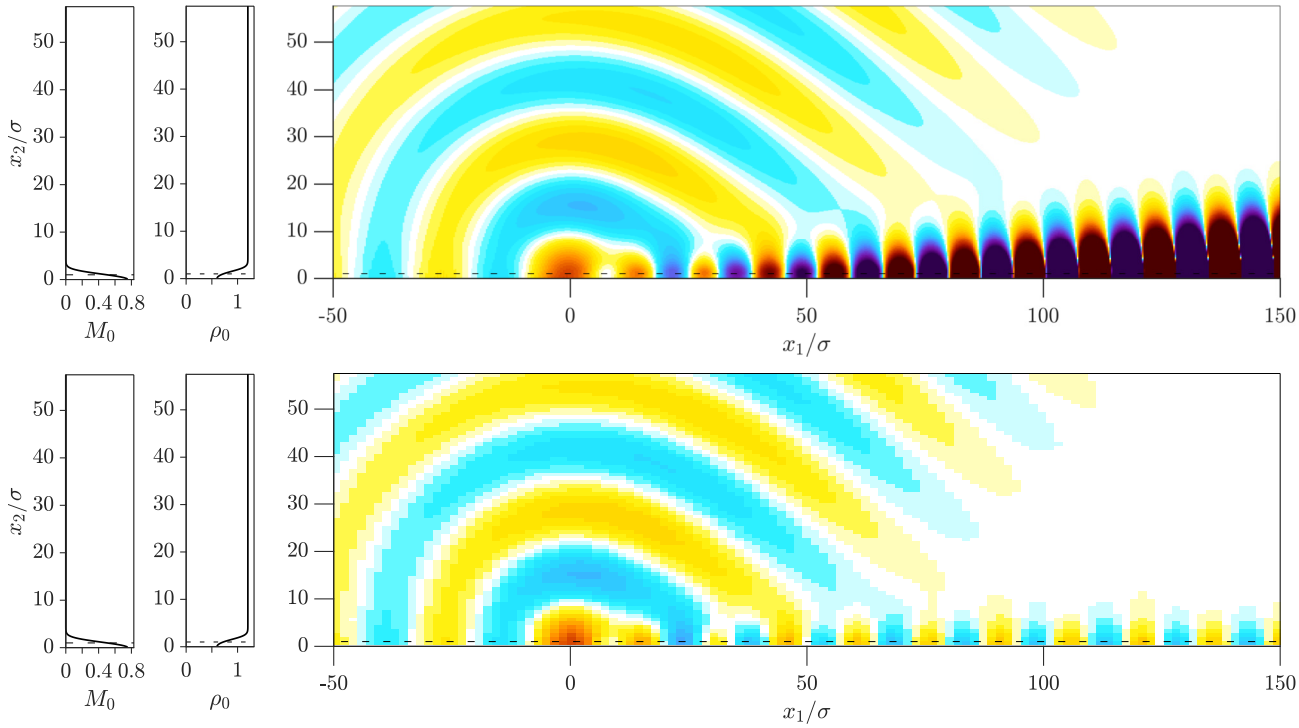

Figure 3.4: Solution to the fourth CAA workshop computed with Lilley's equation for the fine mesh (top) and the coarse mesh (bottom). Mach number M_0 and density ρ_0 profiles of the parallel mean flow considered are shown (left). Dashed lines represent the position of maximal shearing ($x_2/\sigma = 1$).

the development of the instability wave is found grid dependant and is only visible on the fine mesh. More insight is gained with figure 3.5, where the numerical solutions are compared with the analytical solution computed by Agarwal et al. (2004). For the extract along $x_2/\sigma \approx 45.3$ that is not affected by the development of the instability wave, a perfect match is found between the analytical solution and the fine grid solution. Some small discrepancies can be observed with the coarse mesh, but the fit remains very satisfactory. For the extract along $x_2/\sigma \approx 13.6$, the three set of data collapse before $x_1/\sigma = 50$. Further downstream, while the coarse grid solution fairly well strikes the reference solution, the instability wave develops its exponential growth on the fine mesh. From the confrontation of this instability wave solution with this of Rao and Morris (2006), discordance is found. While for this second extract, at $x_1/\sigma \approx 135$ (i.e. $x_1 = 150m$), an amplitude of 4.10^6 Pa is found by Rao and Morris (2006), this fine grid solution indicates an amplitude of 6.10^6 Pa. The high sensitivity of the instability wave solution on the grid discretisation must be acknowledged. A mesh convergence study is required here, and most likely, the fine grid solution is not sufficiently refined. That instability waves are mesh sensitive, could be drawn from (Li et al., 2004; Richter and Thiele, 2007), who proposed to remove the unstable hydrodynamic mode of

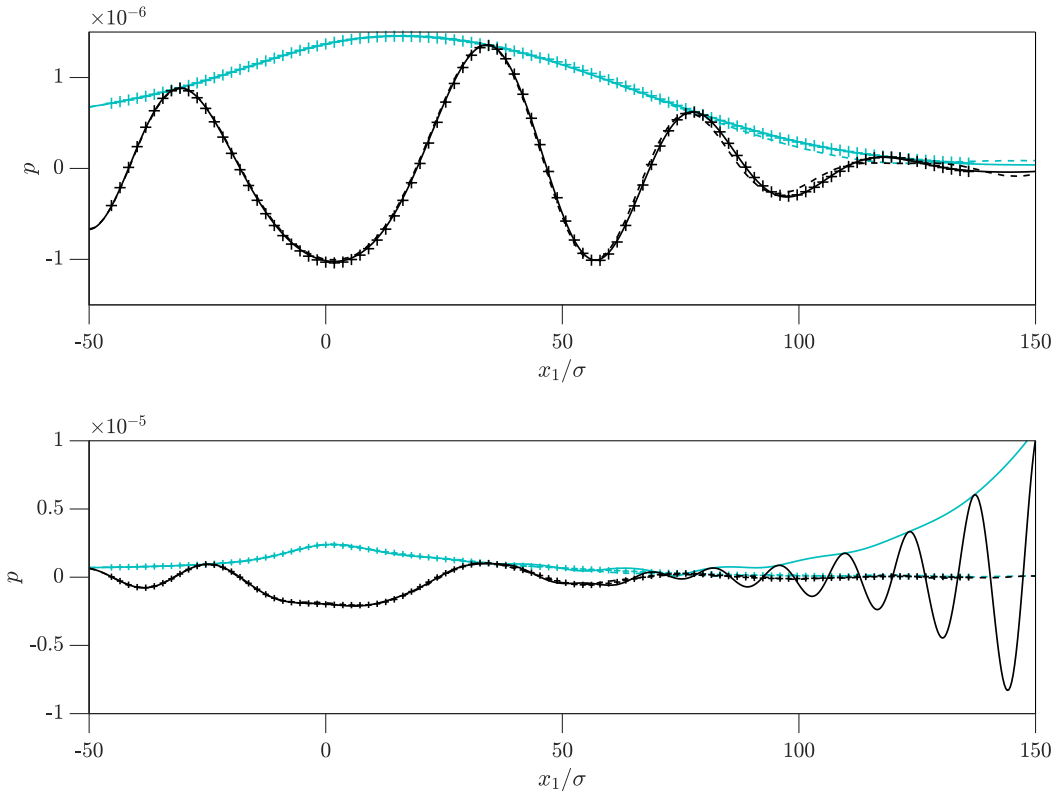

Figure 3.5: Pressure field along $x_2/\sigma \approx 45.3$ (top) and $x_2/\sigma \approx 13.6$ (bottom). The analytical solution + (Agarwal et al., 2004), the fine grid solution —— and the coarse grid solution - - - are compared. The pressure real part is in **black**, its absolute value is in **turquoise**.

the fourth CAA workshop using coarse meshes. Note that if this trick is used, then the convergence of the solution is not guaranteed if a finer grid and smaller time step is chosen. The occurrence of an instability wave in solutions of PROPA comes in opposition with a result of Rao and Morris (2006), who argued that no instability wave solution can occur when a direct inversion method is used in the frequency domain. This contradiction has already been pointed out in the literature, and (Casalino, 2012; Angeloski et al., 2014) stressed that the use of a direct inversion method is not a sufficient condition to guarantee stability. Karabasov and Hynes (2005); Karabasov et al. (2007) have shown that iterative solver are able to filter out the unstable solution, note that this may be the temporal correspondence of grid filtering.

These observations motivated the use of an mesh discretised very finely to assess the stability properties of the acoustic equations analysed in this chapter, and a grid spacing $(\mathrm{d}x_1/\sigma, \mathrm{d}x_2/\sigma)$ of $(0.1, 0.06)$ is chosen. A grid of 650×300 elements (including a 50 cells thick PML layer) is considered in the following and the meaningful computation region is shown in figure 3.6. In this figure the acoustic source S_p is visible. As previously, a symmetry boundary condition is used in the south frontier to simplify the calculations. In chapter 2, linearised Euler's wave equation (LEWE) is derived. Applied to a parallel mean flow, this equation, given in equation (2.18), is claimed to be the equal of the wave equation proposed by Lilley et al. (1972). Both equations are exact reformulation of the LEE for an isobar steady flow, and, in a linearised framework, describe accurately the acoustic mode, the vorticity mode and their interaction. For both wave equations, the entropy mode is not computed. LEWE's fluctuating velocity $\boldsymbol{u}$ is solved for the fourth workshop configuration with PROPA, and its two components are presented in figure 3.7. The Kelvin-Helmholtz instability, characterised by the change of sign for u_1 across the line of maximal

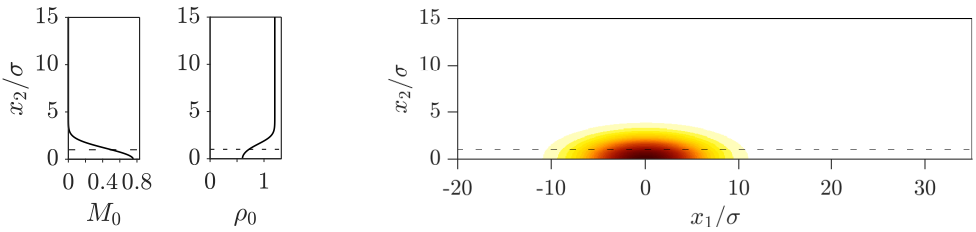

Figure 3.6: Mach number M_0 and density ρ_0 profiles of the mean flow (left), and the broadband acoustic source distirbution S_p (right). Dashed lines represent the position of maximal shearing ($x_2/\sigma = 1$).

shear, and the steady growth of the amplitude when the spots are convected downstream are fairly easy recognisable.

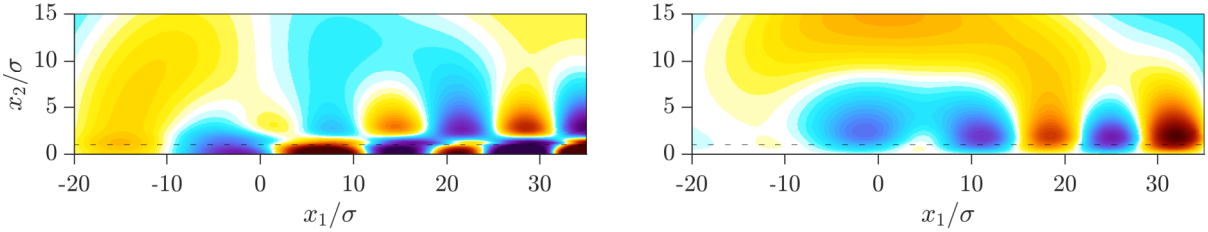

Figure 3.7: Solution of the fourth CAA workshop as computed with LEWE. The real part of the fluctuating velocity $\boldsymbol{u}$, u_1 in the x_1 direction(left), and, u_2 in the x_2 direction (right) are shown.

For a validation of LEWE, against the analytical solution (Agarwal et al., 2004) and the solution to Lilley's wave equation computed with PROPA, the fluctuating pressure p is rebuilt from the fluctuating velocity $\boldsymbol{u}$, by using the linearised energy equation,

$$\mathrm{D}_{\boldsymbol{u}_0}(p) = S_p - \gamma p_0 \nabla \cdot \boldsymbol{u} \tag{3.6}$$

The comparison between the pressure fields obtained with LEWE and Lilley's equation is presented in figure 3.8. The agreement is excellent for the instability wave, as well for the acoustic field, and matches the available analytical solution Agarwal et al. (2004). The correctness of the new wave equation proposed, its implementation in PROPA, and the *a posteriori* reconstruction method of the fluctuating pressure p used for LEWE's solution is thereby validated. For predicting identically the instability wave with different acoustic operators, it can reasonably be deemed that mesh convergence is now satisfied.

If LEWE is equivalent to Lilley's equation when applied to a parallel mean flow, some philosophical differences may however be pointed out. First while Lilley's formulation is a third order operator, LEWE keeps the structure of a second order d'Alembertian so that, in a region at rest LEWE shrinks into the wave equation for the fluctuating velocity $\boldsymbol{u}$. The source term for LEWE is then interestingly simpler than for Lilley's equation. Lilley's equation source term is given in (3.16) of part II, and LEWE's source term in equation (2.19) (to be simplified for a parallel mean flow). In LEWE's source, no mean-flow derivative appear any more in the term associated with S_p. According to Goldstein (2010, §3), the presence of such contributions in the source term indicates that generation and propagation mechanisms are not fully decoupled. This seems to be achieved here for the source term S_p of the energy equation.

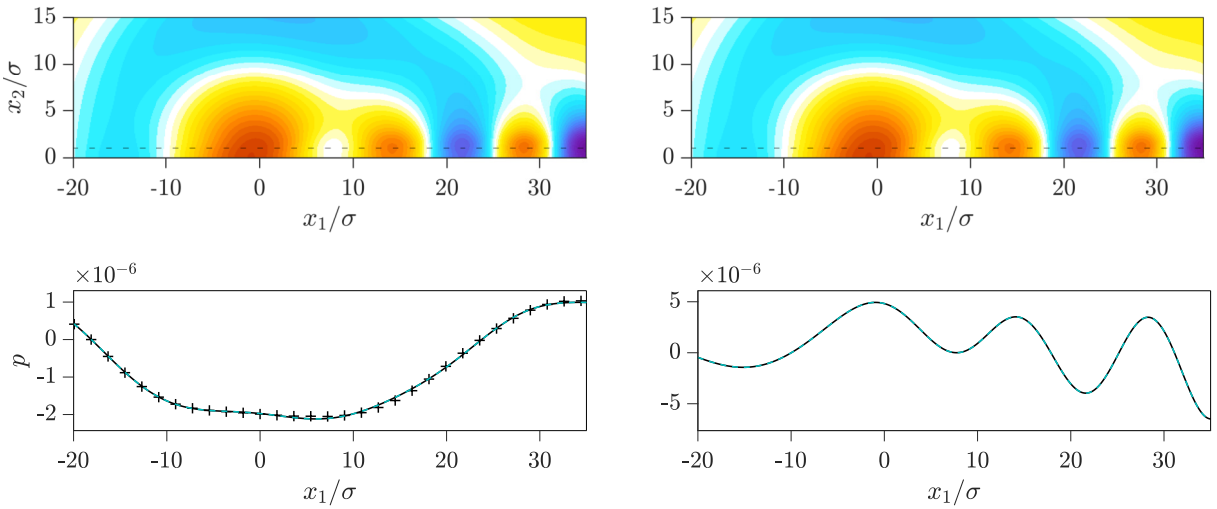

Figure 3.8: Pressure field p computed from LEWE's velocity fluctuations $\boldsymbol{u}$ (top-left) and from Lilley's equation (top-right). Pressure p extracts taken along $x_2/\sigma \approx 13.6$ (bottom-left) and along $x_2/\sigma = 0$ (bottom-right). $+ + +$ analytical solution Agarwal et al. (2004), ——Lilley's equation and - - - LEWE.

3.2.2 Self-adjoint kernels of wave equations

The concept of self-adjoint kernel of a linear operator is introduced in this paragraph. The reader not familiar with the adjoint may refer to (Stone and Goldbart, 2009, chap. 4), or in this script to §3.2 of part II and appendix §B.1. In this paragraph, the discussion is conducted in the frequency domain for convenience. The idea introduced is to split a linear operator $\mathcal{L}_0$ into a self-adjoint contribution $\mathcal{K}_0$, the so-called self-adjoint kernel, and a non-self-adjoint part $\mathcal{N}_0$,

$$\mathcal{L}_0 = \mathcal{K}_0 + \mathcal{N}_0 \tag{3.7}$$

The stabilisation strategy proposed here consists in restricting a linear operator $\mathcal{L}_0$ to its self-adjoint kernel, i.e. $\mathcal{L}_0 \approx \mathcal{K}_0$, and is based on a remark of Möhring (1999, §2.4). This author presented how a variational principle can be derived from a self-adjoint equation, and simultaneously highlighted, that this guarantees the energy conservation in the system. In this paragraph, the notion of self-adjointness of a linear operator $\mathcal{K}_0$ is understood as $\mathcal{K}_0^\dagger = \pm\mathcal{K}_0$, according to the enlarged acceptance introduce in §3.2.2 of part II. The decomposition given in equation (3.7) is obviously not unique, the idea is to find the best approximation $\mathcal{K}_0$ of $\mathcal{L}_0$ that minimises the error in the acoustic computation when $\mathcal{N}_0$ is neglected.

To make this concept less abstract, this theory is applied to Lilley's operator $\mathcal{L}_0$, which adjoint operator $\mathcal{L}_0^\dagger$ is computed in §3.3.1. These two wave equations write for a variable p as,

$$\begin{aligned}
\mathcal{L}_0\ p &= \mathrm{D}_{\boldsymbol{u}_0}\left(\mathrm{D}^2_{\boldsymbol{u}_0}(p) - \nabla\cdot(a_0^2\nabla p)\right) + 2a_0^2\nabla u_{0,1}\cdot\nabla\left(\frac{\partial p}{\partial x_1}\right)\\
\mathcal{L}_0^\dagger\ p^\dagger &= -\mathrm{D}_{\boldsymbol{u}_0}\left(\mathrm{D}^2_{\boldsymbol{u}_0}(p^\dagger) - \nabla\cdot(a_0^2\nabla p^\dagger)\right) + 4a_0^2\nabla u_{0,1}\cdot\nabla\left(\frac{\partial p^\dagger}{\partial x_1}\right) + 3a_0^2\Delta u_{0,1}\frac{\partial p^\dagger}{\partial x_1} + 3\frac{\partial p^\dagger}{\partial x_1}\nabla a_0^2\cdot\nabla u_{0,1}
\end{aligned} \tag{3.8}$$

Blatantly, $\mathcal{L}_0^\dagger \neq \pm\mathcal{L}_0$ and Lilley's wave equation is not self-adjoint. This is obvious, since this linear operator could otherwise not describe any instability wave. A possible self-adjoint kernel decomposition

of Lilley's operator could be achieved in identifying $\mathcal{K}_0$ and $\mathcal{N}_0$ with,

$$\left\{ \begin{array}{l} \mathcal{K}_0 = \mathrm{D}_{\boldsymbol{u}_0}\left(\mathrm{D}^2_{\boldsymbol{u}_0}(p) - \nabla\cdot(a_0^2\nabla p)\right) \\ \\ \mathcal{N}_0 = 2a_0^2\nabla u_{0,1}\cdot\nabla\left(\dfrac{\partial p}{\partial x_1}\right) \end{array} \right. \tag{3.9}$$

This self-adjoint kernel of Lilley's equation verifies $\mathcal{K}_0^\dagger = -\mathcal{K}_0$ and is stable; it is simply the material derivative of Phillips' wave equation (1960). Because in discarding the non-self-adjoint part, the mean velocity gradients $\nabla u_{0,1}$ have been simultaneously removed, the ability of Phillips' equation to account for the flow acoustic refraction is expected to be altered with respect to Lilley's equation.

It is crucial to bear in mind that the adjoint framework always relies upon the prior definition of a scalar product, so does the self-adjointness concept. For Lilley's equation which is scalar, the scalar product introduced in §3.3.1 of part II seems self-evident. For a multi-dimensional linear operator, some non-obvious scalar product may reveal interesting symmetry features in the equations. Let $\mathbf{H}\left(\equiv\mathbf{H}(\boldsymbol{x})\right)$ be an hermitian matrix from which a scalar product $<\ ,\ >_{\mathbf{H}}$ can be built for a domain $\boldsymbol{x}\in\Omega$, and let $\boldsymbol{q}_H^\dagger\left(\equiv\boldsymbol{q}_H^\dagger(\boldsymbol{x})\right)$ be the adjoint field associated to $\boldsymbol{q}\left(\equiv\boldsymbol{q}(\boldsymbol{x})\right)$ with respect to $<\ ,\ >_{\mathbf{H}}$. Lagrange's identity can be written in this matricial context as,

$$<\boldsymbol{q}_H^\dagger,\mathcal{L}_0\boldsymbol{q}>_{\mathbf{H}} = \int_{\boldsymbol{x}\in\Omega} {\boldsymbol{q}_H^\dagger}^{T*}\cdot\mathbf{H}\cdot\mathcal{L}_0\boldsymbol{q} = \int_{\boldsymbol{x}\in\Omega}\left(\mathcal{L}_0^\dagger\boldsymbol{q}_H^\dagger\right)^{T*}\cdot\mathbf{H}\cdot\boldsymbol{q} = <\mathcal{L}_0^\dagger\boldsymbol{q}_H^\dagger,\boldsymbol{q}>_{\mathbf{H}} \tag{3.10}$$

Note that this change in the scalar product should echo consistently on the representation theorem, which may become more complex. Underline that the adjoint field $\boldsymbol{q}_H^\dagger$ intrinsically relies upon an operator and a scalar product. Thus, no comparison between adjoint fields obtained with different scalar products can make sense Spieser and Bailly (2018), even less adjoint variables obtained with different operator, e.g. adjoint Lilley's equation and Phillips' equation.

The multiple possibilities to define scalar products $<\ ,\ >_{\mathbf{H}}$ are as many occasions to find an appropriate self-adjoint kernel $\mathcal{K}_0$ to approximate a linear operator $\mathcal{L}_0$. Another stable alternative to Lilley's equation is presented thanks to this enhanced multi-variable framework. This is achieved by recalling that Lilley's wave equation is equivalent to the linearised Euler's equations $\mathcal{L}_0$ for a parallel base flow,

$$\mathcal{L}_0\begin{pmatrix}\boldsymbol{u}\\ p\end{pmatrix} \equiv \left\{ \begin{array}{l} \mathrm{D}_{\boldsymbol{u}_0}(\boldsymbol{u}) + (\nabla\boldsymbol{u}_0)\cdot\boldsymbol{u} + \dfrac{\nabla p}{\rho_0} = \mathbf{0} \\ \\ \mathrm{D}_{\boldsymbol{u}_0}(p) + \gamma p_0(\nabla\cdot\boldsymbol{u}) = 0 \end{array} \right. \tag{3.11}$$

A self-adjoint kernel $\mathcal{K}_0$ for this operator can be defined as,

$$\mathcal{K}_0\begin{pmatrix}\boldsymbol{u}\\ p\end{pmatrix} \equiv \left\{ \begin{array}{l} \mathrm{D}_{\boldsymbol{u}_0}(\boldsymbol{u}) + \dfrac{\nabla p}{\rho_0} = \mathbf{0} \\ \\ \mathrm{D}_{\boldsymbol{u}_0}(p) + \gamma p_0(\nabla\cdot\boldsymbol{u}) = 0 \end{array} \right. \tag{3.12}$$

That is, by removing the $(\nabla\boldsymbol{u}_0)\cdot\boldsymbol{u}$ term. It is known that these set of equations are skew-symmetric (Serre et al., 2012), and a symmetriser $\mathbf{S}$ for the latter therefore exists. The scalar product $<\ ,\ >_{\mathbf{S}}$, for

which $\mathcal{K}_0$ is self adjoint is given by,

$$\mathbf{S} = \begin{pmatrix} \rho_0 \mathbf{I} & \mathbf{0} \\ \mathbf{0}^T & \dfrac{1}{\gamma p_0} \end{pmatrix} \tag{3.13}$$

Note that a similar symmetriser was proposed in (Barone et al., 2009, eq. (26)). It is straightforward to verify that for a parallel mean flow, $\mathcal{K}_0^\dagger = -\mathcal{K}_0$ with respect to $< , >_{\mathbf{S}}$. As for Lilley's equation, the set of equations (3.12) can be combined together to eliminate $\boldsymbol{u}$ in favour of p, leading to the stable Lilley equation of Bogey et al. (2002),

$$\mathcal{K}_0\ p = \mathrm{D}_{\boldsymbol{u}_0}\left(\mathrm{D}^2_{\boldsymbol{u}_0}(p) - \nabla\cdot(a_0^2\nabla p)\right) + a_0^2\nabla u_{0,1}\cdot\nabla\left(\frac{\partial p}{\partial x_1}\right) \tag{3.14}$$

When comparing equations (3.9) and (3.14), it is apparent that the second proposition for $\mathcal{K}_0$ approximates more closely Lilley's wave equation. The solution for both wave equations to the fourth CAA workshop with similar settings as shown in figure 3.6 is presented in figure 3.9. It is observed that both wave equations are indeed stable.

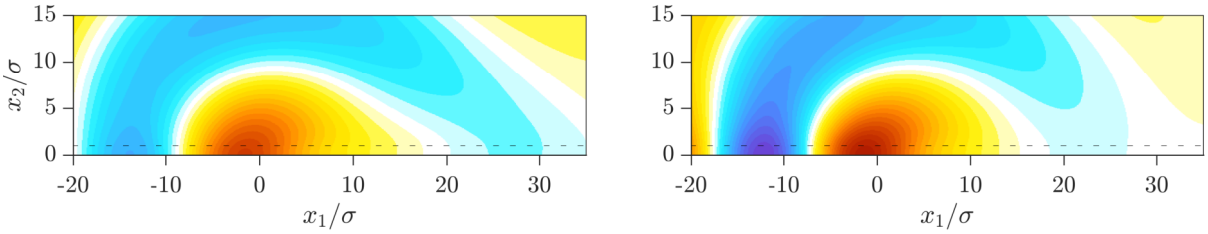

Figure 3.9: Pressure fluctuations p computed for the fourth CAA workshop. The solutions obtained with stable Lilley's equation (left) and Phillips' equation (right) are presented.

3.2.3 Two stable approximates of LEWE

In the LEWE, terms containing mean velocity gradients are manifold. It is expected that the reduction of LEWE to one of his self-adjoint kernel can be achieved with less stringent simplifications of the mean flow derivatives than for Lilley's equation presented here above. The obtained self-adjoint kernels of LEWE would then be twofold, stable and more accurate than stable Lilley's equation. Recall firstly that for a parallel mean flow, the operator of linearised Euler's wave equations simplifies into,

$$\mathcal{L}_0(\boldsymbol{u}) = D^2_{\boldsymbol{u}_0}(\boldsymbol{u}) + \left[(\nabla\boldsymbol{u}_0) + (\nabla\boldsymbol{u}_0)^T\right]\cdot D_{\boldsymbol{u}_0}(\boldsymbol{u}) + (\nabla\boldsymbol{u}_0)^T\cdot(\nabla\boldsymbol{u}_0)\cdot\boldsymbol{u} - a_0^2\nabla(\nabla\cdot\boldsymbol{u}) \tag{3.15}$$

The canonical multivariable scalar product is the simplest variant of equation (3.10) for which $\mathbf{H} = \mathbf{I}$. Computing the adjoint equation of LEWE associated with this scalar product reveals that only the term containing the mean-flow strain rate, i.e. $\left[(\nabla\boldsymbol{u}_0) + (\nabla\boldsymbol{u}_0)^T\right]\cdot D_{\boldsymbol{u}_0}(\boldsymbol{u})$, is non-symmetric. A self-adjoint kernel for LEWE is then realised with,

$$\mathcal{K}_{0,\boldsymbol{I}}(\boldsymbol{u}) = D^2_{\boldsymbol{u}_0}(\boldsymbol{u}) + (\nabla\boldsymbol{u}_0)^T\cdot(\nabla\boldsymbol{u}_0)\cdot\boldsymbol{u} - a_0^2\nabla(\nabla\cdot\boldsymbol{u}) \tag{3.16}$$

This stable wave equation is referred to in the following as LEWE-KI.

Another self-adjoint kernel is introduced from LEWE; it is induced by a scalar product that is worth of

attention. For this parallel flow problem, without loss of generality, the first axis of the coordinate system may be aligned with the mean-flow direction, so that $\boldsymbol{u}_0 = (|\boldsymbol{u}_0|, \mathbf{0})^T$. An interesting hermitian matrix $\mathbf{H} = \mathbf{T}$ is then obtained by a twisting of the axis,

$$\mathbf{T} = \rho_0 \begin{pmatrix} 1 & \mathbf{0}^T \\ \mathbf{0} & \text{- } \mathbf{I} \end{pmatrix} \tag{3.17}$$

From the computation of the associated adjoint operator, nearly all terms are found self-adjoint except one involving $\nabla \times \nabla \times \boldsymbol{u}$. Recalling that, $\nabla(\nabla \cdot \boldsymbol{u}) = \Delta \boldsymbol{u} + \nabla \times \nabla \times \boldsymbol{u}$ an other self-adjoint kernel of LEWE is given by,

$$\mathcal{K}_{0,\boldsymbol{T}}(\boldsymbol{u}) = D^2_{\boldsymbol{u}_0}(\boldsymbol{u}) + \left[(\nabla \boldsymbol{u}_0) + (\nabla \boldsymbol{u}_0)^T\right] \cdot D_{\boldsymbol{u}_0}(\boldsymbol{u}) + (\nabla \boldsymbol{u}_0)^T \cdot (\nabla \boldsymbol{u}_0) \cdot \boldsymbol{u} - a_0^2 \Delta \boldsymbol{u} \tag{3.18}$$

This stable wave equation is baptised as LEWE-KT. The latter wave equation provides hope for an accurate description of acoustic propagation effects, since no mean flow derivatives have been removed in the approximation.

To verify their stability, both operators LEWE-KI and LEWE-KT are implemented in PROPA and their solution to the fourth workshop is calculated. The same source term as for LEWE is used in both cases, and the corresponding pressure fields p are rebuilt *a posteriori* with the same procedure as for the validation of LEWE. The results are shown in figure 3.10. As expected no instability wave are visible and both operators are stable. However the author observed that LEWE-KI appeared to be numerically unstable in the very low-frequency limit when the grid is underdiscretised in regions where the mean-flow field is varying. Indeed, the stabilisation procedure proposed here guaranties the operator to preserve acoustic energy but does not give any guaranty for it numerical well-posedness. No such problem was observe with LEWE-KT.

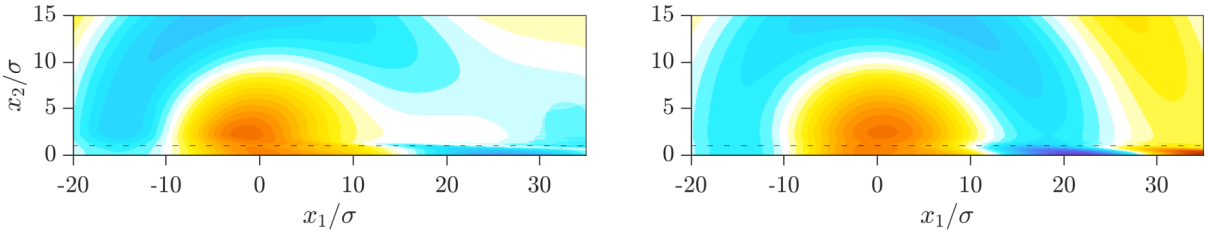

Figure 3.10: Pressure fluctuations p computed for the fourth CAA workshop with LEWE-KI (left) and LEWE-KT (right). Equation (3.6) is used to retrieve the pressure p from the velocity fluctuations $\boldsymbol{u}$.

For completeness, the solution to the fourth CAA workshop on this ultra fine mesh is provided for LEWE-AP and for Pierce's wave equation in figure 3.11. These acoustic potential wave equations are two other stable variants of LEWE which have been derived in §2.5.2.

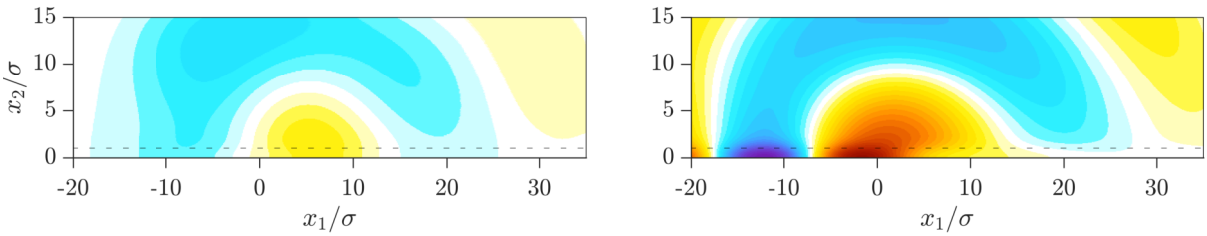

Figure 3.11: Pressure fluctuations p computed for the fourth CAA workshop with LEWE-AP (left) and Pierce's wave equation (right). The pressure field p is retrieved using $p = -\mathrm{D}_{\boldsymbol{u}_0}(\phi)$.

3.3 Benchmark of nine linear acoustic operators

In this section, the acoustic prediction achieved with the eight linear operators mentioned previously are compared on a numerical test case. Two of them, Lilley's equation and LEWE, describe accurately the acoustic mode as well as the vorticity mode, the six other are stable wave equations that meant to account solely for acoustic propagation. For a more complete comparison of stable sound propagation operator, the second version of the acoustic perturbation equations is added to the analysis (Ewert and Schröder, 2003, eq. (53)-(55)). The linear operators corresponding to the here investigated acoustic equations are recalled in table 3.1; all of them have been implemented in PROPA.

The sound propagation of a point source set in a sheared and heated flow profile is considered for the benchmark. For the acoustic field to present a realistic tree-dimensional decay, the configuration is chosen axisymmetric, and the source is set on the symmetry axis. The author noted that axisymmetric configurations are less susceptible to trigger instability waves than corresponding two-dimensional flows; and the present mean flow is stable for the frequency range considered. The same type of base flow as for the fourth workshop is considered, that is a Gaussian velocity $\boldsymbol{u}_0$ profile, as given in equation (3.4), with an evolution of the mean density ρ_0 that obeys Crocco-Busemann's law, equation (3.5). The same temperature ratio $T_j/T_\infty = 2$, and the same ambient pressure p_0 as in the workshop of (2004) are considered. Yet, the jet flow Mach number is set to $M_j = 0.9$, and from Crocco-Busemann's law, the mean density ρ_0 is consequently different from the evolution considered in the CAA workshop. The mesh considered for the resolution is uniform, composed of 350×350 cells, and includes a PML layer of 50 elements. The numerical domain with the PML ranges from $(x_1/\sigma,\, x_2/\sigma) \in [-6, 12] \times [0, 15]$. The standard deviation σ_s taken for the compact Gaussian sound source equals $\sigma_s/\sigma = 0.136$. A synthetic visual of the configuration used for the acoustic operators benchmark is provided in figure 3.12.

This comparative study evaluates the nine linear operators for a set of acoustic pulsations $\omega = 2\pi f$ ranging in $\omega \in (63,\, 126,\, 252,\, 630,\, 1260,\, 3780)$ rad.s^{-1}, and associated with a Strouhal number of $St_{2\sigma} = 2\sigma f/u_j \in (0.05,\, 0.1,\, 0.2,\, 0.5,\, 1.0,\, 3.0)$. Figures 3.13 to 3.18 present the real part of the pressure p computed. Their absolute part, also corresponding to the acoustic root mean square, are presented in figures 3.19 to 3.24. At a given frequency, identical colormaps are considered for all real part and absolute part plots. The range of the colormap is chosen to vary linearly with ω, so to compensate the efficiency increase of the source radiation with the frequency. Lilley's equation and LEWE do not neglect any term in the sound propagation calculus and delivers the reference solutions. From these results some remarks are drawn:

- As a first observation, the more the frequency increases, the better the approximated acoustic equations meet the correct solution. This was to be expected, since in the high frequency limit, the geometrical acoustic limit is retrieved for all wave equations.

Linear operator	**Homogeneous expression**
Lilley's equation	$D_{\boldsymbol{u}_0}\left(D^2_{\boldsymbol{u}_0}(p) - \nabla\cdot(a_0^2\nabla p)\right) + 2a_0^2\nabla u_{0,z}\cdot\nabla\left(\dfrac{\partial p}{\partial z}\right) = 0$
stable Lilley's equation	$D_{\boldsymbol{u}_0}\left(D^2_{\boldsymbol{u}_0}(p) - \nabla\cdot(a_0^2\nabla p)\right) + a_0^2\nabla u_{0,z}\cdot\nabla\left(\dfrac{\partial p}{\partial z}\right) = 0$
Phillips' equation	$D^2_{\boldsymbol{u}_0}(p) - \nabla\cdot(a_0^2\nabla p) = 0$
Linearised Euler's wave equation (LEWE)	$D^2_{\boldsymbol{u}_0}(\boldsymbol{u}) + \left[(\nabla\boldsymbol{u}_0) + (\nabla\boldsymbol{u}_0)^T\right]\cdot D_{\boldsymbol{u}_0}(\boldsymbol{u}) + (\nabla\boldsymbol{u}_0)^T\cdot(\nabla\boldsymbol{u}_0)\cdot\boldsymbol{u} - a_0^2\nabla(\nabla\cdot\boldsymbol{u}) = \boldsymbol{0}$
LEWE-KI	$D^2_{\boldsymbol{u}_0}(\boldsymbol{u}) + (\nabla\boldsymbol{u}_0)^T\cdot(\nabla\boldsymbol{u}_0)\cdot\boldsymbol{u} - a_0^2\nabla(\nabla\cdot\boldsymbol{u}) = \boldsymbol{0}$
LEWE-KT	$D^2_{\boldsymbol{u}_0}(\boldsymbol{u}) + \left[(\nabla\boldsymbol{u}_0) + (\nabla\boldsymbol{u}_0)^T\right]\cdot D_{\boldsymbol{u}_0}(\boldsymbol{u}) + (\nabla\boldsymbol{u}_0)^T\cdot(\nabla\boldsymbol{u}_0)\cdot\boldsymbol{u} - a_0^2\Delta\boldsymbol{u} = \boldsymbol{0}$
LEWE-AP	$\nabla\left[D^2_{\boldsymbol{u}_0}(\Phi) - \nabla\cdot(a_0^2\nabla\Phi)\right] + (\nabla\times\boldsymbol{u}_0)\times\boldsymbol{A}(\Phi) = \boldsymbol{0}$ with $\boldsymbol{A}(\Phi) = \nabla(D_{\boldsymbol{u}_0}(\Phi)) - \left[(\nabla\boldsymbol{u}_0) + (\nabla\boldsymbol{u}_0)^T\right]\cdot\nabla\Phi$ and $\rho_0\boldsymbol{u} = \nabla\Phi$
Pierce's equation	$D^2_{\boldsymbol{u}_0}(\Phi) - \nabla\cdot\left(a_0^2\nabla\Phi\right) = 0 \qquad \text{with} \qquad \rho_0\boldsymbol{u} = \nabla\Phi$
Acoustic perturbation equations (APE v. 2)	$\begin{cases} D_{\boldsymbol{u}_0}(\rho) + \nabla\cdot(\rho_0\boldsymbol{u}) = 0 \\ \dfrac{\partial\boldsymbol{u}}{\partial t} + \nabla(\boldsymbol{u}_0\cdot\boldsymbol{u}) + \nabla\left(\dfrac{p}{\rho_0}\right) = \boldsymbol{0} \end{cases} \quad \text{with} \quad p = a_0^2\rho$

Table 3.1: Summary of the linear acoustic equations investigated.

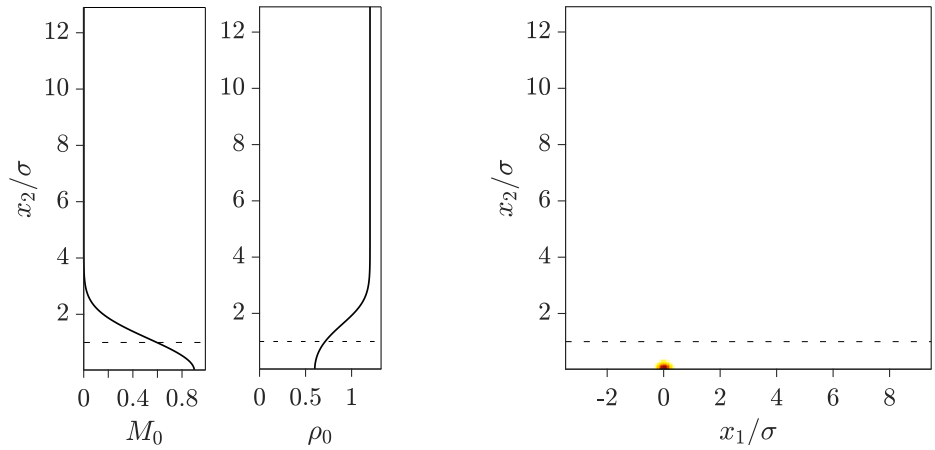

Figure 3.12: Axisymmetric configuration on which the linear operators of table 3.1 are solved.

- An odd behaviour of LEWE-AP is yet to be deplored. The computed wavefronts have singular patterns that significantly differ from the reference solutions (Lilley's equation, LEWE). Very surprisingly with this wave operator, the RMS part of the pressure field does not monotonically decreases with the distance to the sound source. Its numerical implementation in PROPA has been validated in comparing the acoustic potential ϕ computed, with the solution obtained from the linearised Euler's equations for which the relation $\rho_0 \boldsymbol{u} = \nabla\phi$ was enforced; identical results were obtained with both implementations. Different ways to reconstruct the pressure field p of LEWE-AP have been reviewed in appendix §C.4, and none is giving a satisfactory result. It is argued in §2.5.2 of this script, that this wave equation is ill-posed and that Pierce's wave equation must be preferred over LEWE-AP.

- For the lower frequencies that have been investigated, streaks are visible in the solutions of LEWE-KI and LEWE-KT. They likely find their origin in the mathematical simplification that have been conducted in the wave operator without any regard to physics, to create a self-adjoint wave equation. Interestingly stable Lilley's equation does not present such defects. As already mentioned earlier, LEWE-KI, while energetically stable, faces numerical stability issues. Even for the fine grid considered in this study, this is seen in the grid to grid oscillations visible in the low frequency solutions (up to $St = 0.5$) computed by LEWE-KI.

- Even though unphysical streaks are visible in LEWE-KT, the pressure field p out of the sheared flow region seems globally best to be approximated by this wave operator. This is especially true for the lower acoustic frequencies studied. For higher frequencies, Pierce's wave equation and the APE appears to find better agreement with the reference solutions. The comparison of the pressure root mean square given in figure 3.24 indicates this fairly clearly. Strong alikeness is found in the pressure field radiated with stable Lilley's equation and Pierce's equation for the lower frequencies. In this configuration, the low frequency prediction obtained with the APE are not very satisfactory.

- It is instructive also to compare the evolution of the pressure field computed with Lilley's equation, with its stable formulation, and with Phillips' equation. It is observed how the directivity lobe gradually, from Lilley's to Phillips' equation, is tilted in the upstream direction. Phillips's equation consequently overestimates the upstream acoustic radiated field, and this wave equation offers globally the worst acoustic predictions, LEWE-AP excluded. Oppositely, the overall predictions

achieved with Pierce's wave equation are amongst the most accurate. This is paradoxical, because Phillips' and Pierce's wave equations rely upon an identical wave operator. The importance of the choice of the acoustic variable is thereby underlined, the latter is likely to play a more important role than the wave equation itself.

From this comparative benchmark, insight in the behaviour of the acoustic stable equations is gained. Although the predictions achieved with Pierce's equations are not flawless, encouraging results are obtained for the configuration investigated. This result is all the more encouraging, that Pierce's equation is simply a scalar wave equation. For it is seen that the choice of the acoustic variable plays an important role in the propagation, this study could be enhanced by including Möhring's equation in the comparison. The numerical domain is too small to enable a comparison of the far field radiated acoustic field, especially at the lowest frequencies. A larger domain with more points is desirable for such a study. Yet for the configuration investigated, the in-house code PROPA is about to reach the limit in RAM resources of a competitive workstation. In chapter 4 of part II, computations of PROPA are compared to numerical solutions obtained with *Actran TM*, and it is shown that the commercial software handles RAM memory in a much more efficient way than PROPA. Room for improving PROPA seems to exist, and more meaningful domain size may be reached thereby.

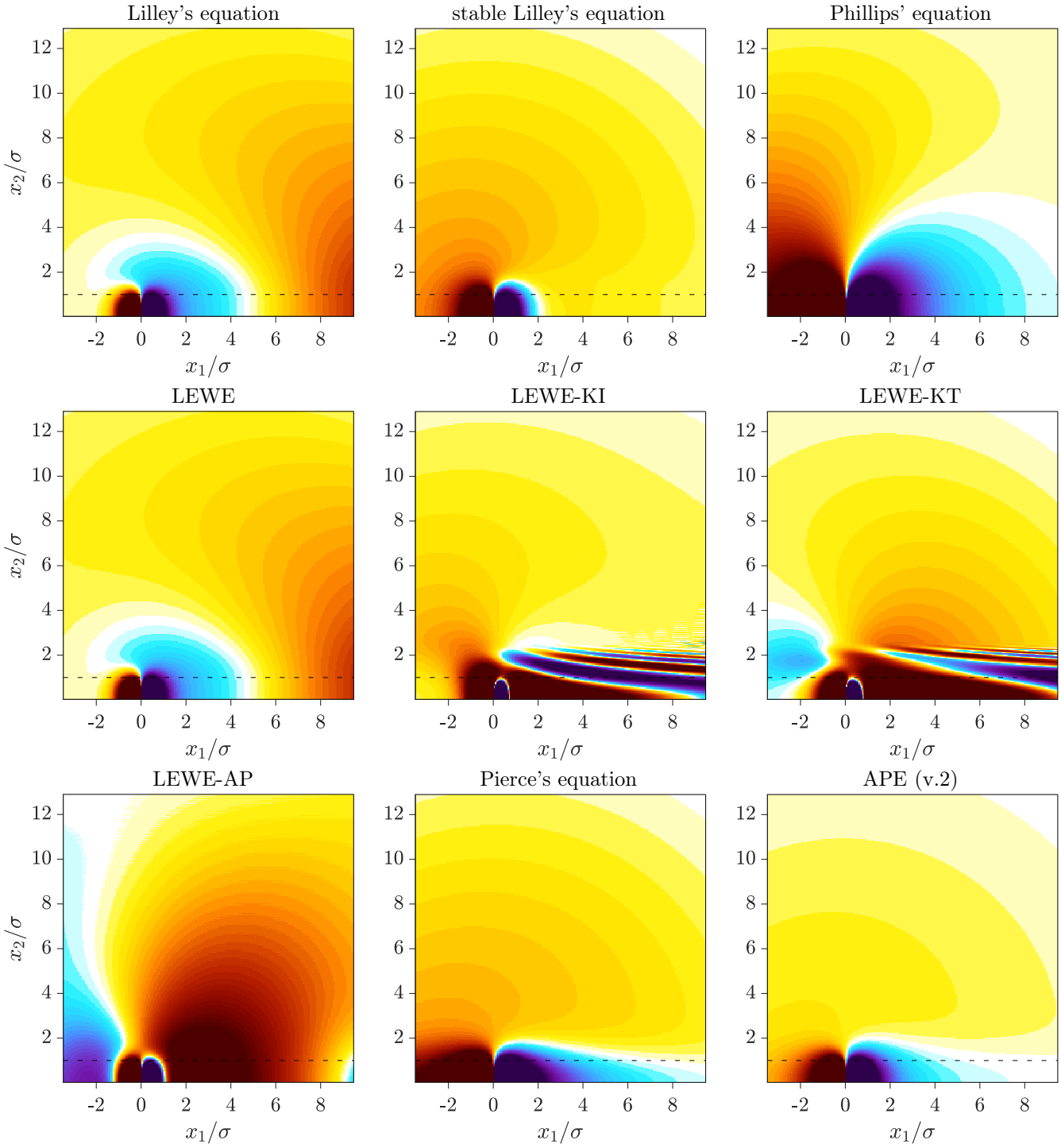

Figure 3.13: Real part of the fluctuating pressure p computed for a Strouhal number of $St = 0.05$.

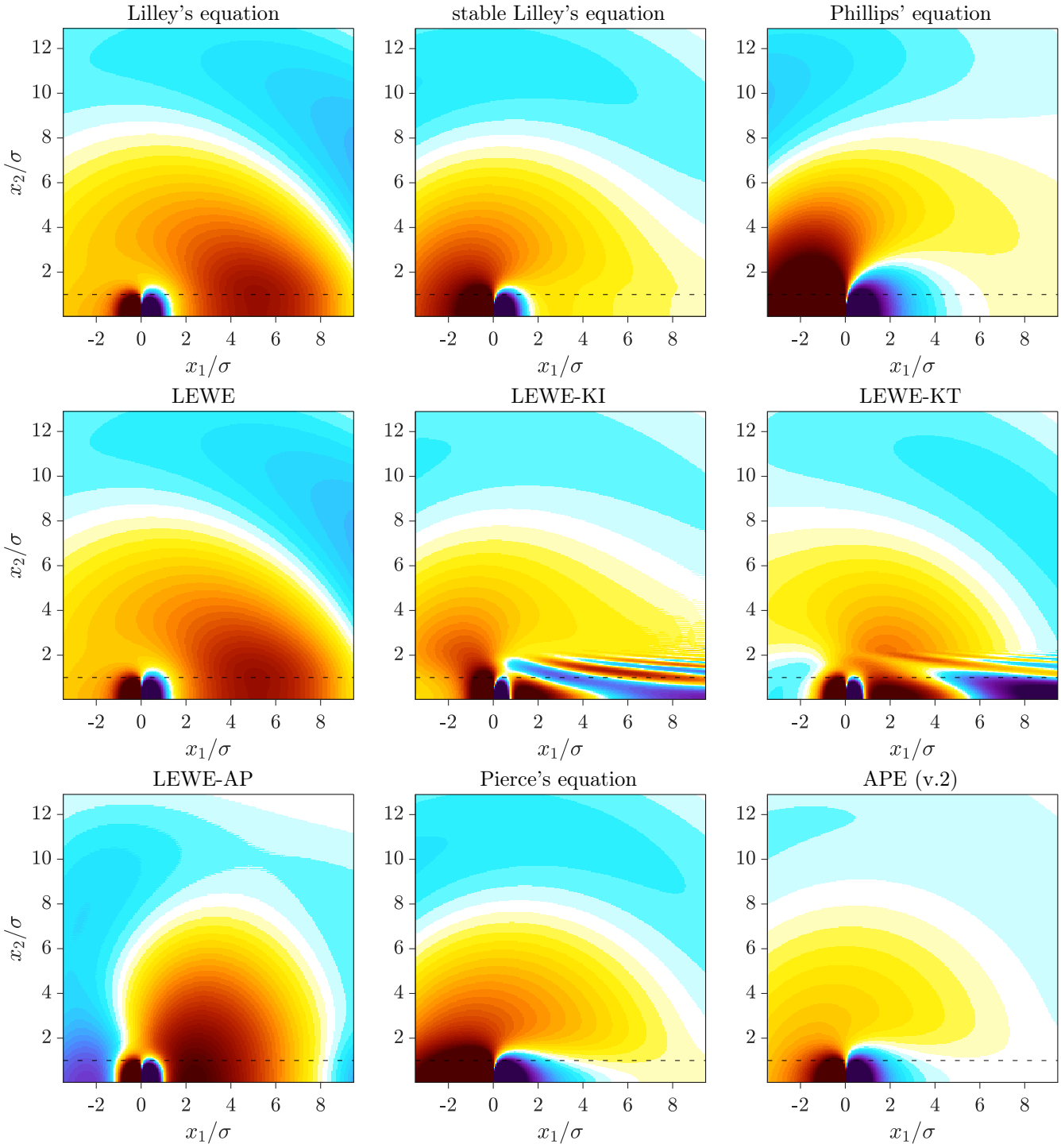

Figure 3.14: Real part of the fluctuating pressure p computed for a Strouhal number of $St = 0.1$.

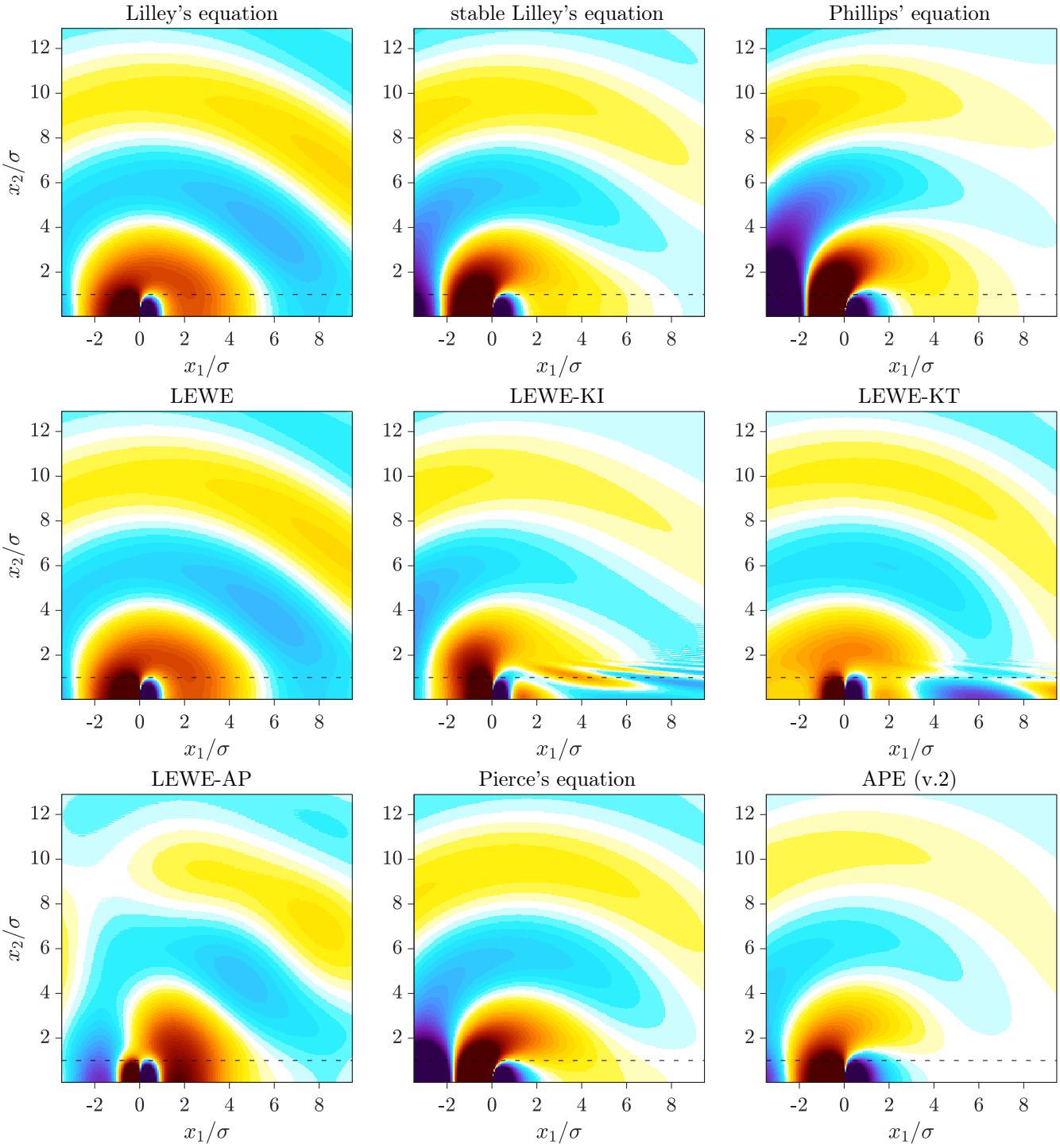

Figure 3.15: Real part of the fluctuating pressure p computed for a Strouhal number of $St = 0.2$.

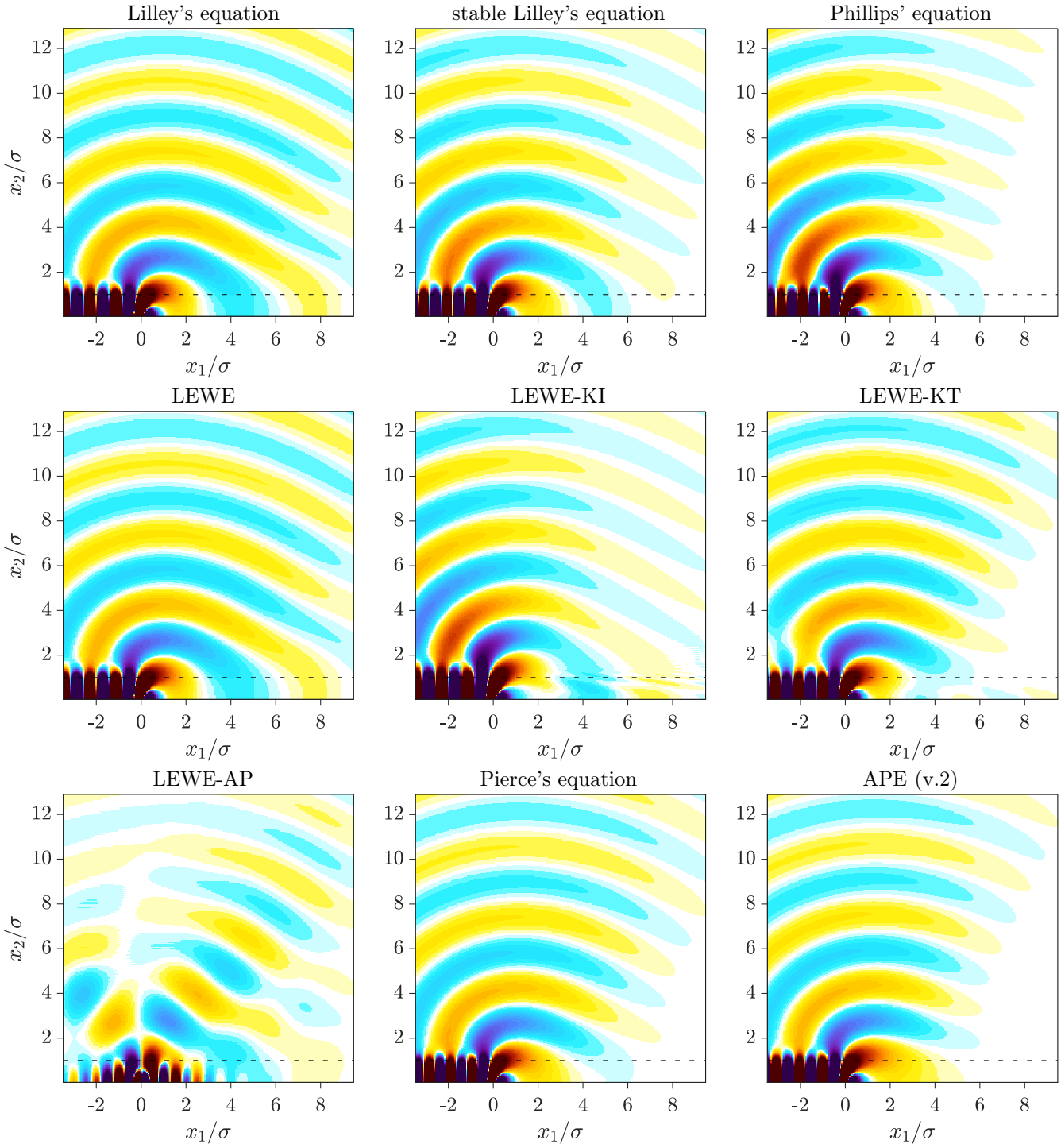

Figure 3.16: Real part of the fluctuating pressure p computed for a Strouhal number of $St = 0.5$.

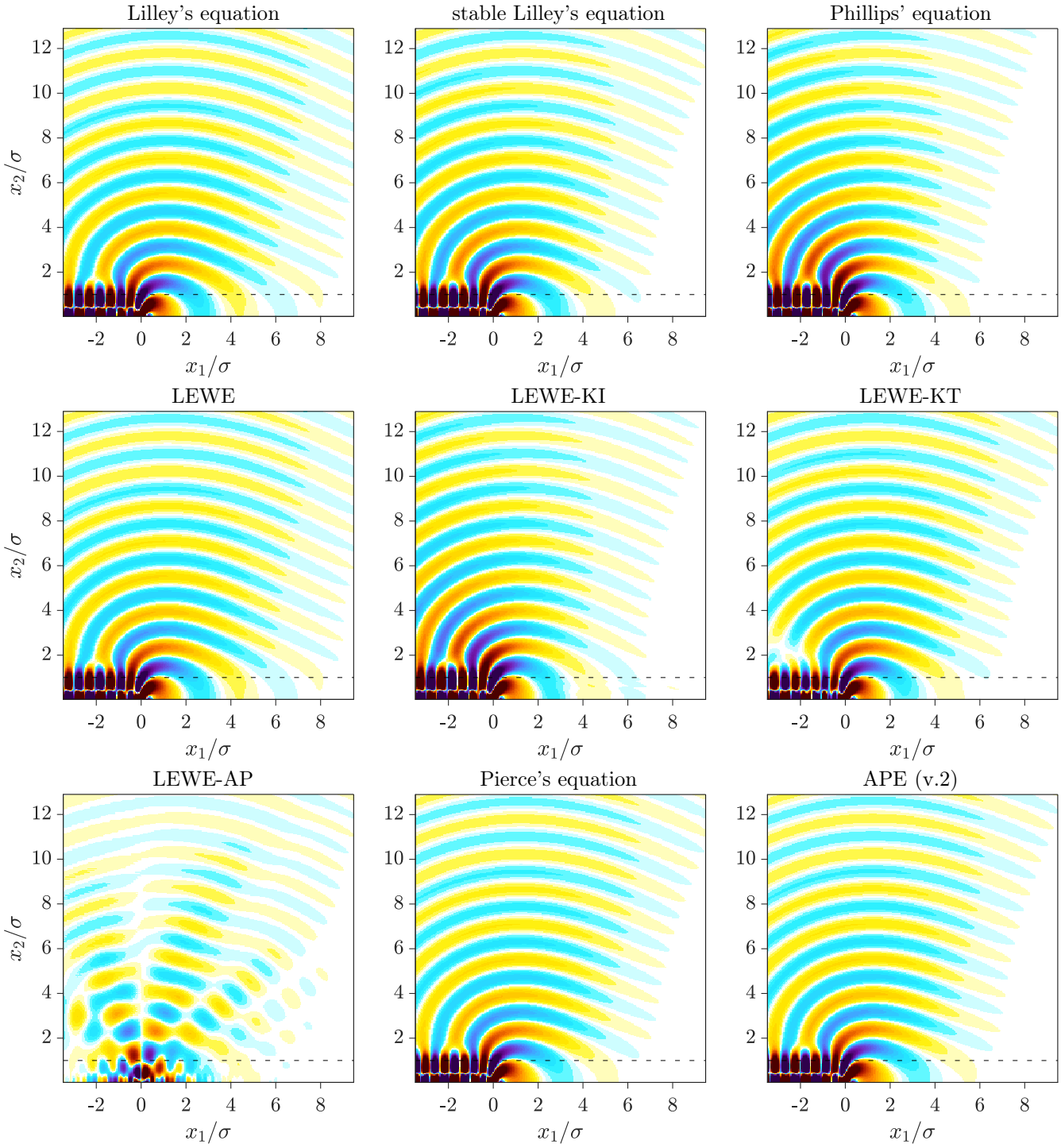

Figure 3.17: Real part of the fluctuating pressure p computed for a Strouhal number of $St = 1$.

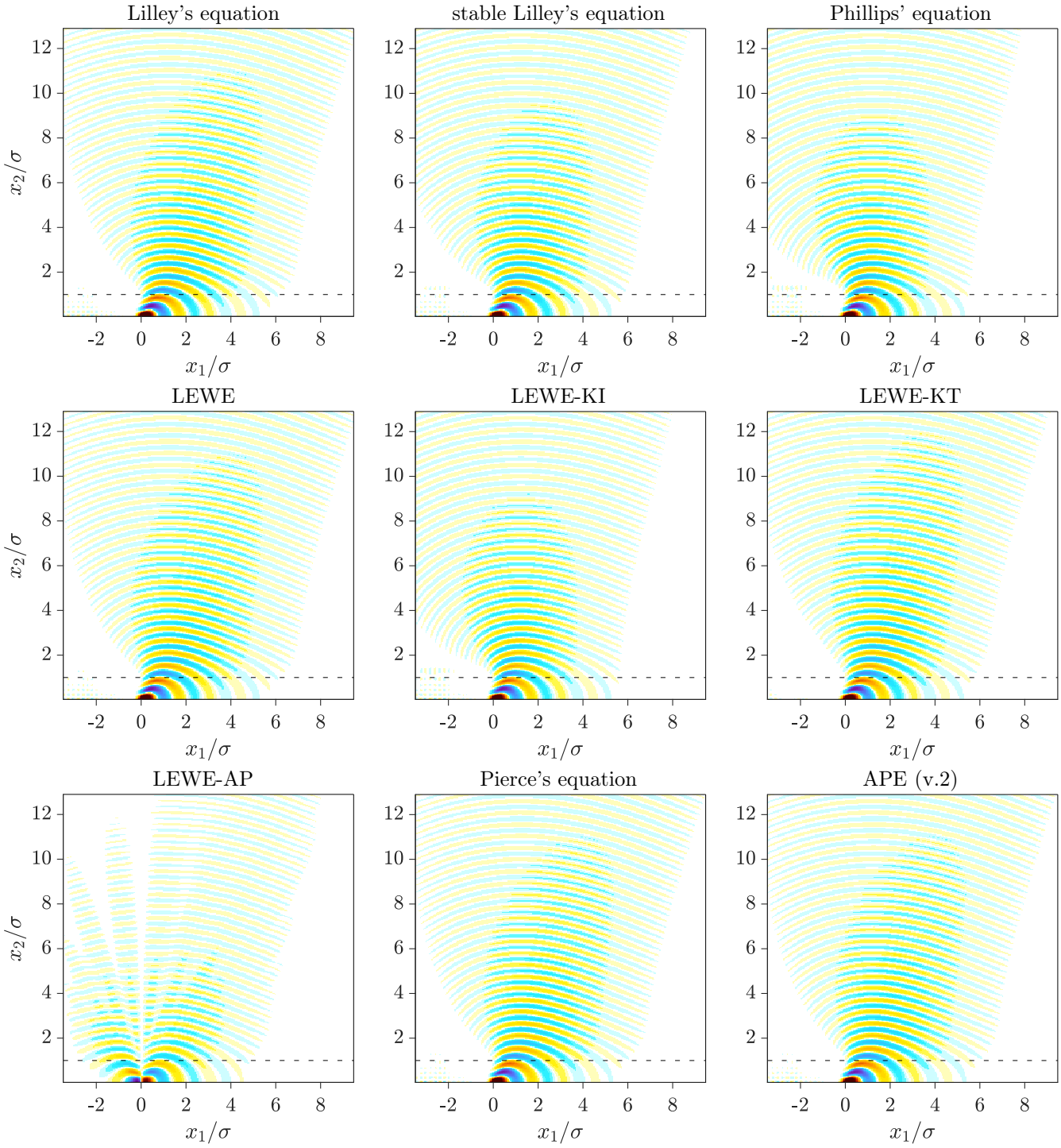

Figure 3.18: Real part of the fluctuating pressure p computed for a Strouhal number of $St = 3$.

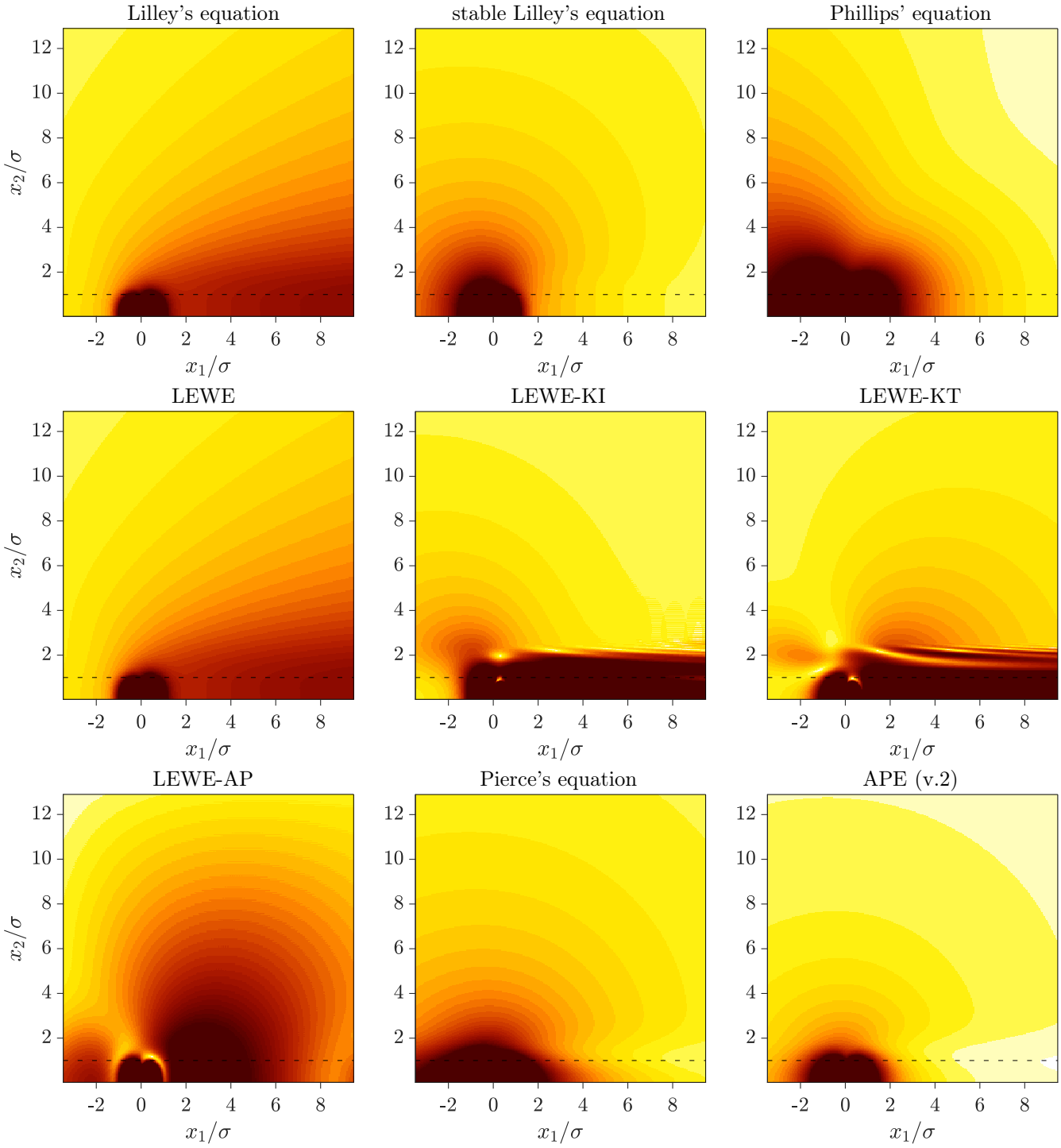

Figure 3.19: Absolute part of the fluctuating pressure p computed for a Strouhal number of $St = 0.05$.

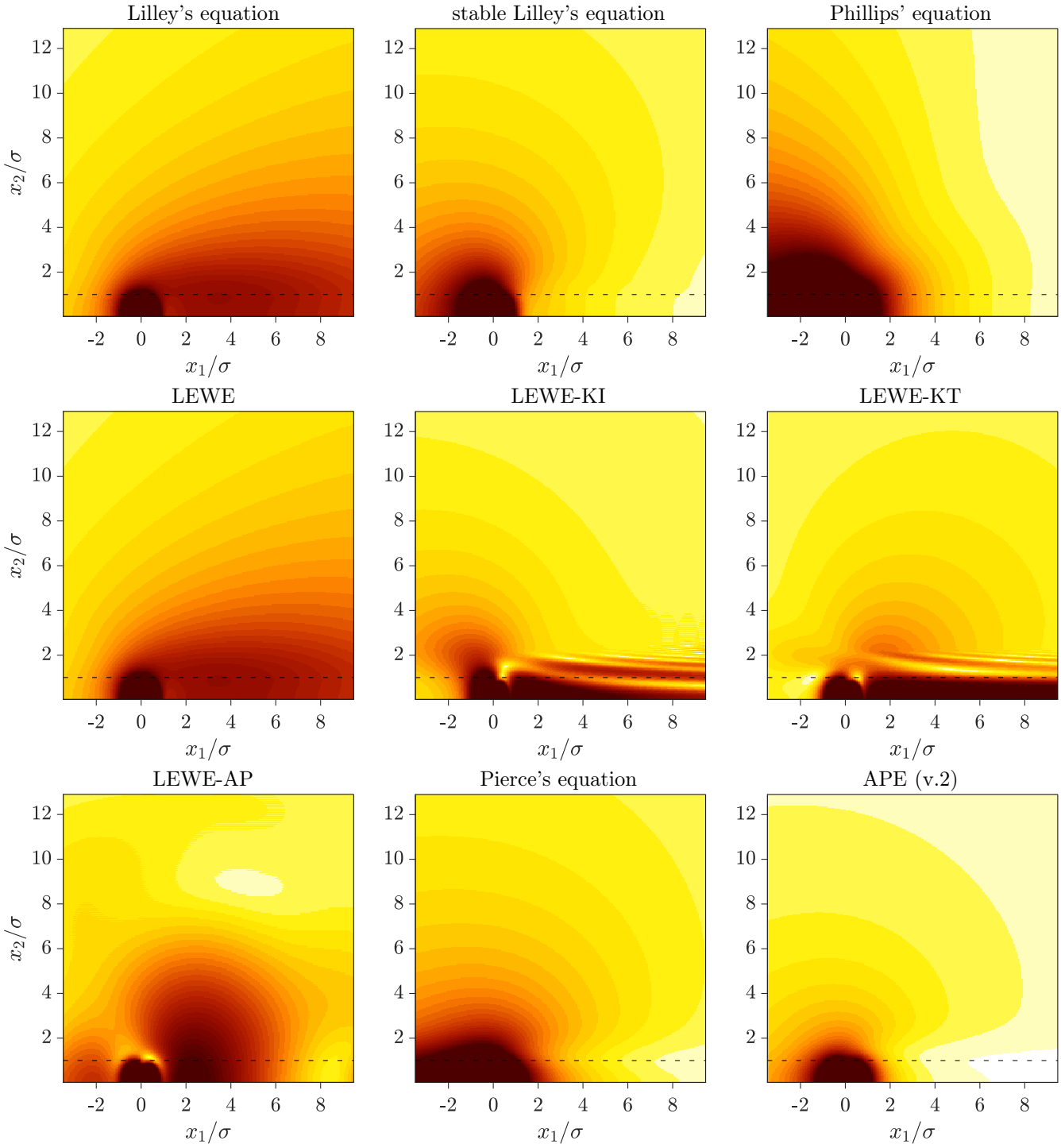

Figure 3.20: Absolute part of the fluctuating pressure p computed for a Strouhal number of $St = 0.1$.

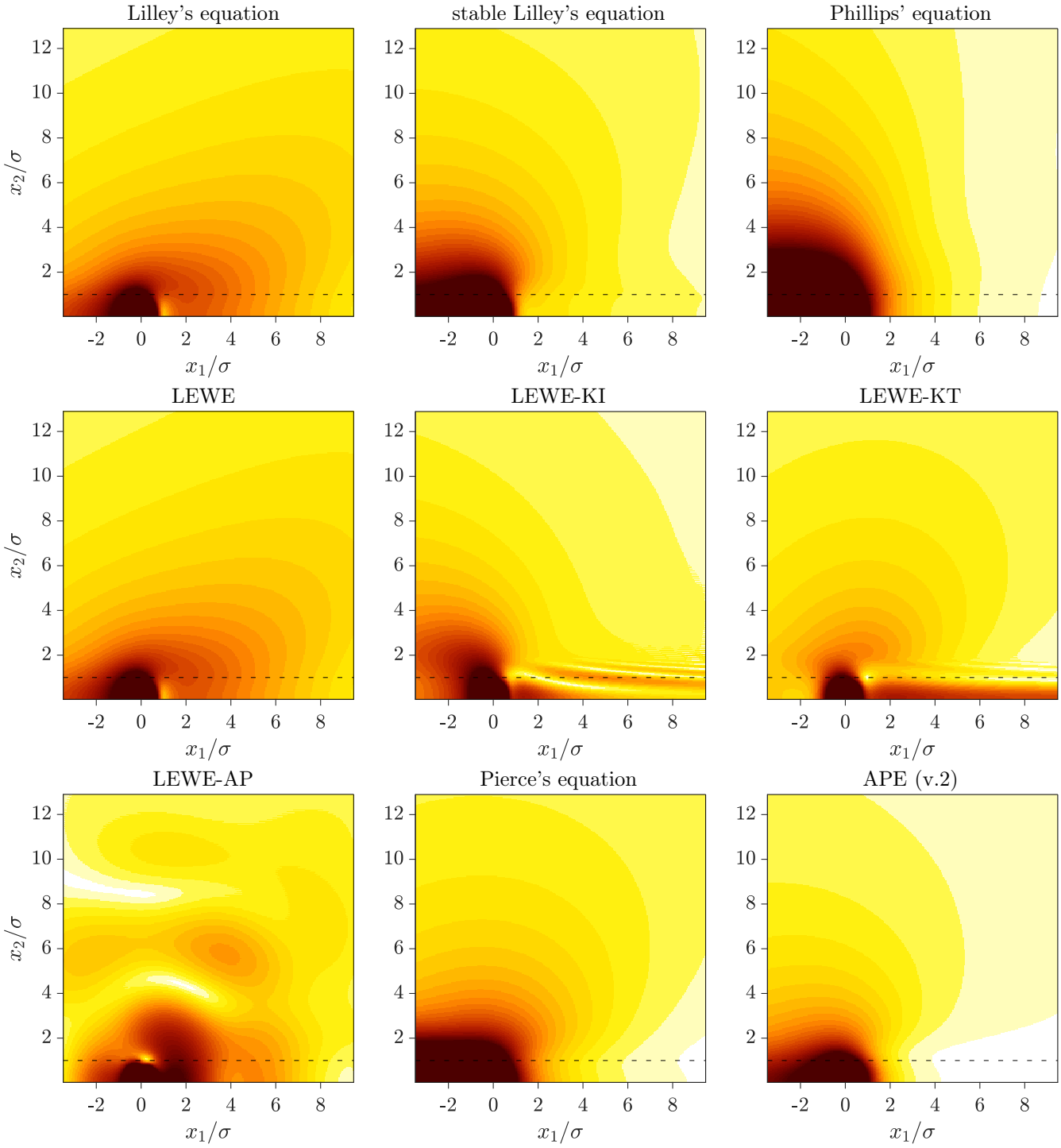

Figure 3.21: Absolute part of the fluctuating pressure p computed for a Strouhal number of $St = 0.2$.

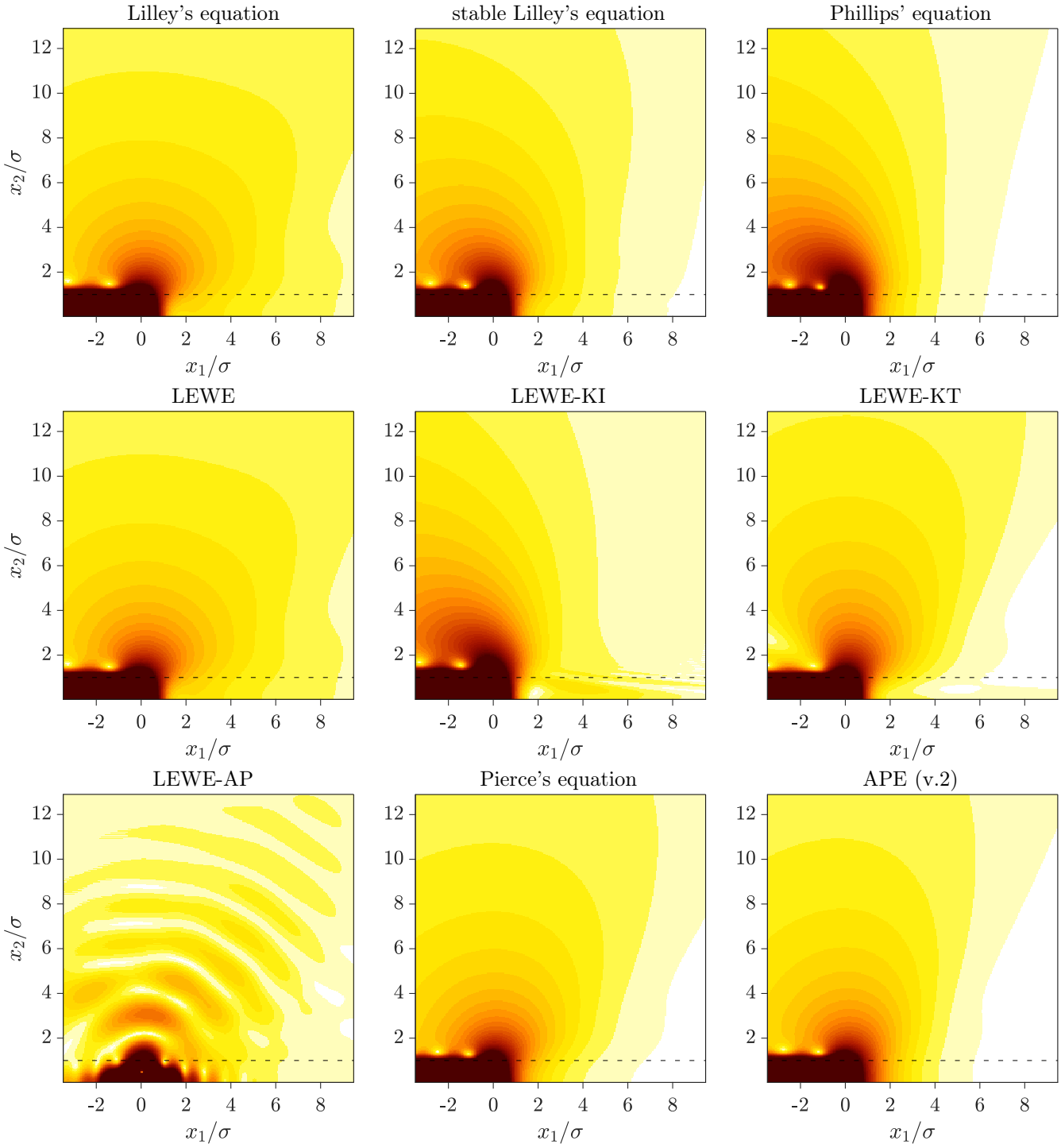

Figure 3.22: Absolute part of the fluctuating pressure p computed for a Strouhal number of $St = 0.5$.

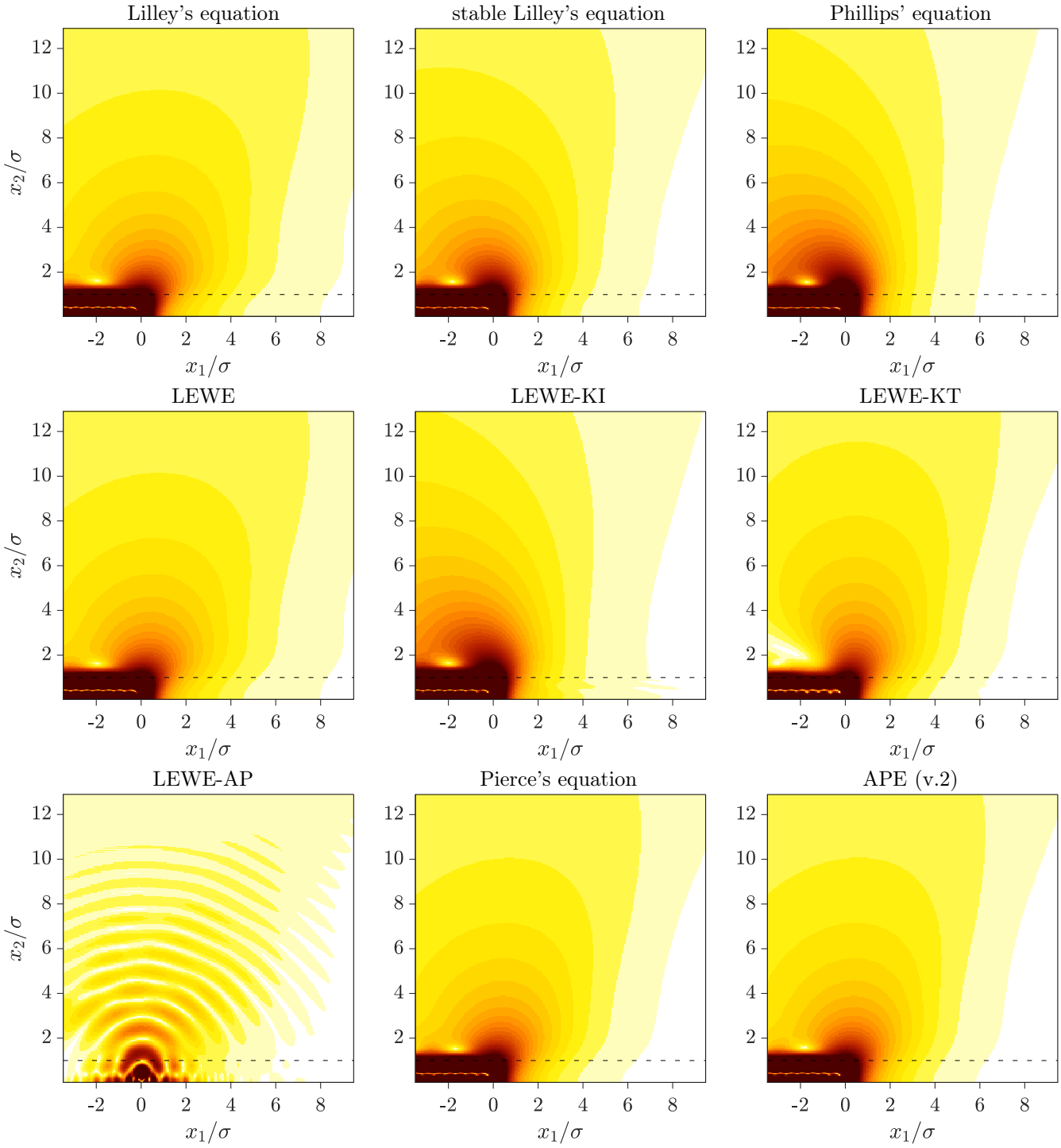

Figure 3.23: Absolute part of the fluctuating pressure p computed for a Strouhal number of $St = 1$.

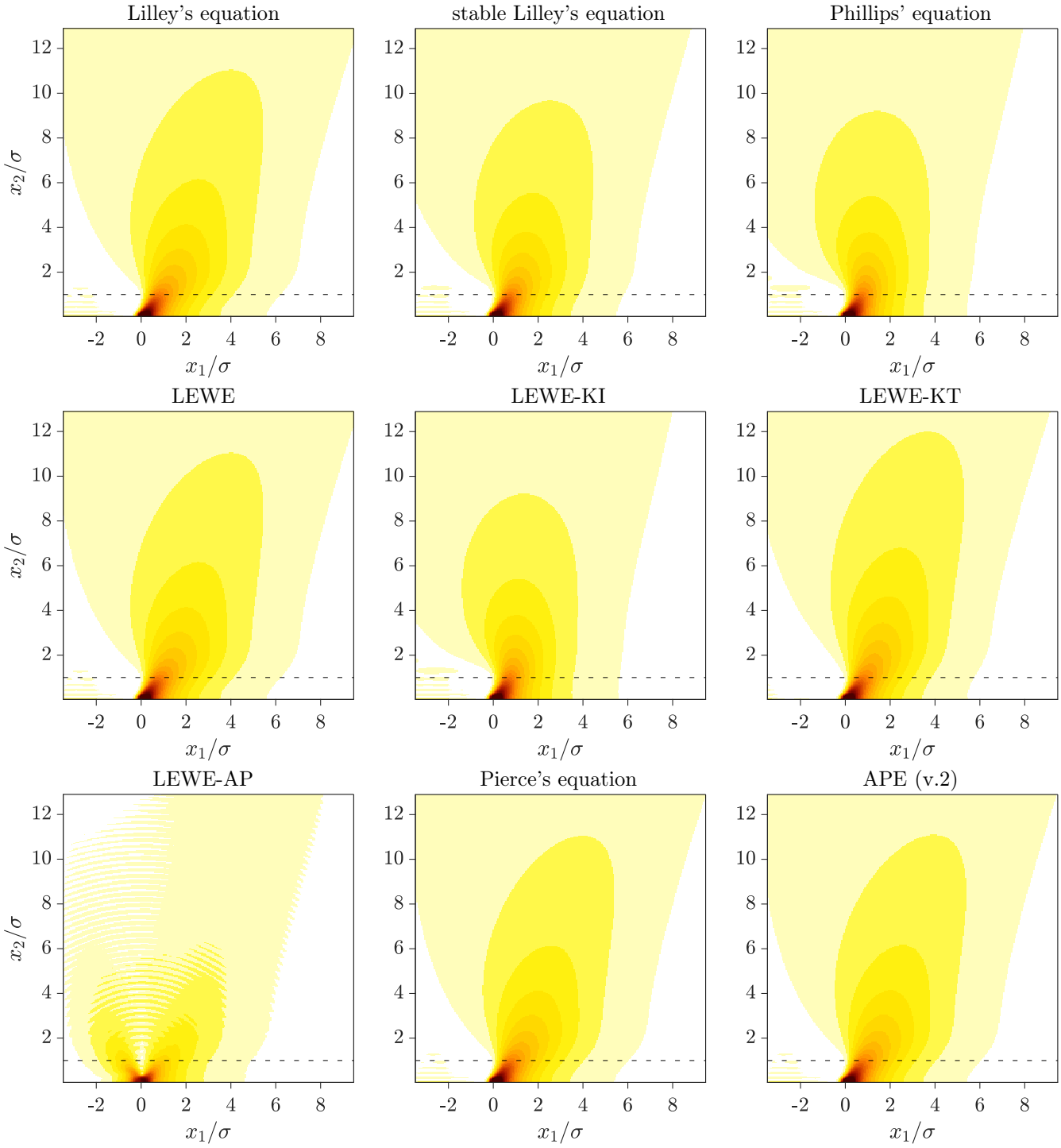

Figure 3.24: Absolute part of the fluctuating pressure p computed for a Strouhal number of $St = 3$.

Part II

Adjoint-based sound propagation for jet noise

1 Motivation for an adjoint-based method

Summary: An introduction to aircraft noise certification and turbofan engine installation effects highlights the need and the stakes for engine manufacturer to develop a reliable jet noise prediction tool. Given the complexity of the geometry encountered in modern aircraft architectures and the available computational capacities, the power spectral density of interest in the certification process needs to be computed from RANS solutions. In such statistical modellings, the noise radiated from jets is accounted for with an adjoint approach. The layout of the second part of the thesis is finally given.

1.1 Aircraft noise certification

Air transportation is constrained by strict noise regulations, which aim is to control the community noise in the vicinity of airport. The legislation in force may vary from one airport to another, nonetheless noise certifications are uniquely defined for all airplanes and are carried out at three positions defined with respect to the take-off runway as presented in figure 1.1. These certification points - namely Approach, Flyover and Lateral - accounts for the noise typically monitored nearby an airport during an aircraft landing and take-off flight operation. This sketch also presents an indicative noise footprint for a commercial airplane. The arrival footprint is significantly smaller than the departure one, this is because the aircraft engine is spool down to idle regime before the touchdown.

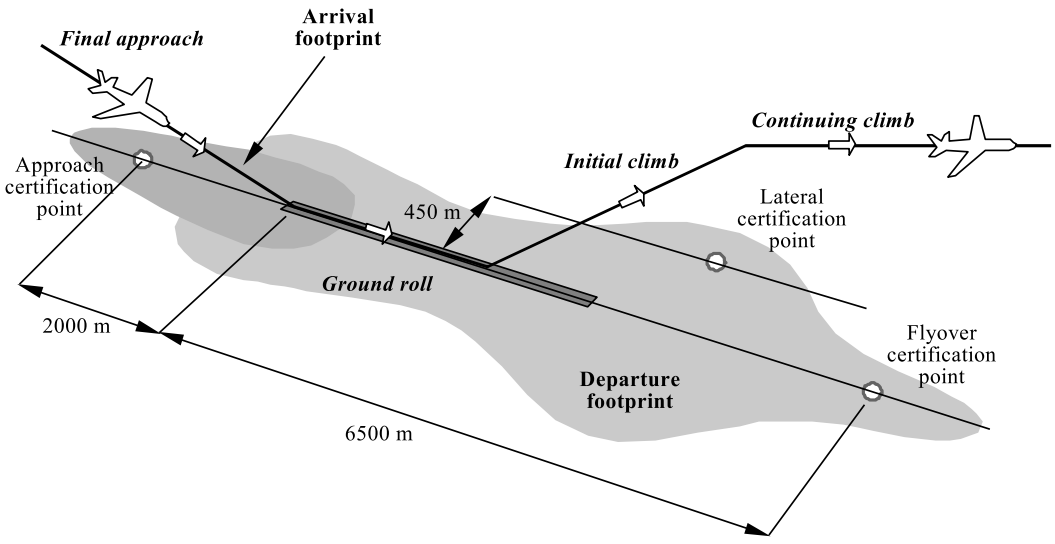

Figure 1.1: Aircraft noise certification points and indicative noise footprint for a commercial flight (ECAC, 2016).

The noisiness of an aircraft pass-by event is measured by the effective perceived noise level (EPNL). This unit measures the intensity of the noise recorded, it accounts also for the physiology of human ears, the annoyance perceived due to the presence of tones and the event duration. The physical input that is relevant to compute EPNL, is the Power Spectral Density (PSD) of the pressure measured at the certification point. Figure 1.2 presents the PSD obtained in a lab measurement for the DGEN 380 turbofan, a dual-stream business jet engine (Berton, 2016). The Fan tonal contribution at the Blade Passing Frequency (BPF) and its harmonics are clearly visible, as well as the turbine tone and its energetic haystack. The noise from the jet is broadband and corresponds to the low frequency hump in the PSD. In general a logarithmic scale is more adapted for its study. Only frequencies below 11220 Hz, marked in the plots of figure 1.2 with a dashed line, contribute to the EPNL metric. The relative importance of the jet noise in the computation of the EPNL is consequently increased.

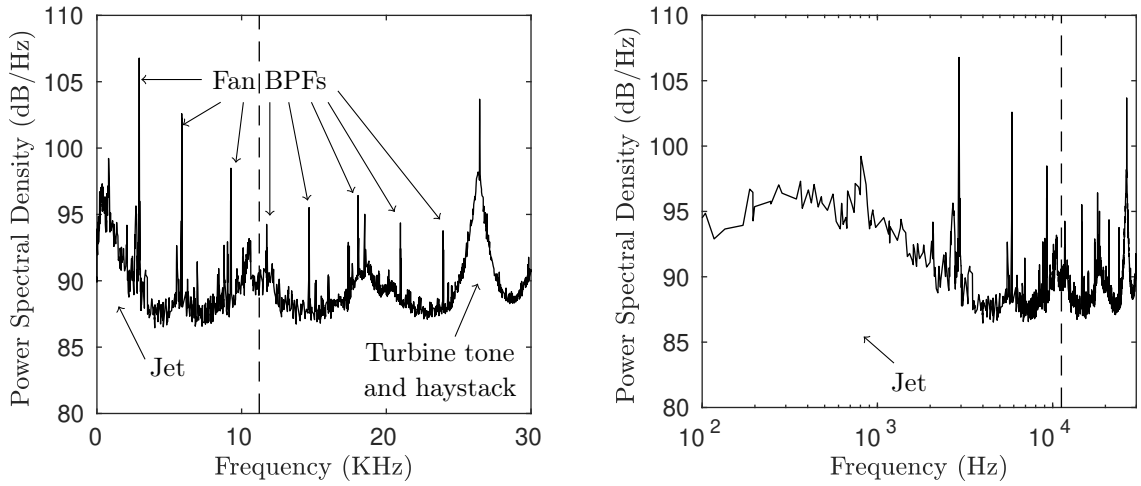

Figure 1.2: DGEN 380 pressure PSD at 118^o from inlet axis operating at 96 % of maximum low-spool shaft speed in linear and logarithmic scales. Results are adapted from (Berton, 2016).

Together with considerations on fuel consumption, the regulation of the noise generated by the air traffic, via the implementation of heavy fines or interdictions to operate in airports, are factors that greatly shaped the design of modern commercial aircraft engines. In particular the bypass ratio (BPR), that is the ratio between the mass flow going through the bypass stream and the one passing through the engine core, largely increased in the last decades. The BPR is now above 10 on typical modern commercial aircraft engines, e.g. of 10 for the GE9X, of 11 for the LEAP-1A and LEAP-1C and of 12.5 for the PW1100G. This evolution leads to a new breakdown in the prominence of noise sources, in reducing significantly the noise from the jet and giving an overriding importance to the noise of the fan as illustrated in figure 1.3. Note that the BPR of business jets are lower, e.g. of 7.6 for DGEN 380, and for such airplanes the noise emitted from the jet is still predominant. Jet noise plays no role at landing, however from figure 1.1, the Lateral and Flyover points correspond to the cases for which the acoustic footprint is the widest, and are thus the most critical ones. For the latter, the contribution of jet noise is substantial. In any event, the acoustic spectrum of an operating turbofan engine is complex and broad over frequencies, so that every relevant noise source needs to be studied and modelled by an engine manufacturer to achieve reliable noise predictions.

Figure 1.3: Noise sources breakdown at certification points for a modern middle-range commercial aircraft (Lempereur, 2018).

1.2 Engine installation effects in modern aircraft architectures

The increase of the BPR leads in practice to the manufacture of larger engines, and yields integration issues in modern aircraft architectures. The reduced space between the engine and the wing drastically modifies the aircraft flight dynamic as well as the engine sound propagation. Figure 1.4 presents the axial mean velocity of the flow exhausted from such an engine as computed with a Reynolds averaged Navier-Stokes (RANS) solver (Mosson et al., 2014). In this study, the radiation of a fan mode is computed over the jet mean flow and the presence of surfaces is accounted for in the propagation. This picture illustrates that aircraft noise is not only broad over frequencies, but its spatial spreading is also complex. This change in the radiated acoustic directivity, induced by the the presence of the mean flow as well as by the geometry, needs to be addressed to enable accurate aircraft noise predictions and may even advantageously be used in the design optimisation processes to reduce the community noise (Morris et al., 1973).

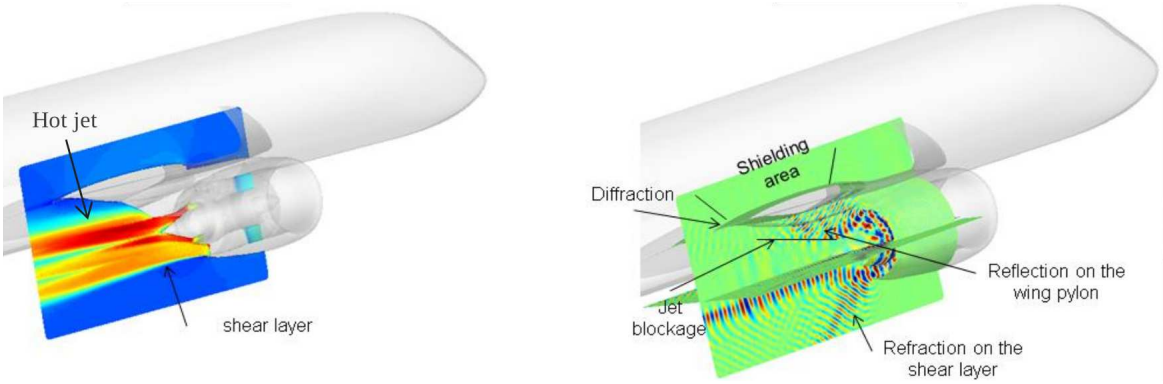

Figure 1.4: Exhaust velocity map and rearward radiation of a fan mode (Mosson et al., 2014).

It also appears from figure 1.4 that the engine installation, especially the presence of the pylon, dissymmetrise the jet flow (Eastwood and Tucker, 2011). This modification in the jet development leads to strong modifications of the jet turbulent kinetic energy field, and have thoroughly been assessed numerically and experimentally in the VITAL project (Dezitter et al., 2009). As will be discussed later, in §2.1, the turbulent kinetic energy of the flow drives the mixing noise generation process of the jet. Thus, in addition to the modification in the acoustic propagation, the engine installation alters the existing sound source distribution as well. The nearness of the engine and the wing is also likely to create new sound sources. Interaction of the jet with the airfoil flap have been observed experimentally (Huber et al., 2014) and tackled numerically (Xia et al., 2012; Tyacke et al., 2016). The flow mean velocity and the Reynolds shear stress tensor as modelled with a hybrid RANS-LES approach, as computed in the latter studies,

is depicted in figure 1.5. The large area of high shearing stress downstream of the wing trailing edge indicates the presence of a new source of sound. It is clear that the unsteady pressure loading of the airfoil is drastically affected by the closeness of the jet as well, so does the airframe radiated noise.

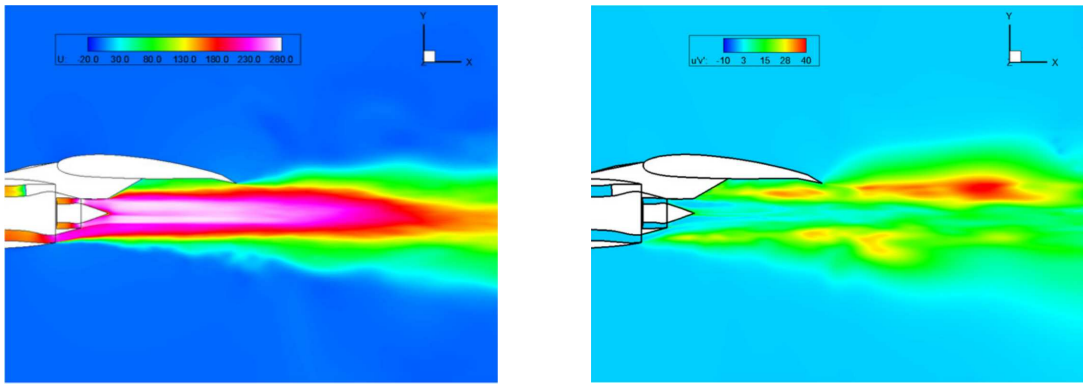

Figure 1.5: Axial mean flow and resolved Reynolds shear stress computed for an installed turbofan (Xia et al., 2012).

All these complex effects due to the engine installation, in the noise generation mechanisms as well as in the sound propagation, need to be taken into account for a modelling strategy to predict accurately the noise radiated from an aircraft engine. The successful design process of modern aircraft architecture will see engine and aircraft manufacturers working side by side with smart numerical tools capable of calculating all acoustic relevant effects in a timely efficient manner. The present study seeks to build a method able to account for all the acoustic propagation effects caused by the presence of the jet mean flow and aircraft surfaces, as encountered in such configurations.

1.3 Jet noise prediction from an engine manufacturer perspective

In the design process of new architectures, aircraft and engine manufacturers need to make sure that their final product passes the acoustic certification process. The direct noise simulation of a complete aircraft is however still technically and timely out of reach. As an illustration, the computation presented in figure 1.5 is based on a timely very competitive hybrid LES-RANS approach and only 53 million grid cells were required (Xia et al., 2012). This computation extended over $7.4 \cdot 10^5$ h.CPU, which represents a month calculation on 1024 CPU cores. This time corresponds solely to the CPU time needed to acquire the useful signal and does not involve the time of residual convergence, and obviously it is not acknowledging the engineer time to set-up such a complex mesh and computation. Moreover the engine studied is a small-scale one, with a diameter D of 18 mm and Reynolds number of $\mathrm{Re_D}$=300 000 only. While it is known that the computational cost of a resolved numerical simulation scales with $\mathrm{Re_D}^{11/4}$, the computation of the same configuration but full-scale would have been roughly 3.10^5 times more expensive. Even though steady encouraging progresses are made in the increase of available computational power, such computations will be unreachable for at least the next twenty years: Optimistically relying on Moore's observation of computational power doubling every 18 months, 30 years of continuous progresses in numerical techniques are required from the publication time of (Xia et al., 2012) before the possible numerical prediction of a full-scale installed engine... As a matter of fact, the numerical predictions of installed aircraft engines needs to be addressed alternatively. This statement needs to be mitigated with the recent progresses made in parallel computation on graphical cards. Markesteijn and Karabasov (2020) indeed demonstrated how

a fully installed engine case of around 250 million cells can be modelled with wall-modelled LES in six days on two workstations, where each of them is equipped with four GPU cards. Realistic simulations can be achieved with the use of smart indirect noise prediction techniques and by the separate investigation of the contribution of each aircraft sub-elements. Then, the closer the design iteration reaches the final aircraft architecture drawing, the more accurate the description should be. The aircraft sub-elements need to be analysed in there environment to compute the impact of installation effects and to describe more precisely the sound propagation. At each iteration step, a trade-off between physical representativeness of the model, - that is the ability of the description to correctly represent the effect of a design parameter change with regards to the overall optimum - and the model cost is to be found.

The following paragraph introduces how jet noise estimation can be addressed indirectly using statistical modelling. Let us first recall here that the final aim of aircraft noise predictions is to obtain the airplane EPNL at certification points. The calculation of EPNL is based on the computation of the Sound Pressure Level (SPL) which simply is the PSD of the normalised pressure recorded at the certification point. From now on, the pressure PSD is referred to as S_{pp} and depends on the microphone position $\boldsymbol{x}_m$ and the frequency f, resp. the pulsation ω of interest expressed in Hz, resp. in rad.s^{-1}, with $\omega = 2\pi f$. The pressure PSD, i.e. S_{pp}, is the Fourier transform of the recorded pressure auto-correlation R_{pp}, these statistical quantities expresses as,

$$R_{pp}(\boldsymbol{x}_m, \tau) = \int_{\mathbb{R}} \mathrm{d}t_m \;\; p(\boldsymbol{x_m}, t_m) p(\boldsymbol{x_m}, t_m + \tau) \qquad \text{and} \qquad S_{pp}(\boldsymbol{x}_m, \omega) = \int_{\mathbb{R}} \mathrm{d}\tau \;\; R_{pp}(\boldsymbol{x}_m, \tau) e^{i\omega\tau} \tag{1.1}$$

where the convention for the Fourier transform considered here is detailed in § A.2. If $p(\boldsymbol{x}_m, \omega)$ is the Fourier transform of the pressure time signal recorded, then from Plancherel's theorem it appears that the pressure PSD is also the square of this quantity.

$$S_{pp}(\boldsymbol{x}_m, \omega) = |p(\boldsymbol{x}_m, \omega)|^2 \tag{1.2}$$

So apart from a phase information which is lost in the autocorrelation procedure, time signal, autocorrelation and PSD are equivalent descriptions of the same signal. To set these ideas down, figure 1.6 depicts qualitatively a sample of the fields previously mentioned. These sketches for R_{pp} and S_{pp} mimic jet noise measurements (Tam et al., 2008), so to qualitatively represent the data of interest in the present study. Because of its broadband and smooth frequency content, it appears intuitively easier for a modelling to account for S_{pp} rather than for the time signal p. In fact, reasons to model statistical quantities are inherent to the physics of turbulence, quoting Lighthill (1952, §5), "*at high Reynolds numbers, when the flow field is fully turbulent, so that presumably the sound field partakes of the same chaotic quality, there is no meaning to be attached to the concept of 'amplitude' for any frequency, or even for any band of frequencies however small. This is because the phase is completely random and discontinuous, so that the fluctuating physical quantities themselves (as distinct from the intensity) possess no spectral density, because the limiting process which is used to define this concept does not converge. Hence intensity and its spectrum are all that can be given a meaning in such cases, not simply all that we need to know.*" When the flow is not deterministic, a statistical modelling of the jet noise is thus 'all that can be given'.

In a celebrated contribution, Tam et al. (1996) advocated for the existence of two components of the jet mixing noise; one originating from the large scale turbulence instabilities and another caused by the fine scale mixing of the turbulence. This view may correspond to the two limits of a generation mechanisms processes that is continuous over the scale of perturbation, refer to §1.3 of part I. These

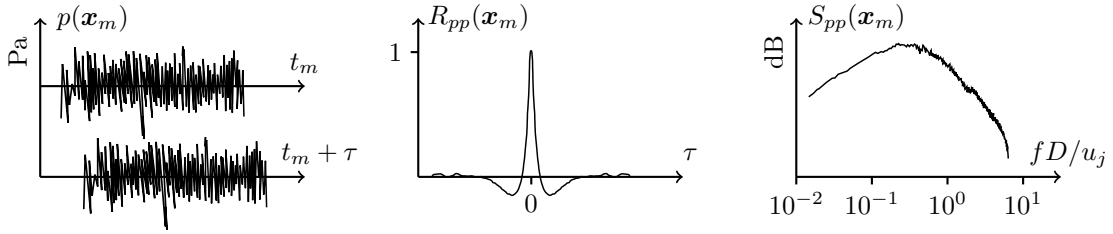

Figure 1.6: Typical mixing noise signature of a jet. From left to right: the pressure time signal recorded at microphone $p(\boldsymbol{x}_m)$, its normalised auto-correlation $R_{pp}(\boldsymbol{x}_m)$ and power spectral density $S_{pp}(\boldsymbol{x}_m)$.

authors convincingly demonstrated how from experimental data self-similar spectra (Powell, 1964, §7) can be deduced for the mixing noise of axisymmetric jets. This is because the turbulence statistics, i.e. the sound sources in the jet core, present themselves self-similarities as pointed out by Tam et al. (1996): *"In the mixing layer of a jet there is no inherent geometrical length scale. Also, it is well-known that at high Reynolds number, viscosity is not a relevant parameter of turbulent jet flows. Based on these observations, it is easy to see that there is no intrinsic length and time scales in the core region of the jet flows. As a result, the mean flow as well as the turbulence statistics must exhibit self-similarity."* Following these authors, two constants are enough to reproduce very closely the S_{pp} associated to the fine scale mixing noise of a simple axisymmetric jet. Note that the scaling parameters enabling data to collapse with self-similar spectra can be deduced theoretically (Tam, 2006; Semiletov and Karabasov, 2017) or experimentally (Witze, 1974; Viswanathan, 2006). Such models, however, do only apply for simple isolated jet configuration.

1.4 Adjoint in RANS-based noise prediction

On this basis, the averaged information on turbulence provided by RANS solvers may be sufficient to characterise statistically the mixing noise sound source, and previous steady flow computations can be intelligently used to predict the S_{pp} associated to jet noise. RANS method are well adapted to industrial and optimisation design processes, they provide indeed fairly accurate descriptions of the mean flow , handle complex geometries and take little time to run. This entailed many contributions in the literature for RANS-based mixing noise prediction tools, which can be sorted in two categories.

1. A first category is based on the deterministic reconstruction of a statistical realisation of the sound sources and their acoustics. The S_{pp} is then rebuilt subsequently at the microphone location $\boldsymbol{x}_m$. The core of this method lies in the reconstruction of the turbulent field time evolution, the acoustic field is then assessed in a second step with an acoustic analogy and a standard Computational Aero-Acoustics (CAA) tool. This is less time consuming than direct noise computations, because only a one-way coupling from turbulence to acoustics is considered, and that turbulence is solely modelled with convection and diffusion processes. Different methods exist in the literature, namely the Stochastic Noise Generation and Radiation (SNGR) (Béchara et al., 1994; Bailly et al., 1995; Lafitte et al., 2012), the fast Random Particle-Mesh (RPM) (Ewert, 2007, 2008; Ewert et al., 2011) and the Adaptive Spectral Reconstruction (ASR) (Di Francescantonio et al., 2015).

2. In the second group of RANS-based prediction techniques the acoustic field is not computed. The power spectral density is evaluated at the microphone location $\boldsymbol{x}_m$ only, and the computation of deterministic statistical realisations of the flow are unnecessary. This is because RANS solutions and

S_{pp}, i.e. the input and output of the noise prediction tool, are both statistical quantities. In these noise prediction methodologies, sound propagation and generation is split thanks to the use of Green's functions. As the sketch bellow illustrates, the autocorrelation of the pressure time signal p is passed on the sound source terms q to form the sound source intercorrelation R_{qq}. Subsequently, the acoustic propagation is tackled in a deterministic approach with the Green technique which can possibly account for mean flow refraction effects, surface reflection or edge diffraction and can be computed by various means.

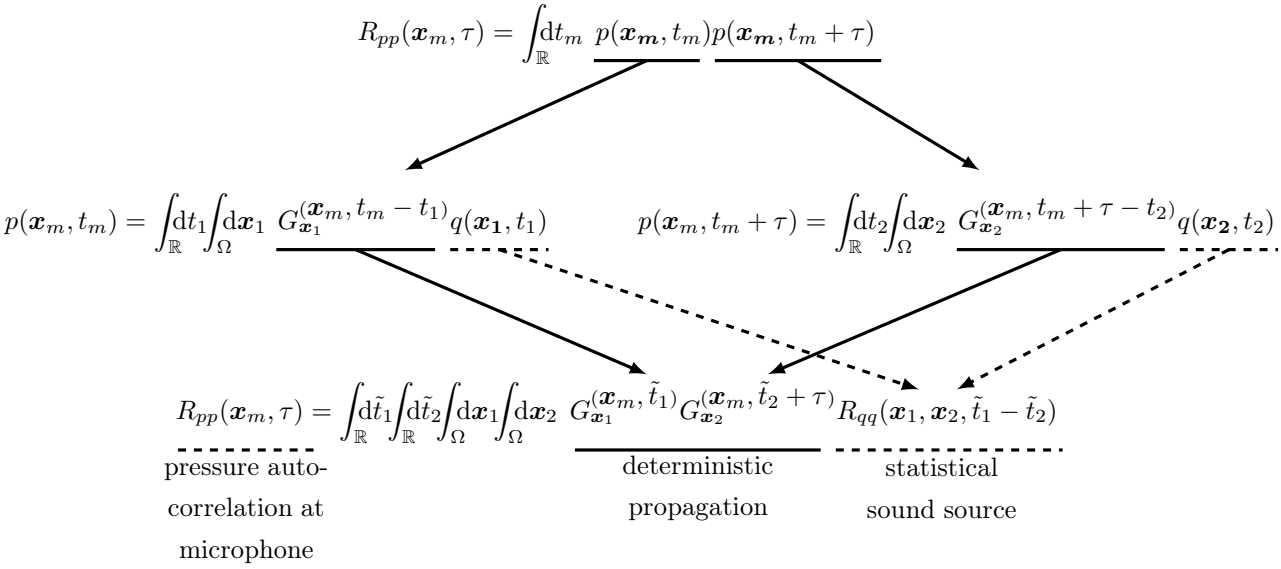

This approach relies on the modelling of the sound source autocorrelation as described by acoustic analogies. Different autocorrelation models exist for different sound sources, and this noise prediction strategy is readily used to model mixing noise, Mach wave radiation and broadband shock associated noise (BBSAN). Note that the computation of different type of sound sources can be tackle simultaneously (Miller, 2014b). The scientific community published prolifically on this methodology in the past thirty years. A non-exhaustive but representative list of contributions published by various researchers and groups is given hereafter. The contributions that are to this author the most significant are underlined: Khavaran et al.[1], Goldstein and Leib[2], Bailly et al.[3], Tam, Pastouchenko et al.[4], (Xu et al., 2015), Morris, Miller et al.[5], Brouwer and Nijboer (2005), Self, Deschamps et al.[6], Karabasov, Afsar et al.[7] A close focus on the numerous previously mentioned contributions is not given here, since they differ *only* by the modelling of the sound source autocorrelation term R_{qq} (Morris and Farassat, 2002, 2003; Tam, 2003) and the taking into account of the propagation effects. For a synthetic review on these contributions, the

[1] (Khavaran et al., 1994), (Das et al., 1997), (Khavaran, 1999), (Barber et al., 2001), (Khavaran et al., 2005), (Khavaran and Bridges, 2005), (Khavaran and Kenzakowski, 2007).

[2] (Goldstein, 1976, chap. 2), (Goldstein and Khavaran, 2005), (Goldstein et al., 2005a), (Goldstein et al., 2005b), (Goldstein, 2005a), (Goldstein, 2006), (Goldstein and Leib, 2008), (Leib and Goldstein, 2011), (Leib, 2013), (Goldstein and Leib, 2018).

[3] (Béchara et al., 1995), (Bailly et al., 1996), (Bailly et al., 1997), (Bodard et al., 2009), (Henry et al., 2012), (Martelet et al., 2019).

[4] (Tam, 1987),(Tam and Auriault, 1999), (Tam et al., 2001), (Tam and Pastouchenko, 2002), (Tam et al., 2005), (Tam and Pastouchenko, 2006), (Tam et al., 2006), (Pastouchenko and Tam, 2007), (Cheung et al., 2015).

[5] (Morris and Farassat, 2002), (Morris and Boluriaan, 2004), (Raizada and Morris, 2006), (Morris and Miller, 2010), (Miller and Morris, 2012),(Miller, 2014b), (Miller, 2015).

[6] (Self, 2005), (Self and Azarpeyvand, 2008), (Azarpeyvand and Self, 2009), (Engel et al., 2014), (Ilário et al., 2017), (Rosa et al., 2017).

[7] (Afsar et al., 2006), (Afsar et al., 2007), (Afsar, 2009), (Afsar, 2010), (Karabasov et al., 2010), (Afsar, 2012), (Depuru Mohan et al., 2015), (Karabasov and Sandberg, 2015), (Afsar et al., 2016a), (Afsar et al., 2016b), (Semiletov and Karabasov, 2016), (Afsar et al., 2017b), (Kalyan and Karabasov, 2017), (Afsar et al., 2017a), (Gryazev and Karabasov, 2018).

reader is referred to (Morris, 2007, 2012). More details on statistical jet noise modelling can also be found in following well-referenced doctoral thesis (Azarpeyvand, 2008; Bassetti, 2009; Almeida, 2009; Martelet, 2020).

To allow the calculation of the pressure autocorrelation R_{pp} with the above formula, it is clear that Green's function $G_{\boldsymbol{x}_s,t_s}$ needs to be determined for each sound source position $\boldsymbol{x}_s$ and time t_s. If an installed aircraft engine is considered, Green's function is not known analytically, and this prediction methodology becomes unreasonably expensive. Indeed the number of sound sources is usually extravagantly high in practice and $G_{\boldsymbol{x}_s,t_s}$ needs to be assessed for each of them. In regard to this, Tam and Auriault (1998) proposed to cleverly use the most general reciprocity principle to redraft Green's function of the direct radiation problem $G_{\boldsymbol{x}_s,t_s}$ with the so called adjoint Green's functions $G^{\dagger}_{\boldsymbol{x}_m,t_m}$. For $\boldsymbol{x}_s$, t_s and $\boldsymbol{x}_m$, t_m, respectively the source and microphone position and time, the general reciprocity principle relates direct and adjoint Green's functions as,

$$G^{(\boldsymbol{x}_m,t_m)}_{\boldsymbol{x}_s,t_s} = G^{\dagger(\boldsymbol{x}_s,t_s)}_{\boldsymbol{x}_m,t_m} \tag{1.3}$$

The Green function needed for the noise prediction is now associated to the microphone rather than to the source as illustrated in figure 1.7. This is timely very efficient, since the acoustic propagation effects from the sound sources to the microphone is handled now in a single computation. Recasting the expression of the pressure autocorrelation R_{pp} with the adjoint Green functions leads to,

$$R_{pp}(\boldsymbol{x}_m,\tau) = \int_{\mathbb{R}}\mathrm{d}\tilde{t}_1\int_{\mathbb{R}}\mathrm{d}\tilde{t}_2\int_{\Omega}\mathrm{d}\boldsymbol{x}_1\int_{\Omega}\mathrm{d}\boldsymbol{x}_2\ G^{\dagger(\boldsymbol{x}_1,-\tilde{t}_1)}_{\boldsymbol{x}_m} G^{\dagger(\boldsymbol{x}_2,-\tilde{t}_2-\tau)}_{\boldsymbol{x}_m} R_{qq}(\boldsymbol{x}_1,\boldsymbol{x}_2,\tilde{t}_1-\tilde{t}_2) \tag{1.4}$$

Tam and Auriault (1999) applied the adjoint approach in their formula to predict jet mixing noise. Its use is now standard in the aeroacoustic community to model acoustic propagation effects in RANS-based models wherever the pressure time evolution is not computed, i.e. in all contributions of the second category of RANS-based prediction techniques previously mentioned. As a matter of fact, statistic jet noise prediction formulae rely intrinsically in their derivation on adjoint.

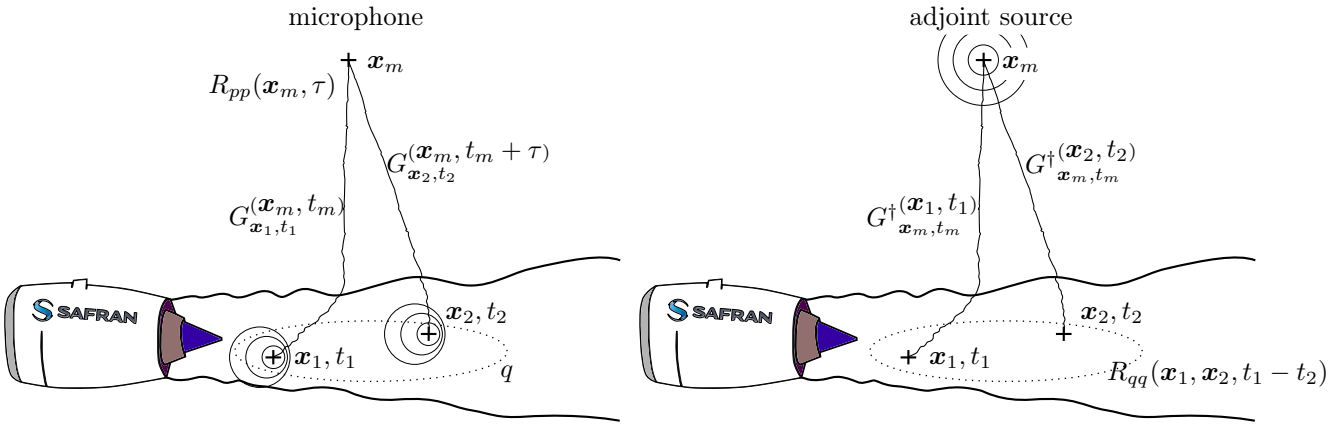

Figure 1.7: Introduction of the adjoint problem to compute the pressure autocorrelation.

The present part of this work focuses on Tam and Auriault's mixing noise model which is detailed in-depth in § 2.1 and recast in § 2.2 for the acoustic potential as governed by Pierce's wave equation. The reasons to use Pierce's equation are numerous. On the one hand Pierce's equation is computationally efficient, acoustic preserving and fairly accurate. This is supported by part I. On the other hand, the self-adjoint

property of Pierce's equation can be advantageously used to compute its adjoint solution. Chapter 3 demonstrates this. Furthermore this equation consists in a simple convected wave equation that many solver readily are able to solve. A procedure to solve Pierce's equation with *FFT*'s commercial solver *Actran TM* is given, and the computation of adjoint field in application to a turbofan engine is finally presented in chapter 4.

2 Recast of Tam and Auriault's mixing noise model for Pierce's equation

Summary: A detailed review on the mixing noise model of Tam and Auriault (1999) is provided here. Effort is given to properly derive the prediction formula anew with a focus on a rigorous use of the adjoint technique. Additionnaly to Tam and Auriault's work, adjoint Green's function correlation (1999, eq. (34)) is modelled using a Taylor expansion. The second part of this chapter is devoted to apply this technique to a potential acoustics formulation based on Pierce's equation. Some remarks on how to model the BBSAN model of Morris and Miller (2010) within the present framework are given as a perspective.

2.1 Tam and Auriault's mixing noise theory

Jet mixing noise is an ever-present and highly emblematic sound source in turbulent flows (Lighthill, 1952, 1954), and its study is of particular interest. Tam and Auriault (1999) developed a RANS-based noise prediction method tackling this sound source, which for the first time, properly accounts for mean flow refraction effects. The acoustic propagation is addressed with a smart use of the adjoint formalism and is presented here succinctly. Deeper insight on the adjoint method is given later in chapter 3 of this part. The model yields very satisfactory results (Morris and Farassat, 2002) and its use is widespread in the aeroacoustic community. These reasons motivated in this work the focus on Tam and Auriault's formula. Note that this methodology can be cast alternatively (Morris and Boluriaan, 2004) and extended to describe other sound sources (Miller, 2014b). The original derivation of Tam and Auriault's formula is duplicated with the greatest possible care here below.

2.1.1 Flow noise modelling based on a RANS

Reynolds averaged Navier-Stokes (RANS) equations are based on the Reynolds decomposition of the variables used in the description of the fluid motion. That is a split of each variable f into its time-averaged part $\overline{f}$ and its fluctuating part f',

$$f = \overline{f} + f' \qquad \text{with} \quad \overline{f'} = 0 \qquad \text{(Reynolds decomposition)} \tag{2.1}$$

The complete set of equations is then time-averaged, and because the fluctuations have zero mean, its expression simplifies greatly. To close the system of equations, the non-vanishing fluctuation correlations are modelled with help of statistical quantities. This is achieved with conservation and transfer equations for the flow energy statistics, e.g. k, ε or ω, leading to different turbulence models (Bailly and Comte-Bellot,

2015, chap. 9). To avoid the modelling of new terms when the mean flow is compressible, it is convenient to consider a Favre decomposition for the velocity field. The Favre average $\widetilde{f}$ and its fluctuation f'' are mass weighted averages defined as,

$$f = \widetilde{f} + f'' \qquad \text{with} \quad \overline{\rho}\widetilde{f} = \overline{\rho f} \quad \text{and} \quad \overline{f''} \neq 0 \qquad \text{(Favre decomposition)} \tag{2.2}$$

This is used in most RANS solvers, and the steady continuity and momentum equations on which statistical noise predictions method relies are (Bailly and Comte-Bellot, 2015, § 9.3.1),

$$\begin{aligned} &\frac{\widetilde{\mathrm{D}}\,\overline{\rho}}{\widetilde{\mathrm{D}}t} + \overline{\rho}\,\nabla\cdot\widetilde{\boldsymbol{u}} = 0 \\ &\overline{\rho}\,\frac{\widetilde{\mathrm{D}}\,\widetilde{\boldsymbol{u}}}{\widetilde{\mathrm{D}}t} + \nabla\,\overline{p} = \nabla\cdot\left(\overline{\Sigma} - \overline{\rho\boldsymbol{u}''\otimes\boldsymbol{u}''}\right) \end{aligned} \tag{2.3}$$

where $\widetilde{\mathrm{D}}/\widetilde{\mathrm{D}}t = \partial/\partial t + \widetilde{\boldsymbol{u}}\cdot\nabla$ is the Favre averaged convective derivative. These equations resemble very much to the general equations of fluid motion, equations (2.2), but with an additional external force $\overline{\rho\boldsymbol{u}''\otimes\boldsymbol{u}''}$ that reminds one of the Lighthill stress tensor in absence of heat source and viscous contributions. This term can be interpreted as the average effect of the turbulent structures on the mean flow evolution. Starting from this RANS correlation tensor, Tam and Auriault proposed a source term to mixing noise for the acoustic equations. To that purpose, they adopted the compressible Boussinesq eddy viscosity model for the Reynolds stress (Bailly and Comte-Bellot, 2015, § 9.3.1), i.e.

$$-\overline{\rho\boldsymbol{u}''\otimes\boldsymbol{u}''} = \mu_t\left[(\nabla\widetilde{\boldsymbol{u}}) + (\nabla\widetilde{\boldsymbol{u}})^T\right] - \frac{2}{3}\mu_t\,(\nabla\cdot\widetilde{\boldsymbol{u}})\,\boldsymbol{I} - \frac{2}{3}\overline{\rho}\,k_s\,\boldsymbol{I} \tag{2.4}$$

where μ_t is the turbulence eddy viscosity, $k_s = \overline{\boldsymbol{u}'\cdot\boldsymbol{u}'}/2$ is the specific kinetic energy of the turbulence and $\boldsymbol{I}$ the identity tensor. The tensor off-diagonal terms weighted by μ_t account for the shearing effect of the turbulence and are deemed negligible. It is indeed reasonable to consider that acoustic fluctuations are caused by fluid compression and dilatation only (Ribner, 1962). These authors proposed in turn an elastic particle collision viewpoint to describe sound generation mechanisms induced by turbulence. Consistently with Boussinesq's model and some experimental evidences measured in the jet far enough from solid boundaries (Fleury et al., 2008), the turbulence is modelled as isotropic in the jet, and hence a single time dependant scalar field q_s is sufficient to account for the mixing noise generation in Tam and Auriault's model,

$$-\overline{\rho\boldsymbol{u}''\otimes\boldsymbol{u}''} \approx -\overline{\rho}\,\overline{\boldsymbol{u}'\cdot\boldsymbol{u}'}/3\;\boldsymbol{I} = -\overline{q_s}\;\boldsymbol{I} \tag{2.5}$$

And finally, if flow noise can be computed with linearised equations (Bogey et al., 2002) by considering the unsteady part of the Lighthill stress tensor (Lighthill, 1952, eq. (7)), Tam and Auriault proposed following alternative to the acoustic analogy source of sound,

$$\nabla\cdot(\overline{\rho}\boldsymbol{u}\otimes\boldsymbol{u}) - \nabla\cdot\left(\overline{\rho}\overline{\boldsymbol{u}\otimes\boldsymbol{u}}\right) = \nabla q_s \tag{2.6}$$

Note that in their model, instead of a classical temporal averaging for the Reynolds decomposition, Tam and Auriault (1999) proposed a spatial averaging with a filtering out of the large scale structures. This is meant to separate the large-scales of turbulence from the fine-scales with reference to (Tam et al., 1996). Yet in practice RANS code are not able to do this distinction, neither does the parabolised RANS equations used to develop the original model (Thies and Tam, 1996). For this reason reference to the

fine-scale to characterise k_s or the mixing noise model proposed in (Tam and Auriault, 1999) are omitted here. Based on the discussions given in section §1.2 and §1.3 of part I, because the modelled momentum source is potential it possesses an acoustic nature and no mode conversion is required for it to radiate. While the turbulent structure scales considered are not necessarily 'fine', they appear to be associated with turbulence self-noise.

2.1.2 Direct acoustic propagation

In their application Tam and Auriault (1999) accounted for the acoustic refraction effects of a steady parallel flow. As in part I, §1.2 of this script, the acoustic propagation problem is sought as the solution to a perturbation problem about a mean flow, as given by a Reynolds decomposition. From now on, the mean flow is indexed by zero $_0$ and the prime $'$ in superscripts of the fluctuating quantities are omitted for the sake of legibility. The direct acoustic propagation problem for Tam and Auriault's mixing noise rewrites then as,

$$\begin{cases} \rho_0 \dfrac{\mathrm{D}(\boldsymbol{u})}{\mathrm{D}t} + \nabla p = -\nabla q_s \\ \dfrac{\mathrm{D}(p)}{\mathrm{D}t} + \gamma p_0 (\nabla \cdot \boldsymbol{u}) = 0 \end{cases} \tag{2.7}$$

where $\mathrm{D}/\mathrm{D}t = \partial/\partial t + \boldsymbol{u}_0 \cdot \nabla$ is the convective derivative. If the associated linear operator $\mathcal{L}_0$ is defined, previous expression can be recast into,

$$\mathcal{L}_0 \begin{pmatrix} \boldsymbol{u} \\ p \end{pmatrix} = \begin{pmatrix} -\nabla q_s \\ 0 \end{pmatrix} \tag{2.8}$$

Note that the mean flow considered for the acoustic propagation is parallel and that $\mathcal{L}_0$ thus corresponds to the linearised Euler equations (LEE). Unlike Tam and Auriault's contribution (1999), it seems more straightforward in the derivations of the model to consider the time domain problem.

2.1.3 Governing adjoint equations

For an introduction on the adjoint framework and the definition of direct and adjoint problems, the reader is referred to § 3.2 of this script. The governing adjoint equations are given by Lagrange's identity,

$$< \begin{pmatrix} \boldsymbol{u}^\dagger \\ p^\dagger \end{pmatrix}, \mathcal{L}_0 \begin{pmatrix} \boldsymbol{u} \\ p \end{pmatrix} > = < \mathcal{L}_0^\dagger \begin{pmatrix} \boldsymbol{u}^\dagger \\ p^\dagger \end{pmatrix}, \begin{pmatrix} \boldsymbol{u} \\ p \end{pmatrix} > \tag{2.9}$$

where the scalar product $<,>$ is introduced in §A.4 of the appendix. Accordingly to Tam and Auriault's model (1999), the free-space propagation problem will be considered, i.e. $\Omega \equiv \mathbb{R}^3$, for which all boundary conditions vanish for the direct problem as well as for the adjoint problem. In particular the radiating boundary conditions associated with the direct problem and their associated anti-causal adjoint boundary will be discarded. Taking benefit from the mean flow parallelism, multiple integration by parts in above

expression lead to following adjoint operator $\mathcal{L}_0^\dagger$,

$$\begin{cases} -\rho_0 \dfrac{\mathrm{D}(\boldsymbol{u}^\dagger)}{\mathrm{D}t} - \gamma p_0 \nabla p^\dagger = \boldsymbol{S}^\dagger_{\rho_0 \boldsymbol{u}^\dagger} \\ -\dfrac{\mathrm{D}(p^\dagger)}{\mathrm{D}t} - \nabla \cdot \boldsymbol{u}^\dagger = S^\dagger_{p^\dagger} \end{cases} \tag{2.10}$$

where $\boldsymbol{S}^\dagger = (S^\dagger_{\rho_0 u_1^\dagger}, S^\dagger_{\rho_0 u_2^\dagger}, S^\dagger_{\rho_0 u_3^\dagger}, S^\dagger_{p^\dagger})^T$ is a generic writing of the adjoint source term. Because Tam and Auriault's model intends to compute the pressure field autocorrelation S_{pp} at a microphone position $\boldsymbol{x}_m$, and that the adjoint method relies on the reciprocity principle for which source and observer position are switched, for more see § 3.2.2, a Dirac source term $\delta_{\boldsymbol{x}_m,t_m}$ ($\equiv \delta(\boldsymbol{x}-\boldsymbol{x}_m)\delta(t-t_m)$) in the equation governing the adjoint field associated to the pressure $p^\dagger$ is considered. This is depicted in figure 2.1.

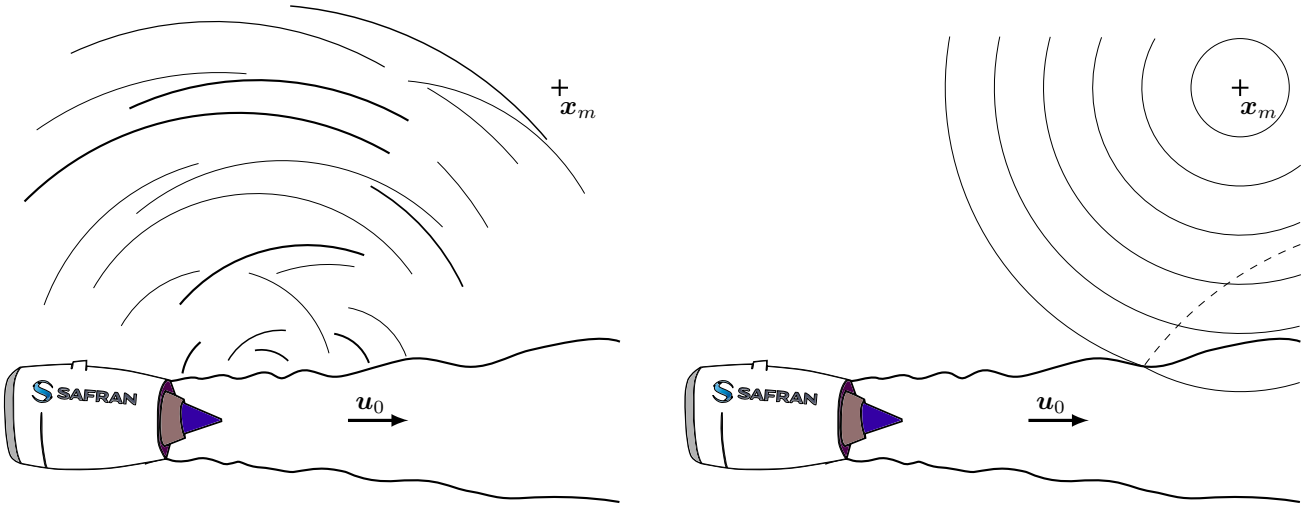

Figure 2.1: The adjoint problem is solved for an impulsive source set at the observer location $\boldsymbol{x}_m$.

What is more, because an impulse response is considered the corresponding adjoint fields $\boldsymbol{u}^\dagger$ and $p^\dagger$ are Green's functions. In the manipulations of Green's functions, it is crucial to bear in mind the source position $\boldsymbol{x}_m$ and time t_m at which they apply, so that this information will be specified in the notations. Considering following adjoint problem,

$$\mathcal{L}_0^\dagger \begin{pmatrix} \boldsymbol{u}^\dagger_{\boldsymbol{x}_m,t_m} \\ p^\dagger_{\boldsymbol{x}_m,t_m} \end{pmatrix} = \begin{pmatrix} \boldsymbol{0} \\ \delta_{\boldsymbol{x}_m,t_m} \end{pmatrix} \tag{2.11}$$

then readily gives in the time domain an expression analogue to (Tam and Auriault, 1999, eq. (21)), when replaced in Green Lagrange's identity together with the direct problem source term. That is,

$$< \begin{pmatrix} \boldsymbol{u}^\dagger_{\boldsymbol{x}_m,t_m} \\ p^\dagger_{\boldsymbol{x}_m,t_m} \end{pmatrix}, \begin{pmatrix} -\nabla q_s \\ 0 \end{pmatrix} > = < \begin{pmatrix} \boldsymbol{0} \\ \delta_{\boldsymbol{x}_m,t_m} \end{pmatrix}, \begin{pmatrix} \boldsymbol{u} \\ p \end{pmatrix} > \tag{2.12}$$

and finally, taking benefit from the delta Dirac property,

$$p(\boldsymbol{x}_m,t_m) = - < \boldsymbol{u}^\dagger_{\boldsymbol{x}_m,t_m}, \nabla q_s > \tag{2.13}$$

Following Tam and Auriault's steps, using integration by parts and the governing equation for $p^\dagger$, the

previous right hand side is recast as,

$$-<\boldsymbol{u}^{\dagger}_{\boldsymbol{x}_m,t_m},\nabla q_s>=<\nabla\cdot\boldsymbol{u}^{\dagger}_{\boldsymbol{x}_m,t_m},q_s>=\ -<\frac{\mathrm{D}(p^{\dagger}_{\boldsymbol{x}_m,t_m})}{\mathrm{D}t},q_s>=<p^{\dagger}_{\boldsymbol{x}_m,t_m},\frac{\mathrm{D}(q_s)}{\mathrm{D}t}> \tag{2.14}$$

where again, all the contour integrals are omitted since they vanish in free field and on solid boundaries where q_s is null. Note that $<,>$ has been used above indifferently for different size of vectors without ambiguity because the canonical scalar product is considered. This procedure can be applied for any scalar product, notice however that, as a step by step derivation would show, the latter needs to be adapted to each new couple of field considered.

2.1.4 Calculation of the pressure autocorrelation

Let the pressure p time-autocorrelation R_{pp} for a time-shift τ at position $\boldsymbol{x}_m$ be defined as,

$$R_{pp}(\boldsymbol{x}_m,\tau)=\int_{\mathbb{R}}\mathrm{d}t_m\ p(\boldsymbol{x_m},t_m)p(\boldsymbol{x_m},t_m+\tau) \tag{2.15}$$

then Tam and Auriault's expression for the autocorrelation (1999, eq. (24)) is retrieved:

$$\begin{aligned}R_{pp}(\boldsymbol{x}_m,\tau)\ &=\int_{\mathbb{R}}\mathrm{d}t_m\ \left\langle p^{\dagger}_{\boldsymbol{x}_m,t_m},\frac{\mathrm{D}(q_s)}{\mathrm{D}t}\right\rangle\left\langle p^{\dagger}_{\boldsymbol{x}_m,t_m+\tau},\frac{\mathrm{D}(q_s)}{\mathrm{D}t}\right\rangle\\ &=\int_{\mathbb{R}}\mathrm{d}t_m\ \left(\int_{\Omega}\mathrm{d}\boldsymbol{x}_1\int_{\mathbb{R}}\mathrm{d}t_1\ p^{\dagger(\boldsymbol{x}_1,t_1)}_{\boldsymbol{x}_m,t_m}\frac{\mathrm{D}(q_s(\boldsymbol{x}_1,t_1))}{\mathrm{D}t,1}\right)\left(\int_{\Omega}\mathrm{d}\boldsymbol{x}_2\int_{\mathbb{R}}\mathrm{d}t_2\ p^{\dagger(\boldsymbol{x}_2,t_2)}_{\boldsymbol{x}_m,t_m+\tau}\frac{\mathrm{D}(q_s(\boldsymbol{x}_2,t_2))}{\mathrm{D}t,2}\right)\end{aligned} \tag{2.16}$$

where $\mathrm{D}/\mathrm{D}t_i=\partial/\partial t_i+\boldsymbol{u_0}\cdot\nabla_i$ is applied to time variable t_i and space variable $\boldsymbol{x}_i$. After simple rearranging,

$$R_{pp}(\boldsymbol{x}_m,\tau)\ =\int_{\Omega}\mathrm{d}\boldsymbol{x}_1\int_{\Omega}\mathrm{d}\boldsymbol{x}_2\int_{\mathbb{R}}\mathrm{d}t_1\int_{\mathbb{R}}\mathrm{d}t_2\int_{\mathbb{R}}\mathrm{d}t_m\ p^{\dagger(\boldsymbol{x}_1,t_1-t_m)}_{\boldsymbol{x}_m}p^{\dagger(\boldsymbol{x}_2,t_2-t_m-\tau)}_{\boldsymbol{x}_m}\frac{\mathrm{D}(q_s(\boldsymbol{x}_1,t_1))}{\mathrm{D}t_1}\frac{\mathrm{D}(q_s(\boldsymbol{x}_2,t_2))}{\mathrm{D}t_2} \tag{2.17}$$

By defining following new variables $\tilde{t}_1=t_1-t_m$ and $\tilde{t}_2=t_2-t_m$,

$$R_{pp}(\boldsymbol{x}_m,\tau)\ =\int_{\Omega}\mathrm{d}\boldsymbol{x}_1\int_{\Omega}\mathrm{d}\boldsymbol{x}_2\int_{\mathbb{R}}\mathrm{d}\tilde{t}_1\int_{\mathbb{R}}\mathrm{d}\tilde{t}_2\ p^{\dagger(\boldsymbol{x}_1,\tilde{t}_1)}_{\boldsymbol{x}_m}p^{\dagger(\boldsymbol{x}_2,\tilde{t}_2-\tau)}_{\boldsymbol{x}_m}\int_{\mathbb{R}}\mathrm{d}t_m\ \frac{\mathrm{D}(q_s(\boldsymbol{x}_1,\tilde{t}_1+t_m))}{\mathrm{D}(\tilde{t}_1+t_m)}\frac{\mathrm{D}(q_s(\boldsymbol{x}_2,\tilde{t}_2+t_m))}{\mathrm{D}(\tilde{t}_2+t_m)} \tag{2.18}$$

When in the $\mathrm{d}t_m$ integral $\tilde{t}_i$ are constants with respect to t_m, thus $\mathrm{D}/\mathrm{D}(\tilde{t}_i+t_m)=\mathrm{D}/\mathrm{D}t_m$. Moreover by setting $\tilde{t}_m=t_m+\tilde{t}_2$ and $\tilde{\tau}=\tilde{t}_1-\tilde{t}_2=t_1-t_2$ then,

$$\int_{\mathbb{R}}\mathrm{d}t_m\ \frac{\mathrm{D}(q_s(\boldsymbol{x}_1,\tilde{t}_1+t_m))}{\mathrm{D}(\tilde{t}_1+t_m)}\frac{\mathrm{D}(q_s(\boldsymbol{x}_2,\tilde{t}_2+t_m))}{\mathrm{D}(\tilde{t}_2+t_m)}\ =\int_{\mathbb{R}}\mathrm{d}\tilde{t}_m\ \frac{\mathrm{D}(q_s(\boldsymbol{x}_1,\tilde{t}_m+\tilde{\tau}))}{\mathrm{D}\tilde{t}_m}\frac{\mathrm{D}(q_s(\boldsymbol{x}_2,\tilde{t}_m))}{\mathrm{D}\tilde{t}_m} \tag{2.19}$$

Above appears clearly the space-time autocorrelation of the quantity $Q\equiv\mathrm{D}(q_s)/\mathrm{D}t$, namely $R_{QQ}(\boldsymbol{x}_1,\boldsymbol{x}_2,\tilde{\tau})$. The pressure time autocorrelation R_{pp}, hence simply expresses without assumptions,

$$\boxed{R_{pp}(\boldsymbol{x}_m,\tau)\ =\int_{\Omega}\mathrm{d}\boldsymbol{x}_1\int_{\Omega}\mathrm{d}\boldsymbol{x}_2\int_{\mathbb{R}}\mathrm{d}\tilde{t}_1\int_{\mathbb{R}}\mathrm{d}\tilde{t}_2\ p^{\dagger(\boldsymbol{x}_1,\tilde{t}_1)}_{\boldsymbol{x}_m}p^{\dagger(\boldsymbol{x}_2,\tilde{t}_2-\tau)}_{\boldsymbol{x}_m}R_{QQ}(\boldsymbol{x}_1,\boldsymbol{x}_2,\tilde{t}_1-\tilde{t}_2)} \tag{2.20}$$

In our applications the Fourier transformed pressure autocorrelation S_{pp} is of interest which is defined as,

$$S_{pp}(\boldsymbol{x}_m,\omega)=\int_{\mathbb{R}}\mathrm{d}\tau\ R_{pp}(\boldsymbol{x}_m,\tau)e^{i\omega\tau} \tag{2.21}$$

Note that the convention for the Fourier transform considered here, given in § A.2 of the appendix, differs from the one in use in (Tam and Auriault, 1999). Since, adjoint Green's functions $p^\dagger_{\boldsymbol{x}_m}$ will be computed in the frequency domain in the present study, the above integrand needs therefore to be Fourier transformed.

$$S_{pp}(\boldsymbol{x}_m,\omega) = \frac{1}{(2\pi)^2}\int_\Omega \mathrm{d}\boldsymbol{x}_1\int_\Omega \mathrm{d}\boldsymbol{x}_2\int_{\mathbb{R}}\mathrm{d}\tilde{t}_1\int_{\mathbb{R}}\mathrm{d}\tilde{t}_2\int_{\mathbb{R}}\mathrm{d}\omega_1\int_{\mathbb{R}}\mathrm{d}\omega_2\int_{\mathbb{R}}\mathrm{d}\tau\ p^{\dagger(\boldsymbol{x}_1,\omega_1)}_{\boldsymbol{x}_m}p^{\dagger(\boldsymbol{x}_2,\omega_2)}_{\boldsymbol{x}_m}e^{i\omega\tau-i\omega_1\tilde{t}_1-i\omega_2(\tilde{t}_2-\tau)}R_{QQ}(\boldsymbol{x}_1,\boldsymbol{x}_2,\tilde{t}_1-\tilde{t}_2) \tag{2.22}$$

The $\mathrm{d}\tau$ integral can be readily performed with,

$$\int_{\mathbb{R}}\mathrm{d}\tau\ e^{i\tau(\omega+\omega_2)} = 2\pi\delta(\omega+\omega_2) \tag{2.23}$$

and following expression is finally obtained:

$$S_{pp}(\boldsymbol{x}_m,\omega) = \frac{1}{2\pi}\int_\Omega \mathrm{d}\boldsymbol{x}_1\int_\Omega \mathrm{d}\boldsymbol{x}_2\int_{\mathbb{R}}\mathrm{d}\tilde{t}_1\int_{\mathbb{R}}\mathrm{d}\tilde{t}_2\int_{\mathbb{R}}\mathrm{d}\omega_1\int_{\mathbb{R}}\mathrm{d}\omega_2\ p^{\dagger(\boldsymbol{x}_1,\omega_1)}_{\boldsymbol{x}_m}p^{\dagger(\boldsymbol{x}_2,\omega_2)}_{\boldsymbol{x}_m}e^{-i\omega_1\tilde{t}_1-i\omega_2\tilde{t}_2}R_{QQ}(\boldsymbol{x}_1,\boldsymbol{x}_2,\tilde{t}_1-\tilde{t}_2)\delta(\omega+\omega_2) \tag{2.24}$$

2.1.5 Modelling of the source autocorrelation term

The modelling of R_{QQ} cannot be further postponed, since its expression is needed to perform analytically the time integrations over $\mathrm{d}\tilde{t}_1$ and $\mathrm{d}\tilde{t}_2$. The Q-quantity space-time autocorrelation model proposed by Tam and Auriault (1999, eq. (27)) is shift-invariant, i.e. by defining $\boldsymbol{r}=\boldsymbol{x}_1-\boldsymbol{x}_2$, then $R_{QQ}(\boldsymbol{x}_1,\boldsymbol{x}_2,\tilde{\tau}) = R_{QQ}(\boldsymbol{r},\tilde{\tau})$, and writes,

$$\boxed{R_{QQ}(\boldsymbol{r},\tilde{\tau}) = \frac{\hat{q}_s^2}{c^2\tau_s^2}\exp\left(-\frac{|\boldsymbol{r}\cdot\boldsymbol{u}_0|}{u_0^2\tau_s}-\frac{\ln(2)}{l_s^2}\left(\boldsymbol{r}-\tilde{\tau}\boldsymbol{u}_0\right)^2\right)} \tag{2.25}$$

with $u_0=|\boldsymbol{u}_0|$. The reader can refer to Tam and Auriault (1999, §3) for the definition of the above other variables and their origin. Simply note, that $\hat{q}_s$, τ_s and l_s are measures of the turbulence intensity, decay time and correlation length and are informed by RANS. Notice also that a similar Gaussian autocorrelation function was introduced by Ribner (1962, § III.) and proved to be able to account for a number of directivity effects encountered in jets.

Reproducing Tam and Auriault's change of variable for the integration, let $s=\tilde{\tau}-\boldsymbol{r}\cdot\boldsymbol{u}_0/u_0^2$, then it comes $\boldsymbol{r}-\tilde{\tau}\boldsymbol{u}_0=\boldsymbol{r}_\perp-s\boldsymbol{u}_0$, where $\boldsymbol{r}_\perp=\boldsymbol{r}-(\boldsymbol{r}\cdot\boldsymbol{u}_0)\boldsymbol{u}_0/u_0^2$ is the projection of $\boldsymbol{r}$ on the hyperplane associated to $\boldsymbol{u}_0$ so that $\boldsymbol{r}_\perp\cdot\boldsymbol{u}_0=0$, and

$$R_{QQ}(\boldsymbol{r},\tilde{\tau}) = \frac{\hat{q}_s^2}{c^2\tau_s^2}\exp\left(-\frac{|\boldsymbol{r}\cdot\boldsymbol{u}_0|}{u_0^2\tau_s}-\frac{\ln(2)|\boldsymbol{r}_\perp|^2}{l_s^2}-\frac{\ln(2)u_0^2s^2}{l_s^2}\right) \tag{2.26}$$

When applying the same change of variable on $\tilde{t}_1$, i.e., $\tilde{t}_1=s+\tilde{t}_2+\boldsymbol{r}\cdot\boldsymbol{u}_0/u_0^2$, in the integrand it follows,

$$S_{pp}(\boldsymbol{x}_m,\omega) = \int_\Omega \mathrm{d}\boldsymbol{x}_1\int_\Omega \mathrm{d}\boldsymbol{x}_2\int_{\mathbb{R}}\mathrm{d}\tilde{t}_2\int_{\mathbb{R}}\mathrm{d}\omega_1\int_{\mathbb{R}}\mathrm{d}\omega_2\int_{\mathbb{R}}\mathrm{d}s\ \frac{\hat{q}_s^2}{2\pi c^2\tau_s^2}\exp\left(-\frac{|\boldsymbol{r}\cdot\boldsymbol{u}_0|}{u_0^2\tau_s}-\frac{\ln(2)|\boldsymbol{r}_\perp|^2}{l_s^2}-\frac{\ln(2)u_0^2s^2}{l_s^2}\right)\delta(\omega+\omega_2)$$
$$\times p^{\dagger(\boldsymbol{x}_1,\omega_1)}_{\boldsymbol{x}_m}p^{\dagger(\boldsymbol{x}_2,\omega_2)}_{\boldsymbol{x}_m}e^{-i\omega_1(s+\tilde{t}_2+\boldsymbol{r}\cdot\boldsymbol{u}_0/u_0^2)-i\omega_2\tilde{t}_2} \tag{2.27}$$

The integration over $\mathrm{d}s$ can now be performed making use of (Gradshteyn and Ryzhik, 1963, eq. (3.323),

p.337 in 7th ed.),

$$\int_{\mathbb{R}} \mathrm{d}s \ \exp\left(-\frac{\ln(2)u_0^2 s^2}{l_s^2} - i\omega_1 s\right) = \frac{l_s}{u_0}\sqrt{\frac{\pi}{\ln(2)}}\exp\left(\frac{-\omega_1^2 l_s^2}{4\ln(2)u_0^2}\right) \tag{2.28}$$

The integral over $\mathrm{d}\tilde{t}_2$ is simpler,

$$\int_{\mathbb{R}} \mathrm{d}\tilde{t}_2 \ e^{-i(\omega_1+\omega_2)\tilde{t}_2} = 2\pi\delta(\omega_1+\omega_2) \tag{2.29}$$

Defining $\alpha = \dfrac{l_s^2}{4\ln(2)u_0^2}$ and $\beta = \dfrac{\hat{q}_s^2 l_s}{c^2\tau_s^2 u_0}\sqrt{\dfrac{\pi}{\ln(2)}}$, the pressure autocorrelation S_{pp} now writes,

$$\begin{aligned} S_{pp}(\boldsymbol{x}_m,\omega) \quad &= \int_\Omega \mathrm{d}\boldsymbol{x}_1 \int_\Omega \mathrm{d}\boldsymbol{x}_2 \int_{\mathbb{R}} \mathrm{d}\omega_1 \int_{\mathbb{R}} \mathrm{d}\omega_2 \ \beta \exp\left(-\frac{|\boldsymbol{r}\cdot\boldsymbol{u}_0|}{u_0^2\tau_s} - \frac{\ln(2)|\boldsymbol{r}_\perp|^2}{l_s^2}\right)\delta(\omega+\omega_2)\delta(\omega_1+\omega_2) \\ &\qquad \times p^{\dagger(\boldsymbol{x}_1,\omega_1)}_{\boldsymbol{x}_m} p^{\dagger(\boldsymbol{x}_2,\omega_2)}_{\boldsymbol{x}_m} \exp\left(-i\omega_1\frac{\boldsymbol{r}\cdot\boldsymbol{u}_0}{u_0^2} - \alpha\omega_1^2\right) \end{aligned} \tag{2.30}$$

Evaluating the $\mathrm{d}\omega_1$ and $\mathrm{d}\omega_2$ integral is straightforward,

$$S_{pp}(\boldsymbol{x}_m,\omega) \quad = \int_\Omega \mathrm{d}\boldsymbol{x}_1 \int_\Omega \mathrm{d}\boldsymbol{x}_2 \ \beta \exp\left(-\frac{|\boldsymbol{r}\cdot\boldsymbol{u}_0|}{u_0^2\tau_s} - \frac{\ln(2)|\boldsymbol{r}_\perp|^2}{l_s^2}\right) p^{\dagger(\boldsymbol{x}_1,\omega)}_{\boldsymbol{x}_m} p^{\dagger(\boldsymbol{x}_2,-\omega)}_{\boldsymbol{x}_m} \exp\left(-i\omega\frac{\boldsymbol{r}\cdot\boldsymbol{u}_0}{u_0^2} - \alpha\omega^2\right) \tag{2.31}$$

By property of the Fourier transform of real valued signals, $p^{\dagger(\boldsymbol{x}_2,-\omega)}_{\boldsymbol{x}_m} = p^{\dagger(\boldsymbol{x}_2,\omega)^*}_{\boldsymbol{x}_m}$, and a last change of variable $\boldsymbol{x}_1 = \boldsymbol{r} + \boldsymbol{x}_2$ leads to Tam and Auriault's equation (33),

$$\boxed{S_{pp}(\boldsymbol{x}_m,\omega) \quad = \int_\Omega \mathrm{d}\boldsymbol{x}_2 \int_\Omega \mathrm{d}\boldsymbol{r} \ \beta \ p^{\dagger(\boldsymbol{r}+\boldsymbol{x}_2,\omega)}_{\boldsymbol{x}_m} p^{\dagger(\boldsymbol{x}_2,\omega)^*}_{\boldsymbol{x}_m} \exp\left(-\frac{|\boldsymbol{r}\cdot\boldsymbol{u}_0|}{u_0^2\tau_s} - \frac{\ln(2)|\boldsymbol{r}_\perp|^2}{l_s^2} - i\omega\frac{\boldsymbol{r}\cdot\boldsymbol{u}_0}{u_0^2} - \alpha\omega^2\right)} \tag{2.32}$$

2.1.6 Approximated calculation of the double space integration

The computation of the above double space integral is numerically costly and a simplification is required.

Fraunhofer approximation

Because in Tam and Auriault's work the observer is set in the acoustic far field, those authors proposed to model two neighbour acoustic ray paths from the source region by a Fraunhofer-like approximation (Tam and Auriault, 1999, fig. 4, eq. (34)) (Ribner, 1962, § 2.3), which expresses with vector notations as[1],

$$p^{\dagger(\boldsymbol{r}+\boldsymbol{x}_2,\omega)}_{\boldsymbol{x}_m} \approx p^{\dagger(\boldsymbol{x}_2,\omega)}_{\boldsymbol{x}_m} \exp\left(\frac{i\omega \ \boldsymbol{x}_m\cdot\boldsymbol{r}}{a_\infty|\boldsymbol{x}_m|}\right) \tag{2.33}$$

[1] In Fraunhofer's approximation, only the difference in travel time between rays is accounted for, so that the ray coming from $\boldsymbol{x}_2$ is the same as the one from $\boldsymbol{x}_2+\boldsymbol{r}$ but with an additional phase $\phi = \boldsymbol{k}\cdot\boldsymbol{r}$, i.e. for the direct problem $p^{(\boldsymbol{x}_m,\omega)}_{\boldsymbol{x}_2} = p^{(\boldsymbol{x}_m,\omega)}_{\boldsymbol{x}_2+\boldsymbol{r}} e^{i\phi}$, where $\boldsymbol{k}$ is the wave number pointing toward the observer point $\boldsymbol{x}_m$. Then for a medium at rest, $\phi = \boldsymbol{k}\cdot\boldsymbol{r} = \frac{\omega}{a_\infty}\frac{(\boldsymbol{x}_m-\boldsymbol{x}_2)}{|\boldsymbol{x}_m-\boldsymbol{x}_2|}\cdot\boldsymbol{r} \approx \frac{\omega}{a_\infty}\frac{\boldsymbol{x}_m}{|\boldsymbol{x}_m|}\cdot\boldsymbol{r}$, so that, $p^{(\boldsymbol{x}_m,\omega)}_{\boldsymbol{x}_2+\boldsymbol{r}} = p^{(\boldsymbol{x}_m,\omega)}_{\boldsymbol{x}_2}\exp\left(-i\frac{\omega}{a_\infty}\frac{\boldsymbol{x}_m}{|\boldsymbol{x}_m|}\cdot\boldsymbol{r}\right)$, the use of the reciprocity principle $p^{(\boldsymbol{x}_m,\omega)}_{\boldsymbol{x}_s} = p^{(\boldsymbol{x}_s,\omega)^*}_{\boldsymbol{x}_m}$ then permits to conclude. The difference between the expression proposed here and given in (Tam and Auriault, 1999) is likely to be a consequence of differences in the considered reciprocity relations, see (Tam and Auriault, 1998, eq. (2)).

where a_∞ is the ambient speed of sound. Note that this expression differs from the one proposed in the literature by the phase shift sign (Tam and Auriault, 1999),(Raizada and Morris, 2006, eq. 14). Replacing this formula in the expression of S_{pp} leads to,

$$S_{pp}(\boldsymbol{x}_m,\omega) = \int_\Omega \mathrm{d}\boldsymbol{x}_2 \int_\Omega \mathrm{d}\boldsymbol{r}\ \beta \left| p^{\dagger(\boldsymbol{x}_2,\omega)}_{\boldsymbol{x}_m} \right|^2 \exp\left(-\frac{|\boldsymbol{r}\cdot\boldsymbol{u}_0|}{u_0^2\tau_s} - \frac{\ln(2)|\boldsymbol{r}_\perp|^2}{l_s^2} - \alpha\omega^2 + i\omega\boldsymbol{r}\cdot\left(\frac{\boldsymbol{x}_m}{a_\infty|\boldsymbol{x}_m|} - \frac{\boldsymbol{u}_0}{u_0^2}\right)\right) \tag{2.34}$$

The integration over $\boldsymbol{r}$ can be performed using the split $\boldsymbol{r} = \boldsymbol{r}_\perp + \boldsymbol{r}_{/\!/}$ defined by the mean flow direction $\boldsymbol{u}_0$, where $\boldsymbol{r}_\perp \cdot \boldsymbol{u}_0 = 0$ and $\boldsymbol{r}_{/\!/} \times \boldsymbol{u}_0 = \boldsymbol{0}$. Previous integral then rewrites as,

$$\begin{aligned} S_{pp}(\boldsymbol{x}_m,\omega) = \int_\Omega \mathrm{d}\boldsymbol{x}_2\ \beta \left| p^{\dagger(\boldsymbol{x}_2,\omega)}_{\boldsymbol{x}_m} \right|^2 e^{-\alpha\omega^2} \int_{\mathbb{R}} \mathrm{d}\boldsymbol{r}_{/\!/}\ \exp\left(-\frac{|\boldsymbol{r}_{/\!/}\cdot\boldsymbol{u}_0|}{u_0^2\tau_s} + i\omega\boldsymbol{r}_{/\!/}\cdot\left(\frac{\boldsymbol{x}_m}{a_\infty|\boldsymbol{x}_m|} - \frac{\boldsymbol{u}_0}{u_0^2}\right)\right) \\ \times \int_{\mathbb{R}^2} \mathrm{d}\boldsymbol{r}_\perp\ \exp\left(-\frac{\ln(2)|\boldsymbol{r}_\perp|^2}{l_s^2} + \frac{i\omega\boldsymbol{r}_\perp\cdot\boldsymbol{x}_m}{a_\infty|\boldsymbol{x}_m|}\right) \end{aligned} \tag{2.35}$$

The integral over $\boldsymbol{r}_{/\!/}$ is evaluated using classical integral formula with $\alpha = \dfrac{1}{u_0\tau_s}$ and $\beta = \pm\dfrac{\omega}{u_0}\left(1 - \dfrac{\boldsymbol{u}_0\cdot\boldsymbol{x}_m}{a_\infty|\boldsymbol{x}_m|}\right)$,

$$\int_{\mathbb{R}} \mathrm{d}\boldsymbol{r}_{/\!/}\ \exp\left(-\frac{|\boldsymbol{r}_{/\!/}\cdot\boldsymbol{u}_0|}{u_0^2\tau_s} + \frac{i\omega(\boldsymbol{r}_{/\!/}\cdot\boldsymbol{u}_0)}{u_0^2}\left(\frac{\boldsymbol{u}_0\cdot\boldsymbol{x}_m}{a_\infty|\boldsymbol{x}_m|} - 1\right)\right) = \frac{2u_0\tau_s}{1+\omega^2\tau_s^2\left(1 - \dfrac{\boldsymbol{u}_0\cdot\boldsymbol{x}_m}{a_\infty|\boldsymbol{x}_m|}\right)^2} \tag{2.36}$$

Similarly, the one running over $\boldsymbol{r}_\perp$ is obtaining with formula (Gradshteyn and Ryzhik, 1963, eq. (3.323), p.337 in 7th ed.) setting $p_i = \dfrac{\sqrt{\ln(2)}}{l_s}$ and $q_i = \dfrac{i\omega x_i}{a_\infty|\boldsymbol{x}_m|}$ leading to,

$$\int_{\mathbb{R}^2} \mathrm{d}\boldsymbol{r}_\perp\ \exp\left(-\frac{\ln(2)|\boldsymbol{r}_\perp|^2}{l_s^2} + \frac{i\omega\boldsymbol{r}_\perp\cdot\boldsymbol{x}_m}{a_\infty|\boldsymbol{x}_m|}\right) = \frac{\pi l_s^2}{\ln(2)} \exp\left(\frac{-\omega^2 l_s^2|\boldsymbol{x}_{m,\perp}|^2}{4\ln(2)a_\infty^2|\boldsymbol{x}_m|^2}\right) \tag{2.37}$$

where $\boldsymbol{x}_{m,\perp} = \boldsymbol{x}_m - (\boldsymbol{x}_m\cdot\boldsymbol{u}_0)\boldsymbol{u}_0/u_0^2$. The double integral finally simplifies with Tam and Auriault's simplification into,

$$\boxed{S_{pp}(\boldsymbol{x}_m,\omega) = \int_\Omega \mathrm{d}\boldsymbol{x}_2\ \frac{2\hat{q}_s^2 l_s^3}{c^2\tau_s}\left(\frac{\pi}{\ln(2)}\right)^{3/2}\left| p^{\dagger(\boldsymbol{x}_2,\omega)}_{\boldsymbol{x}_m}\right|^2 \frac{\exp\left(\dfrac{-\omega^2 l_s^2}{4\ln(2)u_0^2}\left(1 + \dfrac{u_0^2|\boldsymbol{x}_{m,\perp}|^2}{a_\infty^2|\boldsymbol{x}_m|^2}\right)\right)}{1+\omega^2\tau_s^2\left(1 - \dfrac{\boldsymbol{u}_0\cdot\boldsymbol{x}_m}{a_\infty|\boldsymbol{x}_m|}\right)^2}} \tag{2.38}$$

which is Tam and Auriault's mixing noise formula (1999, eq. (35)). Note that above expression differs from the original one by a factor of 2π, which is related to a different Green's function definition, refer to (1999, eq. (19)), from which a $4\pi^2$ factor appears; then because of differences in the Fourier transform conventions, see (1999, eq. (25)), the present relation should be divided by 2π to comply with Tam and Auriault's relation. Note furthermore that the here presented expression is slightly enhanced compared to the original one, since it can tackle three dimensional propagation problems. If an axisymmetric jet flow is considered, the microphone polar angle θ_m, defined as in figure 2.2, is enough to characterise the

observer position. Tam and Auriault's mixing noise formula can then be recast in

$$S_{pp}(\theta_m,\omega) = \int_\Omega \mathrm{d}\boldsymbol{x}_2 \ \frac{2\hat{q}_s^2 l_s^3}{c^2\tau_s}\left(\frac{\pi}{\ln(2)}\right)^{3/2}\left|p^{\dagger(\boldsymbol{x}_2,\omega)}_{\theta_m}\right|^2 \frac{\exp\left(\frac{-\omega^2 l_s^2}{4\ln(2)u_0^2}\left(1+M_\infty^2\sin^2\theta_m\right)\right)}{1+\omega^2\tau_s^2\left(1-M_\infty\cos\theta_m\right)^2} \tag{2.39}$$

where $M_\infty = u_0/a_\infty$. Note that the $\sin^2\theta_m$ term appears to be missing in Tam and Auriault's model (1999, eq. (35)), this observation complies with independent alternative derivations of the mixing noise formula (Brouwer and Nijboer, 2005; Martelet et al., 2019, eq. (39)).

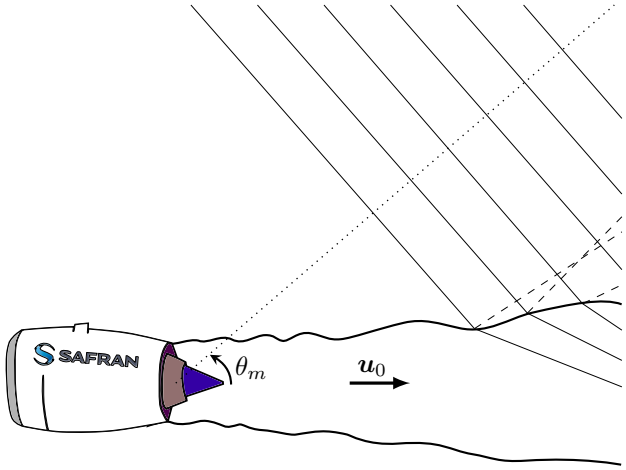

Figure 2.2: When the microphone is in the acoustic far field, the polar angle θ_m is enough to characterise the adjoint function of a round jet.

Taylor expansion

As suggested by Lielens (2019), if the adjoint Green function $p^\dagger_{\boldsymbol{x}_m}$ is computed numerically in the whole space, benefit can be taken from the knowledge of its spatial evolution and the Fraunhofer approximation can be replaced by a Taylor expansion; this will be done in this paragraph. If $\boldsymbol{r} = \boldsymbol{x}_1 - \boldsymbol{x}_2$ is small $p^{\dagger(\boldsymbol{r}+\boldsymbol{x}_2,\omega)}_{\boldsymbol{x}_m}$ can be approximated by the first order Taylor expansion,

$$p^{\dagger(\boldsymbol{r}+\boldsymbol{x}_2,\omega)}_{\boldsymbol{x}_m} \approx p^{\dagger(\boldsymbol{x}_2,\omega)}_{\boldsymbol{x}_m} + \boldsymbol{r}\cdot\frac{\partial p^{\dagger(\boldsymbol{x}_2,\omega)}_{\boldsymbol{x}_m}}{\partial \boldsymbol{x}_2} \tag{2.40}$$

Replacing this expression in the formula for S_{pp} leads to,

$$\begin{aligned} S_{pp}(\boldsymbol{x}_m,\omega) &= \int_\Omega \mathrm{d}\boldsymbol{x}_2 \int_\Omega \mathrm{d}\boldsymbol{r}\ \beta\ \left|p^{\dagger(\boldsymbol{x}_2,\omega)}_{\boldsymbol{x}_m}\right|^2 \exp\left(-\frac{|\boldsymbol{r}\cdot\boldsymbol{u}_0|}{u_0^2\tau_s} - \frac{\ln(2)|\boldsymbol{r}_\perp|^2}{l_s^2} - i\omega\frac{\boldsymbol{r}\cdot\boldsymbol{u}_0}{u_0^2} - \alpha\omega^2\right) \\ &\quad + \int_\Omega \mathrm{d}\boldsymbol{x}_2 \int_\Omega \mathrm{d}\boldsymbol{r}\ \beta\ p^{\dagger(\boldsymbol{x}_2,\omega)^*}_{\boldsymbol{x}_m}\left(\boldsymbol{r}\cdot\frac{\partial p^{\dagger(\boldsymbol{x}_2,\omega)}_{\boldsymbol{x}_m}}{\partial \boldsymbol{x}_2}\right)\exp\left(-\frac{|\boldsymbol{r}\cdot\boldsymbol{u}_0|}{u_0^2\tau_s} - \frac{\ln(2)|\boldsymbol{r}_\perp|^2}{l_s^2} - i\omega\frac{\boldsymbol{r}\cdot\boldsymbol{u}_0}{u_0^2} - \alpha\omega^2\right) \end{aligned} \tag{2.41}$$

Again, both integral can be computed analytically considering a decomposition for $\boldsymbol{r}$ parallel and perpendicular to the mean flow direction, i.e. $\boldsymbol{r} = \boldsymbol{r}_\perp + \boldsymbol{r}_{/\!/}$, so that according to this split for the first integral,

$$\int_\Omega \mathrm{d}\boldsymbol{x}_2 \ \beta \ \left|p^{\dagger(\boldsymbol{x}_2,\omega)}_{\boldsymbol{x}_m}\right|^2 e^{-\alpha\omega^2} \int_{\mathbb{R}^2} \mathrm{d}\boldsymbol{r}_\perp \ \exp\left(-\frac{\ln(2)|\boldsymbol{r}_\perp|^2}{l_s^2}\right) \int_{\mathbb{R}} \mathrm{d}\boldsymbol{r}_{/\!/} \ \exp\left(-\frac{|\boldsymbol{r}_{/\!/}\cdot\boldsymbol{u}_0|}{u_0^2\tau_s} - i\omega\frac{\boldsymbol{r}_{/\!/}\cdot\boldsymbol{u}_0}{u_0^2}\right)$$
$$= \int_\Omega \mathrm{d}\boldsymbol{x}_2 \ \beta \ \left|p^{\dagger(\boldsymbol{x}_2,\omega)}_{\boldsymbol{x}_m}\right|^2 e^{-\alpha\omega^2} \frac{\pi l_s^2}{\ln(2)} \ \frac{2u_0\tau_s}{1+\omega^2\tau_s^2} \tag{2.42}$$

and for the second integral,

$$\int_\Omega \mathrm{d}\boldsymbol{x}_2 \ \beta \ p^{\dagger(\boldsymbol{x}_2,\omega)^*}_{\boldsymbol{x}_m} e^{-\alpha\omega^2} \frac{\partial p^{\dagger(\boldsymbol{x}_2,\omega)}_{\boldsymbol{x}_m}}{\partial \boldsymbol{x}_2} \cdot \left(\int_{\mathbb{R}^2} \mathrm{d}\boldsymbol{r}_\perp \ \boldsymbol{r}_\perp \exp\left(-\frac{\ln(2)|\boldsymbol{r}_\perp|^2}{l_s^2}\right) \int_{\mathbb{R}} \mathrm{d}\boldsymbol{r}/\!/ \ \boldsymbol{r}_{/\!/} \exp\left(-\frac{|\boldsymbol{r}\cdot\boldsymbol{u}_0|}{u_0^2\tau_s} - i\omega\frac{\boldsymbol{r}_{/\!/}\cdot\boldsymbol{u}_0}{u_0^2}\right)\right)$$
$$= \int_\Omega \mathrm{d}\boldsymbol{x}_2 \ \beta \ p^{\dagger(\boldsymbol{x}_2,\omega)^*}_{\boldsymbol{x}_m} e^{-\alpha\omega^2} \left(\frac{\boldsymbol{u}_0}{u_0}\cdot\frac{\partial p^{\dagger(\boldsymbol{x}_2,\omega)}_{\boldsymbol{x}_m}}{\partial \boldsymbol{x}_2}\right) \frac{\pi l_s^2}{\ln(2)} \ \frac{-4i\omega\tau_s^3 u_0^2}{(1+\tau_s^2\omega^2)^2} \tag{2.43}$$

leading to following final formula for the pressure autocorrelation S_{pp} where the double integral is approximated with a Taylor expansion,

$$S_{pp}(\boldsymbol{x}_m,\omega) \ = \int_\Omega \mathrm{d}\boldsymbol{x}_2 \ \frac{2\hat{q}_s^2 l_s^3}{c^2\tau_s}\left(\frac{\pi}{\ln(2)}\right)^{3/2} p^{\dagger(\boldsymbol{x}_2,\omega)^*}_{\boldsymbol{x}_m} \frac{\exp\left(-\frac{\omega^2 l_s^2}{4\ln(2)u_0^2}\right)}{1+\omega^2\tau_s^2}\left(p^{\dagger(\boldsymbol{x}_2,\omega)}_{\boldsymbol{x}_m} - \frac{2i\omega\tau_s^2}{1+\omega^2\tau_s^2}\left(\boldsymbol{u}_0\cdot\frac{\partial p^{\dagger(\boldsymbol{x}_2,\omega)}_{\boldsymbol{x}_m}}{\partial \boldsymbol{x}_2}\right)\right) \tag{2.44}$$

Discussion on the approximations

Comparing this simplified formula with Tam and Auriault's one is not straightforward. If a plane wave propagation toward the observer $\boldsymbol{x}_m$ direction is assumed, then $p^{(\boldsymbol{x}_m,\omega)}_{\boldsymbol{x}_2} \propto \exp\left(i\boldsymbol{k}\cdot(\boldsymbol{x}_m-\boldsymbol{x}_2)\right) \propto \exp\left(-i\boldsymbol{k}\cdot\boldsymbol{x}_2\right)$ with $\boldsymbol{k} = \frac{\omega}{a_\infty}\frac{(\boldsymbol{x}_m-\boldsymbol{x}_2)}{|\boldsymbol{x}_m-\boldsymbol{x}_2|} \approx \frac{\omega\ \boldsymbol{x}_m}{a_\infty|\boldsymbol{x}_m|}$ and following adjoint Green's function $p^{\dagger(\boldsymbol{x}_2,\omega)}_{\boldsymbol{x}_m} = p^{(\boldsymbol{x}_m,\omega)^*}_{\boldsymbol{x}_2} \propto \exp\left(i\boldsymbol{k}\cdot\boldsymbol{x}_2\right)$ is obtained. It can be noted that for a plane wave propagation, Tam and Auriault's approach is exact, indeed $\exp(i\boldsymbol{k}\cdot(\boldsymbol{x}_2+\boldsymbol{r})) = \exp(i\boldsymbol{k}\cdot\boldsymbol{x}_2)\exp(i\boldsymbol{k}\cdot\boldsymbol{r})$, while the Taylor expansion only gives a first order estimate $\exp(i\boldsymbol{k}\cdot(\boldsymbol{x}_2+\boldsymbol{r})) = \exp(i\boldsymbol{k}\cdot\boldsymbol{x}_2)(1+i\boldsymbol{k}\cdot\boldsymbol{r}) + O(\boldsymbol{k}\cdot\boldsymbol{r})$. To verify the correctness of the here presented formula, a Taylor expansion of Tam and Auriault's expression should be considered. This is however not feasible since the source autocorrelation distance $\boldsymbol{r}$ −the small parameter− do not appear any more in the final formula. Nonetheless, some comparison can be achieved, if in the calculation steps a plane wave propagation is assumed, so to permit following estimate $\partial p^{\dagger(\boldsymbol{x}_2,\omega)}_{\boldsymbol{x}_m}/\partial\boldsymbol{x}_2 = i\boldsymbol{k}p^{\dagger(\boldsymbol{x}_2,\omega)}_{\boldsymbol{x}_m}$. With this additional simplification, the second integral can then be integrated anew, leading to,

$$\int_\Omega \mathrm{d}\boldsymbol{x}_2 \int_\Omega \mathrm{d}\boldsymbol{r} \ \beta \ \left|p^{\dagger(\boldsymbol{x}_2,\omega)}_{\boldsymbol{x}_m}\right|^2 (i\boldsymbol{k}\cdot\boldsymbol{r}) \exp\left(-\frac{|\boldsymbol{r}\cdot\boldsymbol{u}_0|}{u_0^2\tau_s} - \frac{\ln(2)|\boldsymbol{r}_\perp|^2}{l_s^2} - i\omega\frac{\boldsymbol{r}\cdot\boldsymbol{u}_0}{u_0^2} - \alpha\omega^2\right)$$
$$= \int_\Omega \mathrm{d}\boldsymbol{x}_2 \ \beta \ \left|p^{\dagger(\boldsymbol{x}_2,\omega)}_{\boldsymbol{x}_m}\right|^2 e^{-\alpha\omega^2}\left(\frac{\boldsymbol{u}_0\cdot\boldsymbol{x}_m}{a_\infty|\boldsymbol{x}_m|}\right)\frac{\pi l_s^2}{\ln(2)} \ \frac{4\omega^2\tau_s^3 u_0}{(1+\omega^2\tau_s^2)^2} \tag{2.45}$$

Adding the unchanged first integral gives for this verification analysis,

$$S_{pp}(\boldsymbol{x}_m,\omega) \quad = \int_\Omega \mathrm{d}\boldsymbol{x}_2 \; \frac{2\hat{q}_s^2 l_s^3}{c^2\tau_s}\left(\frac{\pi}{\ln(2)}\right)^{3/2}\left|p^{\dagger}_{\boldsymbol{x}_m}(\boldsymbol{x}_2,\omega)\right|^2 \frac{\exp\left(\dfrac{-\omega^2 l_s^2}{4\ln(2)u_0^2}\right)}{1+\omega^2\tau_s^2}\left(1+2\left(\frac{\boldsymbol{u}_0\cdot\boldsymbol{x}_m}{a_\infty|\boldsymbol{x}_m|}\right)\frac{\omega^2\tau_s^2}{1+\omega^2\tau_s^2}\right) \tag{2.46}$$

For frequencies of interest $\omega\tau_s \approx 1$, then if $\frac{\boldsymbol{u}_0\cdot\boldsymbol{x}_m}{a_\infty|\boldsymbol{x}_m|}$ is small as for an observer angle close to 90^o fom the jet axis, above formula can be obtained from a Taylor expansion of following expression,

$$S_{pp}(\boldsymbol{x}_m,\omega) \quad = \int_\Omega \mathrm{d}\boldsymbol{x}_2 \; \frac{2\hat{q}_s^2 l_s^3}{c^2\tau_s}\left(\frac{\pi}{\ln(2)}\right)^{3/2}\left|p^{\dagger}_{\boldsymbol{x}_m}(\boldsymbol{x}_2,\omega)\right|^2 \frac{\exp\left(\dfrac{-\omega^2 l_s^2}{4\ln(2)u_0^2}\right)}{(1+\omega^2\tau_s^2)\left(1-\left(\dfrac{\boldsymbol{u}_0\cdot\boldsymbol{x}_m}{a_\infty|\boldsymbol{x}_m|}\right)\dfrac{\omega^2\tau_s^2}{1+\omega^2\tau_s^2}\right)^2} \tag{2.47}$$

which has common features with the original formula of Tam and Auriault. For far-field noise predictions, preference should be given to a Fraunhofer approximation, while for near-field noise predictions, a Taylor expansion seems more accurate. Future investigations will have to verify this guess.

2.2 Tam and Auriault's formula applied to Pierce's wave equation

Tam and Auriault's formula (1999, eq. (35)) relies on the prior computation of adjoint Green's function $p^{\dagger}_{\boldsymbol{x}_m}$ given by the above set of equations. This presents two limitations for the practical use of this theory; firstly efficient solvers that can twofold compute these adjoint equations and handle complex geometries are scarce, and secondly as for the direct problem, these equations do also present a physical unstable mode. A reformulation of Tam and Auriault's formula with a propagation operator based on Pierce's equation (1990, eq. (27)) is a way to overcome these hardships. The formulation proposed by Pierce for the potential acoustic ϕ is indeed energy preserving and solvers, e.g. *Actran TM* from *FFT*, do exist that solve this wave equation.

The acoustic analogy based on Pierce's wave equation was introduced in § 2.5 of part I and writes,

$$\frac{\mathrm{D}^2(\phi)}{\mathrm{D}t^2} - \nabla\cdot(a_0^2\nabla\phi) = \frac{\mathrm{D}(S_m)}{\mathrm{D}t} - S_p \qquad \text{and} \qquad \Delta S_m = \nabla\cdot(\rho_0 \boldsymbol{S_u}) \tag{2.48}$$

where ($\boldsymbol{S_u}$,S_p) is the general formulation of a source term for the linearised momentum and the linearised energy equations. Because Pierce's wave equation describes solely the propagation of acoustic fluctuations ϕ defined as the potential part of the fluctuating momentum $\rho_0\boldsymbol{u}$, the source term for this equation needs to be potential as well. This is the meaning of the introduction of the linearised momentum source potential S_m. From the source model for mixing noise of Tam and Auriault's, it directly follows,

$$S_m = -q_s \qquad \text{and} \qquad S_p = 0 \tag{2.49}$$

The pressure field p is rebuilt subsequently from the acoustic potential ϕ considering $p = -\mathrm{D}(\phi)/\mathrm{D}t$ while the fluctuating velocity field is rebuilt with $\rho_0\boldsymbol{u} = \nabla\phi$.

2.2.1 Calculation of the pressure autocorrelation

The adjoint equation for Pierce's wave equation is obtained with the canonical scalar product, associated Green's function is defined as,

$$\frac{\mathrm{D}^2(\phi^\dagger_{\boldsymbol{x}_m,t_m})}{\mathrm{D}t^2} - \nabla\cdot(a_0^2\nabla\phi^\dagger_{\boldsymbol{x}_m,t_m}) = \delta(\boldsymbol{x}-\boldsymbol{x}_m)\delta(t-t_m) \tag{2.50}$$

The application of Lagrange's identity then directly gives,

$$\phi(\boldsymbol{x}_m,t_m) = <\phi^\dagger_{\boldsymbol{x}_m,t_m}, -\frac{\mathrm{D}(q_s)}{\mathrm{D}t}> \tag{2.51}$$

The pressure time autocorrelation is defined by,

$$R_{pp}(\boldsymbol{x}_m,\tau) = \int_{\mathbb{R}}\mathrm{d}t_m\ p(\boldsymbol{x}_m,t_m)p(\boldsymbol{x}_m,t_m+\tau) = \int_{\mathbb{R}}\mathrm{d}t_m\ \frac{\mathrm{D}(\phi)}{\mathrm{D}_{t_m,\boldsymbol{x}_m}}\frac{\mathrm{D}(\phi)}{\mathrm{D}_{t_m+\tau,\boldsymbol{x}_m}} \tag{2.52}$$

where $\dfrac{\mathrm{D}}{\mathrm{D}_{t_i,\boldsymbol{x}_j}} = \dfrac{\partial}{\partial t_i} + \boldsymbol{u}_0\cdot\dfrac{\partial}{\partial \boldsymbol{x}_j}$ is the material derivative with respect to the position $\boldsymbol{x}_j$ and the reference time t_i. This cumbersome notation is used in the following whenever there may be a confusion in the variables on which the material derivative applies and is omitted elsewhere. Recasting ϕ with Lagrange's identity,

$$\begin{aligned} R_{pp}(\boldsymbol{x}_m,\tau) \quad &= \int_{\mathbb{R}}\mathrm{d}t_m\ \frac{\mathrm{D}}{\mathrm{D}_{t_m,\boldsymbol{x}_m}}\left[\int_\Omega \mathrm{d}\boldsymbol{x}_1\int_{\mathbb{R}}\mathrm{d}t_1\ -\phi^{\dagger(\boldsymbol{x}_1,t_1)}_{\boldsymbol{x}_m,t_m}\frac{\mathrm{D}(q_s(\boldsymbol{x}_1,t_1))}{\mathrm{D}_{t_1,\boldsymbol{x}_1}}\right] \\ &\qquad\qquad \times\frac{\mathrm{D}}{\mathrm{D}_{t_m+\tau,\boldsymbol{x}_m}}\left[\int_\Omega \mathrm{d}\boldsymbol{x}_2\int_{\mathbb{R}}\mathrm{d}t_2\ -\phi^{\dagger(\boldsymbol{x}_2,t_2)}_{\boldsymbol{x}_m,t_m+\tau}\frac{\mathrm{D}(q_s(\boldsymbol{x}_2,t_2))}{\mathrm{D}_{t_2,\boldsymbol{x}_2}}\right] \end{aligned} \tag{2.53}$$

Because τ is constant with respect to t_m, $\mathrm{D}/\mathrm{D}_{t_m+\tau,\boldsymbol{x}_m} = \mathrm{D}/\mathrm{D}_{t_m,\boldsymbol{x}_m}$, moreover $\boldsymbol{x}_1$, $\boldsymbol{x}_2$, t_1 and t_2 are independent of $\boldsymbol{x}_m$, t_m so that previous material derivatives only applies on the $\phi^\dagger$ fields leading to,

$$R_{pp}(\boldsymbol{x}_m,\tau) \quad = \int_{\mathbb{R}}\mathrm{d}t_m\int_\Omega\mathrm{d}\boldsymbol{x}_1\int_\Omega\mathrm{d}\boldsymbol{x}_2\int_{\mathbb{R}}\mathrm{d}t_1\int_{\mathbb{R}}\mathrm{d}t_2\ \frac{\mathrm{D}\left(\phi^{\dagger(\boldsymbol{x}_1,t_1)}_{\boldsymbol{x}_m,t_m}\right)}{\mathrm{D}_{t_m,\boldsymbol{x}_m}}\frac{\mathrm{D}\left(\phi^{\dagger(\boldsymbol{x}_2,t_2)}_{\boldsymbol{x}_m,t_m+\tau}\right)}{\mathrm{D}_{t_m,\boldsymbol{x}_m}}\frac{\mathrm{D}(q_s(\boldsymbol{x}_1,t_1))}{\mathrm{D}_{t_1,\boldsymbol{x}_1}}\frac{\mathrm{D}(q_s(\boldsymbol{x}_2,t_2))}{\mathrm{D}_{t_2,\boldsymbol{x}_2}} \tag{2.54}$$

Recalling the equivalent notation for the Green functions, $G^{(\boldsymbol{x}_m,t_m)}_{\boldsymbol{x}_s,t_s} \equiv G^{(\boldsymbol{x}_m,t_m-t_s)}_{\boldsymbol{x}_s}$, and applying to t_1 and t_2 the change of variable $\tilde{t}_1 \equiv t_1 - t_m$ and $\tilde{t}_2 \equiv t_2 - t_m$ gives,

$$R_{pp}(\boldsymbol{x}_m,\tau) \quad = \int_{\mathbb{R}}\mathrm{d}t_m\int_\Omega\mathrm{d}\boldsymbol{x}_1\int_\Omega\mathrm{d}\boldsymbol{x}_2\int_{\mathbb{R}}\mathrm{d}\tilde{t}_1\int_{\mathbb{R}}\mathrm{d}\tilde{t}_2\ \frac{\mathrm{D}\left(\phi^{\dagger(\boldsymbol{x}_1,\tilde{t}_1)}_{\boldsymbol{x}_m}\right)}{\mathrm{D}_{t_m,\boldsymbol{x}_m}}\frac{\mathrm{D}\left(\phi^{\dagger(\boldsymbol{x}_2,\tilde{t}_2-\tau)}_{\boldsymbol{x}_m}\right)}{\mathrm{D}_{t_m,\boldsymbol{x}_m}}\frac{\mathrm{D}(q_s(\boldsymbol{x}_1,\tilde{t}_1+t_m))}{\mathrm{D}_{\tilde{t}_1+t_m,\boldsymbol{x}_1}}\frac{\mathrm{D}(q_s(\boldsymbol{x}_2,\tilde{t}_2+t_m))}{\mathrm{D}_{\tilde{t}_2+t_m,\boldsymbol{x}_2}} \tag{2.55}$$

Due to the time-shift invariance of $\phi^\dagger_{\boldsymbol{x}_m}$, their material derivatives can be expressed as function of $\tilde{t}_1$ and $\tilde{t}_2$,

$$\frac{\partial}{\partial t_m}\phi^{\dagger(\boldsymbol{x}_1,\tilde{t}_1)}_{\boldsymbol{x}_m} = \frac{\partial}{\partial t_m}\phi^{\dagger(\boldsymbol{x}_1,t_1-t_m)}_{\boldsymbol{x}_m} = -\frac{\partial}{\partial(t_1-t_m)}\phi^{\dagger(\boldsymbol{x}_1,t_1-t_m)}_{\boldsymbol{x}_m} = -\frac{\partial}{\partial\tilde{t}_1}\phi^{\dagger(\boldsymbol{x}_1,\tilde{t}_1)}_{\boldsymbol{x}_m} \tag{2.56}$$

and similarly,

$$\frac{\partial}{\partial t_m}\phi^{\dagger(\boldsymbol{x}_2,\tilde{t}_2-\tau)}_{\boldsymbol{x}_m} = -\frac{\partial}{\partial\tilde{t}_2}\phi^{\dagger(\boldsymbol{x}_2,\tilde{t}_2-\tau)}_{\boldsymbol{x}_m} \tag{2.57}$$

Since $\tilde{t}_1$ and $\tilde{t}_2$ are independent of t_m the pressure time autocorrelation R_{pp} rewrites as,

$$R_{pp}(\boldsymbol{x}_m,\tau) = \int_\Omega \mathrm{d}\boldsymbol{x}_1 \int_\Omega \mathrm{d}\boldsymbol{x}_2 \int_{\mathbb{R}} \mathrm{d}\tilde{t}_1 \int_{\mathbb{R}} \mathrm{d}\tilde{t}_2 \; \frac{\mathrm{D}\left(\phi^\dagger_{\boldsymbol{x}_m}(\boldsymbol{x}_1,\tilde{t}_1)\right)}{\mathrm{D}_{-\tilde{t}_1,\boldsymbol{x}_m}} \frac{\mathrm{D}\left(\phi^\dagger_{\boldsymbol{x}_m}(\boldsymbol{x}_2,\tilde{t}_2-\tau)\right)}{\mathrm{D}_{-\tilde{t}_2,\boldsymbol{x}_m}} \times \int_{\mathbb{R}} \mathrm{d}t_m \; \frac{\mathrm{D}(q_s(\boldsymbol{x}_1,\tilde{t}_1+t_m))}{\mathrm{D}_{t_m,\boldsymbol{x}_1}} \frac{\mathrm{D}(q_s(\boldsymbol{x}_2,\tilde{t}_2+t_m))}{\mathrm{D}_{t_m,\boldsymbol{x}_2}} \tag{2.58}$$

Eventually the change of variables $\tilde{t}_m \equiv t_m + \tilde{t}_2$ and $\tilde{\tau} \equiv \tilde{t}_1 - \tilde{t}_2 = t_1 - t_2$ allows to retrieve the Q-term space-time autocorrelation R_{QQ} defined as,

$$R_{QQ}(\boldsymbol{x}_1,\boldsymbol{x}_2,\tilde{\tau}) \equiv \int_{\mathbb{R}} \mathrm{d}\tilde{t}_m \; \frac{\mathrm{D}(q_s(\boldsymbol{x}_1,\tilde{t}_m+\tilde{\tau}))}{\mathrm{D}_{t_m,\boldsymbol{x}_1}} \frac{\mathrm{D}(q_s(\boldsymbol{x}_2,\tilde{t}_m))}{\mathrm{D}_{t_m,\boldsymbol{x}_2}} \tag{2.59}$$

The pressure time autocorrelation R_{pp} expressed with the acoustic potential ϕ writes thus as,

$$\boxed{R_{pp}(\boldsymbol{x}_m,\tau) = \int_\Omega \mathrm{d}\boldsymbol{x}_1 \int_\Omega \mathrm{d}\boldsymbol{x}_2 \int_{\mathbb{R}} \mathrm{d}\tilde{t}_1 \int_{\mathbb{R}} \mathrm{d}\tilde{t}_2 \; \frac{\mathrm{D}\left(\phi^\dagger_{\boldsymbol{x}_m}(\boldsymbol{x}_1,\tilde{t}_1)\right)}{\mathrm{D}_{-\tilde{t}_1,\boldsymbol{x}_m}} \frac{\mathrm{D}\left(\phi^\dagger_{\boldsymbol{x}_m}(\boldsymbol{x}_2,\tilde{t}_2-\tau)\right)}{\mathrm{D}_{-\tilde{t}_2,\boldsymbol{x}_m}} R_{QQ}(\boldsymbol{x}_1,\boldsymbol{x}_2,\tilde{t}_1-\tilde{t}_2)} \tag{2.60}$$

As previously, the Fourier transformed pressure autocorrelation S_{pp} can be computed, and after decomposing in the Fourier space the material derivatives of $\phi^\dagger_{\boldsymbol{x}_m}$, i.e.

$$\begin{aligned} \frac{\mathrm{D}\left(\phi^\dagger_{\boldsymbol{x}_m}(\boldsymbol{x}_1,\tilde{t}_1)\right)}{\mathrm{D}_{-\tilde{t}_1,\boldsymbol{x}_m}} &= \int_{\mathbb{R}} \frac{\mathrm{d}\omega_1}{2\pi} \left(i\omega_1 \phi^\dagger_{\boldsymbol{x}_m}(\boldsymbol{x}_1,\omega_1) + \boldsymbol{u}_0 \cdot \nabla \phi^\dagger_{\boldsymbol{x}_m}(\boldsymbol{x}_1,\omega_1) \right) e^{-i\omega_1 \tilde{t}_1} \\ &= -\int_{\mathbb{R}} \frac{\mathrm{d}\omega_1}{2\pi} \mathrm{D}_{-\boldsymbol{u}_0,\boldsymbol{x}_m} \left(\phi^\dagger_{\boldsymbol{x}_m}(\boldsymbol{x}_1,\omega_1) \right) e^{-i\omega_1 \tilde{t}_1} \end{aligned} \tag{2.61}$$

in a similar fashion,

$$\frac{\mathrm{D}\left(\phi^\dagger_{\boldsymbol{x}_m}(\boldsymbol{x}_2,\tilde{t}_2-\tau)\right)}{\mathrm{D}_{-\tilde{t}_2,\boldsymbol{x}_m}} = -\int_{\mathbb{R}} \frac{\mathrm{d}\omega_2}{2\pi} \mathrm{D}_{-\boldsymbol{u}_0,\boldsymbol{x}_m} \left(\phi^\dagger_{\boldsymbol{x}_m}(\boldsymbol{x}_2,\omega_2) \right) e^{-i\omega_2(\tilde{t}_2-\tau)} \tag{2.62}$$

where $\mathrm{D}_{\boldsymbol{u}_0}$ is the material derivative along $\boldsymbol{u}_0$ written in the frequency domain, possible additional variables in index refer to position or frequency for which this material derivative applies. After calculation, following formula is obtained,

$$S_{pp}(\boldsymbol{x}_m,\omega) = \frac{1}{2\pi} \int_\Omega \mathrm{d}\boldsymbol{x}_1 \int_\Omega \mathrm{d}\boldsymbol{x}_2 \int_{\mathbb{R}} \mathrm{d}\tilde{t}_1 \int_{\mathbb{R}} \mathrm{d}\tilde{t}_2 \int_{\mathbb{R}} \mathrm{d}\omega_1 \int_{\mathbb{R}} \mathrm{d}\omega_2 \; \mathrm{D}_{-\boldsymbol{u}_0,\boldsymbol{x}_m} \left(\phi^\dagger_{\boldsymbol{x}_m}(\boldsymbol{x}_1,\omega_1) \right) \mathrm{D}_{-\boldsymbol{u}_0,\boldsymbol{x}_m} \left(\phi^\dagger_{\boldsymbol{x}_m}(\boldsymbol{x}_2,\omega_2) \right) \times e^{-i\omega_1\tilde{t}_1 - i\omega_2\tilde{t}_2} R_{QQ}(\boldsymbol{x}_1,\boldsymbol{x}_2,\tilde{t}_1-\tilde{t}_2)\delta(\omega+\omega_2) \tag{2.63}$$

2.2.2 Modelling of the source autocorrelation term

The Q-term space-time autocorrelation is modelled accordingly with Tam and Auriault's work (1999, eq. (27)). Repeating previous derivations, with $\boldsymbol{r} = \boldsymbol{x}_1 - \boldsymbol{x}_2 = \boldsymbol{r}_\perp + \boldsymbol{r}_{/\!/}$, all integrals except the double space integration are evaluated,

$$\begin{aligned} S_{pp}(\boldsymbol{x}_m,\omega) \;&= \int_\Omega \mathrm{d}\boldsymbol{x}_2 \int_\Omega \mathrm{d}\boldsymbol{r}\;\; \beta\; \mathrm{D}_{-\boldsymbol{u}_0,\boldsymbol{x}_m}\left(\phi^\dagger_{\boldsymbol{x}_m}(\boldsymbol{x}_2+\boldsymbol{r},\omega)\right)\left[\mathrm{D}_{-\boldsymbol{u}_0,\boldsymbol{x}_m}\left(\phi^\dagger_{\boldsymbol{x}_m}(\boldsymbol{x}_2,\omega)\right)\right]^* \\ &\qquad \times \exp\left(-\frac{|\boldsymbol{r}\cdot\boldsymbol{u}_0|}{u_0^2\tau_s} - \frac{\ln(2)|\boldsymbol{r}_\perp|^2}{l_s^2} - i\omega\frac{\boldsymbol{r}\cdot\boldsymbol{u}_0}{u_0^2} - \alpha\omega^2\right) \end{aligned} \tag{2.64}$$

where $\alpha = \dfrac{l_s^2}{4\ln(2)u_0^2}$ and $\beta = \dfrac{\hat{q}_s^2 l_s}{c^2\tau_s^2 u_0}\sqrt{\dfrac{\pi}{\ln(2)}}$ have already been introduced previously.

2.2.3 Approximated calculation of the double space integration

The computation of the above double space integral is conducted analytically again with a Fraunhofer approximation and a Taylor expansion.

Fraunhofer approximation

The Fraunhofer approximation for the adjoint acoustic potential $\phi^\dagger$ writes,

$$\phi^\dagger_{\boldsymbol{x}_m}(\boldsymbol{r}+\boldsymbol{x}_2,\omega) \approx \phi^\dagger_{\boldsymbol{x}_m}(\boldsymbol{x}_2,\omega)\exp\left(\frac{i\omega\;\boldsymbol{x}_m\cdot\boldsymbol{r}}{a_\infty|\boldsymbol{x}_m|}\right) \tag{2.65}$$

The quantity appearing in the integrand expresses then as,

$$\mathrm{D}_{-\boldsymbol{u}_0,\boldsymbol{x}_m}\left(\phi^\dagger_{\boldsymbol{x}_m}(\boldsymbol{x}_2+\boldsymbol{r},\omega)\right) = \mathrm{D}_{-\boldsymbol{u}_0,\boldsymbol{x}_m}\left(\phi^\dagger_{\boldsymbol{x}_m}(\boldsymbol{x}_2,\omega)\right)\exp\left(\frac{i\omega\;\boldsymbol{x}_m\cdot\boldsymbol{r}}{a_\infty|\boldsymbol{x}_m|}\right) - \phi^\dagger_{\boldsymbol{x}_m}(\boldsymbol{x}_2,\omega)\,\boldsymbol{u}_0\cdot\frac{\partial}{\partial\boldsymbol{x}_m}\left(\exp\left(\frac{i\omega\;\boldsymbol{x}_m\cdot\boldsymbol{r}}{a_\infty|\boldsymbol{x}_m|}\right)\right) \tag{2.66}$$

Since $\dfrac{\partial}{\partial\boldsymbol{x}_m}\left(\dfrac{\boldsymbol{x}_m\cdot\boldsymbol{r}}{|\boldsymbol{x}_m|}\right) = \dfrac{|\boldsymbol{x}_m|^2\boldsymbol{r} - (\boldsymbol{r}\cdot\boldsymbol{x}_m)\boldsymbol{x}_m}{|\boldsymbol{x}_m|^3}$, the derivative along $\boldsymbol{u}_0$ expresses as,

$$\boldsymbol{u}_0\cdot\frac{\partial}{\partial\boldsymbol{x}_m}\left(\exp\left(\frac{i\omega\;\boldsymbol{x}_m\cdot\boldsymbol{r}}{a_\infty|\boldsymbol{x}_m|}\right)\right) = i\omega\frac{|\boldsymbol{x}_m|^2(\boldsymbol{u}_0\cdot\boldsymbol{r}) - (\boldsymbol{r}\cdot\boldsymbol{x}_m)(\boldsymbol{u}_0\cdot\boldsymbol{x}_m)}{a_\infty|\boldsymbol{x}_m|^3}\exp\left(\frac{i\omega\;\boldsymbol{x}_m\cdot\boldsymbol{r}}{a_\infty|\boldsymbol{x}_m|}\right) \approx \mathrm{O}\left(\frac{|\boldsymbol{r}|}{|\boldsymbol{x}_m|}\right) \tag{2.67}$$

where $|\boldsymbol{r}|/|\boldsymbol{x}_m|$ tends toward zero in the Fraunhofer approximation. Replacing this expression in the formula for S_{pp} gives,

$$S_{pp}(\boldsymbol{x}_m,\omega) = \int_\Omega \mathrm{d}\boldsymbol{x}_2\int_\Omega \mathrm{d}\boldsymbol{r}\;\;\beta\;\left|\mathrm{D}_{-\boldsymbol{u}_0,\boldsymbol{x}_m}\left(\phi^\dagger_{\boldsymbol{x}_m}(\boldsymbol{x}_2,\omega)\right)\right|^2\exp\left(-\frac{|\boldsymbol{r}\cdot\boldsymbol{u}_0|}{u_0^2\tau_s} - \frac{\ln(2)|\boldsymbol{r}_\perp|^2}{l_s^2} - \alpha\omega^2 + i\omega\boldsymbol{r}\cdot\left(\frac{\boldsymbol{x}_m}{a_\infty|\boldsymbol{x}_m|} - \frac{\boldsymbol{u}_0}{u_0^2}\right)\right) \tag{2.68}$$

The integrand is almost the same as the one evaluated previously, hence the expression for the pressure autocorrelation S_{pp} results straightly from former derivations,

$$S_{pp}(\boldsymbol{x}_m,\omega) = \int_\Omega \mathrm{d}\boldsymbol{x}_2 \ \frac{2\hat{q}_s^2 l_s^3}{c^2\tau_s}\left(\frac{\pi}{\ln(2)}\right)^{3/2}\left|\mathrm{D}_{-\boldsymbol{u}_0,\boldsymbol{x}_m}\left(\phi^\dagger_{\boldsymbol{x}_m}(\boldsymbol{x}_2,\omega)\right)\right|^2 \frac{\exp\left(\frac{-\omega^2 l_s^2}{4\ln(2)u_0^2}\left(1+\frac{u_0^2|\boldsymbol{x}_{m,\perp}|^2}{a_\infty^2|\boldsymbol{x}_m|^2}\right)\right)}{1+\omega^2\tau_s^2\left(1-\frac{\boldsymbol{u}_0\cdot\boldsymbol{x}_m}{a_\infty|\boldsymbol{x}_m|}\right)^2} \tag{2.69}$$

This relation is identical to the one proposed by Tam and Auriault (1999, eq. (35)), apart from original adjoint Green's function $p^\dagger_{\boldsymbol{x}_m}(\boldsymbol{x}_2,\omega)$ that is replaced by $\mathrm{D}_{-\boldsymbol{u}_0,\boldsymbol{x}_m}\left(\phi^\dagger_{\boldsymbol{x}_m}(\boldsymbol{x}_2,\omega)\right)$.

Taylor expansion

For completeness, the pressure autocorrelation S_{pp} double integral is approximated here using a Taylor expansion. At first order in $\boldsymbol{r}=\boldsymbol{x}_1-\boldsymbol{x}_2$,

$$\phi^\dagger_{\boldsymbol{x}_m}(\boldsymbol{r}+\boldsymbol{x}_2,\omega) \approx \phi^\dagger_{\boldsymbol{x}_m}(\boldsymbol{x}_2,\omega) + \boldsymbol{r}\cdot\frac{\partial\phi^\dagger_{\boldsymbol{x}_m}(\boldsymbol{x}_2,\omega)}{\partial\boldsymbol{x}_2} \tag{2.70}$$

Because $\boldsymbol{r}$ and $\boldsymbol{x}_2$ are independent of $\boldsymbol{x}_m$, the material derivative of previous relation gives,

$$\mathrm{D}_{-\boldsymbol{u}_0,\boldsymbol{x}_m}\left(\phi^\dagger_{\boldsymbol{x}_m}(\boldsymbol{r}+\boldsymbol{x}_2,\omega)\right) \approx \mathrm{D}_{-\boldsymbol{u}_0,\boldsymbol{x}_m}\left(\phi^\dagger_{\boldsymbol{x}_m}(\boldsymbol{x}_2,\omega)\right) + \boldsymbol{r}\cdot\frac{\partial\left(\mathrm{D}_{-\boldsymbol{u}_0,\boldsymbol{x}_m}\left(\phi^\dagger_{\boldsymbol{x}_m}(\boldsymbol{x}_2,\omega)\right)\right)}{\partial\boldsymbol{x}_2} \tag{2.71}$$

Mimic former derivations leads to following approximation for the sound pressure autocorrelation S_{pp},

$$\begin{aligned} S_{pp}(\boldsymbol{x}_m,\omega) = \int_\Omega \mathrm{d}\boldsymbol{x}_2 \ & \frac{2\hat{q}_s^2 l_s^3}{c^2\tau_s}\left(\frac{\pi}{\ln(2)}\right)^{3/2}\frac{\exp\left(-\frac{\omega^2 l_s^2}{4\ln(2)u_0^2}\right)}{1+\omega^2\tau_s^2}\left[\mathrm{D}_{-\boldsymbol{u}_0,\boldsymbol{x}_m}\left(\phi^\dagger_{\boldsymbol{x}_m}(\boldsymbol{x}_2,\omega)\right)\right]^* \\ & \times\left(\mathrm{D}_{-\boldsymbol{u}_0,\boldsymbol{x}_m}\left(\phi^\dagger_{\boldsymbol{x}_m}(\boldsymbol{x}_2,\omega)\right) - \frac{2i\omega\tau_s^2}{1+\omega^2\tau_s^2}\left(\boldsymbol{u}_0\cdot\frac{\partial\left(\mathrm{D}_{-\boldsymbol{u}_0,\boldsymbol{x}_m}\left(\phi^\dagger_{\boldsymbol{x}_m}(\boldsymbol{x}_2,\omega)\right)\right)}{\partial\boldsymbol{x}_2}\right)\right) \end{aligned} \tag{2.72}$$

2.2.4 Computation of $\mathrm{D}_{-\boldsymbol{u}_0,\boldsymbol{x}_m}\left(\phi^\dagger_{\boldsymbol{x}_m}(\boldsymbol{x}_2,\omega)\right)$

In previous expression the material derivative with reversed flow $\mathrm{D}_{-\boldsymbol{u}_0,\boldsymbol{x}_m}$ of $\phi^\dagger_{\boldsymbol{x}_m}$ needs to be evaluated. When the observer is set in a region were the fluid is at rest, the derivation is straightforward. In other cases, the knowledge of the gradient of $\phi^\dagger_{\boldsymbol{x}_m}$ is required along the exterior mean flow $\boldsymbol{u}_{ext}$. However with the adjoint approach, Green's functions are solely known at the position $\boldsymbol{x}_m$. From a general point of view, the calculation of an estimate of $\boldsymbol{u}_0\cdot\nabla\phi^\dagger_{\boldsymbol{x}_m}$ is possible by additionally computing the adjoint Green

function $\phi^\dagger_{\widetilde{\boldsymbol{x}_m}}$, where $\widetilde{\boldsymbol{x}_m} = \boldsymbol{x}_m + \varepsilon \dfrac{\boldsymbol{u}_{ext}}{|\boldsymbol{u}_{ext}|}$ and $\varepsilon > 0$. An estimate for the material derivative follows,

$$\begin{aligned} \mathrm{D}_{-\boldsymbol{u}_0,\boldsymbol{x}_m}\left(\phi^\dagger_{\boldsymbol{x}_m}(\boldsymbol{x}_2,\omega)\right) &= -i\omega\phi^\dagger_{\boldsymbol{x}_m}(\boldsymbol{x}_2,\omega) - \boldsymbol{u}_0\cdot\nabla\phi^\dagger_{\boldsymbol{x}_m}(\boldsymbol{x}_2,\omega) \\ &= -i\omega\phi^\dagger_{\boldsymbol{x}_m}(\boldsymbol{x}_2,\omega) - |\boldsymbol{u}_{ext}|\left(\frac{\phi^\dagger_{\widetilde{\boldsymbol{x}_m}}(\boldsymbol{x}_2,\omega) - \phi^\dagger_{\boldsymbol{x}_m}(\boldsymbol{x}_2,\omega)}{\varepsilon}\right)_{\varepsilon\to 0} \end{aligned} \tag{2.73}$$

If the observer is set in the acoustic far-field this calculation can be done analytically even in presence of an ambient flow. Indeed $\phi^\dagger_{\widetilde{\boldsymbol{x}_m}}(\boldsymbol{x}_2,\omega)$ then differs from $\phi^\dagger_{\boldsymbol{x}_m}(\boldsymbol{x}_2,\omega)$ by only a phase shift φ, this is illustrated in the sketch given in figure 2.3. The anti-causal adjoint field travels with a phase velocity

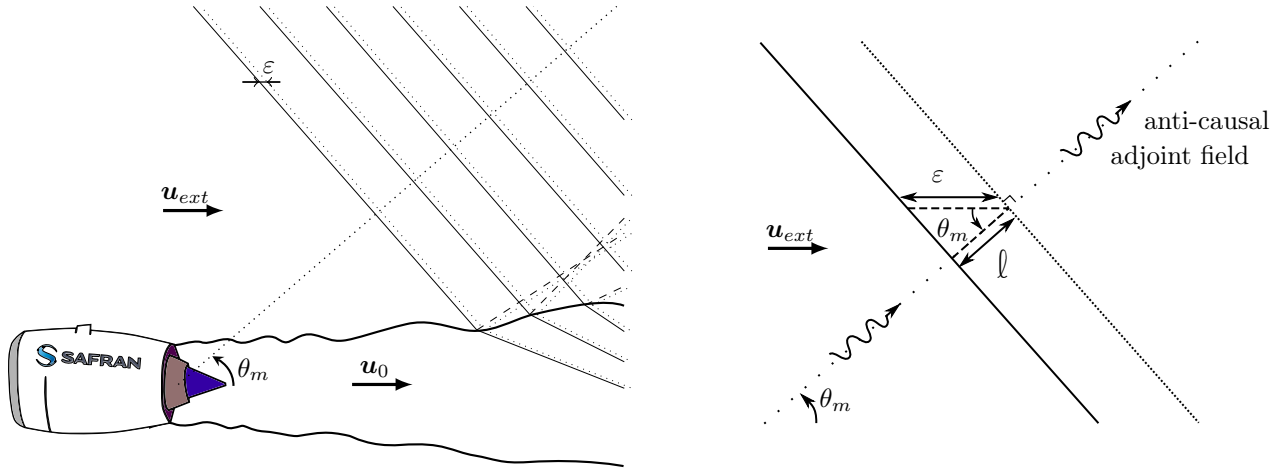

Figure 2.3: Moving from ε the adjoint source in the acoustic far-field is equivalent to add a phase shift φ.

$|\boldsymbol{v}_p| = a_\infty + |\boldsymbol{u}_{ext}|\cos\theta_m$ towards the observer set in the far-field. From the anti-causality property it comes $\phi^\dagger_{\widetilde{\boldsymbol{x}_m}}(\boldsymbol{x}_2,\omega)/\phi^\dagger_{\boldsymbol{x}_m}(\boldsymbol{x}_2,\omega) = e^{i\omega\varphi}$ with $\varphi > 0$. And the previous expression is recast into,

$$\mathrm{D}_{-\boldsymbol{u}_0,\boldsymbol{x}_m}\left(\phi^\dagger_{\boldsymbol{x}_m}(\boldsymbol{x}_2,\omega)\right) = \left(-i\omega - |\boldsymbol{u}_{ext}|\left[\frac{e^{i\omega\varphi}-1}{\varepsilon}\right]_{\varepsilon\to 0}\right)\phi^\dagger_{\boldsymbol{x}_m}(\boldsymbol{x}_2,\omega) \tag{2.74}$$

The computation of φ with help of figure 2.3 follows straightly, $\cos\theta_m = \ell/\varepsilon$ with $\ell = \varphi|\boldsymbol{v}_p|$. A Taylor expansion for small ε of the exponential function then readily gives,

$$\mathrm{D}_{-\boldsymbol{u}_0,\boldsymbol{x}_m}\left(\phi^\dagger_{\boldsymbol{x}_m}(\boldsymbol{x}_2,\omega)\right) = \left(-i\omega - i\frac{\omega|\boldsymbol{u}_{ext}|\cos\theta_m}{a_\infty + |\boldsymbol{u}_{ext}|\cos\theta_m}\right)\phi^\dagger_{\boldsymbol{x}_m}(\boldsymbol{x}_2,\omega) \tag{2.75}$$

Since the previous expression depends on the adjoint source location only by its polar angle θ_m, by defining $\phi^\dagger_{\boldsymbol{x}_m}(\boldsymbol{x}_2,\omega) \to \phi^\dagger_{\theta_m}(\boldsymbol{x}_2,\omega)$, a far-field expression for Tam and Auriault's mixing noise formula is obtained,

$$S_{pp}(\theta_m,\omega) = \int_\Omega \mathrm{d}\boldsymbol{x}_2\ \frac{2\omega^2\hat{q}_s^2 l_s^3}{c^2\tau_s}\left(\frac{\pi}{\ln(2)}\right)^{3/2}\left|\phi^\dagger_{\theta_m}(\boldsymbol{x}_2,\omega)\right|^2\left(1+\frac{M_{ext}\cos\theta_m}{1+M_{ext}\cos\theta_m}\right)^2\frac{\exp\left(\dfrac{-\omega^2 l_s^2}{4\ln(2)u_0^2}\left(1+M_\infty^2\sin^2\theta_m\right)\right)}{1+\omega^2\tau_s^2\left(1-M_\infty\cos\theta_m\right)^2} \tag{2.76}$$

where $M_\infty = u_0/a_\infty$ and $M_{ext} = |\boldsymbol{u}_{ext}|/a_\infty$. It is fairly straightforward to include in these derivations an azimuthal dependency on the microphone position ψ_m as well.

2.3 Ideas to proceed with Miller's BBSAN model

Tam and Auriault's mixing noise model can equivalently be recast for the acoustic potential ϕ as given by Pierce's equation (2.48). This is because the momentum source term of Tam and Auriault's mixing noise model, equation (2.7), is itself potential, see equation (2.49). Though a promising statistic noise modelling strategy needs to be able to account for all kind of sound sources. In perspective for future improvements, some indications are given here on how Miller's Broadband Shock Associated Noise (BBSAN) model could be recast for the acoustic potential.

Assuming the mean flow is parallel to mimic Tam and Auriault's model, Miller's BBSAN noise model (Morris and Miller, 2010) could be recast into,

$$\begin{cases} \rho_0 \dfrac{\mathrm{D}(\boldsymbol{u})}{\mathrm{D}t} + \nabla p = \rho_0 \boldsymbol{f}^v \\ \\ \dfrac{\mathrm{D}(p)}{\mathrm{D}t} + \gamma p_0 (\nabla \cdot \boldsymbol{u}) = 0 \end{cases} \tag{2.77}$$

where $\boldsymbol{f}^v = -(\nabla \boldsymbol{v}_t) \cdot \boldsymbol{v}_s - (\nabla \boldsymbol{v}_s) \cdot \boldsymbol{v}_c$ is the sound source responsible for the BBSAN, $\boldsymbol{v}_t$ and $\boldsymbol{v}_s$ are the velocity perturbations associated with the turbulence and the shock cells respectively. Miller (2010) modelled the noise source $\boldsymbol{f}^v$ with help of the shock-cell characteristic pressure p_s and a characteristic turbulent velocity fluctuation $\boldsymbol{v}_t$ such as $\boldsymbol{f}^v \propto p_s \boldsymbol{v}_t$. For this acoustic analogy to be recast identically with Pierce's equation, $\rho_0 p_s \boldsymbol{v}_t$ would need to derive from a potential, what seems to be a tall order. Two approaches are proposed here to proceed with an implementation of Miller's BSSAN model, such bypasses may possibly be used to model also other stochastic sound sources.

1. Miller's BBSAN model is based on an ad-hoc dimensional analysis. The driving parameters are then modelled from a RANS solution. This procedure can be fairly easily adapted to alternative expressions that derive from a potential source term, e.g. $\rho_0 \boldsymbol{f}^v \approx -\nabla(\rho_0 \boldsymbol{v}_t \cdot \boldsymbol{v}_s)$. This strategy requires a new calibration of the constants and a direct comparison with the original model of Miller may not be possible any more. Though this action plan seems the most robust of the both proposed here.

2. Previous effort to retrieve Tam and Auriault's mixing noise theory with a potential acoustic formulation simply turned out to be equivalent to replace $p^\dagger$ with $-D_{\boldsymbol{u}_0}(\phi^\dagger)$ in the final formula. To this end, compare the prediction formula obtained within the Fraunhofer approximation equations (2.38) and (2.69). Yet, if $p = -D_{\boldsymbol{u}_0}(\phi)$, the equality between $p^\dagger$ and $-D_{\boldsymbol{u}_0}(\phi^\dagger)$ is wrong in general, a counter-example is provided in (Spieser and Bailly, 2018, §§5-6). It is believed that this coincidence is due to the self-adjoint property of Pierce's equation. As this will be discussed later in § (3.4.3), if self-adjoint operators are considered the flow reversal theorem (FRT) applies. The adjoint equation then corresponds to the direct problem solution but with the flow direction reversed, and the equalities $p^\dagger = -D_{\boldsymbol{u}_0}(\phi^\dagger)$ and $\rho_0 \boldsymbol{u}^\dagger = \nabla \phi^\dagger$ are operable. Miller's BBSAN model can then be reused as is, but for adjoint Green's function correspondingly approximated with $\phi^\dagger$, i.e. the adjoint variable to the acoustic potential. More generally, whatever $\mathcal{L}_0$ and $\mathcal{L}_0^\dagger$ may be, by defining,

$$\mathcal{L}_0 \begin{pmatrix} \boldsymbol{u} \\ p \end{pmatrix} = \begin{pmatrix} \rho_0 \boldsymbol{f}^v \\ 0 \end{pmatrix} \qquad \text{and} \qquad \mathcal{L}_0^\dagger \begin{pmatrix} \boldsymbol{u}^\dagger_{\boldsymbol{x}_m, t_m} \\ p^\dagger_{\boldsymbol{x}_m, t_m} \end{pmatrix} = \begin{pmatrix} \boldsymbol{0} \\ \delta_{\boldsymbol{x}_m, t_m} \end{pmatrix} \tag{2.78}$$

as long $\mathcal{L}_0^\dagger$ is computed from $\mathcal{L}_0$ with the canonical scalar product, then Lagrange's identity applies,

$$p(\boldsymbol{x}_m, t_m) = < \rho_0 \boldsymbol{f}^v, \boldsymbol{u}^\dagger_{\boldsymbol{x}_m,t_m} > \tag{2.79}$$

Then by setting $S^\dagger_{p^\dagger} = \delta_{\boldsymbol{x}_m,t_m}$ and solving Pierce's adjoint equation, see equation (2.50), the adjoint variable to the velocity field can be approximated with $\boldsymbol{u}^\dagger_{\boldsymbol{x}_m,t_m} \approx \nabla\phi^\dagger/\rho_0$. This strategy needs still to be validated but seems more elegant and general than the previous one.

2.4 Calculus formulae

For $Re(\alpha) > 0$,

$$\int_{\mathbb{R}} \mathrm{d}x \ \exp\left(-\alpha x^2\right) = \sqrt{\frac{\pi}{\alpha}} \tag{2.80}$$

$$\int_{\mathbb{R}} \mathrm{d}x \ x \exp\left(-\alpha x^2\right) = 0 \tag{2.81}$$

For $Re(\alpha) + Im(\beta) > 0$,

$$\int_{\mathbb{R}} \mathrm{d}x \ \exp\left(-\alpha|x| + i\beta x\right) = \frac{1}{\alpha - i\beta} + \frac{1}{\alpha + i\beta} = \frac{2\alpha}{\alpha^2 + \beta^2} \tag{2.82}$$

$$\int_{\mathbb{R}} \mathrm{d}x \ x \exp\left(-\alpha|x| + i\beta x\right) = \frac{1}{(\alpha - i\beta)^2} - \frac{1}{(\alpha + i\beta)^2} = \frac{4i\alpha\beta}{(\alpha^2 + \beta^2)^2} \tag{2.83}$$

Integral computation found in (Gradshteyn and Ryzhik, 1963, eq. (3.323), p.337 in 7th ed.) for $Re(p^2) > 0$,

$$\int_{\mathbb{R}} \mathrm{d}x \ \exp\left(-p^2x^2 \pm qx\right) = \frac{\sqrt{\pi}}{p} \exp\left(\frac{q^2}{4p^2}\right) \tag{2.84}$$

3 Reciprocity principle for self-adjoint wave equations

Summary: The most general statement for reciprocity principle is based upon adjoint formalism. In this chapter, a comprehensive description of the adjoint approach is proposed and the benefit of using self-adjoint wave equations to solve acoustic propagation problem is highlighted. Tam and Auriault (1998) presented how an adjoint approach can be built to predict the noise of distributed stochastic sources in a complex environment (Tam and Auriault, 1999). A clear statement is also provided about the application of the flow reversal theorem (FRT), and about its restriction to self-adjoint wave equations. As an illustration, sound propagation is computed numerically over a sheared and stratified mean flow for Lilley's and Pierce's wave equations. Acoustic solutions obtained with the adjoint approach are then compared to predictions obtained with the FRT. The reader not familiar with the adjoint method is referred to § B.1 for a very simple illustrative execution of the technique.

3.1 Introduction

In the early beginning of acoustics, Helmholtz (1860) already formulated the well known reciprocity principle: *a disturbance produced at a source location A and recorded at a receiver point B, is identical to what would have been recorded at the source location A if the same disturbance occurred in B.* This principle, generalised to dissipative systems by Lord Rayleigh (Strutt, 1877, §§ 72-78, 107-111), indicates that sound propagation is not a matter of the features of the sound emitter or receiver, but only depends on the property of the considered medium. Despite this early discovery, the reciprocity principle has not been widely used by the acoustics community. Eversman (1976) and Cho (1980) for ducted systems, and Bojarski (1983) for the free-field problem, derived general reciprocity relations for acoustic media at rest. An outstanding work was done by Levine and Schwinger (1948) who first used the reciprocity principle to determine the directivity pattern of a complex sound propagation problem. In their investigation of the far-field radiation from an unflanged duct, the authors exchanged observer and source positions, and turned the complex radiation problem into the equivalent problem of a plane wave coming from infinity and impinging at the duct end. In the same spirit, later the reciprocity principle has also been employed by Crighton and Leppington (1970, 1971, 1973) to analytically derive the far-field radiation of an acoustic source in the vicinity of a refracting body. These contributions permitting the continuation of a near-field acoustic solution to the far-field are important, because they have since motivated most of the investigations involving the reciprocity principle in aeroacoustics.

The failure of the standard reciprocity principle in arbitrary media was also quickly identified. Rayleigh (Strutt, 1877, § 111) already stated that: "*It is important to remember that the Principle of Reciprocity is limited to systems which vibrate about a configuration of equilibrium, and is therefore not to be applied without reservation to such a problem as that presented by the transmission of sonorous waves through the atmosphere when disturbed by wind.*". Several contributions thus aimed at properly delimiting its domain of validity. Landau and Lifshitz (1959) proved the reciprocity principle for a variable index of refraction. Lyamshev (1961) generalised the reciprocity principle in the presence of a uniform mean flow with the so-called flow reversal theorem (FRT), illustrated in figure 3.1. A similar formulation was used by Dowling et al. (1978) and by Dowling (1983) for piecewise uniform flows. Howe (1975b) proved the reciprocity principle for potential mean flows to first order in Mach number. Möhring then extended the FRT to all potential mean flows (Möhring, 1978, 1979) and gave indications on reciprocity for rotational flow (Möhring, 2001). Godin et al. attempted to generalise the FRT to arbitrary mean flows (Godin, 1997), and proved a general version of Fermat's principle for ray acoustics (Godin and Voronovich, 2004). One of the objectives of this study is to carry out computations of reciprocal solutions involving the FRT in order to assess the validity of this technique for propagation problems in complex mean flows.

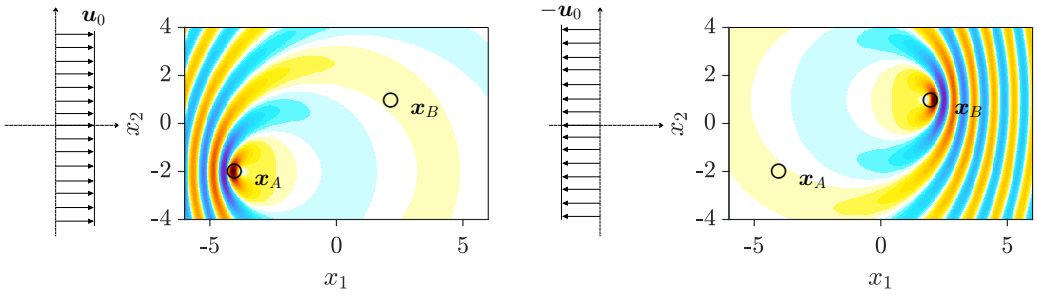

Figure 3.1: Green's function for the acoustic pressure field $G_{\boldsymbol{x}_A}$ generated by a harmonic source in a uniform mean flow with an observer set at $\boldsymbol{x}_B$ (left); $G^-_{\boldsymbol{x}_B}$ for the reversed flow is depicted where source and receiver locations have been switched (right). The FRT states that $G_{\boldsymbol{x}_A}(\boldsymbol{x}_B) = G^-_{\boldsymbol{x}_B}(\boldsymbol{x}_A)$.

A proper mathematical generalisation of the reciprocity principle, however, requires the introduction of the adjoint formalism (Morse and Feshbach, 1953, § 7.5; Lamb Jr., 1995, § 4.6.1; Stone and Goldbart, 2009, § 4.2.1). Although the use of the adjoint formalism is long-standing in the flow receptivity community (Roberts, 1960; Hill, 1995; Luchini and Bottaro, 1998; Barone and Lele, 2005) and became a staple in optimisation and control (Jameson, 1988; Giles and Pierce, 1997; Wei and Freund, 2006), its use in aeroacoustic computations is fairly recent. The first correct generalisation of the reciprocity principle to tackle acoustic propagation in arbitrary mean flows was formulated by Tam and Auriault (1998) for the linearised Euler equations (LEE) and for Lilley's equation (Lilley et al., 1972). Another aim of this study is to recall the adjoint methodology in a synoptic and broader way.

Besides the general derivation of the methodology, Tam and Auriault (1998) mainly focuses on the formulation of the adjoint as the sum of a quasi-analytical solution of a propagation problem on an axisymmetric parallel mean flow for the adjoint Lilley equation, and an additional contribution induced by the jet spreading is solved numerically using a Fourier mode decomposition. This remarkable analytical solution has since been widely reused in the literature to assess jet noise polar directivity (Tam and Auriault, 1999; Tam et al., 2005; Khavaran and Bridges, 2005; Afsar et al., 2006; Raizada and Morris, 2006; Miller, 2014b; Gryazev et al., 2018), and has been simplified by Afsar (2009). This handy analytical model has been improved by Goldstein and Leib (2008) in the low-frequency range to include jet spreading and then

used repeatedly (Afsar, 2010; Goldstein et al., 2012; Afsar et al., 2016b,a). Afsar et al. (2017b) improved the formulation further with a composite solution for Green's function uniformly valid for all frequencies. In the same line, Cheung et al. (2015) developed a method to solve semi-analytically Lilley's equation for non-axisymmetric parallel flows to address azimuthal directivity, yet without falling back to an adjoint formalism.

In numerous relevant configurations, the mean flow topology in which acoustics propagates is complex, e.g. consider the dissymmetric dual stream hot jet flow behind an aircraft engine as computed by Mosson et al. (2014), and computational aeroacoustics tools are needed to address correctly the propagation problem. In the present work a purely numerical method is therefore presented to solve adjoint-based propagation problems. The aeroacoustics community has already computed numerically adjoint Green's function for arbitrary mean flows: Tam and Pastouchenko (2002), Pastouchenko and Tam (2007), and recently Xu et al. (2015), used the method to assess the azimuthal directivity of non-axisymmetric jets. Tam et al. (2010) also achieved with this method continuation of a near-field acoustic solution to the far-field in the presence of flow heterogeneities. In parallel to these studies, the group of Karabasov et al. implemented the adjoint linearised Euler equations first two-dimensionally (Karabasov and Hynes, 2005) then three-dimensionally (Semiletov and Karabasov, 2013) and tackled numerically the acoustic far-field radiation for an arbitrary jet profile (Karabasov et al., 2013; Depuru Mohan et al., 2015). Nevertheless, except some scarce contributions (Alonso and Burdisso, 2007), in all the studies mentioned above, the adjoint solution is always sought as the solution to a scattering problem, with furthermore the adjoint source set in the far-field. In the present study, the adjoint method is recalled in a systematic and general way valid for any linear operator, any propagation media and propagation distance. Even if some adjoint computations including surfaces have been conducted (Pastouchenko and Tam, 2007; Tam et al., 2010; Xu et al., 2015), including liners in (Alonso and Burdisso, 2007), as pointed out by Miller (Miller, 2014a) the currently used formulation of the adjoint method cannot account for diffraction at surface edges. This is because the adjoint field is already sought as the solution to a scattering problem to account for flow refraction effects. Analogously with Barone and Lele (2005), the adjoint method as presented here has the capability to tackle adequately diffraction phenomena.

The general derivation of the adjoint methodology, its validation for a non-trivial case, and its comparison against the FRT are the main purposes of this chapter. To achieve these objectives, two different waves equations − Pierce's wave equation (Pierce, 1990) which is self-adjoint, and Lilley's wave equation (Lilley et al., 1972) − are considered. The script is organised here as follows: the theoretical background of the adjoint formalism is laid out in §3.2, the adjoint method is then executed for a well-documented sheared and stratified mean flow case for Lilley's equation and compared with results obtained with the FRT in §3.3. In §3.4 both methodology are compared for Pierce's wave equation to illustrate numerically the equivalence between the adjoint approach and the FRT for a self-adjoint wave equation. Concluding remarks are finally drawn.

3.2 The adjoint method in the propagation problem

3.2.1 Lagrange's identity

In the framework of the adjoint method, the physical relevant problem is often qualified as *direct* in opposition to what is defined as the *adjoint* problem. Consider a pressure field p and a source term s,

a linear acoustic propagation problem may be described by a linear operator $\mathcal{L}_0$ so that the physical problem of interest − the direct problem − may be written over a domain Ω as

$$\begin{cases} \mathcal{L}_0\ p = s & \text{in } \Omega \\ \mathcal{B}_0\ p = 0 & \text{on } \partial\Omega \end{cases} \tag{3.1}$$

with $\mathcal{B}_0$ the boundary conditions that are necessary for the problem to be well-posed. A cornerstone for the adjoint method is Lagrange's identity (Morse and Feshbach, 1953, § 7.5; Stone and Goldbart, 2009, § 4.2.1) which relates the direct and adjoint fields with help of a scalar product and reads: given a scalar product $<,>$, there exists a unique operator $\mathcal{L}_0^\dagger$ and specific boundary conditions $\mathcal{B}_0^\dagger$ (Giles and Pierce, 1997) such that for any field $p^\dagger$:

$$< p^\dagger, \mathcal{L}_0\ p > = < \mathcal{L}_0^\dagger\ p^\dagger, p > \tag{3.2}$$

where $p^\dagger$ is referred to as the adjoint field. Introducing the adjoint source $s^\dagger$, such that $s^\dagger = \mathcal{L}_0^\dagger\ p^\dagger$, the adjoint problem associated with (3.1) with respect to $<,>$ may be written as

$$\begin{cases} \mathcal{L}_0^\dagger\ p^\dagger = s^\dagger & \text{in } \Omega \\ \mathcal{B}_0^\dagger\ p^\dagger = 0 & \text{on } \partial\Omega \end{cases} \tag{3.3}$$

Lagrange's identity can then be recast in the following convenient form:

$$< p^\dagger, s > = < s^\dagger, p > \tag{3.4}$$

From this relation it is clear that there is no strict equality between the direct field p and the adjoint field $p^\dagger$. Only the source and field projections are cross-related as defined in (3.4). Adjoint fields $p^\dagger$ and sources $s^\dagger$ are only mathematical tools with consistent units. Let $\boldsymbol{X}_m$ be the coordinate of a microphone point, then adjoint Green's function $G^\dagger_{\boldsymbol{X}_m}$ for an impulse Dirac source $\delta_{\boldsymbol{X}_m}$ is defined by

$$\begin{cases} \mathcal{L}_0^\dagger\ G^\dagger_{\boldsymbol{X}_m} = \delta_{\boldsymbol{X}_m} & \text{in } \Omega \\ \mathcal{B}_0^\dagger\ G^\dagger_{\boldsymbol{X}_m} = 0 & \text{on } \partial\Omega \end{cases} \tag{3.5}$$

Lagrange's relation then directly gives the formula used in practice to rebuild the direct solution from the adjoint one:

$$p(\boldsymbol{X}_m) = < G^\dagger_{\boldsymbol{X}_m}, s > \tag{3.6}$$

These statements are general and apply in the time domain, where $\boldsymbol{X}_m \equiv (\boldsymbol{x}_m; t_m)$ and $\delta_{\boldsymbol{X}_m} \equiv \delta(\boldsymbol{x} - \boldsymbol{x}_m)\delta(t - t_m)$, as well as in the Fourier domain for which $\boldsymbol{X}_m \equiv \boldsymbol{x}_m$ and $\delta_{\boldsymbol{X}_m} \equiv \delta(\boldsymbol{x} - \boldsymbol{x}_m)$. In the rest of this study for the sake of simplicity only scalar wave equations are considered, but it is straightforward to transpose these results to multivariable linear operators (Wapenaar, 1996) by making use of a multivariable Hermitian scalar product, resulting in turn in the computation of vector adjoint Green's functions.
In the literature, the relation (3.6) is sometimes referred to as the *representation theorem* (Vasconcelos et al., 2009). In their pioneering work, Tam and Auriault (1998, eq. (A 12)), derived a first version of this relation enabling fluctuating pressure predictions for sources of the momentum equations. An extension to sources set in the energy equation has been given by Afsar et al. (2006, 2007). The expression given here is its general expression and handles any linear operator $\mathcal{L}_0$ and any scalar product, any source term s can be used to rebuild any field variable p from the considered linear operator $\mathcal{L}_0$ if corresponding adjoint

Green's function $G^{\dagger}_{\boldsymbol{X}_m}$ is computed.
One convenient feature of the adjoint method, is to change the convolution nature of Green's integral representation of the solution into a correlation type representation (Vasconcelos et al., 2009). As an illustration, consider a time domain problem, with $< f, g > = \int_{\mathbb{R}} dt \int_{\Omega} d\boldsymbol{x}\ f(\boldsymbol{x},t)g(\boldsymbol{x},t)$, then Green's formula reads

$$p(\boldsymbol{x}_m, t_m) = \int_{\mathbb{R}} dt_s \int_{\Omega} d\boldsymbol{x}_s\ G_{\boldsymbol{x}_s,t_s}(\boldsymbol{x}_m, t_m) s(\boldsymbol{x}_s, t_s) \tag{3.7}$$

where for the sake of clarity boundary conditions have been omitted. If now a shift-invariant problem is considered, i.e. $G_{\boldsymbol{x}_s,t_s}(\boldsymbol{x}_m, t_m) \equiv G(\boldsymbol{x}_m - \boldsymbol{x}_s, t_m - t_s)$, the previous expression can be expressed as a double convolution product over the source position $\boldsymbol{x}_s$ and emission time t_s. In contrast, the operational expression of Lagrange's identity given in (3.6) writes

$$p(\boldsymbol{x}_m, t_m) = \int_{\mathbb{R}} dt_s \int_{\Omega} d\boldsymbol{x}_s\ G^{\dagger}_{\boldsymbol{x}_m,t_m}(\boldsymbol{x}_s, t_s) s(\boldsymbol{x}_s, t_s) = < G^{\dagger}_{\boldsymbol{x}_m,t_m}, s > \tag{3.8}$$

Relying on conventional Green's integral method, $G_{\boldsymbol{x}_s,t_s}$ should be recomputed for each $\boldsymbol{x}_s$, whereas if the solution p of the propagation problem is sought at one single point $\boldsymbol{x}_m$, the adjoint method requires only a single calculation of $G^{\dagger}_{\boldsymbol{x}_m,t_m}$ at $\boldsymbol{x}_m$. This approach shows to be very efficient from a computational point of view, for acoustic prediction to a finite number of points of widespread stochastic sources; this is precisely the appeal of this technique. What is more, as long as the mean flow of the propagation problem and the observer are unchanged, adjoint Green's function $G^{\dagger}_{\boldsymbol{x}_m,t_m}$ can be reused.
At last, recall that the adjoint representation is not unique (Roberts, 1960), different scalar products lead indeed to different adjoint formulations. Attention must therefore be paid when comparing, for instance, the adjoint pressure $p^{\dagger}$ computed from the set of adjoint LEE with the adjoint pressure $p^{\dagger}$ computed with adjoint Lilley's equation (Tam and Auriault, 1998, fig. 9), in general those both variables have no common points.

3.2.2 Reciprocity relation and the notion of self-adjointness

Adjoint Green's function $G^{\dagger}_{\boldsymbol{x}_m,t_m}$ for a source position $\boldsymbol{x}_m$ at time t_m, is defined by

$$\begin{cases} \mathcal{L}_0^{\dagger}\ G^{\dagger}_{\boldsymbol{x}_m,t_m}(\boldsymbol{x},t) = \delta(\boldsymbol{x}-\boldsymbol{x}_m)\delta(t-t_m) & \text{in } \Omega \\ \mathcal{B}_0^{\dagger}\ G^{\dagger}_{\boldsymbol{x}_m,t_m}(\boldsymbol{x},t) = 0 & \text{on } \partial\Omega \end{cases} \tag{3.9}$$

when instead of the physical problem defined in (3.1), an impulsive problem at position $\boldsymbol{x}_s$ and time t_s is considered:

$$\begin{cases} \mathcal{L}_0\ G_{\boldsymbol{x}_s,t_s}(\boldsymbol{x},t) = \delta(\boldsymbol{x}-\boldsymbol{x}_s)\delta(t-t_s) & \text{in } \Omega \\ \mathcal{B}_0\ G_{\boldsymbol{x}_s,t_s}(\boldsymbol{x},t) = 0 & \text{on } \partial\Omega \end{cases} \tag{3.10}$$

The general scalar reciprocity principle is recovered with help of Lagrange's identity (3.4) and the above-introduced scalar product $< , >$:

$$G_{\boldsymbol{x}_s,t_s}(\boldsymbol{x}_m, t_m) = G^{\dagger}_{\boldsymbol{x}_m,t_m}(\boldsymbol{x}_s, t_s) \tag{3.11}$$

As the direct problem is causal, its adjoint is then necessary anti-causal, e.g. (Goldstein, 2006, eq. (A8)),

$$t_m < t_s, \quad G_{\boldsymbol{x}_s,t_s}(\boldsymbol{x}_m, t_m) = 0 \qquad \Longrightarrow \qquad t_s > t_m, \quad G^{\dagger}_{\boldsymbol{x}_m,t_m}(\boldsymbol{x}_s, t_s) = 0 \tag{3.12}$$

This complies with the analysis of Karabasov et al. (Semiletov and Karabasov, 2013;Karabasov and Sandberg, 2015) and Afsar et al. (2017b) who stressed that, the adjoint source acts as a sink and that the adjoint acoustic solution is inward-going, but goes beyond. The adjoint solution needs furthermore to go backward in time and is intrinsically anti-causal (Lamb Jr., 1995, §§ 4.5, 4.6;Stone and Goldbart, 2009, § 4.2). This has been pointed out in the flow receptivity community by Luchini and Bottaro (1998) and since then is well-established (Wei and Freund, 2006; Barone and Lele, 2005). A proof for this can be found in the literature for the heat equation (Stone and Goldbart, 2009, § 6.4.2) and is given in appendix B.2 for the convected Helmholtz's wave equation.
As a consequence, only some very specific problems may verify (3.1) ≡ (3.3). Such problems are referred to as self-adjoint (or symmetric) for which the well known symmetry property of Green's function is recovered. Strictly speaking, due to the boundary conditions, no self-adjoint problem exists for time-dependant problems. The solution would indeed need to be causal and anti-causal at the same time. In this work, the mathematical self-adjoint definition is gently relaxed so to also call self-adjoint, time problems for which Green's function, for the usual scalar product, verifies $G^{\dagger}_{\boldsymbol{x}_m,t_m}(\boldsymbol{x}_s,t_s) = G_{\boldsymbol{x}_s,-t_s}(\boldsymbol{x}_m,-t_m)$. From this standpoint, the acoustic problem governed by Helmholtz's equation is self-adjoint, see Morse and Feshbach (1953, § 7.3) or Eisler (1969). Skew-symmetric problems are also included in this enlarged definition of self-adjointness. This seems reasonable, since for some well-chosen scalar products, the LEE for a uniform and steady mean flow are skew-symmetric while Helmholtz's equation, which is physically equivalent in its description, is symmetric. This result, moreover complies with the work of Möhring (2001), in which the classical reciprocity principle is derived from antisymmetric relations. Thus for an acoustic propagation problem with ordinary boundary conditions to verify this enlarged definition of self-adjointness, it is sufficient that $\mathcal{L}_0^{\dagger} = \pm\mathcal{L}_0$.

3.3 Application to Lilley's equation

3.3.1 Derivation of Lilley's adjoint problem

Acoustic propagation in a steady parallel mean flow is considered. In spite of their apparent limitations, these mean flows are of practical importance since they correspond to configurations encountered in jets and many subtle phenomena can be described with them. The equation derived by Lilley et al. (1972) is known to take exactly the acoustic propagation effects over such parallel mean flows into account. This section shows how an adjoint method based upon this wave equation can be used.
From now on, and in later sections, all results will be derived in the frequency domain for a pulsation frequency ω, which is related to the time domain through Fourier transform,

$$F(\boldsymbol{x},\omega) = \int_{-\infty}^{\infty} f(\boldsymbol{x},t)e^{+i\omega t}dt \quad \text{and} \quad f(\boldsymbol{x},t) = \frac{1}{2\pi}\int_{-\infty}^{\infty} F(\boldsymbol{x},\omega)e^{-i\omega t}d\omega \tag{3.13}$$

Following this convention, the material derivative along the mean flow writes as $D_{\boldsymbol{u}_0} = \{-i\omega + \boldsymbol{u}_0\cdot\nabla\}$. Consistently, the canonical scalar product for complex valued functions, defined for f and g by

$$< f, g > = \int_{\Omega} d\boldsymbol{x}\ f(\boldsymbol{x})^* g(\boldsymbol{x}) \tag{3.14}$$

is considered, where f^* denotes the complex conjugate of f. Let $\boldsymbol{u}_0 = u_{0,1}\boldsymbol{e}_1$ be the mean velocity field with $\boldsymbol{e}_1$ a unit vector in the flow direction, ρ_0 the mean density and p_0 the mean pressure considered. The evolution of the fluctuating pressure p is governed by Lilley's equation and obeys some radiating

boundary condition $\mathcal{B}_0$, leading to the direct problem

$$\begin{cases} \mathcal{L}_0\ p = D_{\boldsymbol{u}_0}\left(D^2_{\boldsymbol{u}_0}(p) - \nabla\cdot(a_0^2\nabla p)\right) + 2a_0^2\nabla u_{0,1}\cdot\nabla\left(\dfrac{\partial p}{\partial x_1}\right) = S_{Lilley} & \text{in } \Omega \\ \mathcal{B}_0\ p = 0 & \text{on } \partial\Omega \end{cases} \tag{3.15}$$

where $a_0 = \sqrt{\gamma p_0/\rho_0}$ is the mean speed of sound. The source term S_{Lilley} of Lilley's equation can be expressed with some generic source term definition $(S_\rho, \boldsymbol{S_u}, S_p)$ of the LEE, and can be found in the literature, e.g. in Bailly et al. (2010, eq. (26)),

$$S_{Lilley} = D_{\boldsymbol{u}_0}\left(D_{\boldsymbol{u}_0}(S_p) - \gamma p_0\left(\nabla\cdot\boldsymbol{S_u}\right)\right) + 2\gamma p_0\nabla u_{0,1}\cdot\left(\frac{\partial \boldsymbol{S_u}}{\partial x_1}\right) \tag{3.16}$$

To define the corresponding adjoint problem, the linear operator $\mathcal{L}_0^\dagger$ and adjoint boundary conditions $\mathcal{B}_0^\dagger$ which fulfil Lagrange's identity are now sought. Starting with the left-hand side of Lagrange's identity (3.2),

$$< p^\dagger, \mathcal{L}_0\ p > = \int_\Omega d\boldsymbol{x}\ p^{\dagger *}\left\{D_{\boldsymbol{u}_0}\left(D^2_{\boldsymbol{u}_0}(p) - \nabla\cdot(a_0^2\nabla p)\right) + 2a_0^2\nabla u_{0,1}\cdot\nabla\left(\frac{\partial p}{\partial x_1}\right)\right\} \tag{3.17}$$

the right-hand side of the equality is obtained after using integration by parts and other vector calculus formulas, leading to

$$\begin{aligned} < p^\dagger, \mathcal{L}_0\ p > = \int_\Omega d\boldsymbol{x}\ \Bigg\{ & -D_{\boldsymbol{u}_0}\left(D^2_{\boldsymbol{u}_0}(p^\dagger) - \nabla\cdot(a_0^2\nabla p^\dagger)\right) \\ & +4a_0^2\nabla u_{0,1}\cdot\nabla\left(\frac{\partial p^\dagger}{\partial x_1}\right) + 3\nabla\cdot\left(a_0^2\nabla u_{0,1}\right)\frac{\partial p^\dagger}{\partial x_1}\Bigg\}^* p \\ & +\nabla\cdot\left[\left(D^2_{\boldsymbol{u}_0}(p^\dagger)^*p - D_{\boldsymbol{u}_0}(p^\dagger)^* D_{\boldsymbol{u}_0}(p)\right)\boldsymbol{u}_0\right] \\ & +\nabla\cdot\left[p^{\dagger *}\left(D^2_{\boldsymbol{u}_0}(p) - \nabla\cdot(a_0^2\nabla p)\right)\boldsymbol{u}_0\right] \\ & +\nabla\cdot\left[\left(-2a_0^2\frac{\partial p^{\dagger\ *}}{\partial x_1}\nabla u_{0,1} - a_0^2\nabla(D_{\boldsymbol{u}_0}(p^\dagger))^*\right)p\right] \\ & +\nabla\cdot\left[-2a_0^2 p^{\dagger *}(\nabla p\cdot\nabla u_{0,1})\boldsymbol{x_1} + a_0^2 D_{\boldsymbol{u}_0}(p^\dagger)^*\nabla p\right] \end{aligned} \tag{3.18}$$

The Green-Ostrogradsky theorem helps to express the divergence term as a contour integral. $\mathcal{B}_0^\dagger$ is defined so that together with $\mathcal{B}_0$ this boundary term is zero. Thus, if p and $p^\dagger$, respectively, satisfy their boundary conditions, the previous contour integral does not contribute and Lagrange's identity, $< p^\dagger, \mathcal{L}_0\ p > = < \mathcal{L}_0^\dagger\ p^\dagger, p >$ is retrieved. Finally by identification, the adjoint problem associated with Lilley's equation is obtained as

$$\begin{cases} \mathcal{L}_0^\dagger\ p^\dagger = & -D_{\boldsymbol{u}_0}\left(D^2_{\boldsymbol{u}_0}(p^\dagger) - \nabla\cdot(a_0^2\nabla p^\dagger)\right) + 4a_0^2\nabla u_{0,1}\cdot\nabla\left(\dfrac{\partial p^\dagger}{\partial x_1}\right) \\ & +3a_0^2\Delta u_{0,1}\dfrac{\partial p^\dagger}{\partial x_1} + 3\dfrac{\partial p^\dagger}{\partial x_1}\nabla a_0^2\cdot\nabla u_{0,1} \end{cases} \quad \text{in } \Omega$$

$$\mathcal{B}_0^\dagger\ p^\dagger = 0 \quad \text{on } \partial\Omega \tag{3.19}$$

One has $\mathcal{L}_0^\dagger \neq \pm\mathcal{L}_0$ and Lilley's equation is therefore not self-adjoint.
In the following, a numerical execution of the adjoint method is conducted for a sheared and stratified mean

flow, for which Lilley's equation and its adjoint are solved. Computations are achieved with PROPA, an in-house frequency domain code using a direct inversion method[1]. Care must be taken in the implementation of the adjoint anti-causality conditions. A description of the numerical procedure is provided in §3.1 of part I.

3.3.2 Solution to the direct problem

The direct problem under consideration here is the two-dimensional radiation of an acoustic source set in a sheared and stratified flow and corresponds to the well-documented mean flow analysed in the fourth computational aeroacoustic workshop (Dahl, 2004). The mean velocity profile follows a Gaussian evolution in the transverse direction

$$\frac{u_{0,1}(x_2)}{u_j} = \exp\left(-\frac{x_2^2}{2\sigma^2}\right) \tag{3.20}$$

where $\boldsymbol{x} = (x_1, x_2)$, $u_j = M_j a_j$, $a_j = \sqrt{\gamma R T_j}$ and $\sigma = \sqrt{0.845 \cdot \log(2)}\,\mathrm{m}$ is its standard deviation. To model a high-speed and heated jet flow, the following values are taken: $M_j = 0.756$, $T_j = 600\,\mathrm{K}$, $T_\infty = 300\,\mathrm{K}$, $\gamma = 1.4$ and $R = 287\,\mathrm{m^2{\cdot}s^{-2}{\cdot}K^{-1}}$. Considering $\rho_j = \gamma p_0 / a_j^2$ and $p_0 = 103330\,\mathrm{Pa}$, the mean density $\rho_0(x_2)$ is defined with Crocco-Busemann's law

$$\frac{\rho_j}{\rho_0(x_2)} = \frac{T_\infty}{T_j} - \left(\frac{T_\infty}{T_j} - 1\right)\frac{u_{0,1}(x_2)}{u_j} + \frac{\gamma - 1}{2} M_j^2 \frac{u_{0,1}(x_2)}{u_j}\left(1 - \frac{u_{0,1}(x_2)}{u_j}\right) \tag{3.21}$$

The stability analysis of this mean flow profile has been performed and the spatial growth rate of the Kelvin-Helmholtz instability wave is given in Bailly and Bogey (2003, fig. 1). To avoid the triggering of these hydrodynamic waves, a source pulsation of $\omega = 200\pi\,\mathrm{rad{\cdot}s^{-1}}$ is chosen, which ensures possible vortical disturbances are damped and do not corrupt the acoustic solution. This frequency corresponds to a Strouhal number of $St_{2\sigma} = 2\sigma f / u_j = 0.60$ and to $\omega b / u_j = 2.20$ according to the notation given in Bailly and Bogey (2003). The source for Lilley's equation chosen here corresponds to a quadrupole source $\rho_0 \boldsymbol{S_u}$ of unitary amplitude, computed as the gradient of a Gaussian monopolar source S_m whose spatial variation is given by $S_m = \sigma_s \sqrt{e}\, e^{-(x_1^2 + x_2^2)/(2\sigma_s^2)}$, where $\sigma_s = \sigma/4$. This sound source for the direct problem $\rho_0 \boldsymbol{S_u} = \nabla S_m$ is taken into account in Lilley's equation with the relation (3.16), and is depicted in figure 3.2. The channelling of acoustic waves propagating in the opposite direction to the mean flow inside the jet, and the generation of a cone of silence downstream, can be easily identified in the computed fields; however, the quadrupole nature of the acoustic source is not.

3.3.3 Reconstruction of the solution with the adjoint method

The adjoint method is now used to recover the direct field solution. For this analysis a sample of 69 equispaced adjoint sources along a line $\boldsymbol{x}_2/\sigma = 9.0$ is considered. For each of these adjoint sources the anti-causal adjoint Lilley's problem (3.19) is solved. The same base flow, the same mesh and the same frequency as for the direct problem are considered. Figure 3.3 shows two samples of adjoint Green's problem solved among a total set of 69. Wherever the mean velocity gradient is zero, the adjoint Lilley equation behaves like a classical acoustic propagation operator. This can be observed in figure 3.3 and inferred from the self-adjoint property of Lilley's equation for a constant flow profile (compare (3.15) and (3.19)). Yet wherever the mean flow is sheared, the propagation problem ceases to be self-adjoint and

[1] Comment of a jury member: since the inverse system matrix is not directly computed, the system is solved with a *factorisation* rather than with a *direct inversion* technique.

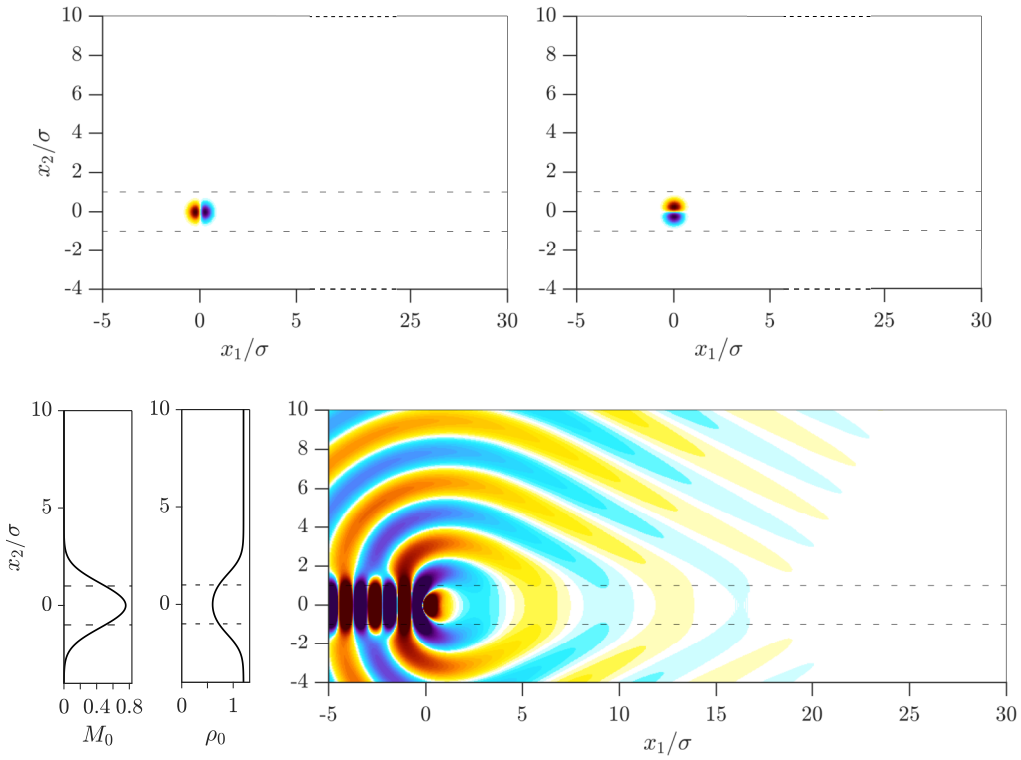

Figure 3.2: Direct problem for Lilley's wave equation. Linearised Euler equations equivalent quadrupole source $\rho_0 \boldsymbol{S_u}$ forcing the direct problem $\rho_0 S_{u_1}$ (top-left), and $\rho_0 S_{u_2}$ (top-right). Mach number M_0 and density ρ_0 profiles of the parallel mean flow considered (bottom-left), and the real part of the pressure field is shown (bottom-right). Dashed lines represent the position of maximal shearing ($x_2/\sigma = 1$).

specific features of the adjoint formulation (3.19) are expected. The wave patterns warped in the flow channel for numerical adjoint Green's function computed at $\boldsymbol{x}_m/\sigma = (25, 9.0)$ and shown in figure 3.3 is such a phenomenon. Recall that the fields presented in figure 3.3 are anti-causal and focus toward the adjoint source term.

To properly define adjoint Green's function $G^\dagger_{\boldsymbol{x}_m}$, the impulse response of the linear operator $\mathcal{L}_0^\dagger$ should be considered, that is $\mathcal{L}_0^\dagger \; G^\dagger_{\boldsymbol{x}_m} = \delta_{\boldsymbol{x}_m}$. For most numerical solvers, computing the solution to an exact Dirac delta function $\delta_{\boldsymbol{x}_m}$ is tricky. A bypass to this is considered here; narrow Gaussian sources are chosen to force the linear operator $\mathcal{L}_0^\dagger$ given in (3.19). Then when the size L of the numerical adjoint source $S^{\dagger,N}_{\boldsymbol{x}_m}$ is small with respect to the acoustic wavelength λ, mathematical Green's function $G^\dagger_{\boldsymbol{x}_m}$ can be approximated with the following normalisation of numerical Green's function $G^{\dagger,N}_{\boldsymbol{x}_m}$:

$$G^\dagger_{\boldsymbol{x}_m}(\boldsymbol{x}) \;\approx\; G^{\dagger,N}_{\boldsymbol{x}_m}(\boldsymbol{x}) \Big/ \int_\Omega S^{\dagger,N^*}_{\boldsymbol{x}_m}(\boldsymbol{y}) d\boldsymbol{y} \tag{3.22}$$

where $S^{\dagger,N}_{\boldsymbol{x}_m}$ is the numerical source term of the adjoint problem, chosen presently to be a sharp Gaussian around $\boldsymbol{x}_m$. For a Gaussian source, its size L is measured by its standard deviation σ_s, for the present analysis, $\lambda/\sigma_s \approx 23$. Following this procedure, for each adjoint solution adjoint Green's function $G^\dagger_{\boldsymbol{x}_m}$ is defined. Lagrange's identity (3.2) then readily gives at each sample position $\boldsymbol{x}_m$ the physical pressure field $p(\boldsymbol{x}_m)$:

$$p(\boldsymbol{x}_m) \;= < G^\dagger_{\boldsymbol{x}_m}, S_{Lilley} >= \int_\Omega G^{\dagger^*}_{\boldsymbol{x}_m}(\boldsymbol{x}) \; S_{Lilley}(\boldsymbol{x}) d\boldsymbol{x} \tag{3.23}$$

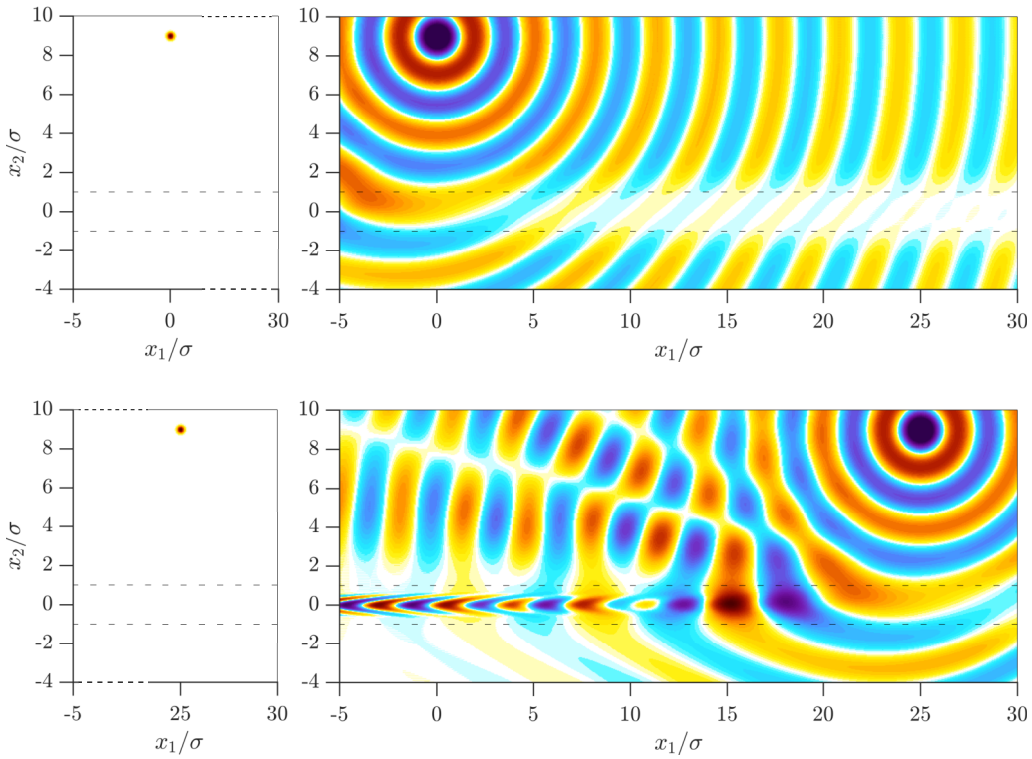

Figure 3.3: Numerical adjoint Green's problems associated with Lilley's equation at $\boldsymbol{x}_m = (x_1, x_2)$ for the axial positions $x_1/\sigma = 0.0$, $x_1/\sigma = 25$ and $x_2/\sigma = 9.0$. Adjoint Gaussian source terms $S^{\dagger,N}_{\boldsymbol{x}_m}$ considered to mimic an impulse forcing (left); the associated adjoint fields $p^\dagger$ regarded as numerical adjoint Green's functions $G^{\dagger,N}_{\boldsymbol{x}_m}$ (right).

Results obtained for the investigated sampled line are compared in figure 3.4 against the direct problem

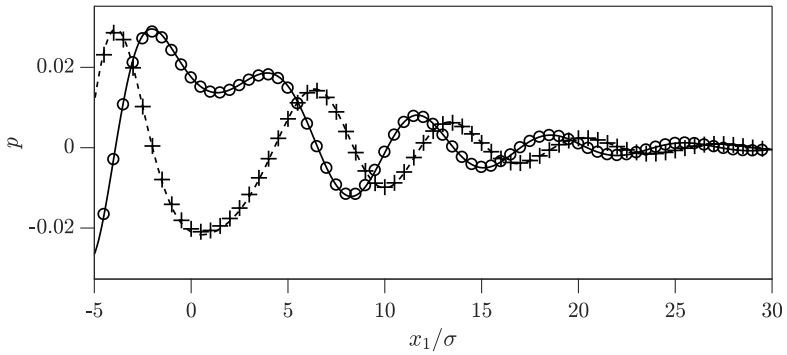

Figure 3.4: Validation of the adjoint method along the line $x_2/\sigma = 9.0$ for Lilley's equation. Reference data for the pressure p (real part: ——, imaginary part: - - -) is taken from the direct field computation presented in figure 3.2. Rebuilt pressure field p (real part: ∘, imaginary part: +) is obtained with Lagrange's identity.

solution seen as a reference. Figure 3.4 shows an almost perfect reconstruction of the reference field with the adjoint method, demonstrating thus the viability of the approach, and gives an *a posteriori* validation of the utilised numerical trick to compute an anti-causal solution (refer to appendix B.2). In practice, the only limitation of the method is the ability to properly compute numerical adjoint Green's function.

The bypass procedure, given in (3.22), requiring that the adjoint source is compact ($\lambda/L >> 1$) proves to work correctly as well.

3.3.4 Reconstruction of the solution with the flow reversal theorem (FRT)

The FRT introduced by Lyamshev (1961) and Howe (1975b), and formulated in a more general statement by Godin (1997), exploits alternatively the reciprocity principle to rebuild the physical field. The FRT is used here and applied to Lilley's wave equation to enable comparison with the adjoint method.
In the framework of the FRT, the reciprocal problem is obtained from the direct one (3.1) by turning the velocity dependences in $\boldsymbol{u}_0$ in the linear operators $\mathcal{L}_0$ and $\mathcal{B}_0$ into $-\boldsymbol{u}_0$. The corresponding operators will be referred to as $\mathcal{L}_0^-$ and $\mathcal{B}_0^-$, the reciprocal field p^- is then governed by the FRT equations

$$\begin{cases} \mathcal{L}_0^- \; p^- = s^- & \text{in } \Omega \\ \mathcal{B}_0^- \; p^- = 0 & \text{on } \partial\Omega \end{cases} \tag{3.24}$$

where s^- is the source for the FRT problem considered. In practice, it is sufficient to invert the mean flow $\boldsymbol{u}_0$ direction in the direct problem solver to compute p^-. This has been achieved for Lilley's wave equation for which simulations are conducted for the same sampling of sources as for the adjoint problem presented in the previous paragraph, that is by taking $s^- \equiv s^\dagger$. The same mean density ρ_0, pulsation frequency ω and mesh as for the direct problem are considered. Again, Green's solutions to $\mathcal{L}_0^-$ are considered and (3.16) is therefore discarded. Some realisations for the reciprocal field p^- for different sample locations are shown in figure 3.5.
A normalisation procedure similar to (3.22) is used to compute from the numerical FRT field $G^{-,N}_{\boldsymbol{x}_m}$ FRT reciprocal Green's function $G^-_{\boldsymbol{x}_m}$. In a similar fashion to (3.2), the pressure field p solution of the direct problem is rebuilt with

$$p(\boldsymbol{x}_m) = < G^-_{\boldsymbol{x}_m}, S_{Lilley} >_{\mathbb{R}} \tag{3.25}$$

where the scalar product for real-valued functions $<,>_{\mathbb{R}}$ should be used, according to (Lyamshev, 1961, eq. (14)), defined for the functions f and g by

$$< f, g >_{\mathbb{R}} = \int_\Omega d\boldsymbol{x} \; f(\boldsymbol{x}) g(\boldsymbol{x}) \tag{3.26}$$

The explanation why a non-Hermitian scalar product in the application of the FRT is needed, is discussed later in § 3.4.3. The pressure field p obtained along the sampled line with the FRT is compared in figure 3.6 against the direct problem solution taken as reference.
In this example, the FRT recovers very poorly the direct problem solution both qualitatively as quantitatively. In this configuration a relative error greater than 300% is observed at some observer locations, this error grows when the considered pulsation frequency ω decreases. A comparative look at the reciprocal fields obtained with the FRT, in figure 3.5, and with the adjoint method, in figure 3.3, reveals striking differences in both computed reciprocal fields. Subtle phenomena seem indeed to occur in the region of flow gradients in the adjoint approach which are not described by the FRT methodology; note that this region coincides with the region for which $\mathcal{L}_0$ is not self-adjoint. Furthermore this region of flow gradient is precisely where the source S_{Lilley} for the direct problem is located and, according to (3.23) and (3.25), it is the part of the reciprocal fields that contributes to the value of the rebuilt pressure p at the sample locations $\boldsymbol{x}_m$. This paragraph highlights hence, that the rigorous computation of an acoustic field over a shear mean flow is typically a case for which the commonly used reciprocity principle − even if extended

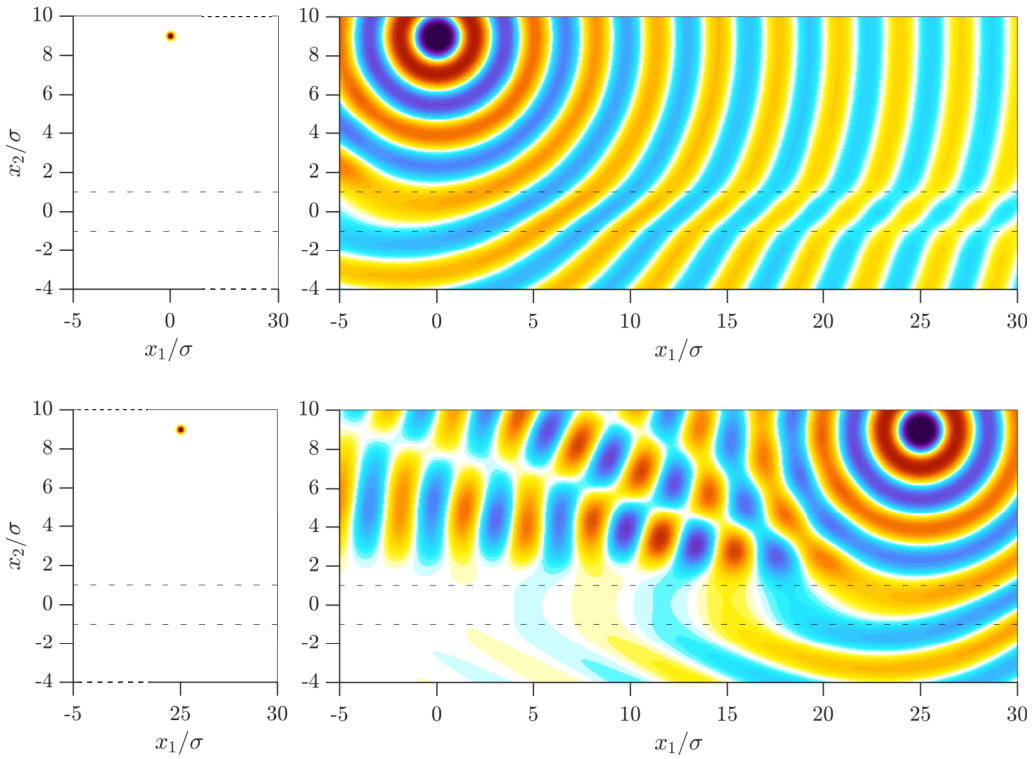

Figure 3.5: Numerical FRT Green's problems associated with Lilley's equation at $\boldsymbol{x}_m = (x_1, x_2)$ for the axial positions $x_1/\sigma = 0.0$, $x_1/\sigma = 25$ and $x_2/\sigma = 9.0$. Gaussian source terms $S^{-,N}_{\boldsymbol{x}_m}$ considered to mimic an impulse forcing (left); the associated reciprocal fields p^- regarded as numerical FRT Green's functions $G^{-,N}_{\boldsymbol{x}_m}$ (right). The same range for the colourmaps as in figure 3.3 is used.

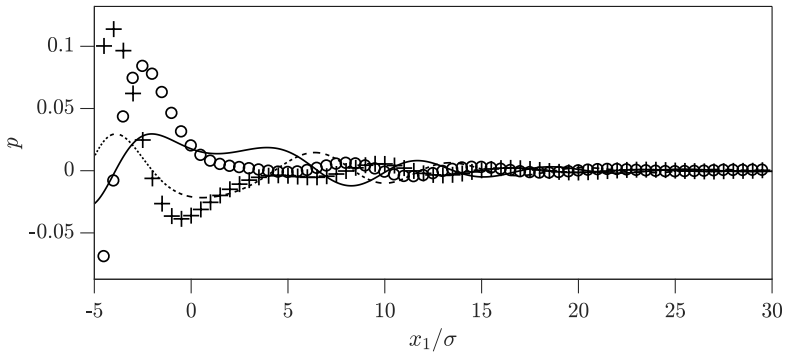

Figure 3.6: Validation of the FRT method along the line $x_2/\sigma = 9.0$ for Lilley's equation. Reference data for the pressure p (real part, ——; imaginary part, - - -) is taken from the direct field computation presented in figure 3.2. Rebuilt pressure field p (real part, ∘; imaginary part, +) is obtained with (3.25).

with the FRT − fails and where the general adjoint framework is required.

3.4 Application to Pierce's equation

The adjoint method is a general and powerful technique which could be applied to any linearised operator. However, to compute acoustic propagation with this technique, there is an interest in operators which are self-adjoint. Reasons for this are twofold. First, from a practical point of view, if a self-adjoint operator is chosen, the set of equations governing the direct and the adjoint problem are identical apart from the causality/anti-causality conditions, leading obviously to an easier implementation of the technique and enabling the use of some off-the-shelf solvers. Second, the adjoint method suffers from the same stumbling block as for the direct problem, in particular when the mean flow field considered is sheared, instability waves may also occur in the adjoint space (Karabasov and Hynes, 2005) and corrupt the acoustic solution. Möhring (1999) pointed out that self-adjoint propagation operators are energy preserving and, in turn, do not trigger any instability waves. Choosing a self-adjoint operator is then an elegant means to guarantee the stability of the acoustic propagation problem.
In the present section, the study conducted for Lilley's wave equation is repeated for Pierce's wave equation (Pierce, 1990). This wave operator is self-adjoint for the usual scalar product (3.14) and relies on a potential description of acoustic fluctuations. From the authors' investigations, this wave equation has been found to be among the most accurate stable operator governing acoustic propagation in an arbitrary mean flow. Note that, unlike Blokhintzev's wave equation for the acoustic potential (Blokhintzev, 1946) or the acoustic perturbation equations (Ewert and Schröder, 2003), no barotropic assumption of the mean flow is required. If ϕ refers to the acoustic potential, Pierce's wave equation reads

$$\left\{\begin{array}{l} p = -D_{\boldsymbol{u}_0}(\phi) \\ D^2_{\boldsymbol{u}_0}(\phi) - \nabla\cdot(a_0^2\nabla\phi) = S_{Pierce} \equiv D_{\boldsymbol{u}_0}(S_m) - S_p \\ \Delta S_m = \nabla\cdot(\rho_0 \boldsymbol{S_u}) \end{array}\right. \tag{3.27}$$

where the first equation relates the fluctuating pressure p to the acoustic potential ϕ (Pierce, 1990, eq. (26)). Because this wave equation relies upon a potential description of the flow and the acoustics, the source term should be potential as well. The third equation links the linearised momentum equation source term $\boldsymbol{S_u}$ to the corresponding filtered potential term S_m. The adjoint method could be applied to the first and second equations of (3.27) taken as a whole, provided that a suitable multivariable scalar product is defined. But for the sake of considering an unambiguous self-adjoint operator in the sense of § 3.2.2 and for simplicity, the adjoint method and the FRT will only be applied here to the wave equation for ϕ and for the scalar product (3.14). The fluctuating pressure p will be rebuilt subsequently.

3.4.1 Solution to the direct problem

The direct problem under consideration is made of Pierce's wave equation completed with some radiating boundary conditions $\mathcal{B}_0$

$$\left\{\begin{array}{ll} \mathcal{L}_0\ \phi = D^2_{\boldsymbol{u}_0}(\phi) - \nabla\cdot(a_0^2\nabla\phi) = S_{Pierce} & \text{in } \Omega \\ \\ \mathcal{B}_0\ \phi = 0 & \text{on } \partial\Omega \end{array}\right. \tag{3.28}$$

where S_{Pierce} is built according to (3.27) and is based on the same LEE equivalent source terms $(S_\rho, \boldsymbol{S_u}, S_p)$ as used for S_{Lilley}. For simplicity, the quadrupole source $\rho_0\boldsymbol{S_u}$ considered in § 3.3.2 was chosen in this study to derive from a potential source S_m. For arbitrary sources, a filtering process based on a Poisson

solver has proved to give very satisfactory results for Pierce's equation when compared with the solution for the unfiltered source computed with Lilley's equation. The computation of ϕ described in Pierce's direct problem (3.28) is achieved with the in-house code PROPA. The same mean flow field and the same frequency are analysed as previously for Lilley's wave equation. The fluctuating pressure p is then straightforwardly rebuilt with $p = -D_{\boldsymbol{u}_0}(\phi)$ and is shown in figure 3.7.

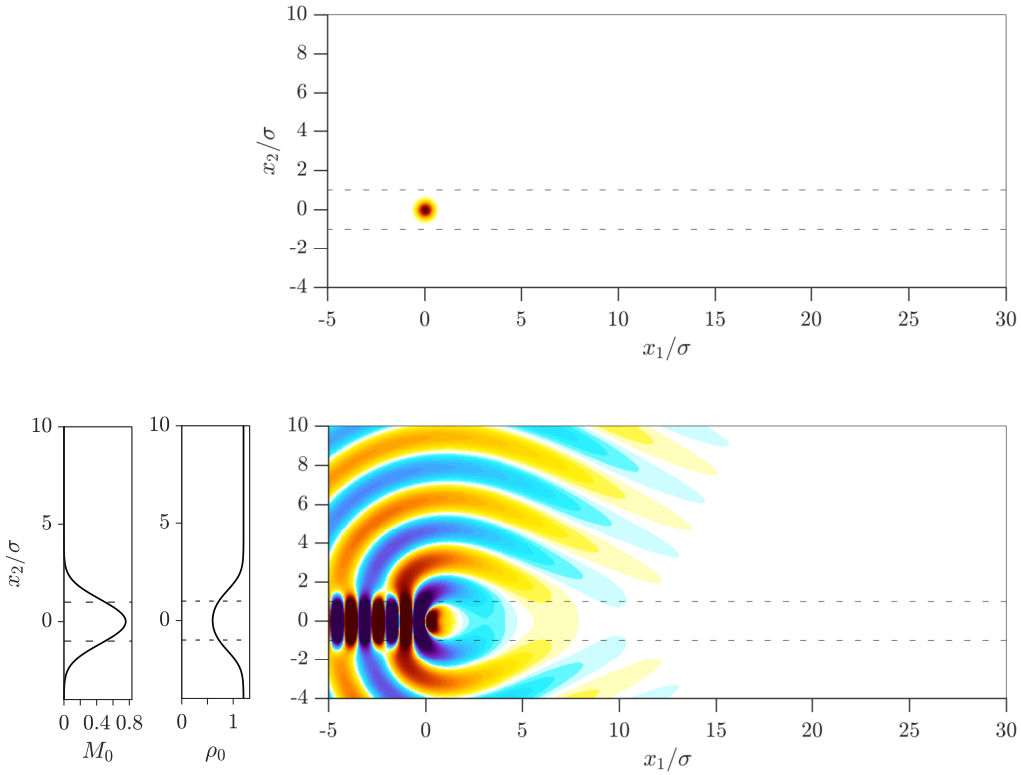

Figure 3.7: Direct problem for Pierce's wave equation. Source for Pierce's potential acoustic wave equation S_m equivalent to the quadrupole $\rho_0 \boldsymbol{S}_{\boldsymbol{u}} (= \nabla S_m)$ shown in figure 3.2 (top). Mach number M_0 and density ρ_0 profiles of the parallel mean flow considered (bottom-left); and the real part of the pressure field $p = -D_{\boldsymbol{u}_0}(\phi)$ is shown with the same range for the colourmap as in figure 3.2 (bottom-right). Dashed lines represent the position of maximal shearing ($x_2/\sigma = 1$).

3.4.2 Reconstruction of the solution with the adjoint method

Repeating the procedure given in § 3.3.3, the adjoint method is used here to recover the acoustic potential ϕ associated with the direct field. The fluctuating pressure p is rebuilt subsequently. The same sampling of adjoint sources used previously, partly shown in figure 3.3, is considered here. Each of these adjoint sources is defined as a sink term to the anti-causal adjoint Pierce problem

$$\begin{cases} \mathcal{L}_0^\dagger \ \phi^\dagger = D^2_{\boldsymbol{u}_0}(\phi^\dagger) - \nabla \cdot (a_0^2 \nabla \phi^\dagger) & \text{in } \ \Omega \\ \\ \mathcal{B}_0^\dagger \ \phi^\dagger = 0 & \text{on } \ \partial\Omega \end{cases} \tag{3.29}$$

Because Pierce's wave equation is self-adjoint for the scalar product (3.14) chosen here, its associated adjoint problem is nothing other than Pierce's wave equation completed with some anti-radiating boundary conditions $\mathcal{B}_0^\dagger$. The same features for the mean flow and the numerical settings as for previous calculations

are considered. Figure 3.8 shows the adjoint acoustic potential fields $\phi^\dagger$ solution to Pierce's adjoint problem taken at two sample locations.

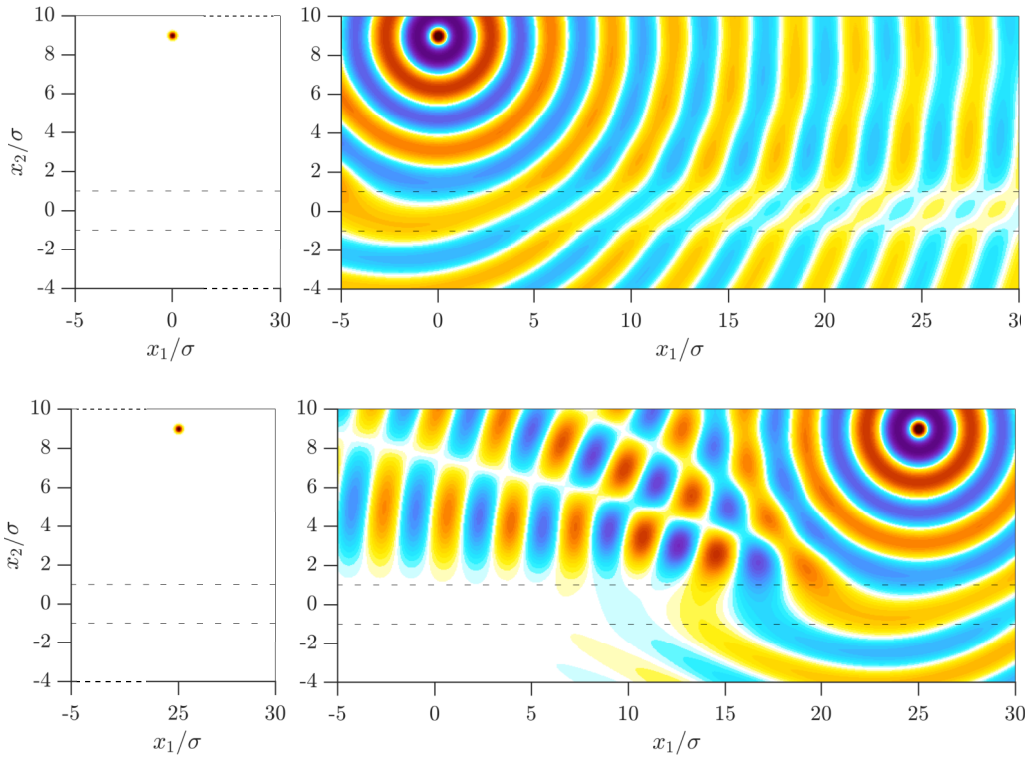

Figure 3.8: Numerical adjoint Green's problems associated with Pierce's equation at $\boldsymbol{x}_m = (x_1, x_2)$ for the axial positions $x_1/\sigma = 0.0$, $x_1/\sigma = 25$ and $x_2/\sigma = 9.0$. Adjoint Gaussian source terms $S^{\dagger,N}_{\boldsymbol{x}_m}$ considered to mimic an impulse forcing (left); the associated adjoint fields $\phi^\dagger$ regarded as numerical adjoint Green's functions $G^{\dagger,N}_{\boldsymbol{x}_m}$ (right). The range for the colourmaps used here differs from the one used in figure 3.3 and 3.5.

As previously, adjoint Green's functions $G^\dagger_{\boldsymbol{x}_m}$ are computed from previous numerical adjoint functions $G^{\dagger,N}_{\boldsymbol{x}_m}$ using the compacity assumption of the adjoint source. Lagrange's identity then gives straightforwardly at each sample position $\boldsymbol{x}_m$,

$$\phi(\boldsymbol{x}_m) \ = < G^\dagger_{\boldsymbol{x}_m}, S_{Pierce} > \tag{3.30}$$

and subsequently the acoustic pressure $p = -D_{\boldsymbol{u}_0}(\phi)$. Results obtained for the fluctuating pressure p along the sampled line are compared in figure 3.9 against Pierce's direct problem solution taken as reference. Again in figure 3.9, an almost perfect reconstruction of the reference pressure field p is obtained with the adjoint method. On an indicative basis, figure 3.9 also shows the pressure field p computed previously with Lilley's wave equation. The satisfactory ability of Pierce's wave equation to compute acoustic refraction effects for the high-speed heated sheared mean flow encountered here is enlightening. This potential acoustic prediction is all the more satisfactory, since Pierce's equation is known to be accurate in the high-frequency limit (Pierce, 1990), which is not fulfilled here, $\lambda/\sigma \approx 3$.

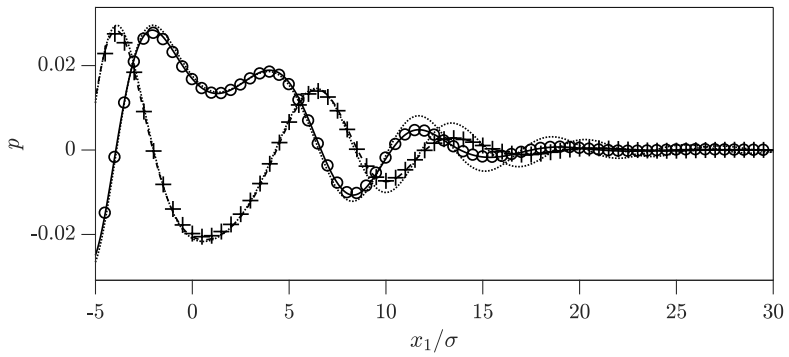

Figure 3.9: Validation of the adjoint method along the line $x_2/\sigma = 9.0$ for Pierce's equation. Reference data for the pressure p (real part, ——; imaginary part, - - -) is rebuilt from the direct field computation using $p = -D_{\boldsymbol{u}_0}(\phi)$ as presented in figure 3.7. Similarly, the rebuilt pressure field p (real part, ∘; imaginary part, +) is computed from the acoustic potential field ϕ computed with Lagrange's identity. Dotted lines, ·····, display the corresponding real and imaginary parts of the pressure p solution to Lilley's equation given in figure 3.4.

3.4.3 The adjoint method and the FRT equivalence for self-adjoint operators

In this study on Pierce's wave equation, the field reconstruction achieved with the FRT is not shown. Rigorously the same results as those presented for the adjoint method in figures 3.8 and 3.9 would have indeed been obtained. This is because the adjoint method and the FRT are fully equivalent for self-adjoint operators. A proof for this is given here for Helmholtz's wave equation written for a uniform steady background flow. Three-dimensional Green's function for the latter is recalled in appendix B.2 and solutions to the direct and adjoint propagation problems can be expressed as

$$G_{\boldsymbol{x}_s}(\boldsymbol{x},\omega) = \exp\left(-i\frac{\omega}{a_0}\frac{\boldsymbol{M}_0\cdot(\boldsymbol{x}-\boldsymbol{x}_s)}{1-M_0^2}\right)\frac{\exp\left(i\dfrac{1}{1-M_0^2}\dfrac{\omega}{a_0}r_{\boldsymbol{x}_s}\right)}{4\pi r_{\boldsymbol{x}_s}} \tag{3.31}$$

and

$$G^{\dagger}_{\boldsymbol{x}_m}(\boldsymbol{x},\omega) = \exp\left(-i\frac{\omega}{a_0}\frac{\boldsymbol{M}_0\cdot(\boldsymbol{x}-\boldsymbol{x}_m)}{1-M_0^2}\right)\frac{\exp\left(-i\dfrac{1}{1-M_0^2}\dfrac{\omega}{a_0}r_{\boldsymbol{x}_m}\right)}{4\pi r_{\boldsymbol{x}_m}} \tag{3.32}$$

where $r_{\boldsymbol{x}_i} = \sqrt{(1-M_0^2)|\boldsymbol{x}-\boldsymbol{x}_i|^2 + (\boldsymbol{M}_0\cdot(\boldsymbol{x}-\boldsymbol{x}_i))^2}$ and $\boldsymbol{M}_0 = \boldsymbol{u}_0/a_0$ is the vectorial Mach number. Furthermore, let $G^{-}_{\boldsymbol{x}_m}$ be Green's function in $\boldsymbol{x}_m$ solution of the FRT. Then $G^{-}_{\boldsymbol{x}_m}$ can be deduced from the expression of $G_{\boldsymbol{x}_s}$ by switching the source $\boldsymbol{x}_s$ and the observer $\boldsymbol{x}_m$ positions and reversing the mean velocity $\boldsymbol{u}_0$ direction. Consistently with what is carried out for the numerical simulations in the frequency domain, it is argued that the anti-causal solution for the adjoint problem $G^{\dagger}_{\boldsymbol{x}_m}$ can be selected considering the usual radiating solution, but for an opposite pulsation frequency ω. From the above obtained analytical expressions, the equivalence of the reciprocal fields computed with the adjoint method or the FRT are then easily verified:

$$G^{\dagger}_{\boldsymbol{x}_m}(\boldsymbol{x},\omega) = G^{-}_{\boldsymbol{x}_m}(\boldsymbol{x},-\omega) \tag{3.33}$$

Since analytical solutions to acoustic propagation problems are scarce, directly assessing this symmetry with respect to the flow reversal on general analytical solutions is hopeless. However, this symmetry in the exchange of the mean flow direction and the sign of the pulsation frequency ω of the acoustic solution

can already be assessed from the linear operator $\mathcal{L}_0$ governing the wave propagation. And effectively, in Pierce's wave operator, changing the sign of ω or $\boldsymbol{u}_0$ appears to be fully equivalent. This remark holds for all self-adjoint wave equations describing acoustic propagation over a moving flow, namely the ones introduced by Galbrun (1931), Phillips (1960), Goldstein (1978) Godin (1997) and Möhring (1999).
On top of that, a critical literature review reveals that in the studies illustrating the FRT, only self-adjoint wave equations written in the frequency domain are considered. The proof for the FRT reciprocity relation, classically starts with the multiplication of the wave equation governing the direct propagation problem by a field variable, and its integration over the entire propagation domain. In fact, this operation closely resembles a scalar product multiplication with a test function or a Lagrange multiplier. Integration by parts of the direct problem wave equation then frees the direct field variable and defines the reciprocal wave equation with reversed flow to which the previously introduced test function is subject, i.e. the FRT for the considered wave equation is readily demonstrated. The difference with the adjoint method lies in the scalar product which is not well-posed for the FRT. As a matter of fact, manipulating a wave equation written in the frequency domain requires the introduction of a Hermitian scalar products. If the latter condition were fulfilled in the FRT proof, the self-adjoint property of the equation would have been retrieved and in turn no flow reversal needed. It appears now clearly why only $\mathbb{R}$ space scalar products should be considered in the final solution reconstruction with the FRT, to say,

$$\phi = < G^{\dagger}_{\boldsymbol{x}_m}, S_{Pierce} >= < G^{-}_{\boldsymbol{x}_m}, S_{Pierce} >_{\mathbb{R}} \tag{3.34}$$

The reciprocal field $G^{-}_{\boldsymbol{x}_m}$ computed with the FRT is in fact, the complex conjugate of the adjoint field $G^{\dagger}_{\boldsymbol{x}_m}$. This is easily seen, taking benefit of the Fourier transform property of a real-valued field $G^{-}_{\boldsymbol{x}_m}(\boldsymbol{x}, -\omega) = G^{-^*}_{\boldsymbol{x}_m}(\boldsymbol{x}, \omega)$ for which it follows from (3.33):

$$G^{-}_{\boldsymbol{x}_m}(\boldsymbol{x}, \omega) = G^{\dagger^*}_{\boldsymbol{x}_m}(\boldsymbol{x}, \omega) \tag{3.35}$$

The equivalence between the adjoint method and the FRT for self-adjoint operators has pragmatic implications. The solving of anti-causal adjoint equations can indeed be advantageously replaced by direct computations over reversed flow. An interesting question to answer is whether some linear operators may all at once describe exactly acoustic propagation over a sheared mean flow and be self-adjoint. Möhring (1999) answered this question and illustrated how from a self-adjoint operator an energy-conserving law could be derived for the acoustic field. Yet, it is well known that for sheared flows, instability waves may occur converting acoustic energy into vortical energy (Yates, 1978; Maestrello et al., 1981) and thus that no such conservation law for acoustic energy exist. Hence for arbitrary mean flows, acoustic energy is not preserved, and a linear operator which is twofold self-adjoint and exactly describes acoustic propagation does not exist. If acoustic propagation in a complex media needs to be conducted very accurately, a non-self-adjoint operator needs therefore to be considered. Nevertheless if a decoupling of the acoustic with the vortical mode is required for stability purposes, and approximations tolerated, Pierce's wave equation seems to achieve nicely the prediction of flow refraction effects on sound.

3.5 Final remarks

3.5.1 Conclusion

In the present study, the adjoint method is analysed in-depth and demonstratively applied to the model problem of a source radiating in a sheared and stratified mean flow. This approach offers a fully equivalent alternative to ordinary computational aeroacoustics to rebuild locally the solution of a non-trivial propagation problem. With respect to the pioneering work of Tam and Auriault (1998), the adjoint field is not sought as the solution of a scattering problem. The presented approach wraps around Lagrange's identity, which offers a robust mathematical basis for the method. A well-defined scalar product is considered leading to a consistent expression of the representation formula. The anti-causality of the adjoint field is also stressed. In addition, the adjoint method is compared against the flow reversal theorem, that is shown to work properly only for self-adjoint wave equations. This property is sometimes overseen or confusingly addressed in aeroacoustics. Finally, solving an adjoint problem can be sometimes cumbersome due to the presence of instability waves, and to the numerical implementation of anti-causality boundary conditions, for instance. Another contribution of this work is to propose a stable and accurate alternative methodology based on Pierce's equation and the rigorous use of the flow reversal theorem. A general expression of the source terme is derived that enables the prediction of aerodynamic noise. No limitation on the physical source is imposed, and this method has already changed the game for computation of acoustic radiation of widely distributed physical sources such as those found in jets (Tam and Auriault, 1999; Morris and Farassat, 2002; Raizada and Morris, 2006), and there is some interest in computing accurately the quantities appearing in the model for complex configurations. Compared with the classical adjoint formulation encountered in aeroacoustics, the presented approach has the ability to account for acoustic diffraction at surface edges (Barone and Lele, 2005) and describes near-field propagation as well. Future contributions should verify the ability of the technique to properly account for realistic configurations.

3.5.2 Perspectives

In its essence, the adjoint method furnishes an equality between, in one hand, the projection of a physical unknown field on a adjoint source, and in the other hand, the projection of the physical sound source on the computed adjoint field. This is what states Lagrange's identity. This techniques is attractive as long as the observer is 'simpler' as the physical sound source, and suits therefore very well to the computation of the acoustic propagation toward sensors. What is more, since adjoint Green's functions are computed irrespectively from the physical sound source, this technique appears to be tailored to sound source localisation algorithms. Analogously to Tam and Auriault (1998), the adjoint method has been outlined here as an alternative approach to locally compute the noise originating from a broadband stochastic sound source. The adjoint source is defined as a delta Dirac source and in turn acoustic is only predicted locally at the microphone position. If different shapes of adjoint sources are considered, the method possibilities are enhanced. For instance, if the fundamental vibration modes of a surface panel are identified, they can then be taken as adjoint sources for the propagation problem. Lagrange's identity would straightforwardly give the amplitude of the considered mode when exited by the physical sound source. There is thus a large scope of application of the adjoint method in interior noise assessment. Just as the noise perceived in cabin of an plane or in a car (Khalighi et al., 2010; Blanchet and Golota, 2014). The vibration of a surface due to turbulent boundary layers is often modelled with empirical models (e.g. Corcos, Chase), thanks to the adjoint method the contribution of exterior acoustic sound sources on the

surface vibration could be predicted from a simple RANS solution. The expense of this approach increases with the number of Fourier mode considered to account for the surface vibration.

3.5.3 Tribute to Lagrange

Reading original material from pioneer researcher is always edifying. Such an investigation reveals that Lagrange (1761) applied the adjoint methodology to solve the motion of a vibrating string. He then applied his technique to the acoustic propagation of spherical waves in air. It is striking to remark that the philosophy of his technique remained unchanged over the years. As for Tam and Auriault's work (1998), the present study relies on the same idea. For documentation, let us recopy and translate here below Lagrange's comments on his technique (1761, p. 176). This remark was written in investigations on the movement of arbitrarily perturbed vibrating string. Note how close these statements could apply for acoustic propagation of stochastic sound sources as encountered in turbulent jet flows.

"*Since the question is to determine the movement of an infinite number of mobile points, with the supposition that their equilibrium state is arbitrarily disturbed, one cannot, as we have previously proven, express all these movements by a unique and general formula. Contrariwise, each moving point must be treated separately, and its movement determined by solving as many isolated problems as there are mobile points in the given system. Such a question therefore requires, for it to be entirely solved, other means than those ordinarily provided by analysis.*"

His next sentences highlights how groundbreaking his discovery was,

"*This is what M. d'Alembert took care to underline on the subject of the vibrating strings in the article II he added to his Mémoire sur la courbe que forme une corde tendue mise en vibration and printed in the year 1750 in the Mémoires de l'Académie de Berlin. «In any case, he said [...], the problem cannot be solved, with my method at least, and I do not even know whether the strength of any known analysis would succeed.»*"

This analysis unknown by d'Alembert was the adjoint. But Lagrange's talent is only equalled by his humility, and few lines later he wrote,

"*The main foundation of both of these methodologies is the ingenious analysis invented by M. d'Alembert to integrate differential equations of any order, and containing any number of variables, as long as they appear with a linear dependence. Hence it is only justice for this erudite Geometrician for us to recognise that we owe him the principal support of overcoming the difficulties that apparently he himself believed impassable.*"

3.5.4 Afterword

A variant of this chapter has been accepted for a journal publication (Spieser and Bailly, 2020). The article is in very close similitude with this chapter, only a footnote, the perspective paragraph, the historical paragraph on Lagrange, the appendix B.1 and the present paragraph have been added here. I long hesitated about the most appropriate name to give to equation (3.2). Indeed, in the literature the relationship defining the adjoint is rather called Lagrange's identity by mathematicians (Stone and Goldbart, 2009), whereas physicists refer to it rather as Green's identity (Lanczos, 1996; Morse and Feshbach, 1953). I found then myself lucky to discover the online recordings of Lagrange's works (available at `https://gallica.bnf.fr`). In fact, not only his work, but also the faithful epistolary correspondences he had with his fellow European scientists (d'Alembert, Condorcet, Euler, Laplace, Gauss, Monge) was

gathered. Reading the private communications, steeped in immense respect, he had with Euler was moving. At the same time, as I meant to illustrate with previous paragraph, many of his ideas were incredibly modern. The literature dedicated to the history of mathematics (Kline, 1990; Roy, 2011), associates the origin of adjoints to Lagrange. Even though strictly speaking the name of 'adjoint' was introduced more than a century later by Fuchs (1873). Considering this, I resolved to render unto Caesar the things that are Caesar's, and name this fundamental relation of functional analysis after the name of this brilliant mind.

4 Solving adjoint Pierce's equation with *Actran TM*

Summary: This section details how *Actran TM*, designed to solve Möhring's equation, is turned into a solver for Pierce's equation. After presenting the normalised Möhring equation solved by *Actran TM*, the accuracy of the solver is compared with respect to the in-house code PROPA. Because Pierce's equation is self-adjoint, the adjoint problem is solved with help of *Actran TM* using the FRT. A template enabling the computation of adjoint Green's function for a bidimensional jet flow is provided. As a proof of concept, the reciprocal acoustic solution for a realistic dual-stream aircraft engine with flight effects is presented.

4.1 Insight into *Actran TM*

4.1.1 Introduction to *FFT*'s software

FFT (*Free Field Technologies*) commercialises a software suite to model and solve linear acoustic propagation problems for industry relevant applications. In 2011, *FFT* has been acquired by *MSC Software Company* the multi-physics simulation company which owns numerous code among which *MSC Nastran*, *Patran*, *Adams* and since recently, the flow solver *Cradle*. *Actran* is the generic name for the different software developed by *FFT*. Each of them can be regarded as add-ons to the basic *Actran Acoustics* tool which can be initiate in command lines or manipulated with the dedicated GUI *Actran VI*. This GUI enables amongst other the creation of meshes of intermediate degree of complexity with the inbuilt *Boxpro* tool. *Actran Parallel* enables to solve the linear propagation in a HPC environment using MPI. The overlayer of *FFT*'s products are coded in a python environment with a devoted library `actranpy` enabling thus fairly easy and extensive post-processing possibilities but also scripting. *FFT*'s programs are using FEM (see `femtown` environment in `actranpy`) and provides efficient means to interpolate fields on unstructured meshes for complex geometries. The software suite is composed of *Actran TM*, *Actran DGM*, *Actran SNGR*, *Actran SEA*, *Actran Aero-Acoustics*, *Actran Trimmed Body* and *Actran Vibro-Acoustics*. *Actran DGM* is a discontinuous Galerkin time-domain solver for the LEE and finds application in the computation of noise from aircraft engines (Mosson et al., 2014) and jets (Legendre et al., 2016). In the present work, the *Actran TM* solution is considered.

Actran TM (TM: Turbo-Machinery) aims at predicting the propagation of tonal engine noise components in a moving fluid in the presence of acoustically lined ducts and is typically meant for the acoustic design of engine nacelles. *Actran TM* solves a normalised Möhring's equation in the frequency domain and can rely on state of the art numerical sparse parallel solvers (*Mumps*, *Pardiso*, ...). More details on *Actran TM*

can be found in its user guide (Free Field Technologies, 2018b,c), refer to the user interface user guide (Free Field Technologies, 2018a) for setting up *Actran TM* computations in practice.

4.1.2 Möhring's equation as implemented in *Actran TM*

In his work, Möhring (1999) defined an acoustic analogy based on a wave equation for the total enthalpy B. His wave equation describes the propagation of sound over an irrotational and isentropic flow. As in Lighthill's acoustic analogy, vortices and entropy fluxes occur as sources term of the analogy. But while the paragon acoustic analogy is valid for a flow at rest, Möhring's wave analogy is exact for steady irrotational and isentropic base flows. But its use is not restricted to such flow. Möhring notably insists on the self-adjointness of his operator which guarantees that the acoustic energy is preserved (Möhring, 1999). This makes his operator very handy to use in complex configurations.

Actran TM is a frequency domain solver, as such it is known that the group velocity locally vanishes wherever the flow speed is sonic leading to singularities in the system matrix. To prevent from this numerical issue the equation solved in *Actran TM* is normalised by the total density ρ_T. With this normalisation it is possible to rescale the mean flow variables so the flow remains subsonic and hence to guarantee robustness (ref. to *CUT_SOS* (Free Field Technologies, 2018b, § 51.7)). Note that this normalisation is effective even though no flow region is supersonic. Möhring's equation governs the total enthalpy $B = h + \boldsymbol{v}^2/2$, which is computed from the first thermodynamic principle $\delta h = T\delta s + (\delta p)/\rho$. Where $\boldsymbol{v}$ is the fluid velocity, p its pressure, ρ its density, T the fluid temperature and s its entropy. If S_ρ, $\boldsymbol{S_u}$, S_p are generic forcing terms for the Navier-Stokes equation when written for the principal variables ρ, $\boldsymbol{u}$ and p (see appendix E), then the normalised Möhring equation writes,

$$\begin{aligned}\frac{\partial}{\partial t}\left[\frac{\rho}{\rho_T a^2}\frac{\mathrm{D}B}{\mathrm{D}t}\right] + \nabla\cdot\left[\frac{\rho\boldsymbol{u}}{\rho_T a^2}\frac{\mathrm{D}B}{\mathrm{D}t} - \frac{\rho}{\rho_T}\nabla B\right] = \quad & \nabla\cdot\left[-\frac{\rho}{\rho_T}\boldsymbol{S_u} + \frac{\rho\boldsymbol{u}}{\rho_T a^2}(\boldsymbol{u}\cdot\boldsymbol{S_u}) + \frac{\boldsymbol{u}}{\rho_T a^2(\gamma-1)}S_p - \frac{\boldsymbol{u}}{\gamma\rho_T}S_\rho\right] \\ & + \frac{\partial}{\partial t}\left[\frac{\rho}{\rho_T a^2}(\boldsymbol{u}\cdot\boldsymbol{S_u}) + \frac{1}{(\gamma-1)\rho_T a^2}S_p + \frac{\gamma-1}{\gamma\rho_T}S_\rho\right] + \mathcal{R}\end{aligned} \tag{4.1}$$

$$\begin{aligned}\text{with}\quad \mathcal{R} = \quad & \nabla\cdot\left[\frac{\rho}{\rho_T}\boldsymbol{\omega}\times\boldsymbol{u} - \frac{\rho}{\rho_T}T\nabla s - \frac{\rho_s\boldsymbol{u}}{\rho_T}\frac{\partial s}{\partial t} - \frac{\boldsymbol{u}}{\rho_T a^2}\nabla\cdot\boldsymbol{q} - \frac{\rho}{\rho_T}\nabla\cdot\boldsymbol{\Sigma} + \frac{\boldsymbol{u}}{\rho_T a^2}\nabla\cdot(\boldsymbol{\Sigma}\cdot\boldsymbol{u}) - \rho\boldsymbol{u}\frac{\partial}{\partial t}\left(\frac{1}{\rho_T}\right)\right] \\ & + \frac{\partial}{\partial t}\left[-\frac{\rho_s}{\rho_T}\frac{\partial s}{\partial t} - \frac{\nabla\cdot\boldsymbol{q}}{\rho_T a^2} + \frac{\nabla\cdot(\boldsymbol{\Sigma}\cdot\boldsymbol{u})}{\rho_T a^2} + \rho\boldsymbol{u}\cdot\nabla\left(\frac{1}{\rho_T}\right)\right]\end{aligned} \tag{4.2}$$

where, $\mathrm{D}/\mathrm{D}t = \partial/\partial t + \boldsymbol{u}\cdot\nabla$ is the material derivative, $a = \sqrt{\frac{\partial p}{\partial\rho}\big|_s}$ is the speed of sound, and $\rho_s = \frac{\partial\rho}{\partial s}\big|_p$. $\boldsymbol{\Sigma}$ denotes the friction-related stress tensor, $\boldsymbol{q} = -\lambda\nabla T$ is the heat flux and $\boldsymbol{\omega} = \nabla\times\boldsymbol{u}$ is the vorticity. The detailed derivation of the normalised Möhring equation is provided in appendix E.

In most applications, acoustic fluctuations have weak amplitudes with respect to the base flow, so that it is legitimate to consider the linearised equations to compute sound propagation. As usually in CAA practices, a Reynolds decomposition of the flow ($B = B_0 + B'$, $\rho = \rho_0 + \rho'$, $\boldsymbol{u} = \boldsymbol{u}_0 + \boldsymbol{u}'$, etc.) is considered to derive the equation of *Actran TM*. Legendre (2014, §§ 6.3-6.5), (Legendre et al., 2012) conducted such a linearisation and proposed different formulation for the linearised Möhring equation, one of which is multivariable and is almost equivalent to LEE, and four scalar acoustic-vortical wave equations. The

extension of Möhring's equation proposed by those authors showed promising results for low vorticity but diverges for strongly sheared mean flows (Legendre et al., 2012). Another closure strategy for Möhring's equation is given in Delfs' lecture notes (2016, § 3.2.2). This author argued that if the mean flow is assumed potential, the Lamb vector term appearing in Crocco's equation (see appendix E) solely contributes as a source term. So that, for acoustic propagation over a potential mean flow, the momentum equation furnishes,

$$\nabla B_0 = T_0 \nabla s_0 \tag{4.3}$$

If the mean flow is supposed isentropic, then the stagnation enthalpy B_0 is conserved along the streamlines and equals the Bernoulli constant (Delfs, 2016). This second simplified framework assuming a potential and homentropic base flow is retained for the linearisation procedure. If the viscous stresses and the heat fluxes are discarded in the linearisation, and if moreover the forcing terms have no mean contributions, then the linearised normalised Möhring equation is obtained,

$$\frac{\partial}{\partial t}\left[\frac{\rho_0}{\rho_{T,0}a_0^2}\frac{\mathrm{D}B'}{\mathrm{D}t}\right] + \nabla\cdot\left[\frac{\rho_0\boldsymbol{u}_0}{\rho_{T,0}a_0^2}\frac{\mathrm{D}B'}{\mathrm{D}t} - \frac{\rho_0}{\rho_{T,0}}\nabla B'\right] = \mathcal{R}' \tag{4.4}$$

with,

$$\begin{aligned}\mathcal{R}' = \quad & \nabla\cdot\left[\frac{1}{\rho_{T,0}a_0^2}\left(\rho_0(\boldsymbol{u}_0\otimes\boldsymbol{u}_0 - a_0^2\boldsymbol{Id})\cdot\boldsymbol{S'_u} + \frac{\boldsymbol{u}_0}{(\gamma-1)}S'_p - \frac{\boldsymbol{u}_0}{\gamma}a_0^2 S'_\rho\right)\right] \\ & + \frac{\partial}{\partial t}\left[\frac{1}{\rho_{T,0}a_0^2}\left(\rho_0\boldsymbol{u}_0\cdot\boldsymbol{S'_u} + \frac{1}{\gamma-1}S'_p + \frac{\gamma-1}{\gamma}a_0^2 S'_\rho\right)\right] \\ & + \nabla\cdot\left[\frac{\rho_0}{\rho_{T,0}}\boldsymbol{\omega'}\times\boldsymbol{u}_0 - \frac{\rho_0}{\rho_{T,0}}T_0\nabla s' - \frac{\rho_{s,0}\boldsymbol{u}_0}{\rho_{T,0}}\frac{\partial s'}{\partial t}\right] - \frac{\partial}{\partial t}\left[\frac{\rho_{s,0}}{\rho_{T,0}}\frac{\partial s'}{\partial t}\right]\end{aligned} \tag{4.5}$$

where $\boldsymbol{Id}$ is the identity tensor, and from here on, $\mathrm{D}/\mathrm{D}t = \partial/\partial t + \boldsymbol{u}_0\cdot\nabla$ is the material derivative along the mean flow streamlines. Note that additionally the contributions relative to variations in ρ_T have been discarded in the source term. Eventually, this equation, with a rescaled definition of the stagnation enthalpy b given by,

$$\delta b = \rho_{T,0}\ \delta B' \tag{4.6}$$

and some generic monopole S_m and dipole $\boldsymbol{S}_d$ source definition (Legendre, 2019), is solved in *Actran TM* in the frequency domain,

$$\boxed{\frac{\partial}{\partial t}\left[\frac{\rho_0}{\rho_{T,0}^2 a_0^2}\frac{\mathrm{D}b}{\mathrm{D}t}\right] + \nabla\cdot\left[\frac{\rho_0\boldsymbol{u}_0}{\rho_{T,0}^2 a_0^2}\frac{\mathrm{D}b}{\mathrm{D}t} - \frac{\rho_0}{\rho_{T,0}^2}\nabla b\right] = \frac{\partial S_m}{\partial t} + \nabla\cdot\boldsymbol{S}_d} \tag{4.7}$$

where, by introducing the Mach number $\boldsymbol{M}_0 = \boldsymbol{u}_0/a_0$, the mean total density $\rho_{T,0}$ is given by,

$$\rho_{T,0} = \rho_0\left(1 + \frac{\gamma-1}{2}\boldsymbol{M}_0^2\right)^{1/(\gamma-1)} \tag{4.8}$$

The pressure is built then subsequently with,

$$\frac{\rho_{T,0}}{\rho_0}\frac{\partial p}{\partial t} = \frac{\mathrm{D}b}{\mathrm{D}t} \tag{4.9}$$

4.2 Solving Pierce's equation with *Actran TM*

Pierce's equation is identified previously as a good candidate to compute acoustic propagation over sheared and stratified flows, this section explains how *Actran TM* can be hijacked to solve this wave equation. The general idea, is to manipulate the stagnation enthalpy b computed with *Actran TM* and to rebuilt a posteriori the associated fluctuating pressure field p' with the chosen relevant relationship. In *FFT*'s software, b is referred to as `VELOCITY_POTENTIAL` and p' with the keyword `PRESSURE`.

1. Obviously, by setting $\rho_{T,0} = 1$ and considering $b \leftarrow B'$ Möhring's linearised equation (Delfs, 2016; Legendre, 2014) is retrieved, for which, the fluctuating pressure p' is deduced from $\partial p'/\partial t = \rho_0 \, \mathrm{D}B'/\mathrm{D}t$.

2. Still considering $\rho_{T,0} = 1$ but setting $b \leftarrow -\psi$, and retaining another reconstruction of the pressure field $p' = -\rho_0 \, \mathrm{D}\psi/\mathrm{D}t$, then Blokhintzev's equation (Pierce, 1990, eq. (21) & eq. (23)) is obtained.

3. Choosing $\rho_{T,0} = \rho_0$, linearised and normalised Möhring's equation is equivalent to the linearised Phillips' equation (1960) for a direct identification of the stagnation enthalpy with the fluctuation pressure field $b \leftarrow p'$.

4. At last Pierce's equation (1990) is obtained, setting $\rho_{T,0} = \rho_0$ by identifying the enthalpy with the acoustic potential $b \leftarrow \phi$. The acoustic pressure field is then rebuilt with $p' = -\mathrm{D}\phi/\mathrm{D}t$.

Note that the differences between these wave equations in their ability to describe refraction effects, lays in their proper taking into account of the stratification effects (density gradients) and the choice of the relevant acoustic variable. The latter is the leading order effects and brings back the much addressed issue of what is the correct acoustic variable.

4.2.1 Preprocessing of the mean flow given in input

In *FFT*'s software, it is not possible however to force the equality $\rho_{T,0} = \rho_0$ to solve Pierce's equation, because the expression of the mean stagnation density $\rho_{T,0}$ is directly computed from the mean density ρ_0 and the mean Mach number $\boldsymbol{M}_0$. This hardship is overcome by preprocessing the mean flow fields ρ_0, p_0 and $\boldsymbol{u}_0$ given in input, so to compensate in the solved equation the presence of the total mean density $\rho_{T,0}$. A similar manipulation was performed by Legendre (2019) to rebuilt solutions of Möhring's equation without the stagnation density $\rho_{T,0}$ normalisation encountered in *Actran TM*. Those corrected mean flow fields are defined so to change *Actran TM*'s equation into Pierce's equation for the physically relevant mean flow fields ρ_0, p_0 and $\boldsymbol{u}_0$. Let those customisable variables be renamed by adding a C in subscript. Inspection of *Actran TM*'s equation indicates that subsequent relationship exist between the physical relevant mean flow variables $\boldsymbol{u}_0$, a_0, ρ_0 and the variables $\boldsymbol{u}_{0,C}$, $a_{0,C}$, $\rho_{0,C}$ provided in input of *Actran TM*, so to transform Möhring's wave equation into Pierce's one,

$$\boldsymbol{u}_{0,C} = \boldsymbol{u}_0 \qquad a_{0,C} = a_0 \qquad \frac{\rho_{0,C}}{\rho_{T,0}^2} = \frac{1}{\rho_0} \tag{4.10}$$

where, because in general $\rho_{0,C} \neq \rho_0$, equation (4.8) needs to be replaced by,

$$\rho_{T,0} = \rho_{0,C} \left(1 + \frac{\gamma - 1}{2} \frac{\rho_{0,C}}{\gamma p_{0,C}} \boldsymbol{u}_{0,C}^2 \right)^{1/(\gamma-1)} \tag{4.11}$$

It comes out, that the mean velocities $\boldsymbol{u}_0$ and a_0 are not affected by this transformations. Therefore, because the mean density ρ_0 is modified, the mean pressure p_0 needs to be corrected in order for $a_0 = \sqrt{\gamma p_0/\rho_0}$ to remain unchanged. Finally, to solve Pierce's equation with *Actran TM*, the adjustment that should be applied to the mean flow field to obtain the suitable corrected input fields $\rho_{0,C}$ and $p_{0,C}$ is computed from equations (4.10) and (4.11) and reads,

$$\boxed{\frac{p_{0,C}}{p_0} = \frac{\rho_{0,C}}{\rho_0} = \left[1 + \frac{\gamma-1}{2}\frac{\boldsymbol{u}_0^2}{a_0^2}\right]^{-2/(\gamma-1)}} \tag{4.12}$$

It must be mentioned, that to identically retrieve Pierce's equation from the relation (4.10) and equation (4.7), the gradients in the physical mean flow pressure p_0 have been neglected. These gradients do not exist in steady parallel flows and their effect in acoustic propagation are generally negligible.

4.2.2 Correction of the source amplitude

Because *Actran TM*'s `VELOCITY_POTENTIAL` output is used in a postprocessing procedure to rebuilt manually the fluctuating pressure p', the source amplitude A needs also to be corrected accordingly. In *Actran TM*, there are three kinds of source amplitude definitions, sources referred to as `P` type, `Q` type or `V` type (keyword `AMPLITUDE_TYPE` (Free Field Technologies, 2018c)). The type `P` amplitude is default and is related with the pressure field, while the `Q` type amplitude is related to mass flow rate and the `V` type source is related to volume source (Free Field Technologies, 2018c, § 9.50.3). In the present study, a source amplitude of type `P` is considered. When the above preprocessing step is conducted to turn *Actran TM* into a Pierce's equation solver, the acoustic potential ϕ solution of Pierce's normalised equation, given for $\delta_{\boldsymbol{x}_s}$ a pointwise source in $\boldsymbol{x}_s$ by,

$$\frac{1}{a_0^2}\left(\frac{\mathrm{D}^2\phi}{\mathrm{D}t^2} - \nabla\cdot(a_0^2\nabla\phi)\right) = A\ \delta_{\boldsymbol{x}_s} \tag{4.13}$$

is related to the computed stagnation enthalpy b by,

$$\boxed{\phi^* = \frac{-i\omega A}{4}\left(1 + \frac{\gamma-1}{2}\boldsymbol{M}_{0,S}^2\right)^{-1/(\gamma-1)} b} \tag{4.14}$$

where ϕ^* is the complex conjugate of ϕ, A the complex source amplitude defined in the software, ω the investigated acoustic pulsation and $\boldsymbol{M}_{0,S}$ the Mach number at the source position. This expression is deduced (painstakingly) from the comparison of the computed field b with the reference analytical solution presented in next paragraph.

4.3 Validation of *Actran TM*'s hijacking

The ability of the code to solve Pierce's equation is validated for a uniform mean flow were the analytical solution is available. For a sheared and stratified mean flow, the solution computed with PROPA is taken as a reference. These validations are presented here for a bidimensional configuration, for which a Dirac delta source is computed in *Actran TM* with a cylindrical source. Let $\boldsymbol{x}_s$ be the position of this source.

4.3.1 Validation over an uniform mean flow

For a uniform mean flow when the above flow preprocessing is considered, the equation solved by *Actran TM* reduces to,

$$\frac{1}{\rho_0}\left\{(-k_0 + \boldsymbol{M}_0 \cdot \nabla)^2 - \Delta\right\} b^{(2D)}_{\boldsymbol{x}_s}(\boldsymbol{x}) = A\ \delta(\boldsymbol{x} - \boldsymbol{x}_s) \tag{4.15}$$

where $k_0 = \omega/a_0$ and $b^{(2D)}_{\boldsymbol{x}_s}$ is the bidimensional Green function computed by the software, let similarly $\phi^{(2D)}_{\boldsymbol{x}_s}(\boldsymbol{x})$ be the solution of Pierce's equation. When the amplitude correction is taking into account as well, the solved problem writes,

$$\left\{(-k_0 + \boldsymbol{M}_0 \cdot \nabla)^2 - \Delta\right\} \phi^{(2D)}_{\boldsymbol{x}_s}(\boldsymbol{x}) = A\ \delta(\boldsymbol{x} - \boldsymbol{x}_s) \tag{4.16}$$

For $|\boldsymbol{M}_0| < 1$ and $A = 1$, the analytical solution for the associated radiating problem is,

$$\phi^{(2D)}_{\boldsymbol{x}_s}(\boldsymbol{x}) = \frac{i \exp\left(-ik_0 \dfrac{\boldsymbol{M}_0 \cdot (\boldsymbol{x} - \boldsymbol{x}_s)}{1 - \boldsymbol{M}_0^2}\right)}{4\sqrt{1 - \boldsymbol{M}_0^2}} H_0^{(1)}\left(\frac{|k_0| r_{\boldsymbol{x}_s}}{1 - \boldsymbol{M}_0^2}\right) \tag{4.17}$$

with $r_{\boldsymbol{x}_s} = \sqrt{(1 - \boldsymbol{M}_0^2)|\boldsymbol{x} - \boldsymbol{x}_s|^2 + (\boldsymbol{M}_0 \cdot (\boldsymbol{x} - \boldsymbol{x}_s))^2}$. Figure 4.1 presents $\phi^{(2D)}$ for a pointwise source set at the origin, for $\omega = 20\pi$ rad $\cdot$ s^{-1}, $M_0 = 0.756$, $p_0 = 103330$ Pa and $a_0 = \sqrt{\gamma R T_0}$, where $T_0 = 300$ K.

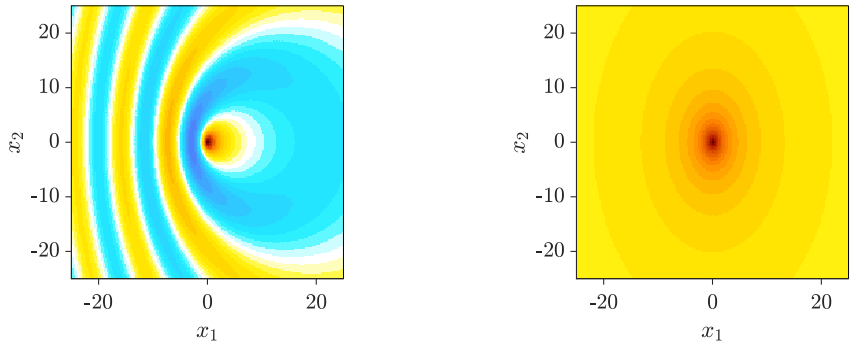

Figure 4.1: Bidimensional acoustic potential field $\phi^{(2D)}$ over the investigated uniform mean flow, real part on the left, absolute part on the right.

The solution to Pierce's equation computed with *Actran TM* is compared to the above analytical solution and the solution obtained with PROPA, for which the acoustic source is modelled by a Gaussian of standard deviation σ_s chosen to be compact $\lambda/\sigma_s \approx 1.4 \cdot 10^2$, where $\lambda = 2\pi a_0/\omega$. To comply with the analytical expression and *Actran TM*'s normalised Pierce's equation, the field computed with PROPA is divided by the integral of the Gaussian source term set in input and multiplied by a_0^2 (evaluated at the source position). Figure 4.2 compares extracts obtained for the different means and shows an almost perfect match. What is more, the ability of *Actran TM* to accurately compute a delta Dirac source term is observed.

4.3.2 Source compactness issue for the solutions of PROPA

PROPA is only capable to mimic a delta Dirac source term with a sharp Gaussian distribution. Yet due to RAM limitations, the regular mesh set in PROPA cannot be fine at will for large domains, leading to broader Gaussian profiles for the source distribution. Obviously for such cases where the

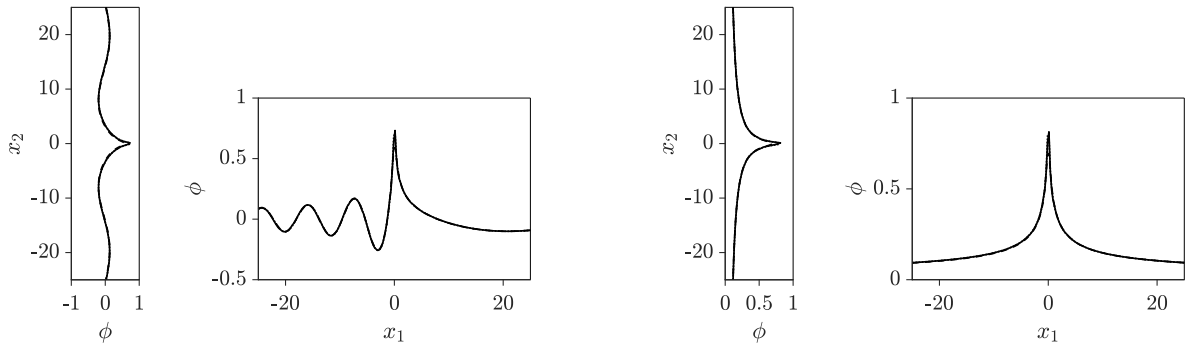

Figure 4.2: Extracts along $x_1 = 0$ and $x_2 = 0$ of the acoustic potential field ϕ computed with *Actran TM* —— with the in-house code PROPA - - - and the analytical solution ·····, real part on the left, absolute part on the right.

source is not compact with respect to the wavelength λ, the source−Green function convolution should be computed properly to be compared with the computed solution. In the next validation step of *Actran TM*'s prediction capabilities over a sheared and stratified flow, a larger domain than previously is considered for PROPA, where $\lambda/\sigma_s \approx 23$ instead of $\lambda/\sigma_s \approx 1.4 \cdot 10^2$. Before further investigations, the effect of this source broadening is presented in figure 4.3 for the uniform mean flow.

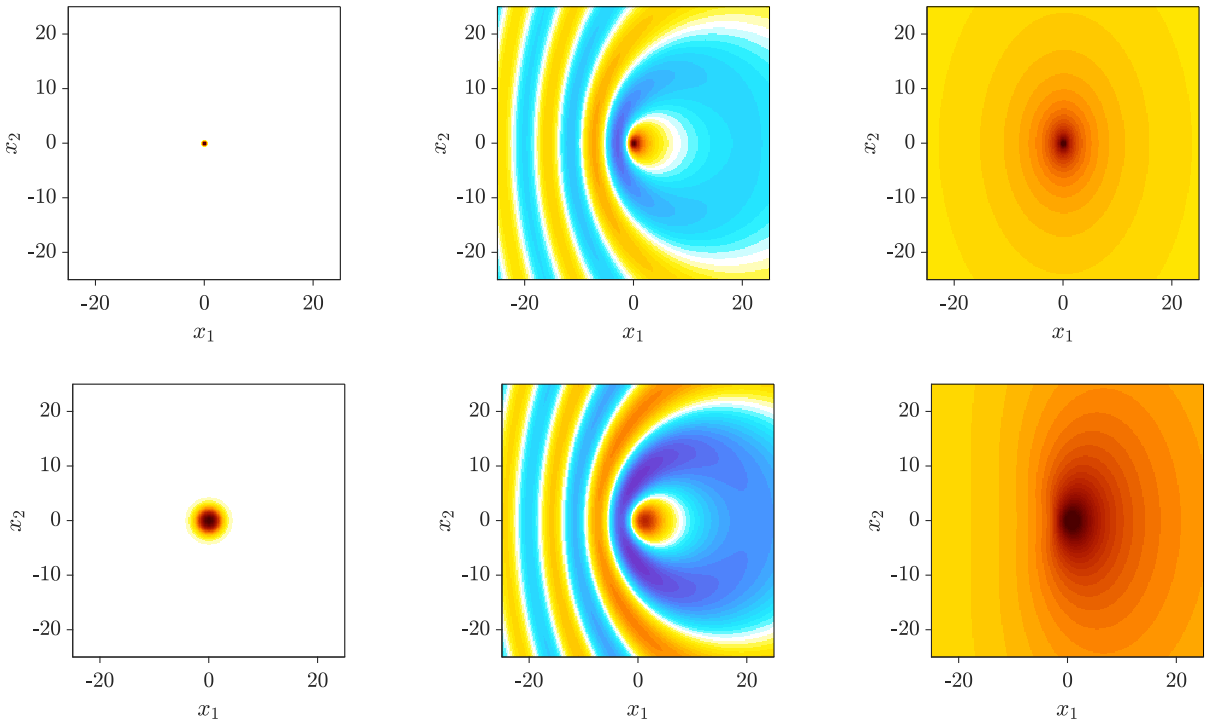

Figure 4.3: Potential field ϕ obtained with PROPA for $\lambda/\sigma_s \approx 1.4 \cdot 10^2$ on the top and $\lambda/\sigma_s \approx 23$ bottom. From left to right, the forcing term, the real part and the absolute part of the computed potential field.

This solution for a broad source is validated with respect to the analytical solution for which the convolution is properly computed. Figure 4.4 presents extracts of computed fields and shows a very satisfactory fit with the corresponding analytical solutions.

From this study, it appears that for the considered Helmholtz and Mach numbers, the loss of compactness blurs the acoustic field in the near field of the source. What is surprising is that this change of the source

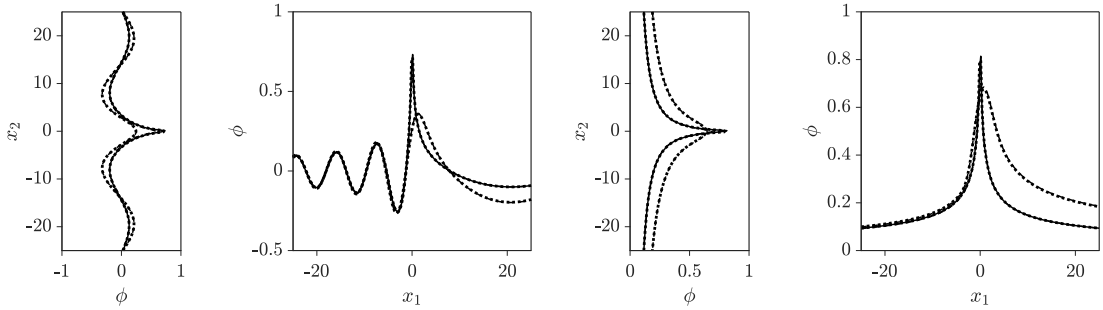

Figure 4.4: Extracts of the acoustic potential field ϕ along $x_1 = 0.0$ and $x_2 = 0.0$ with —— the solution computed with *Actran TM*, and solutions for a compact and a non-compact source - - - computed with PROPA, ▪▪▪▪ the corresponding analytical solution, real part on the left, absolute part on the right.

width has almost no effects upstream where the wavelength paradoxically are shorter and vice-versa has most significant effect in the downstream region where the wavelength are the longest.

4.3.3 Validation on the fourth CAA workshop flow

The ability of *Actran TM* to solve properly Pierce's equation over a sheared and stratified flow is verified for the Gaussian heated jet flow profile taken from the fourth CAA workshop. This parallel flow toy model is presented in §3.3.2 and a source pulsation of $\omega = 200\pi$ rad $\cdot$ s^{-1} set in the flow region is considered. In this paragraph, four simulations are presented and their extracts compared. Two simulations are computed with *Actran TM*, the first with IE (infinite elements) boundary conditions[1] and the other with PML (perfectly matched layers) radiation conditions. Two other simulations are conducted with PROPA, the first on a large domain for a source−wavelength ratio of $\lambda/\sigma_s \approx 23$ and the second on a finer but smaller mesh (with same number of grid points) where a ratio of $\lambda/\sigma_s \approx 1.4 \cdot 10^2$ is achieved, ensuring a proper description of the delta Dirac source term. This later fine mesh calculation is taken as the reference solution. Convergence on the boundary condition tuning parameter have been verified for the *Actran TM* computations. For the IE condition, interpolation order of 25 and 100 have been tested showing no modifications in the computed solution. For the PML condition, a PML width of λ and 2λ have been separately considered giving identical solutions.

Figure 4.5 shows the computed fields without the boundary condition layers. Figure 4.6 and 4.7 compare the horizontal and vertical extracts of the computed fields for $x_2/\sigma = 0.0$, $x_2/\sigma = 9.0$ and $x_1/\sigma = 0.0$, $x_1/\sigma = 25.0$ respectively, where σ corresponds to the standard deviation of the Gaussian velocity profile. Figure 4.5 indicates an overall good qualitative agreement. Except for the field computed in *Actran TM* with IE boundary conditions, the quantitative agreement for the three other fields is excellent. Outside of the shadow zone where the acoustic amplitude is low (and apart from the source compactness issue discussed later on), these three fields coincide with a deviation of less than 2%. The small discrepancies are likely to correspond to acoustic reflection at NRBC. On the cut $x_1/\sigma = 25.0$ in figure 4.7 it appears clearly that the field computed with the IE is not symmetric with respect to the jet axis, while the propagation problem is, suggesting a misbehaviour of the boundary condition in presence of a sheared flow. This appreciable dysfunction of the IE boundary conditions with non-uniform flow at the boundaries is likely to explain the qualitative differences observed. However from a quantitative point of view along the jet axis, see figure 4.6, there is almost no difference between this field, the reference solution (compact

[1]They rely on the multipole expansion of the uniform flow solution of the convected wave equation (Astley et al., 1998).

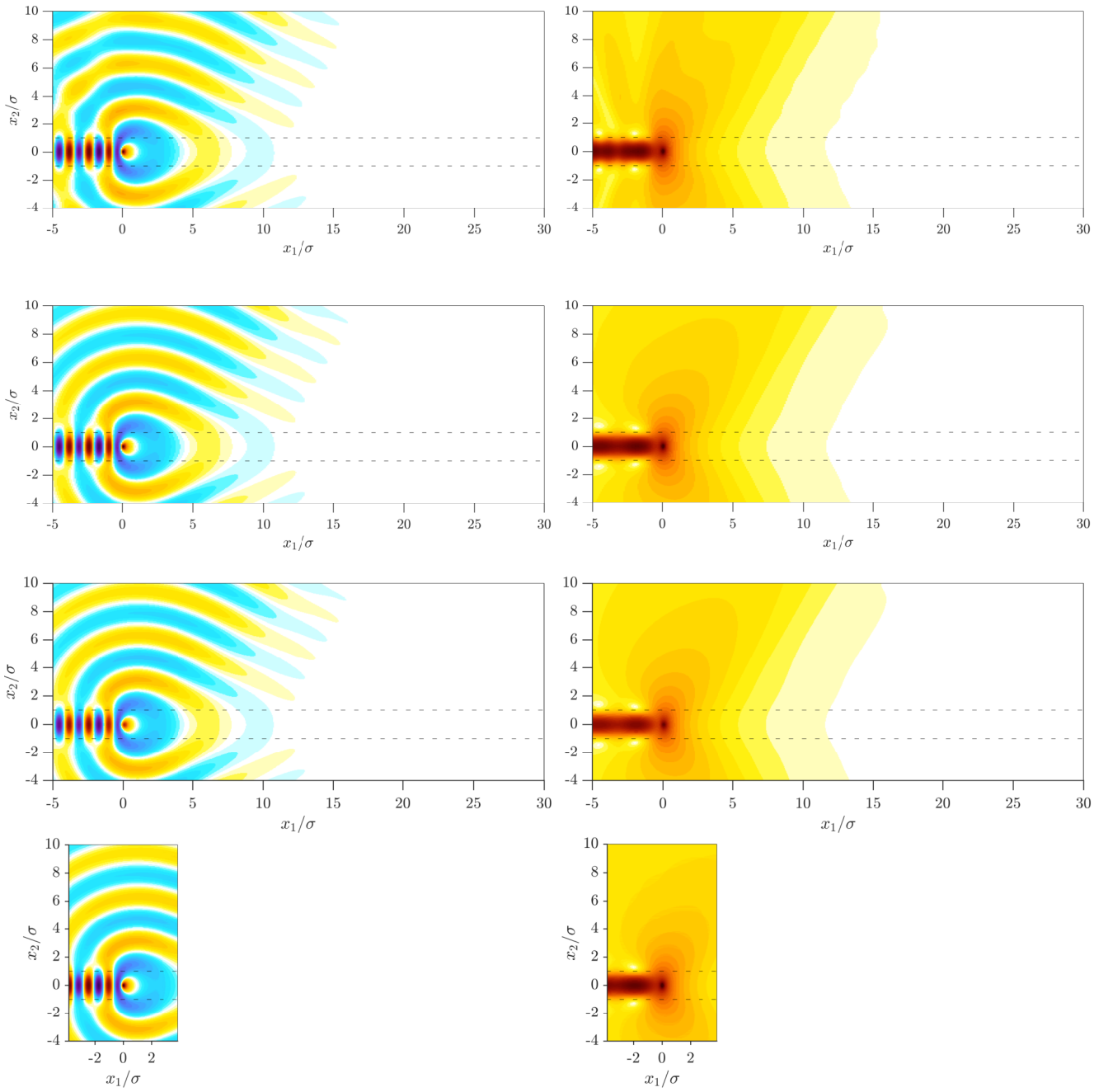

Figure 4.5: Real and absolute map of the acoustic potential field ϕ computed, from top to bottom, with *Actran TM* with IE boundary conditions, *Actran TM* with PML, PROPA with a non-compact source ($\lambda/\sigma_s \approx 23$) and PROPA for a finer mesh enabling the source to be compact ($\lambda/\sigma_s \approx 1.4 \cdot 10^2$).

acoustic computation with PROPA) and the solution obtained with *Actran TM* with PML.

As expected some amplitude differences close to the source for the non-compact PROPA computation exist. This is most easily seen when the absolute part of the potential field ϕ is considered, see the extract along the jet axis in figure 4.6. As for the uniform flow case, the source downstream region has got higher absolute acoustic amplitude than the upstream region, yet this time the acoustic upstream of the broad source does not fit the reference acoustic solution upstream of the compact source. This analysis

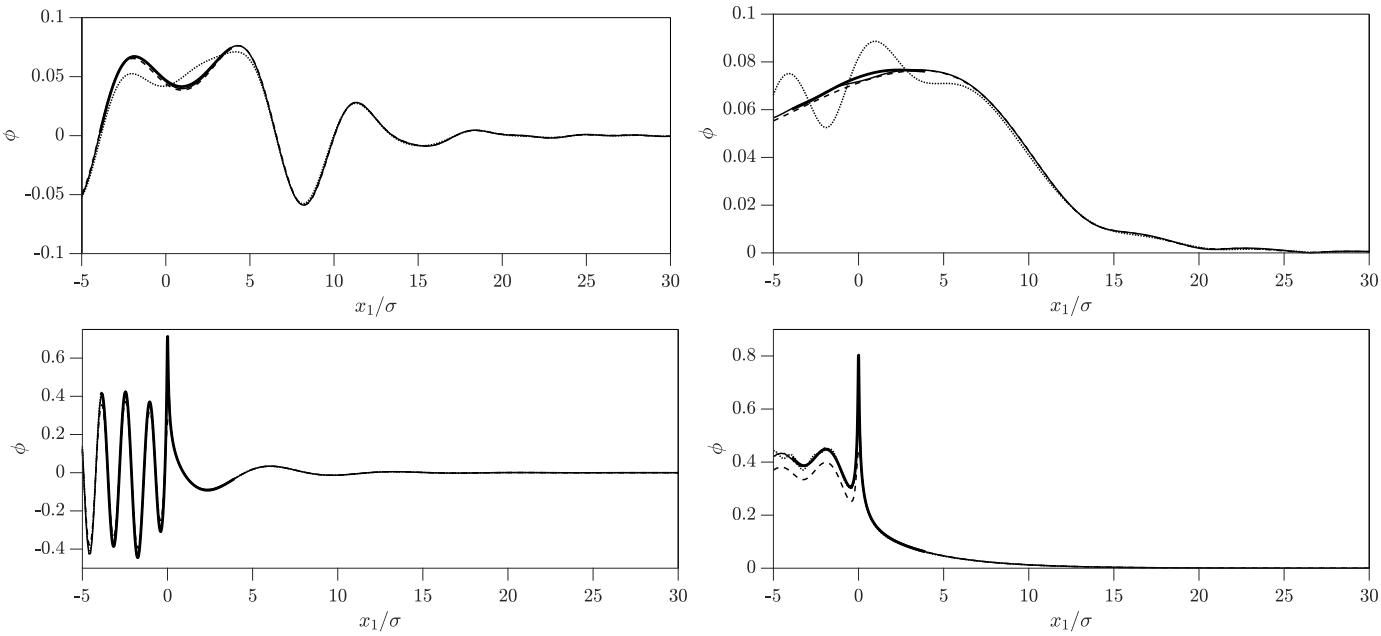

Figure 4.6: Extracts of the acoustic potential field ϕ along $x_2/\sigma = 9.0$ on the top and $x_2/\sigma = 0.0$ on the bottom computed with - - - PROPA with non compact source term, ▬ PROPA with compact source, ── *Actran TM* with PML and ····· *Actran TM* with IE, real part on the left, absolute part on the right.

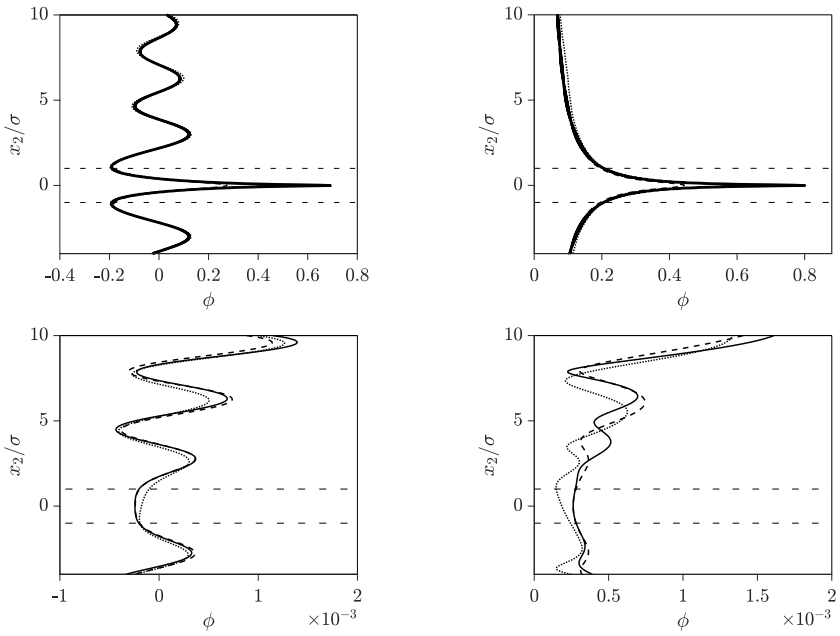

Figure 4.7: Extracts of the acoustic potential field ϕ along $x_1/\sigma = 0.0$ on the top and $x_1/\sigma = 25.0$ on the bottom computed with - - - PROPA with non compact source term, ▬ PROPA with compact source, ── *Actran TM* with PML and ····· *Actran TM* with IE, real part on the left, absolute part on the right.

furthermore highlights that the source compactness has almost no effect further away of the source vertical to the flow direction, since both extracts along $x_2/\sigma = 9.0$, obtained with PROPA for a compact and not compact source coincide and thus that the computation done with PROPA for a broad source term can be taken as reference away from the source. This observation is confirmed in figure 4.7 with the extract at $x_1/\sigma = 0.0$.

In this section, the equation coded in *FFT*'s software are derived. A procedure to transform the solved equation into Pierce's equation is given and proved to work perfectly for a uniform mean flow. For a strongly sheared and stratified flow, IE boundary conditions are not suited to perform *Actran TM* computations and PML are required. When compared to computations performed with PROPA a qualitative and quantitative very good agreement is obtained for Pierce's equation solved with *Actran TM*.

The computations achieved with the code PROPA for Pierce's equation are computed over a regular structured domain of 800×450 requiring 43 GB of RAM. Whereas the resolution with *Actran TM* over a mesh of 430 000 nodes (215 000 quadratic two-dimensional unstructured elements), which has approximatively the size of mesh used in PROPA, needs only 1.7 GB. Finite difference and finite element methods are fairly different techniques and a too strict comparison may not be fair, however PROPA and *Actran TM* with second order elements require both a minimum of 4 elements per wavelength to resolve acoustic travelling waves. This enormous gain in computation cost, and the ability of *Actran TM* to consider complex geometries, represent tremendous advantages over the in-house code, when Pierce's equation has to be solved in realistic applications.

4.4 Illustration of adjoint field in application with jet flows

Capabilities of *Actran TM* to compute adjoint solutions for jet noise relevant configurations is illustrated here. A template based on `actranpy` syntax for the computation of reciprocal solutions in application to a jet flow model is provided in appendix F. As a proof of concept, the second part of this section presents results obtained for a realistic aircraft engine geometry.

4.4.1 A template to compute $\phi^\dagger$ with *Actran TM*

Besides the possibility of handling unstructured geometries at affordable costs, another attractive aspect of *Actran TM* is to enable scripting with the inbuilt python library `actranpy`. This is an advanced feature of the tool that makes parametric studies and optimisation procedures possible. It was found valuable to present here how such a computation could be set-up without resorting to the GUI *ActranVI*.

This template, appendix F, considers a bidimensional heated jet exiting an unflanged duct as presented in figure 4.8. The duct is straight and hard walled, possible internal reflection are discarded by assuming the duct infinitely long. The flow is computed from Panda and Seasholtz (1999) with some slight modifications to fiddle about flight effects. This analytical non-uniform flow is mapped on the numerical grid with help of the `field_data` structures of `actranpy`. With the script variable `WhichFlowField`, the base flow used for the computation is selected. It is possible to compute the direct solution to default Möhring's equation or to Pierce's equation but also to compute the FRT-reciprocal solution associated to Pierce's equation. When solution to Pierce's equation is chosen, the base flow is preprocessed to compensate for the $\rho_{T,0}$. The source amplitude is modified accordingly apart from the pulsation ω and the complex conjugation of the `VELOCITY_POTENTIAL` field that is straightforward to compensate later on in the analysis, compare §4.2.2 and appendix F. The free field boundary condition is modelled either with infinite elements (IE) or with perfectly matched layer (PML). Depending on the choice of the radiating condition, the mesh is automatically generated either with a linear or with a quadratic interpolation order. For a linear interpolation order, 7 elements per wavelength are required while for a quadratic interpolation order, a minimum of 4 elements is needed.

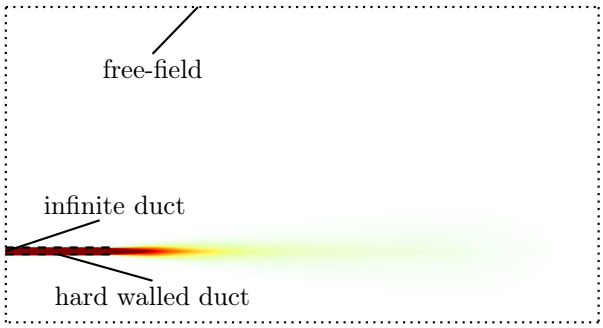

Figure 4.8: Definition of the domain and the flow as computed with the script given in appendix F. The jet Mach number ranging from 0.3 (white) to 0.7 (dark red) is depicted.

The sound sources can be either planar or pointwise. They can be set in or out of the computational domain. This is the keystone to enable far field noise prediction at affordable computational costs. In this way indeed, the mesh does not need to extend up to the adjoint source position, that is the location of the observer. Only flow heterogeneities needs to be meshed. During the design of this template, investigations with the team of *Free Field Technologies* have shown that `field_data` could not be used together with sound sources set out of the computational domain. When far field analysis are done, this means in practice that the mean flow must be uniform at the domain boundaries, unlike what is presented in figure 4.5. This feature is not functional yet and should be fixed in future releases. An alternative solution using IE is employed here instead. That is, an additional region of uniform flow is defined to wrap the region of flow heterogeneities and to achieve the interface with the non reflecting boundary condition. This transition layer can be defined as thin as one cell width as in the template of appendix F or much thicker as in figure 4.11. Since this flow region is uniform, `field_data` are not needed and the definition of exterior sound source is readily operable. To avoid discontinuity in the mean flow field, the flow specified in the `field_data` needs to be uniform at the outer domain frontier. In practice this is achieved here with the use of a buffer domain for the base flow. It was previously observed in figure 4.5, that flow heterogeneities at IE frontier may create spurious reflections. The use of such a buffer layer for the flow is therefore a recommended practice for IE radiating conditions. Results obtained for the jet flow of figure 4.8 for sources set in and out of the meshed domain have been obtained with this alternative procedure and are presented in figure 4.9.

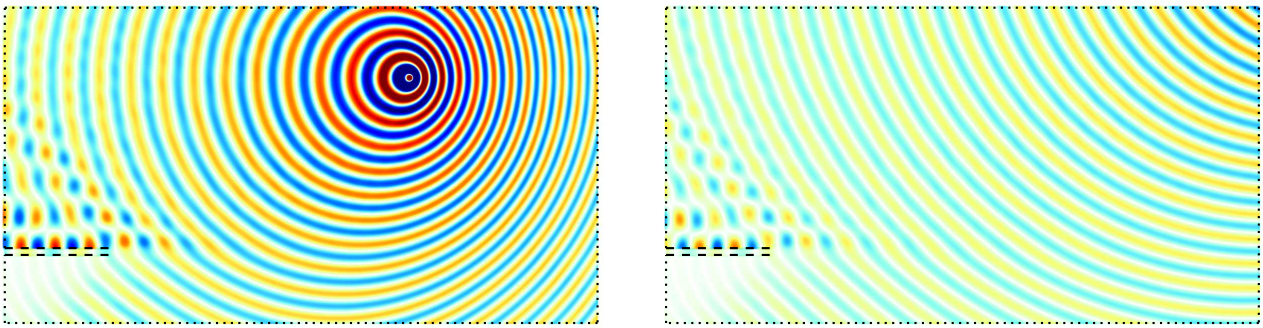

Figure 4.9: Adjoint solution $\phi^\dagger$ to Pierce's equation computed by flow reversal for a Strouhal number of $St = 0.32$. Adjoint sources are set at a distance of 50 and 100 diameter with respect to the duct exit and with a polar angle of 30^o. The transition layer with uniform flow is so thin, it cannot be spot.

4.4.2 Dual stream engine with chevrons

A further benefit of commercial software lies in their robustness, versatility and maintenance. As such *Actran TM* enables amongst others the reading of RANS computations, the generation and the handling of unstructured meshes, the interpolation of the flow on the acoustic grid, the computation and the post-processing of the results. An illustrative implementation of an adjoint computation for a realistic industrial configuration is presented here. The EXEJET dual-stream engine with chevrons is considered for that purpose Huber et al. (2014). The dealt configuration presents realistic features of an aircraft engine. The primary jet exiting the core is heated with respect to the secondary flow originating from the fan with a temperature ratio $T_c/T_f \approx 2.6$. The local jet Mach numbers for both flow are respectively $M_f = 0.84$ and $M_c = 0.67$. Some in-flight effects are moreover accounted for with an external flow of $M_{ext} = 0.27$.

The *Actran TM* analysis is based on a RANS solution computed with the flow solver *ElsA* developed at *Onera*. The geometry presents 9 inner chevrons and 18 outer chevrons, so that the flow simulation could benefit from angular periodicity simplifications, and hence only an angular sector of 20^o of the flow was modelled with RANS. Steps to build an *Actran TM* analysis are overviewed hereafter.

1. In order to rebuilt the complete engine, an intermediate grid of 40^o angle is first created. The *Boxpro* toolbox of *ActranVI* enables to duplicate the 20^o geometry and to generate an unstructured mesh such as presented in figure 4.10 (use `interior shrinkwrap` for multi-bloc geometries).

2. Import the flow field with `actranpy`, if need is, dimensionalise the CFD data and apply flow reversal and/or $\rho_{T,0}$ corrections. Using *iCFD* device of *Actran TM* and the geometry planar symmetry, interpolate the 20^o flow field from structured multi-bloc CFD mesh on the 40^o unstructured grid.

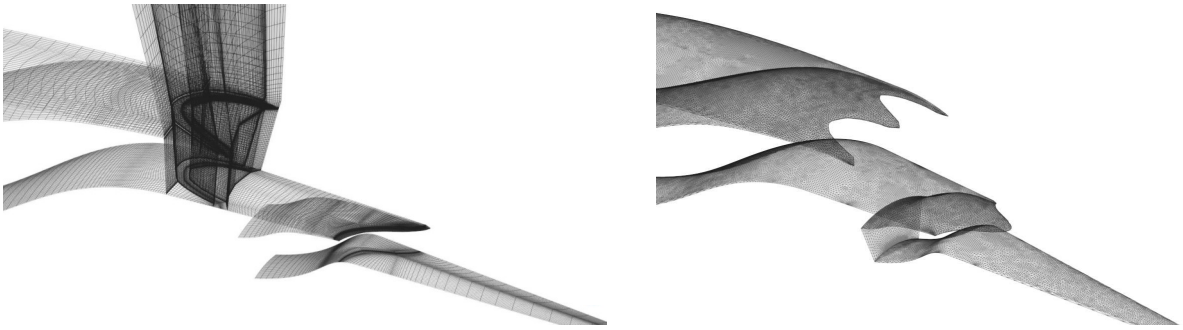

Figure 4.10: Detail of the structured and multi-bloc CFD mesh spanning on 20^o (left) and detail of the unstructured mesh computed with planar symmetry and used for the first flow interpolation (right).

3. With *Boxpro*, an unstructured 360^o acoustic mesh of $3.9\,.10^6$ three-dimensional elements is built (900 000 grid points). The geometry is cylindrical with a diameter three time larger as the engine end extending over 10 diameters In the mesh generation process, the `Hexacore` option is selected, so to use hexahedral elements in the core of the mesh as shown in figure 4.11. This is a recommended practice to diminish the RAM requirements of the computation.

4. With help of the *iCFD* hand-tool, the mean flow previously mapped on the 40^o angular sector is now interpolated using angular periodicity on the complete 360^o geometry, as shown in figure 4.11 (left). Note that it is presently not possible with *iCFD* to map a three-dimensional axisymmetric geometry with a planar axisymmetrical flow.

5. A transition layer is wrapped around the numerical domain so to enable acoustic computations from source set out of the domain. $2.2\,.10^6$ three-dimensional elements are additionally created (440 000 grid points). A buffer region forces smoothly the interpolated flow to uniformity at the domain frontier so to guarantee flow continuity at the interface with the transition layer.

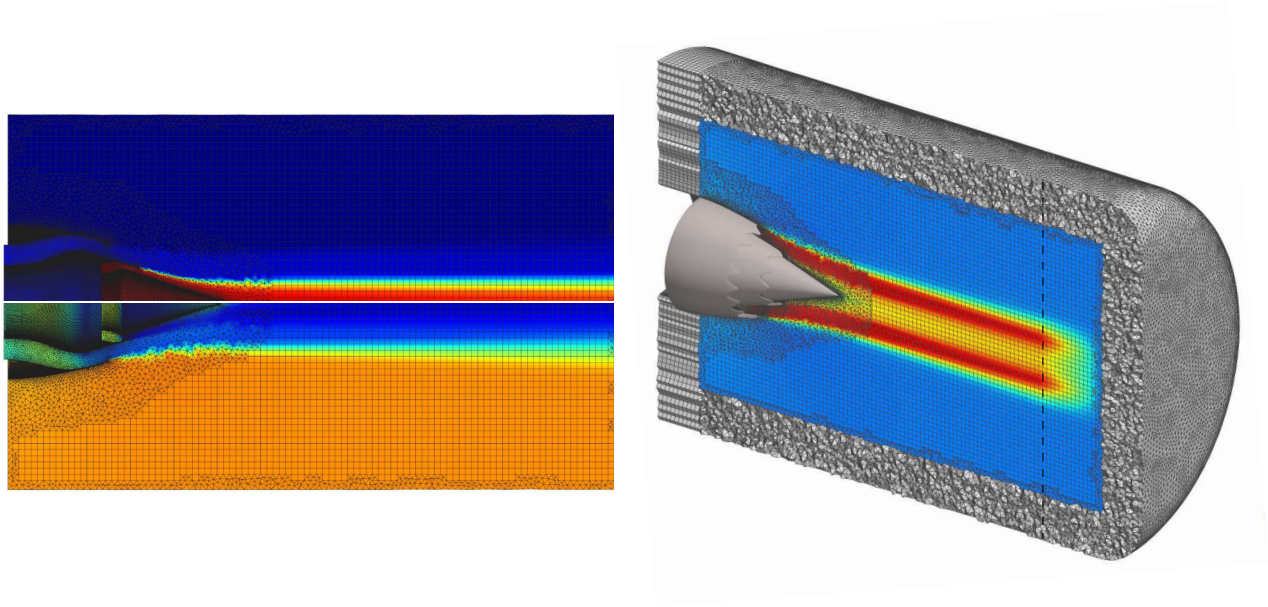

Figure 4.11: Interpolation over the 360^o acoustic grid of the heterogeneous mean-flow. Mean speed of sound a_0 from $331\,\mathrm{m.s^{-1}}$ to $570\,\mathrm{m.s^{-1}}$ (left - top), and reversed mean axial velocity $u_{0,1}$ required to solve the adjoint Pierce problem, from $-377\,\mathrm{m.s^{-1}}$ to $3.37\,\mathrm{m.s^{-1}}$ (left - bottom). To enable far field computations, grid points are created to form a transition layer where uniform flow is specified in the analysis. The present transition layer represents about $1/3$ of the total number of elements. Absolute value of the Mach number M_0 that is specified with `field_data` in the analysis, from 0.04 to 0.94, the ambient Mach number is 0.27. A buffer region delimited with dashed line is build to ensure the base flow continuity (right).

6. Eventually the computation is parametrised as for the previous analysis given in appendix F. For this configuration, 85 GB of RAM and about 45 min per frequency were required. Note that *Actran TM* simulations can be run in parallel and/or with iterative solvers. This figures are indicative for a sequential use of the MUMPS solver. As further indication, 43 GB of RAM would have been required to perform similar computation without the extra layer, i.e. half memory for $1/3$ less grid points. To divide the memory requirement by two, the computations may be achieved with single precision. The price to pay for these cost savings are the errors in the mantissa; the accuracy of this compromise has to be estimated.

A compact monopole oscillating at a Strouhal number of $St_f = 2.0$ is considered in the presented analyses. Where $St_f = \frac{1}{M_f}\frac{D_f}{\lambda}$ is based on the fan flow exit diameter D_f. This corresponds to a mixed Strouhal number Huber et al. (2014) of $St_{\mathrm{mix}} = 1.3$. Before presenting the computed adjoint fields, a qualitative comparison of the effect of the $\rho_{T,0}$ correction procedure is given figure 4.12. In both solutions, the channelling of acoustic wave upstream of the flow is observed. The flow refraction effect is clearly identifiable and fairly similar for both solutions, yet of higher amplitude and slightly more directional for the potential field obtained with Pierce's equation. Larger discrepancies arise downward of the source; while a part

of the amplitude is trapped on the jet axis with the default equation solved in *Actran TM*, the cone of silence is more pronounced in the solution computed with Pierce's wave equation.

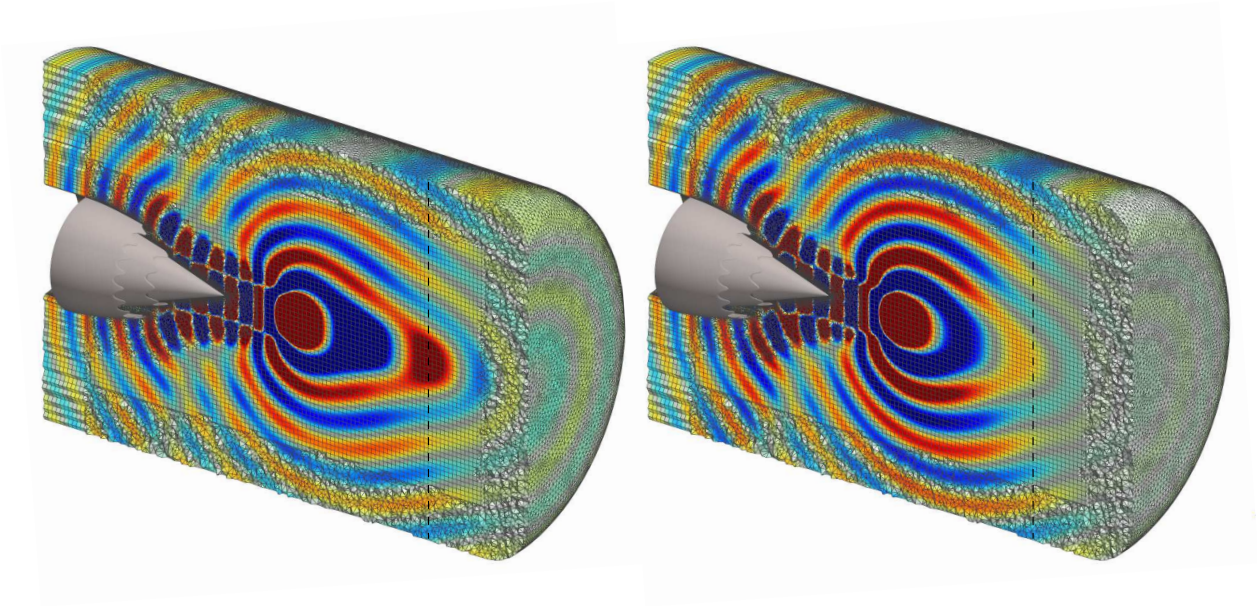

Figure 4.12: Green solution to the direct propagation problem for $St_f = 2.0$. The solution b to the default Möhring's equation of *Actran TM*, with $p = \frac{i\rho_0}{\omega\rho_{T,0}} D_{\boldsymbol{u}_0}(b)$ (left) and ϕ to Pierce's wave equation, with $p = -D_{\boldsymbol{u}_0}(\phi)$ (right) are shown.

The adjoint Green solution $\phi^\dagger$ to Pierce's equation is computed with *Actran TM* by using the FRT. For an illustrative purpose, computations performed for adjoint sources set in the near-field, figure 4.13, and in the middle range to far-field, figure 4.14, are presented. Reminding that the adjoint field $\phi^\dagger$ is relevant in Lagrange's identity where the physical sound source are located, commentaries on these fields must thus focus on the jet sheared flow region. It is seen that in these regions that the adjoint solution $\phi^\dagger$ experiences some sharp variations in phase. This will translate into constructive and destructive interferences of the sound source. From these preliminary results, it is expected that reliable computations of adjoint Green's solutions may notably improve the taking into account of acoustic propagation effects. This work will receive further attention in future work. Attention will be paid in a step by step validation, with increasing geometrical complexities, of the complete jet mixing noise prediction methodology. In particular, it appears instructive to compare the original Tam and Auriault mixing noise model §2.1 with analytical adjoint Green function computation (Afsar et al., 2017b) to the alternative proposed in §2.2 and in the present section.

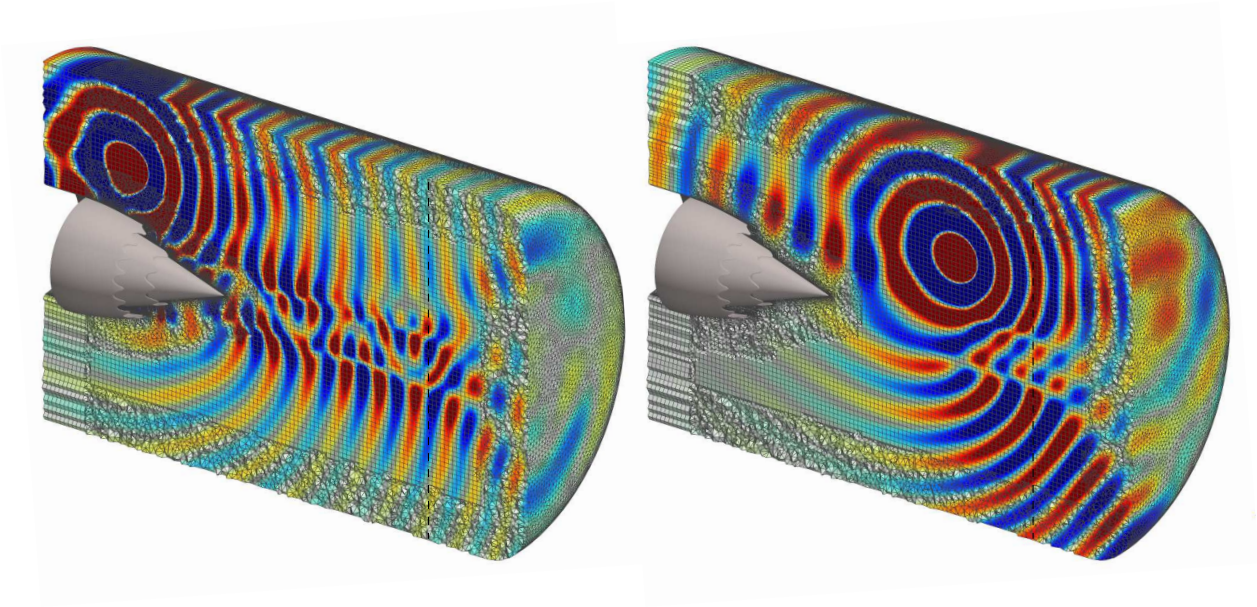

Figure 4.13: Adjoint Green's function $\phi^\dagger$ of Pierce's equation computed with the flow reversal theorem for $St_f = 2.0$. These two near-field solutions to the reciprocal propagation problem exhibit a complex behaviour in the jet flow region.

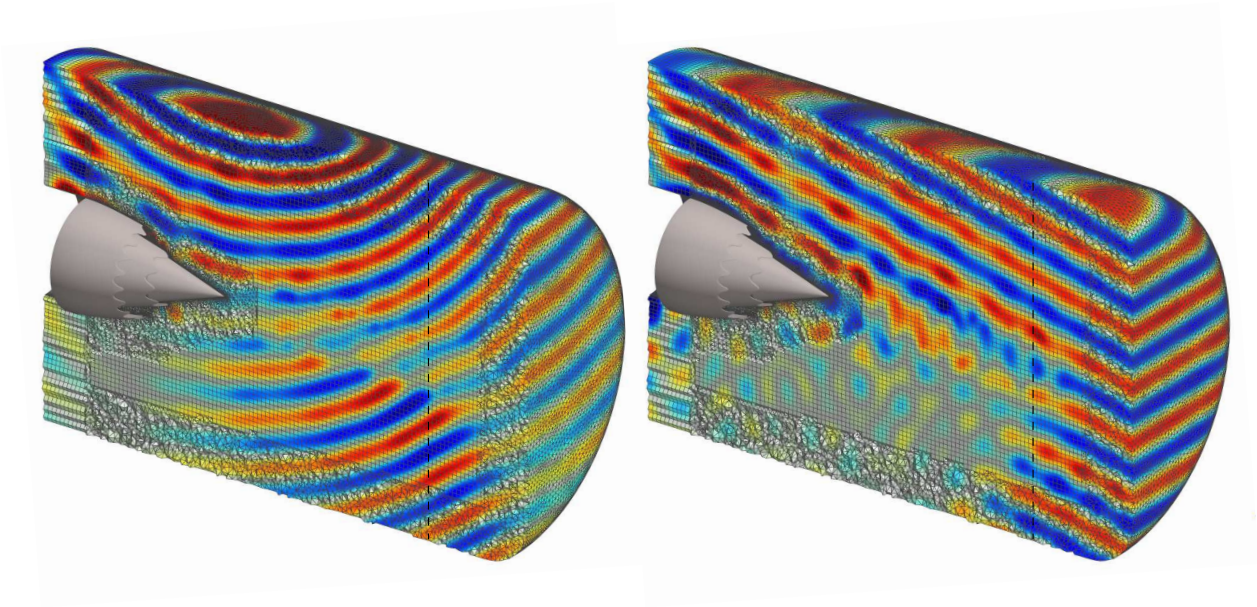

Figure 4.14: Adjoint Green's function $\phi^\dagger$ of Pierce's equation computed with the flow reversal theorem for $St_f = 2.0$. The computations are run for sources set at a distance of $10D_f$ (left) and $500D_f$ (right) from the engine.

Conclusion

This study is concerned with the modelling of the propagation of sound emitted by a high-speed turbulent jet. The standpoint adopted is that of acoustic analogies and the approach selected involves largely analytical modelling. Within this simplified framework, the acoustic field produced by the aerodynamic flow does not retroact on the latter, and the problems of sound generation and propagation can be treated separately. This thesis is divided into two parts as follows.

The objective of this study's first part is to propose a simplified model for the sound propagating on a base flow, that is both accurate and robust. To guarantee the robustness of the approach, a formulation that uses the acoustic potential is proposed. This method conserves acoustic energy. This is an asset of the method, which is found thereby consistent with the two limit cases of sound propagation around a potential flow and geometrical acoustics. This is to say that the model proposed coincides with the only formulations in the literature for which acoustics is unambiguously defined. The enforced conservation of acoustic energy equally means that mode conversion phenomena cannot be dealt from this approximated perspective. This represents a limitation of the methodology presented, which by construction is unable to describe certain noise generation mechanisms, such as instability waves or the acoustic radiation of a vortex sheared as it moves with the flow. Equivalent acoustic sources must be defined to address these noise mechanisms. This appears as a necessary price to pay to ensure that the acoustic energy is conserved.

To arrive at this formulation, Euler's equations are rearranged into Euler's Wave Equation (EWE). Under the assumption of perfect gases, a closing equation for the fluid equations is derived, and it is shown that Euler's equations can be restated with only two variables. From the linearisation of EWE (LEWE), a wave equation for the fluctuating velocity is obtained which is equivalent to linearised Euler's equations provided that the entropic mode is not generated. This is not particularly constraining for Euler's equations which presuppose an adiabatic flow. LEWE is thus more general than the equation of Lilley et al. (1972). For a parallel mean flow, the equivalence of the two equations is verified numerically on a configuration exhibiting an instability wave. Taking good advantage of the energy conservation property of self-adjoint operators (Möhring, 1999), several stable approximations of LEWE are proposed. Then, by opting for a definition of the acoustic potential based on the momentum rather than on the velocity, an acoustic analogy is constructed. The propagation operator so formed corresponds to the wave equation of Pierce (1990), whose operational relevance is greatly enhanced by the novelty of a source term. It is only by choosing this definition of the acoustic potential that the equivalence of potential acoustics and exact ray formalism (Foreman, 1989) could be formally demonstrated. The choice in favour of this original convention for acoustic potential is reinforced through this. The sound field calculated with Pierce's equation is compared with other stable propagation operators on a benchmark case, and its agreement with the reference solution obtained with Lilley's equation is found satisfactory. While Pierce's equation and Phillips' equation (1960) have the same wave operator, it was found that their predictions differ greatly. The paramount importance of judiciously choosing the acoustic variable is emphasised through this. It has not been proven that the definition of the acoustic potential used here offers the best approximation of the acoustic field, and other definitions of acoustic potentials, such as the fluctuating enthalpy (Howe, 1975a), could be explored in future investigations. Thanks to the development of the PROPA in-house code, the stability of the propagation operators that have been proposed could be validated. The accuracy of the different formulations are compared on a test case, which due to the inherent limitations of PROPA that is very greedy in RAM, considers a simple configuration that extends over a relatively small calculation domain. A more thorough comparative study would require the use of a more advanced development environment such as provided by the *FreeFEM* open source libraries (Hecht, 2012).

The second part of this thesis illustrates how the acoustic analogy formed from Pierce's equation can advantageously be used to reformulate existing jet noise models. The targeted application is the prediction of the noise radiated by the jet of an aircraft engine installed under the wing. Due to the complexity of the flow exhausting from such a turbofan engine, only a statistical description of the flow is numerically achievable, and the usual methods for simulating acoustic propagation are rendered inoperable. The adjoint method, initially introduced by Lagrange (1761) and reformulated for jet noise by Tam and Auriault (1998), ingeniously overcomes this difficulty by using the reciprocity principle. This study reviews this technique as meticulously as possible by this author, and compares it to the competing and more intuitive technique of flow reversal. These two techniques, the adjoint method and flow reversal, are then applied to Pierce's equation and Lilley's equation. While the adjoint method is always exact, flow reversal only applies to self-adjoint equations such as Pierce's equation. As a result, the use of Pierce's wave equation has several major advantages in this context. Since flow reversal does not require the development of anti-causal boundary conditions, the numerical resolution of the adjoint field associated with Pierce's equation is simplified, and existing numerical tools can be used to this end. Furthermore, Pierce's wave equation is scalar and its expression is extremely simple, so that the computational cost associated with its resolution is minimal. This is an undeniable advantage when solving problems with a large number of degrees of freedom as encountered in industrial applications. Finally, its self-adjoint nature guarantees the stability of the propagation problem. This seems to have been the stumbling block preventing a more widespread use of the numerical resolution of adjoint equations until now. As a matter of fact, Lilley's equation and linearised Euler's equations used so far in the adjoint formulations (Tam and Auriault, 1998) describe the instability mode, and approximated analytical methods of the WKBJ type have been privileged to a numerical resolution of the equations (Goldstein, 2003).

In order to demonstrate the viability of using Pierce's acoustic analogy to reformulate jet noise models, the turbulent mixing noise model of Tam and Auriault (1999) has been rewritten for the acoustic potential. A methodology to consistently transpose into this framework other noise source modellings, such as the broadband shock-associated noise (BBSAN), has been sketched, and future work will have to prove its appropriateness. To indicate a possible way of implementing the method, that is compatible with the requirements of the aeronautics industry, a calculation strategy based on the commercial software *Actran TM* has been implemented and carefully detailed. A realistic turbofan engine geometry is considered as a proof of concept and different adjoint fields could be computed in near and far field in times compatible with engineering requirements. Future work will have to focus on implementing the entire prediction chain, from the calculation of the RANS solution to the noise spectrum, and to validate each step. The presence of surfaces in acoustic propagation can be taken into account by the adjoint method as formulated here, this represents a major improvement over the original formulation of Tam and Auriault (1998), and awaits to be carried out and validated in concrete applications. The adjoint method reveals its full potential when the noise sources are only known statistically, and has no rival when the acoustic propagation cannot be solved analytically. This technique is moreover general and can be used to tackle the acoustic propagation of all kind of sound sources. The same adjoint fields would thus allow the computation of the sound propagation of all aircraft engine noise sources. This approach treats the sound propagation independently of the noise generation mechanisms, and the adjoint fields fully characterise a propagation medium. In a sense, with the decoupling achieved in the noise computation, this method can be seen as a logical extension to the acoustic analogies.

Appendix

A Conventions and formulae

A.1 Convention for the Fourier transform

In this study, a non-unitary Fourier transform is considered in time,

$$F(\boldsymbol{x},\omega) = \int_{\mathbb{R}} \mathrm{d}t \; f(\boldsymbol{x},t) e^{+i\omega t} \quad \text{and} \quad f(\boldsymbol{x},t) = \frac{1}{2\pi} \int_{\mathbb{R}} \mathrm{d}\omega \; F(\boldsymbol{x},\omega) e^{-i\omega t} \tag{A.1}$$

and in space,

$$\hat{f}(\boldsymbol{k},t) = \int_{\mathbb{R}^n} \mathrm{d}\boldsymbol{x} \; f(\boldsymbol{x},t) e^{-i\boldsymbol{k}\cdot\boldsymbol{x}} \quad \text{and} \quad f(\boldsymbol{x},t) = \frac{1}{(2\pi)^n} \int_{\mathbb{R}^n} \mathrm{d}\boldsymbol{k} \; \hat{f}(\boldsymbol{k},t) e^{+i\boldsymbol{k}\cdot\boldsymbol{x}} \tag{A.2}$$

where n is the dimension of the space considered, $\boldsymbol{x}$ and t are the position and the time, ω corresponds to the pulsation and $\boldsymbol{k}$ is the wave number. If f is a generic function of space and time, F is its Fourier transform in time and $\hat{f}$ in space. Both transformation may possibly be achieved simultaneously,

$$\hat{F}(\boldsymbol{k},\omega) = \int_{\mathbb{R}} \mathrm{d}t \int_{\mathbb{R}^n} \mathrm{d}\boldsymbol{x} \; f(\boldsymbol{x},t) e^{i(\omega t - \boldsymbol{k}\cdot\boldsymbol{x})} \quad \text{and} \quad f(\boldsymbol{x},t) = \frac{1}{(2\pi)^{n+1}} \int_{\mathbb{R}} \mathrm{d}\omega \int_{\mathbb{R}^n} \mathrm{d}\boldsymbol{k} \; \hat{F}(\boldsymbol{k},\omega) e^{-i(\omega t - \boldsymbol{k}\cdot\boldsymbol{x})} \tag{A.3}$$

The space-time Fourier transform of the one dimensional advection equation,

$$\frac{\partial f(x,t)}{\partial t} + a \frac{\partial f(x,t)}{\partial x} = \delta(x-\xi)\delta(t-\tau) \tag{A.4}$$

is considered to observe how these conventions apply on PDE. Here a is the advection speed, ξ and τ are the reference position an time of the impulsive source term considered. If the Fourier transform in time is done first,

$$\int_{\mathbb{R}} \mathrm{d}t \left\{ \quad \frac{\partial f(x,t)}{\partial t} + a \frac{\partial f(x,t)}{\partial x} = \delta(x-\xi)\delta(t-\tau) \quad \right\} e^{i\omega t} \tag{A.5}$$

Since x and t are two independent variables, derivation in space and time integration may be switched,

$$\int_{\mathbb{R}} \mathrm{d}t \; \frac{\partial f(x,t)}{\partial t} e^{i\omega t} + a \frac{\partial}{\partial x} \left(\int_{\mathbb{R}} \mathrm{d}t \; f(x,t) e^{i\omega t} \right) = \delta(x-\xi) e^{i\omega\tau} \tag{A.6}$$

Integrating by parts and because real signal have a finite time support, the first term can be recast into,

$$\int_{\mathbb{R}} \mathrm{d}t \; \frac{\partial f(x,t)}{\partial t} e^{i\omega t} = \Big[f(x,t) e^{i\omega t} \Big]_{t=-\infty}^{t=+\infty} - \int_{\mathbb{R}} \mathrm{d}t \, f(x,t) \frac{\partial e^{i\omega t}}{\partial t} = -i\omega \int_{\mathbb{R}} \mathrm{d}t \, f(x,t) e^{i\omega t} = -i\omega F(x,\omega) \tag{A.7}$$

The advection equation therefore writes in the frequency domain as,

$$-i\omega F(x,\omega) + a\frac{\partial F(x,\omega)}{\partial x} = \delta(x-\xi)e^{i\omega\tau} \tag{A.8}$$

The Fourier transform in space is analogous to the one in time but with an opposite sign. Finally these convention turn the advection equation in the wave number - pulsation domain (k , ω) into,

$$\{-i\omega + iak\}\,\hat{F}(k,\omega) = e^{i(\omega\tau - k\xi)} \tag{A.9}$$

Note that throughout this work, the upper/lowercase convention is not systematically followed for the sake of convenience.

A.2 Fourier transform in time of Green's function

Different time Fourier transform definitions for Green's functions are possible (Chong, 2016), the one chosen for this study takes benefit from the time-shift invariance. Let $\boldsymbol{x}_s$, $\boldsymbol{x}_m$ and t_s, t_m be respectively the source, microphone positions and corresponding times. Source-observer Green's functions are defined in the frequency domain as $G^{(\boldsymbol{x}_m,\omega)}_{\boldsymbol{x}_s}$ and in the time domain as $g^{(\boldsymbol{x}_m,t_m)}_{\boldsymbol{x}_s,t_s} \equiv g^{(\boldsymbol{x}_m,\tau)}_{\boldsymbol{x}_s}$, where $\tau \equiv t_m - t_s$ is the source-observer time-shift. Fourier transform of Green's functions are thus defined as,

$$G^{(\boldsymbol{x}_m,\omega)}_{\boldsymbol{x}_s} = \int_{\mathbb{R}} \mathrm{d}\tau\; g^{(\boldsymbol{x}_m,\tau)}_{\boldsymbol{x}_s} e^{i\omega\tau} = \int_{\mathbb{R}} \mathrm{d}\tau\; g^{(\boldsymbol{x}_m,t_s+\tau)}_{\boldsymbol{x}_s,t_s} e^{i\omega\tau} \tag{A.10}$$

and,

$$g^{(\boldsymbol{x}_m,t_m)}_{\boldsymbol{x}_s,t_s} = g^{(\boldsymbol{x}_m,\tau)}_{\boldsymbol{x}_s} = \frac{1}{2\pi}\int_{\mathbb{R}} \mathrm{d}\omega\; G^{(\boldsymbol{x}_m,\omega)}_{\boldsymbol{x}_s} e^{-i\omega\tau} \tag{A.11}$$

A.3 Free field Green's functions for Helmholtz's equation

Two dimensional analytical solutions can be obtained by integration of the three dimensional analytical solution (Ehrenfried, 2004, §6.6),

Wave equation	Green's function
$\left\{\frac{1}{a_0^2}\frac{\partial^2}{\partial t^2} - \Delta\right\} G_{\boldsymbol{x}_s,t_s}(\boldsymbol{x},t) = \delta(\boldsymbol{x}-\boldsymbol{x}_s)\delta(t-t_s)$	$G^{3D}_{\boldsymbol{x}_s,t_s}(\boldsymbol{x},t) = \frac{\delta\left(t-t_s-\lvert\boldsymbol{x}-\boldsymbol{x}_s\rvert/a_0\right)}{4\pi\lvert\boldsymbol{x}-\boldsymbol{x}_s\rvert}$ $G^{2D}_{\boldsymbol{x}_s,t_s} = \frac{H\left(t-\tau-\lvert\boldsymbol{x}-\boldsymbol{y}\rvert/a_0\right)}{2\pi\sqrt{(t-\tau)^2-\lvert\boldsymbol{x}-\boldsymbol{y}\rvert^2/a_0^2}}$

Table A.1: δ is the Dirac delta function, H corresponds to the Heaviside step function.

and according to the Fourier transform convention considered here,

Wave equation	Green's function
$\left\{\left(-i\frac{\omega}{a_0}+\boldsymbol{M}_0\cdot\nabla\right)^2-\Delta\right\}G_{\boldsymbol{x}_s}(\boldsymbol{x})=\delta(\boldsymbol{x}-\boldsymbol{x}_s)$	$G^{3D}_{\boldsymbol{x}_s}(\boldsymbol{x})=\exp\left(-i\frac{\omega}{a_0}\frac{\boldsymbol{M}_0\cdot(\boldsymbol{x}-\boldsymbol{x}_s)}{1-M_0^2}\right)\frac{\exp\left(i\frac{1}{1-M_0^2}\frac{\omega}{a_0}r_{\boldsymbol{x}_s}\right)}{4\pi r_{\boldsymbol{x}_s}}$ $G^{2D}_{\boldsymbol{x}_s}(\boldsymbol{x})=\frac{i\ \exp\left(-i\frac{\omega}{a_0}\frac{\boldsymbol{M}_0\cdot(\boldsymbol{x}-\boldsymbol{x}_s)}{1-M_0^2}\right)}{4\sqrt{1-M_0^2}}H_0^{(1)}\left(\frac{1}{1-M_0^2}\frac{\omega}{a_0}r_{\boldsymbol{x}_s}\right)$ where, $\quad r_{\boldsymbol{x}_s}=\sqrt{(1-M_0^2)\lvert\boldsymbol{x}-\boldsymbol{x}_s\rvert^2+(\boldsymbol{M}_0\cdot(\boldsymbol{x}-\boldsymbol{x}_s))^2}$

Table A.2: δ is the Dirac delta function, and $H_0^{(1)}$ is the Hankel function of first kind with order zero.

A.4 Choice of the scalar product

Let $\boldsymbol{a}$ and $\boldsymbol{b}$ be two vectors of a space Ω and $\boldsymbol{H}$ a definite positive symmetric matrix. If problems in the time domain are considered, a real valued scalar product $<,>_{\boldsymbol{H}}$ induced by $\boldsymbol{H}$ may be introduced,

$$< \boldsymbol{a},\boldsymbol{b} >_{\boldsymbol{H}} = \int_\Omega \mathrm{d}\boldsymbol{x}\int_{\mathbb{R}}\mathrm{d}t\ \boldsymbol{a}(\boldsymbol{x},t)\cdot\boldsymbol{H}(\boldsymbol{x},t)\cdot\boldsymbol{b}(\boldsymbol{x},t) \tag{A.12}$$

When a frequency domain problem is investigated, the symmetry of the $\boldsymbol{H}$ matrix needs to be hermitian, that is $\boldsymbol{H}=\boldsymbol{H}^{T*}$, where ^{T} is the matrix transpose and * is the element-wise complex conjugation. The hermitian scalar product $<,>_{*\boldsymbol{H}}$ induced by $\boldsymbol{H}$ may then be defined as,

$$< \boldsymbol{a},\boldsymbol{b} >_{*\boldsymbol{H}} = \int_\Omega \mathrm{d}\boldsymbol{x}\ \boldsymbol{a}(\boldsymbol{x},\omega)^*\cdot\boldsymbol{H}(\boldsymbol{x},\omega)\cdot\boldsymbol{b}(\boldsymbol{x},\omega) \tag{A.13}$$

Notice that hermitian symmetry applies on the scalar product $< \boldsymbol{b},\boldsymbol{a} >_{*\boldsymbol{H}}=(< \boldsymbol{a},\boldsymbol{b} >_{*\boldsymbol{H}})^*$. The canonical scalar product are given by defining $\boldsymbol{H}$ as the identity matrix, they express as,

$$< \boldsymbol{a},\boldsymbol{b} > = \int_\Omega \mathrm{d}\boldsymbol{x}\int_{\mathbb{R}}\mathrm{d}t\ \boldsymbol{a}(\boldsymbol{x},t)\cdot\boldsymbol{b}(\boldsymbol{x},t) \quad \text{and} \quad < \boldsymbol{a},\boldsymbol{b} >_* = \int_\Omega \mathrm{d}\boldsymbol{x}\ \boldsymbol{a}(\boldsymbol{x},\omega)^*\cdot\boldsymbol{b}(\boldsymbol{x},\omega) \tag{A.14}$$

In most cases there is no ambiguity whether the real or the hermitian scalar product needs to be considered an the $_*$ in index is omitted for legibility.

A.5 Vector identities for the material derivative

From the chosen Fourier transform conventions, if the material derivative is given in the time domain by $\frac{\mathrm{D}}{\mathrm{D}t}=\left\{\frac{\partial}{\partial t}+\boldsymbol{u}_0\cdot\nabla\right\}$, then the latter writes in the frequency domain as $\mathrm{D}_{\boldsymbol{u}_0}=\{-i\omega+\boldsymbol{u}_0\cdot\nabla\}$, were $\boldsymbol{u}_0$ is the mean velocity. To complete this section, recall following identities which useful to settle the adjoint problem.

$$< \boldsymbol{a},\frac{\mathrm{D}\,\boldsymbol{b}}{\mathrm{D}t} >= - < \frac{\mathrm{D}\,\boldsymbol{a}}{\mathrm{D}t},\boldsymbol{b} > +\nabla\cdot(< \boldsymbol{a},\boldsymbol{b} > \boldsymbol{u}_0) - < \boldsymbol{a},\boldsymbol{b} > (\nabla\cdot\boldsymbol{u}_0) + \Big[< \boldsymbol{a},\boldsymbol{b} >\Big]_{\mathbb{R}} \tag{A.15}$$

$$< \boldsymbol{a}, \mathrm{D}_{\boldsymbol{u}_0}(\boldsymbol{b}) >_* = - < \mathrm{D}_{\boldsymbol{u}_0}(\boldsymbol{a}), \boldsymbol{b} >_* + \nabla \cdot (< \boldsymbol{a}, \boldsymbol{b} >_* \boldsymbol{u}_0) - < \boldsymbol{a}, \boldsymbol{b} >_* (\nabla \cdot \boldsymbol{u}_0) \tag{A.16}$$

Different higher order derivative of the material derivative are given, they identically apply in time or in Fourier domain. The special case in which the flow is parallel, i.e. $\nabla(\boldsymbol{u}/||\boldsymbol{u}||) = \boldsymbol{0}$ simplifies the formulae in some cases and is discussed.

Gradient of the material derivative[1]

$$\begin{aligned} &\forall f \in \mathbb{K}, \forall \boldsymbol{u}_0 \in \mathbb{K}^n, \quad \nabla(D_{\boldsymbol{u}_0}(f)) = D_{\boldsymbol{u}_0}(\nabla f) + (\nabla \boldsymbol{u}_0)^T \nabla f \\ &\text{when } \nabla(\boldsymbol{u}_0/||\boldsymbol{u}_0||) = \boldsymbol{0}, \quad \nabla(D_{\boldsymbol{u}_0}(f)) = D_{\boldsymbol{u}_0}(\nabla f) + \left(\nabla f \cdot \frac{\boldsymbol{u}_0}{||\boldsymbol{u}_0||}\right) \nabla ||\boldsymbol{u}_0|| \end{aligned} \tag{A.17}$$

Divergence of the material derivative [2][3]

$$\begin{aligned} \nabla \cdot \left(D_{\boldsymbol{u}_0}(\boldsymbol{v})\right) &= D_{\boldsymbol{u}_0}(\nabla \cdot \boldsymbol{v}) - (\nabla \times \boldsymbol{u}_0) \cdot (\nabla \times \boldsymbol{v}) + \frac{1}{2}\left[\Delta(\boldsymbol{u}_0 \cdot \boldsymbol{v}) - \boldsymbol{u}_0 \cdot \Delta \boldsymbol{v} - \Delta \boldsymbol{u}_0 \cdot \boldsymbol{v}\right] \\ &= D_{\boldsymbol{u}_0}(\nabla \cdot \boldsymbol{v}) + \mathrm{tr}((\nabla \boldsymbol{u}_0) \cdot (\nabla \boldsymbol{v})) \\ \text{when } \nabla(\boldsymbol{u}_0/||\boldsymbol{u}_0||) = \boldsymbol{0}, \quad \nabla \cdot \left(D_{\boldsymbol{u}_0}(\boldsymbol{v})\right) &= D_{\boldsymbol{u}_0}(\nabla \cdot \boldsymbol{v}) + \left((\nabla \boldsymbol{v}) \frac{\boldsymbol{u}_0}{||\boldsymbol{u}_0||}\right) \cdot \nabla ||\boldsymbol{u}_0|| \end{aligned} \tag{A.18}$$

Curl of the material derivative[4]

$$\nabla \times \left(D_{\boldsymbol{u}_0}(\boldsymbol{v})\right) = D_{\boldsymbol{u}_0}(\nabla \times \boldsymbol{v}) + (\nabla \cdot \boldsymbol{u}_0)(\nabla \times \boldsymbol{v}) - (\nabla \boldsymbol{u}_0) \cdot (\nabla \times \boldsymbol{v}) - \nabla \times \left((\nabla \boldsymbol{u}_0)^T \cdot \boldsymbol{v}\right) \tag{A.19}$$

Laplacien of the material derivative[5]

$$\text{when } \nabla(\boldsymbol{u}_0/||\boldsymbol{u}_0||) = \boldsymbol{0}, \quad \Delta(D_{\boldsymbol{u}}(f)) = D_{\boldsymbol{u}}(\Delta f) + 2\left(\nabla(\nabla f)\frac{\boldsymbol{u}}{||\boldsymbol{u}||}\right) \cdot \nabla ||\boldsymbol{u}|| + \left(\nabla f \cdot \frac{\boldsymbol{u}}{||\boldsymbol{u}||}\right) \Delta ||\boldsymbol{u}|| \tag{A.20}$$

Derivation along the flow direction of the material derivative[6]

$$\text{when } \nabla(\boldsymbol{u}_0/||\boldsymbol{u}_0||) = \boldsymbol{0}, \quad \left(\nabla D_{\boldsymbol{u}_0}(\boldsymbol{v})\right)\frac{\boldsymbol{u}_0}{||\boldsymbol{u}_0||} = D_{\boldsymbol{u}_0}\left((\nabla \boldsymbol{v})\frac{\boldsymbol{u}_0}{||\boldsymbol{u}_0||}\right) + \left(\frac{\boldsymbol{u}_0}{||\boldsymbol{u}_0||} \cdot \nabla ||\boldsymbol{u}_0||\right)(\nabla \boldsymbol{v})\frac{\boldsymbol{u}_0}{||\boldsymbol{u}_0||} \tag{A.21}$$

A.6 Some classical vector identities

In the formulae presented hereafter f, g and h correspond to scalar fields in a space $\mathbb{K}$ ($\mathbb{R}$ or $\mathbb{C}$), $\boldsymbol{u}$, $\boldsymbol{v}$, $\boldsymbol{w}$, $\boldsymbol{x}$ and $\boldsymbol{z}$ are vector fields defined in $\mathbb{K}^n$ where $n \in \mathbb{N}$, $\boldsymbol{T}$ and $\boldsymbol{I}$ are tensor field defined in $\mathbb{K}^{n\times n}$. The tensor

[1] Use of formula (A.63) and of the symmetry property of the Hessian tensor (i.e. $(\nabla\nabla f)^T = \nabla\nabla f$).

[2] Green's vector identity is used: $\forall \boldsymbol{u}, \boldsymbol{v} \in \mathbb{K}^n$, $\nabla \cdot \left[(\boldsymbol{u} \cdot \nabla)\boldsymbol{v}\right] = 1/2\left[\Delta(\boldsymbol{u} \cdot \boldsymbol{v}) + \boldsymbol{u} \cdot \Delta \boldsymbol{v} - \Delta \boldsymbol{u} \cdot \boldsymbol{v}\right] + \nabla \cdot \left[(\nabla \times \boldsymbol{v}) \times \boldsymbol{u}\right]$, the RHS last term needs to be redraft into, $\nabla \cdot \left[(\nabla \times \boldsymbol{v}) \times \boldsymbol{u}\right] = \boldsymbol{u} \cdot (\nabla \times \nabla \times \boldsymbol{v}) - (\nabla \times \boldsymbol{u}) \cdot (\nabla \times \boldsymbol{v}) = \boldsymbol{u} \cdot \nabla(\nabla \cdot \boldsymbol{v}) - \boldsymbol{u} \cdot \Delta \boldsymbol{v} - (\nabla \times \boldsymbol{u}) \cdot (\nabla \times \boldsymbol{v})$, and hence (A.18). The formula involving the trace operator is demonstrated with (A.70).

[3] Starting from $\nabla \cdot (\boldsymbol{u} \cdot \nabla \boldsymbol{v}) = \nabla \cdot ((\nabla \boldsymbol{v})\boldsymbol{u})$, together with the formula (A.41), then $\nabla \cdot (\boldsymbol{u} \cdot \nabla \boldsymbol{v}) = (\nabla \cdot ((\nabla \boldsymbol{v})^T)) \cdot \boldsymbol{u} + \nabla \boldsymbol{v} : \nabla \boldsymbol{u}$. Making use of (A.59) and (locally) decomposing $\boldsymbol{u}$ into its norm and its unitary vector, one obtains, $\nabla \cdot (\boldsymbol{u} \cdot \nabla \boldsymbol{v}) = \boldsymbol{u} \cdot (\nabla(\nabla \cdot \boldsymbol{v})) + ((\nabla \boldsymbol{v})\frac{\boldsymbol{u}}{||\boldsymbol{u}||}) \cdot \nabla ||\boldsymbol{u}||$, and finally the divergence of the material derivative.

[4] Consider $\nabla \times \left((\nabla \boldsymbol{u}) \cdot \boldsymbol{v}\right) = \nabla \times \left(\left[(\nabla \boldsymbol{u}) - (\nabla \boldsymbol{u})^T\right] \cdot \boldsymbol{v}\right) + \nabla \times \left((\nabla \boldsymbol{u})^T \cdot \boldsymbol{v}\right)$ and distribute $\nabla \times \left((\nabla \times \boldsymbol{u}) \times \boldsymbol{v}\right)$.

[5] Successive use of (A.18) and (A.17) is made.

[6] By defining $\boldsymbol{u} = u_z \boldsymbol{z}$, with $\boldsymbol{z} = \frac{\boldsymbol{u}}{||\boldsymbol{u}||}$, one can write, $\nabla\left((\nabla \boldsymbol{v})\boldsymbol{u}\right)\boldsymbol{z} = \boldsymbol{z} \cdot \nabla\left(u_z\{(\nabla \boldsymbol{v})\boldsymbol{z}\}\right)$, equation (A.39) can then be used to recast the formula into $(\boldsymbol{z} \cdot \nabla u_z)(\nabla \boldsymbol{v})\boldsymbol{z} + u_z\left(\nabla\{(\nabla \boldsymbol{v})\boldsymbol{z}\}\boldsymbol{z}\right) = (\boldsymbol{z} \cdot \nabla u_z)(\nabla \boldsymbol{v})\boldsymbol{z} + \boldsymbol{u} \cdot \nabla\{(\nabla \boldsymbol{v})\boldsymbol{z}\}$

product is noted with '$\otimes$' and the double tensor product with ':'. The convention for the latter considered here is $\boldsymbol{T} : \boldsymbol{I} = T^{ji} I_{ij} = T_{ji} I^{ij} = T_i^j I_j^i = T_j^i I_i^j = tr(\boldsymbol{T} \cdot \boldsymbol{I}) = tr(\boldsymbol{I} \cdot \boldsymbol{T}) = tr(\boldsymbol{T}^T \cdot \boldsymbol{I}^T) = tr(\boldsymbol{I}^T \cdot \boldsymbol{T}^T)$. In this work, the following convention is taken $\forall \boldsymbol{u}, \boldsymbol{v} \in \mathbb{K}^n \quad (\boldsymbol{u} \cdot \nabla)\boldsymbol{v} = (\nabla \boldsymbol{v})\boldsymbol{u}$, so that in a bidimensional Cartesian system of coordinate,

$$\nabla \boldsymbol{u} = \left(\frac{\partial u_i}{\partial x_j} \right) = \begin{pmatrix} \dfrac{\partial u_1}{\partial x_1} & \dfrac{\partial u_1}{\partial x_2} \\ \dfrac{\partial u_2}{\partial x_1} & \dfrac{\partial u_2}{\partial x_2} \end{pmatrix} \quad \text{and} \quad \boldsymbol{u} \otimes \boldsymbol{v} = (u_i \, v_j) = \begin{pmatrix} u_1 \, v_1 & u_1 \, v_2 \\ u_2 \, v_1 & u_2 \, v_2 \end{pmatrix} \tag{A.22}$$

The use of vector calculus is widespread in this work, this section is a toolbox of identities gathered from different sources (Bonnet and Luneau, 1989; Plaut, 2017) some are also found in the online encyclopedia *Wikipedia*, from the pages *Vector calculus*[7] and *Green's identities*[8] in particular. Additional useful formulae may be found in the work of Uosukainen (2011).

Mixed scalar product

$$\boldsymbol{u} \cdot (\boldsymbol{v} \times \boldsymbol{w}) = \boldsymbol{w} \cdot (\boldsymbol{u} \times \boldsymbol{v}) = \boldsymbol{v} \cdot (\boldsymbol{w} \times \boldsymbol{u}) \tag{A.23}$$

$$\boldsymbol{u} \times (\boldsymbol{v} \times \boldsymbol{w}) = (\boldsymbol{u} \cdot \boldsymbol{w})\boldsymbol{v} - (\boldsymbol{u} \cdot \boldsymbol{v})\boldsymbol{w} \tag{A.24}$$

Jacobi's identity

$$\boldsymbol{u} \times (\boldsymbol{v} \times \boldsymbol{w}) = (\boldsymbol{u} \times \boldsymbol{v}) \times \boldsymbol{w} + \boldsymbol{v} \times (\boldsymbol{u} \times \boldsymbol{w}) \tag{A.25}$$

$$(\boldsymbol{u} \times \boldsymbol{v}) \cdot (\boldsymbol{w} \times \boldsymbol{x}) = (\boldsymbol{u} \cdot \boldsymbol{w})(\boldsymbol{v} \cdot \boldsymbol{x}) - (\boldsymbol{v} \cdot \boldsymbol{w})(\boldsymbol{u} \cdot \boldsymbol{x}) \tag{A.26}$$

$$(\boldsymbol{u} \cdot (\boldsymbol{v} \times \boldsymbol{w}))\boldsymbol{x} = (\boldsymbol{u} \cdot \boldsymbol{x})(\boldsymbol{v} \times \boldsymbol{w}) + (\boldsymbol{v} \cdot \boldsymbol{x})(\boldsymbol{w} \times \boldsymbol{u}) + (\boldsymbol{w} \cdot \boldsymbol{x})(\boldsymbol{u} \times \boldsymbol{v}) \tag{A.27}$$

$$(\boldsymbol{u} \times \boldsymbol{v}) \times (\boldsymbol{w} \times \boldsymbol{x}) = (\boldsymbol{u} \cdot (\boldsymbol{v} \times \boldsymbol{x}))\boldsymbol{w} - (\boldsymbol{u} \cdot (\boldsymbol{v} \times \boldsymbol{w}))\boldsymbol{x} \tag{A.28}$$

$$(\boldsymbol{u} \otimes \boldsymbol{v}) \cdot \boldsymbol{w} = \boldsymbol{u}(\boldsymbol{v} \cdot \boldsymbol{w}) \tag{A.29}$$

$$(\boldsymbol{u} \otimes \boldsymbol{v})^T = \boldsymbol{v} \otimes \boldsymbol{u} \tag{A.30}$$

$$\boldsymbol{T} : (\boldsymbol{u} \otimes \boldsymbol{v}) = \mathrm{tr}\left(\boldsymbol{T} \cdot (\boldsymbol{u} \otimes \boldsymbol{v})\right) = (\boldsymbol{T} \cdot \boldsymbol{u}) \cdot \boldsymbol{v} \tag{A.31}$$

$$(\boldsymbol{u} \otimes \boldsymbol{v}) \cdot (\boldsymbol{w} \otimes \boldsymbol{x}) = (\boldsymbol{v} \cdot \boldsymbol{w})(\boldsymbol{u} \otimes \boldsymbol{x}) \tag{A.32}$$

$$(\boldsymbol{u} \otimes \boldsymbol{v}) : (\boldsymbol{w} \otimes \boldsymbol{x}) = (\boldsymbol{v} \cdot \boldsymbol{w})(\boldsymbol{u} \cdot \boldsymbol{x}) \tag{A.33}$$

[7] `https://en.wikipedia.org/wiki/Vector_calculus_identities`.
[8] `https://en.wikipedia.org/wiki/Green%27s_identities`.

$$(\boldsymbol{u} \otimes \boldsymbol{v}) \times \boldsymbol{w} = \boldsymbol{u} \otimes (\boldsymbol{v} \times \boldsymbol{w}) \tag{A.34}$$

$$\boldsymbol{w} \times (\boldsymbol{u} \otimes \boldsymbol{v}) = (\boldsymbol{w} \times \boldsymbol{u}) \otimes \boldsymbol{v} \tag{A.35}$$

$$[\boldsymbol{T} \times \boldsymbol{u}]^T = -\left[\boldsymbol{u} \times \boldsymbol{T}^T\right] \tag{A.36}$$

$$\nabla \cdot (\boldsymbol{u} \otimes \boldsymbol{v}) = (\nabla \boldsymbol{u}) \cdot \boldsymbol{v} + \boldsymbol{u}(\nabla \cdot \boldsymbol{v}) \tag{A.37}$$

$$\nabla(f\boldsymbol{v}) = f\nabla\boldsymbol{v} + \boldsymbol{v} \otimes \nabla f \tag{A.38}$$

$$(\boldsymbol{u} \cdot \nabla)(f\boldsymbol{v}) = \boldsymbol{v}(\boldsymbol{u} \cdot \nabla f) + f(\boldsymbol{u} \cdot \nabla)\boldsymbol{v} \tag{A.39}$$

$$\nabla \cdot (f\boldsymbol{T}) = f\nabla \cdot \boldsymbol{T} + \boldsymbol{T} \cdot \nabla f \tag{A.40}$$

$$\nabla \cdot (\boldsymbol{T}\boldsymbol{u}) = \left(\nabla \cdot \left(\boldsymbol{T}^T\right)\right) \cdot \boldsymbol{u} + \operatorname{tr}\left(\boldsymbol{T} \cdot (\nabla \boldsymbol{u})\right) \tag{A.41}$$

$$\nabla \cdot (\nabla f) = \Delta f \tag{A.42}$$

$$\nabla \cdot (\nabla \boldsymbol{u}) = \Delta \boldsymbol{u} \tag{A.43}$$

$$\nabla (\Delta f) = \Delta (\nabla f) \tag{A.44}$$

$$\nabla \cdot (\nabla \times \boldsymbol{u}) = 0 \tag{A.45}$$

$$\nabla \times (\nabla f) = \boldsymbol{0} \tag{A.46}$$

$$\nabla \times (f\boldsymbol{u}) = f\nabla \times \boldsymbol{u} + \nabla f \times \boldsymbol{u} \tag{A.47}$$

$$\nabla \times (\boldsymbol{u} \times \boldsymbol{v}) = (\nabla \boldsymbol{u})\boldsymbol{v} + \boldsymbol{u}(\nabla \cdot \boldsymbol{v}) - (\nabla \boldsymbol{v})\boldsymbol{u} - \boldsymbol{v}(\nabla \cdot \boldsymbol{u}) \tag{A.48}$$

$$\nabla \cdot (\boldsymbol{u} \times \boldsymbol{v}) = (\nabla \times \boldsymbol{u}) \cdot \boldsymbol{v} - (\nabla \times \boldsymbol{v}) \cdot \boldsymbol{u} \tag{A.49}$$

Green's identity (first)

$$\boldsymbol{u} \cdot \nabla f + f\nabla \cdot \boldsymbol{u} = \nabla \cdot (f\boldsymbol{u}) \tag{A.50}$$

Green's identity (second)

$$f\Delta g - g\Delta f = \nabla \cdot (f\nabla g - g\nabla f) \tag{A.51}$$

Green's identity (third)

$$\boldsymbol{u}\cdot\Delta\boldsymbol{v}-\boldsymbol{v}\cdot\Delta\boldsymbol{u}=\nabla\cdot\Big((\nabla\cdot\boldsymbol{v})\boldsymbol{u}+\boldsymbol{u}\times(\nabla\times\boldsymbol{v})-(\nabla\cdot\boldsymbol{u})\boldsymbol{v}-\boldsymbol{v}\times(\nabla\times\boldsymbol{u})\Big) \tag{A.52}$$

Corollary 1

$$\boldsymbol{u}\cdot\Delta\boldsymbol{v}-\boldsymbol{v}\cdot\Delta\boldsymbol{u}=\nabla\cdot\Big((\nabla\boldsymbol{v})\cdot\boldsymbol{u}+\boldsymbol{u}\times(\nabla\times\boldsymbol{v})-(\nabla\boldsymbol{u})\cdot\boldsymbol{v}-\boldsymbol{v}\times(\nabla\times\boldsymbol{u})\Big) \tag{A.53}$$

Corollary 2

$$\nabla\cdot\big[(\nabla\boldsymbol{v})\cdot\boldsymbol{u}-(\nabla\cdot\boldsymbol{v})\boldsymbol{u}\big]=\nabla\cdot\big[(\nabla\boldsymbol{u})\cdot\boldsymbol{v}-(\nabla\cdot\boldsymbol{u})\boldsymbol{v}\big] \tag{A.54}$$

Corollary 3

$$\Delta(\boldsymbol{u}\cdot\boldsymbol{v})=\boldsymbol{u}\cdot\Delta\boldsymbol{v}-\boldsymbol{v}\cdot\Delta\boldsymbol{u}+2\nabla\cdot\Big((\nabla\boldsymbol{u})\cdot\boldsymbol{v}+\boldsymbol{v}\times(\nabla\times\boldsymbol{u})\Big) \tag{A.55}$$

Corollary 4

$$\boldsymbol{u}\cdot\nabla(\nabla\cdot\boldsymbol{v})-\boldsymbol{v}\cdot\nabla(\nabla\cdot\boldsymbol{u})=\nabla\cdot\Big(\boldsymbol{u}(\nabla\cdot\boldsymbol{v})-\boldsymbol{v}(\nabla\cdot\boldsymbol{u})\Big) \tag{A.56}$$

$$(\nabla\boldsymbol{v})\boldsymbol{u}+(\nabla\boldsymbol{u})\boldsymbol{v}=\nabla(\boldsymbol{u}\cdot\boldsymbol{v})+(\nabla\times\boldsymbol{v})\times\boldsymbol{u}+(\nabla\times\boldsymbol{u})\times\boldsymbol{v} \tag{A.57}$$

$$\nabla(\boldsymbol{u}\cdot\boldsymbol{v})=(\nabla\boldsymbol{u})^{T}\cdot\boldsymbol{v}+(\nabla\boldsymbol{v})^{T}\cdot\boldsymbol{u} \tag{A.58}$$

$$\nabla\left(\nabla\cdot\boldsymbol{u}\right)=\nabla\cdot\left((\nabla\boldsymbol{u})^{T}\right) \tag{A.59}$$

$$\Delta(fg)=f\Delta g+2\nabla f\cdot\nabla g+g\Delta f \tag{A.60}$$

$$\Delta(f\boldsymbol{u})=f\Delta\boldsymbol{u}+2(\nabla\boldsymbol{u})\cdot\nabla f+\boldsymbol{u}\Delta f \tag{A.61}$$

$$\Delta\boldsymbol{u}=\nabla(\nabla\cdot\boldsymbol{u})-\nabla\times\nabla\times\boldsymbol{u} \tag{A.62}$$

$$\nabla\left(\boldsymbol{u}\cdot\boldsymbol{v}\right)=(\nabla\boldsymbol{u})^{T}\boldsymbol{v}+(\nabla\boldsymbol{v})^{T}\boldsymbol{u} \tag{A.63}$$

$$\boldsymbol{\nabla}\times\boldsymbol{u}=\nabla\boldsymbol{u}-(\nabla\boldsymbol{u})^{T} \tag{A.64}$$

$$(\boldsymbol{\nabla}\times\boldsymbol{u})\cdot\boldsymbol{v}=(\nabla\times\boldsymbol{u})\times\boldsymbol{v} \tag{A.65}$$

$$\boldsymbol{\nabla}\times(\nabla\boldsymbol{u})=\boldsymbol{0} \tag{A.66}$$

$$\boldsymbol{\nabla}\times(\nabla\boldsymbol{u})^{T}=\nabla(\nabla\times\boldsymbol{u}) \tag{A.67}$$

$$\forall\boldsymbol{z}\in\mathbb{K}^{n},\nabla\boldsymbol{z}=\boldsymbol{0}\quad(\boldsymbol{\nabla}\times\boldsymbol{T})\cdot\boldsymbol{z}=\nabla\times(\boldsymbol{T}^{T}\cdot\boldsymbol{z}) \tag{A.68}$$

A.7 Some original identities involving the trace operator ':'

Starting from the formula,

$$\nabla \cdot (T\boldsymbol{u}) = \Big(\nabla \cdot \big(T^T\big)\Big) \cdot \boldsymbol{u} + T : \nabla \boldsymbol{u}$$

Some alternative writing of the trace operator ':' are proposed. Setting $\boldsymbol{T} = \nabla \boldsymbol{u}$ and making use of $(\nabla \times \boldsymbol{u}) \times \boldsymbol{v} = \left[(\nabla \boldsymbol{u}) - (\nabla \boldsymbol{u})^T\right] \boldsymbol{v}$, it can be shown that, $\nabla \cdot \Big((\nabla \boldsymbol{u})\boldsymbol{v}\Big) = \nabla \cdot \Big((\nabla \times \boldsymbol{u}) \times \boldsymbol{v} + (\nabla \boldsymbol{u})^T \boldsymbol{v}\Big)$. Distributing the divergence in both member of the equality, using $\nabla \cdot (\boldsymbol{u} \times \boldsymbol{v}) = (\nabla \times \boldsymbol{u}) \cdot \boldsymbol{v} - (\nabla \times \boldsymbol{v}) \cdot \boldsymbol{u}$, and the expression involving the trace operator, then

$$\Big(\nabla \cdot \big((\nabla \boldsymbol{u})^T\big)\Big) \cdot \boldsymbol{v} + (\nabla \boldsymbol{u}) : (\nabla \boldsymbol{v}) = (\nabla \times \nabla \times \boldsymbol{u}) \cdot \boldsymbol{v} - (\nabla \times \boldsymbol{u}) \cdot (\nabla \times \boldsymbol{v}) + (\nabla \cdot (\nabla \boldsymbol{u})) \cdot \boldsymbol{v} + (\nabla \boldsymbol{u})^T : (\nabla \boldsymbol{v})$$

Since $\nabla \cdot \big((\nabla \boldsymbol{u})^T\big) = \nabla(\nabla \cdot \boldsymbol{u})$ with the usual relationship $\nabla \times \nabla \times \boldsymbol{u} + \Delta \boldsymbol{u} = \nabla(\nabla \cdot \boldsymbol{u})$, the following formula is shown:

$$\boxed{\left[(\nabla \boldsymbol{u}) - (\nabla \boldsymbol{u})^T\right] : (\nabla \boldsymbol{v}) = -(\nabla \times \boldsymbol{u}) \cdot (\nabla \times \boldsymbol{v})} \tag{A.69}$$

From a corollary of Green's identity, $\boldsymbol{u} \cdot \Delta \boldsymbol{v} - \boldsymbol{v} \cdot \Delta \boldsymbol{u} = \nabla \cdot \Big((\nabla \boldsymbol{v}) \cdot \boldsymbol{u} + \boldsymbol{u} \times (\nabla \times \boldsymbol{v}) - (\nabla \boldsymbol{u}) \cdot \boldsymbol{v} - \boldsymbol{v} \times (\nabla \times \boldsymbol{u})\Big)$ recasting the curl operator with $(\nabla \times \boldsymbol{v}) \times \boldsymbol{u} = \left[(\nabla \boldsymbol{v}) - (\nabla \boldsymbol{v})^T\right] \boldsymbol{u}$, then
$\boldsymbol{u} \cdot \Delta \boldsymbol{v} - \boldsymbol{v} \cdot \Delta \boldsymbol{u} = \nabla \cdot \Big((\nabla \boldsymbol{v})^T \cdot \boldsymbol{u} - (\nabla \boldsymbol{u}) \cdot \boldsymbol{v} - \boldsymbol{v} \times (\nabla \times \boldsymbol{u})\Big)$ Using the same recast of the curl operator, yet reversely, and also $\nabla(\boldsymbol{u} \cdot \boldsymbol{v}) = (\nabla \boldsymbol{u})^T \cdot \boldsymbol{v} + (\nabla \boldsymbol{v})^T \cdot \boldsymbol{u}$, this corollary of Green's identity is obtained,

$$\boldsymbol{u} \cdot \Delta \boldsymbol{v} - \boldsymbol{v} \cdot \Delta \boldsymbol{u} = \nabla \cdot \Big(\nabla(\boldsymbol{u} \cdot \boldsymbol{v}) - 2(\nabla \boldsymbol{u}) \cdot \boldsymbol{v} - 2\boldsymbol{v} \times (\nabla \times \boldsymbol{u})\Big)$$

By distributing the divergence with the formula $\nabla \cdot (\boldsymbol{u} \times \boldsymbol{v}) = (\nabla \times \boldsymbol{u}) \cdot \boldsymbol{v} - (\nabla \times \boldsymbol{v}) \cdot \boldsymbol{u}$ hence,
$\Delta(\boldsymbol{u} \cdot \boldsymbol{v}) = \boldsymbol{u} \cdot \Delta \boldsymbol{v} - \boldsymbol{v} \cdot \Delta \boldsymbol{u} + 2\nabla \cdot \Big((\nabla \boldsymbol{u}) \cdot \boldsymbol{v}\Big) + 2(\nabla \times \boldsymbol{v}) \cdot (\nabla \times \boldsymbol{u}) - 2(\nabla \times \nabla \times \boldsymbol{u}) \cdot \boldsymbol{v}$
From the equality $\nabla \times \nabla \times \boldsymbol{u} + \Delta \boldsymbol{u} = \nabla(\nabla \cdot \boldsymbol{u})$ then,

$$\nabla \cdot \Big((\nabla \boldsymbol{u})\boldsymbol{v}\Big) = \frac{\Delta(\boldsymbol{u} \cdot \boldsymbol{v}) - \boldsymbol{u} \cdot \Delta \boldsymbol{v} - \boldsymbol{v} \cdot \Delta \boldsymbol{u}}{2} - (\nabla \times \boldsymbol{v}) \cdot (\nabla \times \boldsymbol{u}) + (\nabla(\nabla \cdot \boldsymbol{u})) \cdot \boldsymbol{v}$$

After a simple identification with the formula of the divergence involving the trace operator,

$$\boxed{(\nabla \boldsymbol{u}) : (\nabla \boldsymbol{v}) = \frac{\Delta(\boldsymbol{u} \cdot \boldsymbol{v}) - \boldsymbol{u} \cdot \Delta \boldsymbol{v} - \boldsymbol{v} \cdot \Delta \boldsymbol{u}}{2} - (\nabla \times \boldsymbol{v}) \cdot (\nabla \times \boldsymbol{u})} \tag{A.70}$$

Finally from equation (A.69),

$$\boxed{(\nabla \boldsymbol{u})^T : (\nabla \boldsymbol{v}) = \frac{\Delta(\boldsymbol{u} \cdot \boldsymbol{v}) - \boldsymbol{u} \cdot \Delta \boldsymbol{v} - \boldsymbol{v} \cdot \Delta \boldsymbol{u}}{2}} \tag{A.71}$$

B Anti-causality of the adjoint problem

B.1 A toy model to get insight into the adjoint

Summary: The advection equation is investigated with care to understand on this very simple example how adjoint and FRT are related. It is verified that the adjoint is indeed anti-causal and that the generalised reciprocity principle is working. The link between the temporal and frequency domain formulation of adjoint is addressed as well.

B.1.1 Time domain formulation

Computation of the adjoint problem

The Green problem for the advection equation for a source set in $x = \xi$ (xi) at time $t = \tau$ (tau) writes,

$$\left\{ \frac{\partial}{\partial t} + a \frac{\partial}{\partial x} \right\} g_{\xi,\tau}(x,t) = \delta(x-\xi)\delta(t-\tau) \tag{B.1}$$

where a represents the advection speed. For the problem to be well-posed, boundary conditions needs to be settled,

$$\begin{cases} g_{\xi,\tau}(x,-\infty) = 0 \\ g_{\xi,\tau}(-\infty,t) = 0 \end{cases} \tag{B.2}$$

Let the adjoint problem be computed with help of the canonical scalar product $< , >$ for an adjoint source set in $x = \aleph$ ($aleph$) at time $t = \daleth$ ($daleth$). The adjoint Green problem is obtained classically by projection of the adjoint field $g_{\aleph,\daleth}$ on the PDE of the physical problem to form Lagrange's identity (Stone and Goldbart, 2009).

$$< g^{\dagger}_{\aleph,\daleth} \ , \ \left\{ \frac{\partial}{\partial t} + a_0 \frac{\partial}{\partial x} \right\} g_{\xi,\tau} >=< g^{\dagger}_{\aleph,\daleth} \ , \ \delta_\xi \ \delta_\tau > \tag{B.3}$$

The adjoint field is chosen here to be the adjoint Green function, this is to directly recover the reciprocity principle as the derivation will show. By simply detailing previous equation with help of the definition of the scalar product §A.4,

$$\int_{-\infty}^{\infty} dt \int_{-\infty}^{\infty} dx \ g^{\dagger}_{\aleph,\daleth}(x,t) \left\{ \frac{\partial}{\partial t} + a_0 \frac{\partial}{\partial x} \right\} g_{\xi,\tau}(x,t) = \int_{-\infty}^{\infty} dt \int_{-\infty}^{\infty} dx \ g^{\dagger}_{\aleph,\daleth}(x,t) \delta(x-\xi)\delta(t-\tau) \tag{B.4}$$

The right-hand side delivers,

$$\int_{-\infty}^{\infty} dt \int_{-\infty}^{\infty} dx \; g^{\dagger}_{\aleph,\beth}(x,t)\delta(x-\xi)\delta(t-\tau) = g^{\dagger}_{\aleph,\beth}(\xi,\tau) \tag{B.5}$$

The left-hand side can be recast by using integration by parts,

$$\begin{aligned}\int_{-\infty}^{\infty} dt \int_{-\infty}^{\infty} dx \; g^{\dagger}_{\aleph,\beth}(x,t) \left\{ \frac{\partial}{\partial t} + a_0 \frac{\partial}{\partial x} \right\} g_{\xi,\tau}(x,t) = \quad & \int_{-\infty}^{\infty} dt \int_{-\infty}^{\infty} dx \; \left[- \left\{ \frac{\partial}{\partial t} + a_0 \frac{\partial}{\partial x} \right\} g^{\dagger}_{\aleph,\beth}(x,t) \right] g_{\xi,\tau}(x,t) \\ & + \int_{-\infty}^{\infty} dx \; \left[g^{\dagger}_{\aleph,\beth} g_{\xi,\tau} \right]_{t=-\infty}^{t=\infty} \\ & + \int_{-\infty}^{\infty} dt \; \left[a_0 g^{\dagger}_{\aleph,\beth} g_{\xi,\tau} \right]_{x=-\infty}^{x=\infty}\end{aligned} \tag{B.6}$$

The boundary conditions of the adjoint problem are defined so to vanish the contour integral terms of previous expression. Therefore,

$$\left\{ \begin{array}{l} g_{\xi,\tau}(x,-\infty) = 0 \\ g_{\xi,\tau}(-\infty,t) = 0 \end{array} \right. \qquad \Longrightarrow \qquad \left\{ \begin{array}{l} g^{\dagger}_{\aleph,\beth}(x,+\infty) = 0 \\ g^{\dagger}_{\aleph,\beth}(+\infty,t) = 0 \end{array} \right. \tag{B.7}$$

The adjoint PDE to the advection equation is formed by the integrand of the remaining volume integral. It follows that the advection equation is skew-symmetric (skew-self-adjoint),

$$-\left\{ \frac{\partial}{\partial t} + a_0 \frac{\partial}{\partial x} \right\} g^{\dagger}_{\aleph,\beth}(x,t) = \delta(x-\aleph)\delta(t-\beth) \tag{B.8}$$

Finally from Lagrange's identity informed with corresponding Green's functions and appropriate boundary conditions the reciprocity principle is recovered,

$$\boxed{g_{\xi,\tau}(\aleph,\beth) = g^{\dagger}_{\aleph,\beth}(\xi,\tau)} \tag{B.9}$$

Derivation of the analytical solutions

Direct problem

Because the one dimension advection problem is simplistic, its analytical solution can very straightforwardly be obtained by double Fourier transform. The Fourier of the advection equation has readily been computed in § A.2 and writes,

$$\{-i\omega + iak\}\, \hat{G}_{\xi,\tau}(k,\omega) = e^{i(\omega\tau - k\xi)} \tag{B.10}$$

The inverse Fourier transform in time is first considered,

$$\hat{g}_{\xi,\tau}(k,t) = \frac{1}{2\pi} \int_{\mathbb{R}} \hat{G}_{\xi,\tau}(k,\omega) e^{-i\omega t} \, \mathrm{d}\omega = \frac{e^{-ik\xi}}{2i\pi} \int_{\mathbb{R}} \frac{e^{i\omega(\tau-t)}}{-\omega + ak} \, \mathrm{d}\omega \tag{B.11}$$

This integral can be evaluated with help of the residue theorem. For the integral to be well defined when $\tau > t$, the contour needs to be closed in the upper half-plane, while when $t > \tau$ the integration path needs to be defined in the lower half-space. The integrand has a real pole in $\omega = ak$. A priori it is possible to circumvent this singularity by the upper or the lower half-plane. Both possibilities are mathematically correct. The causality of the direct problem resolves this indecision and leads to the following integral

contour drawings.

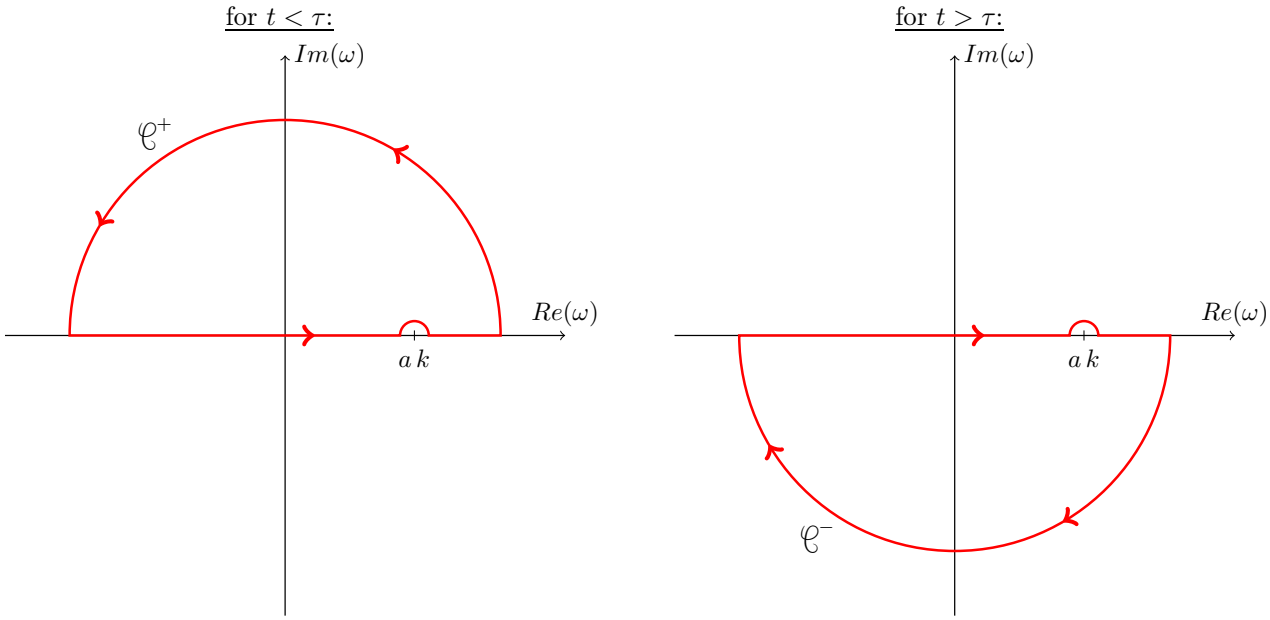

The contours are defined in a way such that $\mathrm{d}\omega$ runs over $\mathbb{R}$ in increasing sense. From Jordan's lemma, it can be shown that the contribution from the outer circle tends to zero when its radius tends to infinite. Since the lace $\mathcal{C}^+$ does not contain any pole, the residue theorem states,

$$\text{for } t < \tau: \qquad \hat{g}_{\xi,\tau}(k,t) = 0 \tag{B.12}$$

The orientation of the lace $\mathcal{C}^-$ is negative and contains one residue. Thus,

$$\int_{\mathcal{C}^-} \frac{e^{i\omega(\tau-t)}}{-\omega + ak}\,\mathrm{d}\omega = \int_{\mathbb{R}} \frac{e^{i\omega(\tau-t)}}{-\omega + ak}\,\mathrm{d}\omega + 0 = -2i\pi Res(ak) \tag{B.13}$$

where, $\quad Res(ak) = \lim_{z\to ak}\left((z-ak)\dfrac{e^{iz(\tau-t)}}{-z+ak}\right) = -e^{iak(\tau-t)} \quad$ which delivers,

$$\text{for } t > \tau: \qquad \hat{g}_{\xi,\tau}(k,t) = e^{-ik\xi}e^{ika(\tau-t)} \tag{B.14}$$

and therefore: $\quad \hat{g}_{\xi,\tau}(k,t) = H(t-\tau)e^{-ik\xi}e^{ika(\tau-t)}$

Considering now the inverse spatial Fourier transform leads to sought answer,

$$g_{\xi,\tau}(x,t) = \frac{1}{2\pi}\int_{\mathbb{R}} \hat{g}_{\xi,\tau}(k,t)e^{ikx}\,\mathrm{d}k = \frac{H(t-\tau)}{2\pi}\int_{\mathbb{R}} e^{ik\left[(x-\xi)-a(t-\tau)\right]}\,\mathrm{d}k \tag{B.15}$$

$$\boxed{g_{\xi,\tau}(x,t) = H(t-\tau)\delta\left((x-\xi)-a_0(t-\tau)\right) = \delta\left(|x-\xi|-a_0(t-\tau)\right)} \tag{B.16}$$

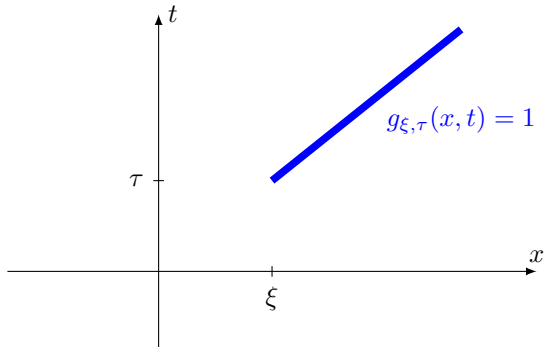

Adjoint problem

The adjoint problem is identical to the direct one apart from the causality condition and sign change. The space-time Fourier transform of the adjoint equation writes

$$\{i\omega - iak\}\,\hat{G}^{\dagger}_{\aleph,\beth}(k,\omega) = e^{i(\omega\beth - k\aleph)} \tag{B.17}$$

Again the inverse Fourier transform in time is first considered,

$$\hat{g^{\dagger}}_{\aleph,\beth}(k,t) = \frac{1}{2\pi}\int_{\mathbb{R}} \hat{G}^{\dagger}_{\aleph,\beth}(k,\omega)e^{-i\omega t}\,\mathrm{d}\omega = \frac{e^{-ik\aleph}}{2i\pi}\int_{\mathbb{R}} \frac{e^{-i\omega(t-\beth)}}{\omega - ak}\,\mathrm{d}\omega \tag{B.18}$$

Again when $\beth > t$, the contour needs to be closed in the upper half-space, whereas when $t > \beth$, the integration path needs to be chosen in lower half-space for the integral to be well defined. Nevertheless this time, to comply with the anti-causality boundary condition, the lace is chosen to pass around the real pole by a downward going integration route. Following contour integral paths follows.

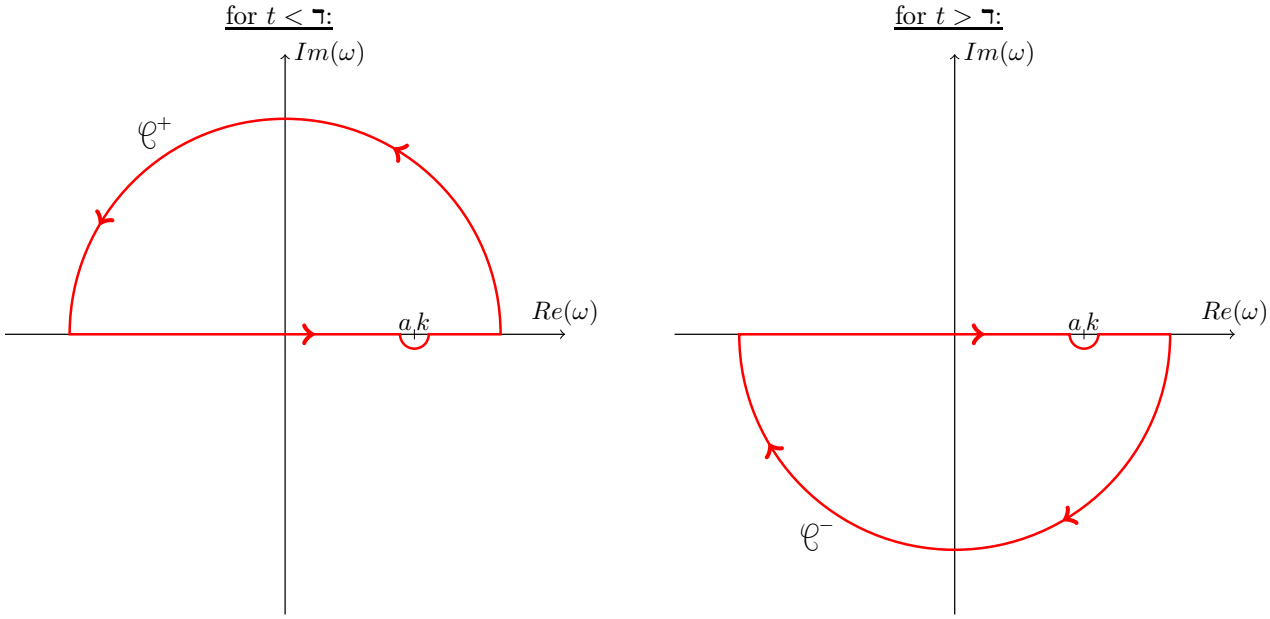

As previously, Jordan's lemma shows that the contribution of the exterior half-circle vanishes when the radius increases. The theorem of residue enable then to calculate the value of the integral along the real axis. The lace $\mathcal{C}^+$ is orientated in positive direction, and

$$\int_{\mathcal{C}^+} \frac{e^{-i\omega(t-\beth)}}{\omega - ak}\,\mathrm{d}\omega = \int_{\mathbb{R}} \frac{e^{-i\omega(t-\beth)}}{\omega - ak}\,\mathrm{d}\omega + 0 = 2i\pi Res(ak) = 2i\pi e^{-iak(t-\beth)} \tag{B.19}$$

therefore,

$$\text{for } t < \beth: \qquad \hat{g}_{\aleph,\beth}(k,t) = e^{-ik\aleph} e^{ika(\beth - t)} \tag{B.20}$$

Since the contour $\mathscr{C}^-$ does not contain any singularity,

$$\text{for } t > \beth: \qquad \hat{g}_{\aleph,\beth}(k,t) = 0 \tag{B.21}$$

Which delivers $\hat{g^\dagger}_{\aleph,\beth}(k,t) = H(\beth - t) e^{-ik\aleph} e^{-iak(t-\beth)}$

By inverse spatial Fourier transform, the expression of $g^\dagger_{\aleph,\beth}$ is readily obtained,

$$g^\dagger_{\aleph,\beth}(x,t) = \frac{1}{2\pi} \int_{\mathbb{R}} \hat{g^\dagger}_{\aleph,\beth}(k,t) e^{ikx} dk = \frac{H(\beth - t)}{2\pi} \int_{\mathbb{R}} e^{ik\left[(x-\aleph) - a_0(t-\beth)\right]} dk \tag{B.22}$$

$$\boxed{g^\dagger_{\aleph,\beth}(x,t) = H(\beth - t)\delta\left((x-\aleph) - a_0(t-\beth)\right) = \delta\left(|x-\aleph| + a_0(t-\beth)\right)} \tag{B.23}$$

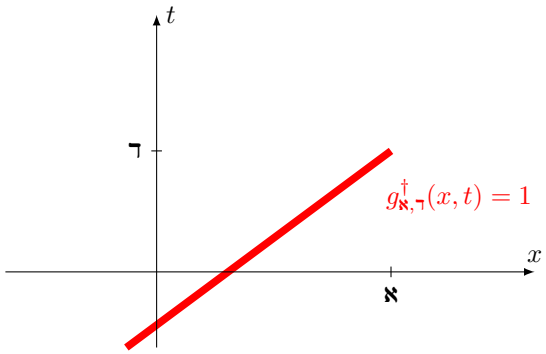

Summary for the time-domain analysis

The adjoint problem to the advection equation is given for the classical scalar product and solved. The adjoint boundary conditions are defined so to cancel the boundary integral appearing in the manipulation of Lagrange's identity. From this procedure, it comes that if the direct problem is causal, its adjoint is necessarily anti-causal. The reciprocity principle is verified from the analytical solutions,

$$g_{\xi,\tau}(\aleph,\beth) = g^\dagger_{\aleph,\beth}(\xi,\tau) \tag{B.24}$$

For the record,the solution for the direct and adjoint advection problem are,

$$\begin{cases} g_{\xi,\tau}(x,t) = \delta\left(|x-\xi| - a_0(t-\tau)\right) \\ \\ g^\dagger_{\aleph,\beth}(x,t) = \delta\left(|x-\aleph| + a_0(t-\beth)\right) \end{cases} \tag{B.25}$$

Notice that no resort to time reversal (see eq. (7.3.3) in Morse and Feshbach, 1953; Eisler, 1969) nor flow reversal (Godin, 1997; Howe, 1975b) was required to achieve the general reciprocity principle. It is easy to observe from the analytical solutions that the Flow Reversal Theorem would however have given the correct answer. Note that the advection equation is skew-symmetric and enters into the enlarged definition of self-adjoint equation as proposed in § 3.2.2. The analysis is performed in the following in the frequency domain.

B.1.2 Frequency domain formulation

The Green problem for the advection equation writes in the frequency domain for a pulsation ω as

$$\left\{-i\omega + a\frac{\partial}{\partial x}\right\} G_\xi(x) = \delta(x-\xi) \tag{B.26}$$

To guarantee the uniqueness of the solution of this PDE, a boundary condition needs to be specified. The causality condition does not apply in the frequency domain, however to be consistent with the problem set in the time domain, following boundary condition is imposed,

$$G_\xi(-\infty) = 0 \tag{B.27}$$

Anew if the Green adjoint problem is considered for an adjoint source set in $x = \aleph$ (*aleph*), the adjoint equations are deduced from Lagrange's identity. The projection of the adjoint Green function on the direct problem PDE is,

$$< G^\dagger_\aleph \ , \ \left\{-i\omega + a\frac{\partial}{\partial x}\right\} G_\xi >_* = < G^\dagger_\aleph \ , \ \delta_\xi \ >_* \tag{B.28}$$

where $<,>_*$ is the hermitian scalar product. The right-hand side delivers $G^{\dagger\,*}_\aleph(\xi)$, while the left-hand side can be recast into,

$$\begin{aligned}\int_{-\infty}^{\infty} G^{\dagger\,*}_\aleph(x) \left\{-i\omega + a\frac{\partial}{\partial x}\right\} G_\xi(x)\,\mathrm{d}x = \quad & \int_{-\infty}^{\infty} \left[-\left\{-i\omega + a\frac{\partial}{\partial x}\right\} G^\dagger_\aleph(x)\right]^* G_\xi(x)\,\mathrm{d}x \\ & + \left[a_0 G^{\dagger\,*}_\aleph G_\xi\right]_{x=-\infty}^{x=\infty}\end{aligned} \tag{B.29}$$

Again, the adjoint boundary condition need to make the contour integral vanish. It follows,

$$G_\xi(-\infty) = 0 \qquad \Longrightarrow \qquad G^\dagger_\aleph(+\infty) = 0 \tag{B.30}$$

The adjoint advection equation is deduced from the remaining volume integrand. And it comes, that in the frequency domain as well, the advection equation is skew-symmetric.

$$-\left\{-i\omega + a\frac{\partial}{\partial x}\right\} G^\dagger_\aleph(x) = \delta(x-\aleph) \tag{B.31}$$

Echoing these definitions in Lagrange's identity, the reciprocity principle in the frequency domain is obtained.

$$\boxed{G_\xi(\aleph) = G^{\dagger\,*}_\aleph(\xi)} \tag{B.32}$$

Derivation of the analytical solutions

Direct problem

The spatial Fourier transform of the direct advection equation is,

$$\{-i\omega + iak\}\,\hat{G}_\xi(k) = e^{-ik\xi} \tag{B.33}$$

The inverse spatial Fourier transform enables the computation of the solution.

$$G_\xi(x) = \frac{1}{2\pi}\int_{\mathbb{R}} \hat{G}_\xi(k) e^{ikx}\,\mathrm{d}k = \frac{1}{2i\pi}\int_{\mathbb{R}} \frac{e^{ik(x-\xi)}}{-\omega + ak}\,\mathrm{d}k \tag{B.34}$$

As previously this integral can be solved with the residue theorem. When $\xi > x$ the integration over k needs to be conducted in the upper half-space, and conversely when $x > \xi$, the integration path needs to be achieved in the lower half-space. For the boundary condition $G_\xi(-\infty) = 0$ to be fulfilled, the real pole $k = \omega/a$ needs to be circumvent from above. Eventually similar integration routes $\mathscr{C}^-$ and $\mathscr{C}^+$ are obtained as for the temporal approach.

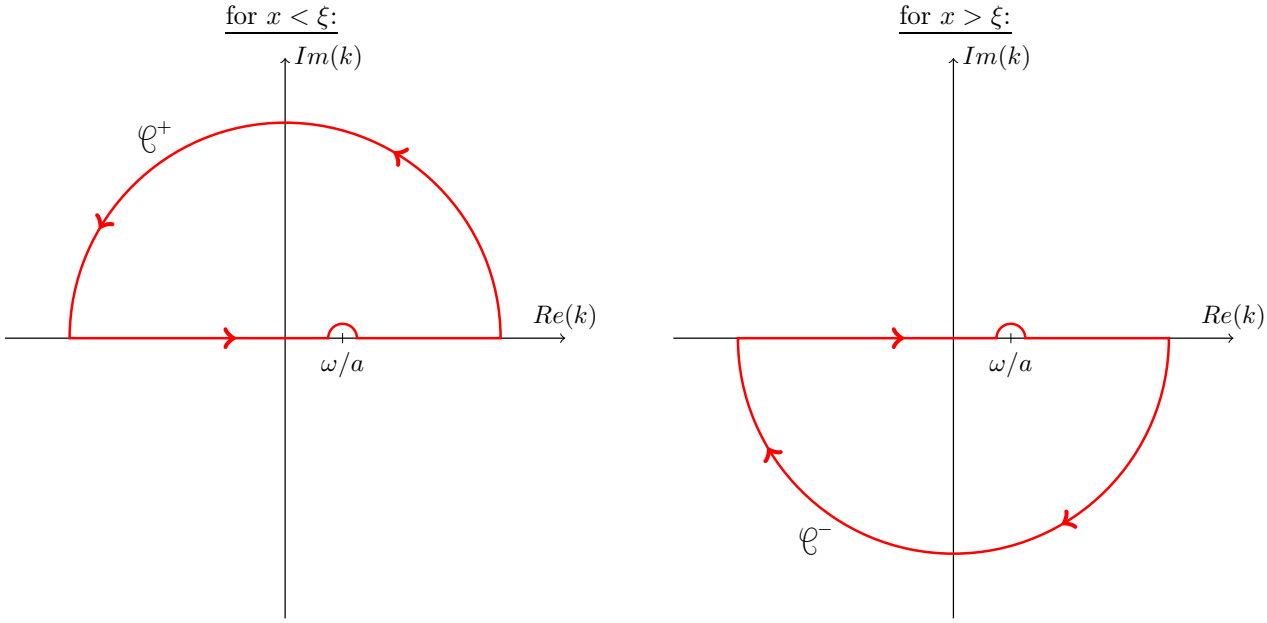

This time also, the residue theorem and Jordan's lemma are used to conclude. Finally,

$$G_\xi(x) = H(x-\xi)\frac{e^{i\omega(x-\xi)/a}}{a} \tag{B.35}$$

Adjoint problem

The computation of the adjoint problem solution is similar to the solving of the direct problem. Yet with the boundary condition $G^\dagger_{\aleph}(+\infty) = 0$, the pole needs to be circumvent from below. After calculations,

$$G^\dagger_{\aleph}(x) = H(\aleph - x)\frac{e^{i\omega(x-\aleph)/a}}{a} \tag{B.36}$$

Summary for the frequency-domain analysis

From this toy example, it is illustrated that adjoint analysis could be achieved as well in the time domain as in the frequency domain. The reciprocity principle in the frequency domain writes,

$$G_\xi(\aleph) = G^{\dagger *}_{\aleph}(\xi) \tag{B.37}$$

The solutions obtained in the frequency domain,

$$\begin{cases} G_\xi(x) = H(x-\xi)\dfrac{e^{i\omega(x-\xi)/a}}{a} \\ \\ G^\dagger_{\aleph}(x) = H(\aleph - x)\dfrac{e^{i\omega(x-\aleph)/a}}{a} \end{cases} \tag{B.38}$$

verify this fundamental relationship. These solutions are moreover consistent with the time-domain solution by recalling that $\delta(ax) = \delta(x)/|a|$.

Care must be taken to the proper definition of a hermitian scalar product. If a non-hermitian scalar product was used, the skew-symmetry behaviour of the advection equation would have been lost. And the conclusion would have been drawn that for the reciprocity to be fulfilled, the sign of the advection speed a should be changed. This is how the flow reversal theorem (FRT) was introduced (Howe, 1975b). In turn, the FRT appears more to be a calculus artefact, than a physically general and meaningful law.

B.2 Anti-causality of adjoint Helmholtz's equation

Summary: The purpose of this section is a reminder that if the direct problem is radiating, its adjoint is not. Illustration for this is given in the frequency domain for the convected Helmholtz's equation. A methodology is proposed moreover to compute the anti-causal solution in the frequency domain by changing the sign of the pulsation in the PDE.

B.2.1 Green's function for the direct problem

Introducing the vectorial Mach number $\boldsymbol{M}_0 = \boldsymbol{u}_0/a_0$, the homogeneous solution F to Helmholtz's equation is defined as

$$\left(-i\omega/a_0 + \boldsymbol{M}_0 \cdot \nabla\right)^2 F(\boldsymbol{x}) - \Delta F(\boldsymbol{x}) = 0 \tag{B.39}$$

If F_1 and F_2 are two independent solutions of the problem, any solution of the homogeneous problem can be expressed in the (F_1,F_2) basis as, $F(\boldsymbol{x}) = A_1\ F_1(\boldsymbol{x}) + A_2\ F_2(\boldsymbol{x})$, where the values of the A_1, A_2 constants are determined from the boundary conditions. One can verify that the following expressions for F_1 and F_2 are independent and are solutions of the homogeneous problem:

$$\begin{cases} F_1(\boldsymbol{x}) = \exp\left(-i\dfrac{\omega}{a_0}\dfrac{\boldsymbol{M}_0\cdot\boldsymbol{x}}{1-M_0^2}\right)\dfrac{\exp\left(i\dfrac{1}{1-M_0^2}\dfrac{\omega}{a_0}\tilde{x}\right)}{4\pi\tilde{x}} \\ \\ F_2(\boldsymbol{x}) = \exp\left(-i\dfrac{\omega}{a_0}\dfrac{\boldsymbol{M}_0\cdot\boldsymbol{x}}{1-M_0^2}\right)\dfrac{\exp\left(-i\dfrac{1}{1-M_0^2}\dfrac{\omega}{a_0}\tilde{x}\right)}{4\pi\tilde{x}} \end{cases} \tag{B.40}$$

where $\tilde{x} = \sqrt{(1-M_0^2)|\boldsymbol{x}|^2 + (\boldsymbol{M}_0\cdot\boldsymbol{x})^2}$. Without flow, the boundary condition of the radiating problem is given by the Sommerfeld conditions. The far-field asymptotic solution to the radiating problem for a uniform mean flow are given by Tam and Webb (1993) in two dimensions, and by Bogey and Bailly (2002) in three dimensions. In the frequency domain, boundary conditions for the three-dimensional uniform

flow case are given by

for $|\boldsymbol{x}| \to \infty$, then $\left\{-i\omega + v_{g,\infty}\left(\frac{\partial}{\partial|\boldsymbol{x}|} + \frac{1}{|\boldsymbol{x}|}\right)\right\} F(\boldsymbol{x}) = O\left(\frac{1}{|\boldsymbol{x}|}\right)$,

with $\frac{v_{g,\infty}}{a_0} = \frac{\tilde{x} + \boldsymbol{M}_0 \cdot \boldsymbol{x}}{|\boldsymbol{x}|}$ From the expression given for F, it can be now deduced that radiating solutions are given by $F \propto F_1$, thus that the F_2 solution to the Helmholtz's equation is not a radiating one. The remaining constant is determined with the forcing term of the problem. It is now possible to define properly the Green function $G_{\boldsymbol{x}_s}$ associated with Helmholtz's radiation problem for a source term in $\boldsymbol{x}_s$ as

$$\begin{cases} \left(-i\omega/a_0 + \boldsymbol{M}_0 \cdot \nabla\right)^2 G_{\boldsymbol{x}_s}(\boldsymbol{x}) - \Delta G_{\boldsymbol{x}_s}(\boldsymbol{x}) = \delta(\boldsymbol{x} - \boldsymbol{x}_s) \\ \text{for } |\boldsymbol{x}| \to \infty, \quad \left\{-i\omega + v_{g,\infty}\left(\frac{\partial}{\partial|\boldsymbol{x}|} + \frac{1}{|\boldsymbol{x}|}\right)\right\} G_{\boldsymbol{x}_s}(\boldsymbol{x}) = O\left(\frac{1}{|\boldsymbol{x}|}\right) \end{cases} \tag{B.41}$$

for which the solution is uniquely defined as

$$G_{\boldsymbol{x}_s}(\boldsymbol{x}) = \exp\left(-i\frac{\omega}{a_0}\frac{\boldsymbol{M}_0 \cdot (\boldsymbol{x} - \boldsymbol{x}_s)}{1 - M_0^2}\right) \frac{\exp\left(i\frac{1}{1 - M_0^2}\frac{\omega}{a_0} r_{\boldsymbol{x}_s}\right)}{4\pi r_{\boldsymbol{x}_s}} \tag{B.42}$$

where $r_{\boldsymbol{x}_s} = \sqrt{(1 - M_0^2)|\boldsymbol{x} - \boldsymbol{x}_s|^2 + (\boldsymbol{M}_0 \cdot (\boldsymbol{x} - \boldsymbol{x}_s))^2}$. It is interesting to note that for the impulse problem, the far-field boundary conditions are more than just an asymptotic solution. In the impulse problem, since the source term is infinitely small, boundaries are always far from the source and the above given far-field solution is everywhere exact for the Green problem, so that the second-order radiating Helmholtz's problem is equivalent to the following first-order problem:

$$\left\{-i\omega + v_g\left(\frac{\partial}{\partial|\boldsymbol{x} - \boldsymbol{x}_s|} + \frac{1}{|\boldsymbol{x} - \boldsymbol{x}_s|}\right)\right\} G_{\boldsymbol{x}_s}(\boldsymbol{x}) = 0, \text{ with } \frac{v_g}{a_0} = \frac{r_{\boldsymbol{x}_s} + \boldsymbol{M}_0 \cdot (\boldsymbol{x} - \boldsymbol{x}_s)}{|\boldsymbol{x} - \boldsymbol{x}_s|}$$

B.2.2 Green's function for the adjoint problem

It is well known that Helmholtz's operator is formally self-adjoint, but that the radiation problem governed by Helmholtz's equation is not, due to non-symmetries of the boundary conditions. Thus, the solution of the adjoint problem is different from the one of the direct problem. This complies with the reciprocity principle for complex valued scalar functions which can be deduced from Lagrange's identity (Alonso and Burdisso, 2007, eq. (48)) (Stone and Goldbart, 2009, § 5.3.1):

$$G_{\boldsymbol{x}_s}(\boldsymbol{x}_m) = {G^\dagger}^*_{\boldsymbol{x}_m}(\boldsymbol{x}_s) \tag{B.43}$$

The adjoint solution to the considered problem can be deduced from this previous fundamental relation,

$$G^\dagger_{\boldsymbol{x}_m}(\boldsymbol{x}) = \exp\left(-i\frac{\omega}{a_0}\frac{\boldsymbol{M}_0 \cdot (\boldsymbol{x} - \boldsymbol{x}_m)}{1 - M_0^2}\right) \frac{\exp\left(-i\frac{1}{1 - M_0^2}\frac{\omega}{a_0} r_{\boldsymbol{x}_m}\right)}{4\pi r_{\boldsymbol{x}_m}} \tag{B.44}$$

where $r_{\boldsymbol{x}_m} = \sqrt{(1 - M_0^2)|\boldsymbol{x} - \boldsymbol{x}_m|^2 + (\boldsymbol{M}_0 \cdot (\boldsymbol{x} - \boldsymbol{x}_m))^2}$. In turns out that the adjoint solution corresponds to the F_2 solution of the homogeneous convected equation studied above. One can verify that this solution has indeed a non-radiating behaviour in the far-field. From the solution to the direct problem and

adjoint problem, the classical out-going (causal) and in-going (anti-causal) waves solution of Helmholtz's equation without flow can be retrieved:

$$G_{\boldsymbol{x}_s}(\boldsymbol{x}) = \frac{\exp\left(i\frac{\omega}{a_0}|\boldsymbol{x}-\boldsymbol{x}_s|\right)}{4\pi|\boldsymbol{x}-\boldsymbol{x}_s|} \quad , \quad G^{\dagger}_{\boldsymbol{x}_m}(\boldsymbol{x}) = \frac{\exp\left(-i\frac{\omega}{a_0}|\boldsymbol{x}-\boldsymbol{x}_m|\right)}{4\pi|\boldsymbol{x}-\boldsymbol{x}_m|} \tag{B.45}$$

where the causal and anti-causal behaviour of the solution is more easily seen.

B.2.3 Recovering the anti-causal adjoint solution

From the Green function of the direct problem, it can be seen that the solution is invariant under source−observer position exchange and flow direction reversal. This is an example where the FRT could be used. In this study the symmetry of the problem with respect to time is used to simplify the numerical implementation. Unlike symmetries from space on which the FRT relies, the time symmetry of the operator cannot be violated. Indeed for real-valued signals $p(t)$, their Fourier transform always verify $p(\omega) = p^*(-\omega)$. Applying this rule to the reciprocity principle yields

$$G^{\dagger}_{\boldsymbol{x}_s}(\boldsymbol{x}_m, \omega) = {G^{\dagger}}^{*}_{\boldsymbol{x}_s}(\boldsymbol{x}_m, -\omega) \tag{B.46}$$

As can be inferred for the case of previously treated convected Helmholtz's equation, solving the non-radiating adjoint equation for positive pulsation ω or solving the radiating problem, that is complex conjugated to the latter, for negative pulsation $-\omega$ are equivalent. The generality of this property is assumed. Instead of developing and coding anti-radiation numerical boundary conditions, standard PML conditions are used. The anti-causality of the adjoint field is accounted for by changing the sign of the pulsation ω in the adjoint linear operator $\mathcal{L}_0^{\dagger}$. The capability of the adjoint method, using this numerical trick, to recover the direct field serves as a verification for the latter assumption.

C Derivation of the wave equations

C.1 Linearised Euler's wave equation (LEWE)

Calculations to obtain the LEWE are presented, these derivations refer to §2.2 of part I of this script. In what follows, the primes are omitted in superscript of the fluctuating quantities. The linearisation could be achieved directly from Euler's wave equation, but it is found easier to cast anew a wave equation for the fluctuating velocity $\boldsymbol{u}$. This equation is referred to as the linearised Euler's wave equation (LEWE). The linearisation considered is performed over an unsteady base flow that obeys,

$$\begin{cases} \mathrm{D}_{\boldsymbol{u}_0}(\rho_0) + \rho_0(\nabla\cdot\boldsymbol{u}_0) = 0 & (a_0) \\ \rho_0\mathrm{D}_{\boldsymbol{u}_0}(\boldsymbol{u}_0) + \nabla p_0 = \boldsymbol{0} & (b_0) \\ \mathrm{D}_{\boldsymbol{u}_0}(p_0) + \gamma p_0(\nabla\cdot\boldsymbol{u}_0) = 0 & (c_0) \end{cases} \tag{C.1}$$

The material derivative along the base flow is introduced, $\mathrm{D}_{\boldsymbol{u}_0} = \partial/\partial t + \boldsymbol{u}_0\cdot\nabla$. The linearised Euler's equations are recalled hereafter for some generic source term $(S_\rho, \boldsymbol{S}_{\boldsymbol{u}}, S_p)$ as,

$$\begin{cases} \mathrm{D}_{\boldsymbol{u}_0}(\rho) + \nabla\cdot(\rho_0\boldsymbol{u}) + (\nabla\cdot\boldsymbol{u}_0)\rho = S_\rho & (a_1) \\ \mathrm{D}_{\boldsymbol{u}_0}(\boldsymbol{u}) + (\nabla\boldsymbol{u}_0)\cdot\boldsymbol{u} + \dfrac{\nabla p}{\rho_0} - \dfrac{\nabla p_0}{\rho_0^2}\rho = \boldsymbol{S}_{\boldsymbol{u}} & (b_1) \\ \mathrm{D}_{\boldsymbol{u}_0}(p) + \nabla p_0\cdot\boldsymbol{u} + \gamma p_0(\nabla\cdot\boldsymbol{u}) + \gamma(\nabla\cdot\boldsymbol{u}_0)p = S_p & (c_1) \end{cases} \tag{C.2}$$

The expression of LEWE is obtained by combining $(b1)$ and $(c1)$ as $\mathrm{D}_{\boldsymbol{u}_0}(b1) + (\nabla\boldsymbol{u}_0)^T\cdot(b1) - \dfrac{\nabla(c1)}{\rho_0}$. Let f be scalar, $\boldsymbol{u}$ and $\boldsymbol{v}$ be vectors, the following two vector identities are particularly useful for the derivations:

$$\begin{aligned} &\nabla(f\boldsymbol{v})\cdot\boldsymbol{w} = (\nabla f\cdot\boldsymbol{w})\boldsymbol{v} + f(\nabla\boldsymbol{v})\cdot\boldsymbol{w} && (d) \\ &\nabla(\boldsymbol{v}\cdot\boldsymbol{w}) = (\nabla\boldsymbol{v})^T\cdot\boldsymbol{w} + (\nabla\boldsymbol{w})^T\cdot\boldsymbol{v} && (e) \end{aligned} \tag{C.3}$$

where following convention $(\nabla\boldsymbol{w})\cdot\boldsymbol{v} = (\boldsymbol{v}\cdot\nabla)\boldsymbol{w}$ is adopted. Based on the below intermediate steps, from equation (C.4) to equation (C.8), the derivation of LEWE is fairly straightforward. From (d) and (a_0),

$$\mathrm{D}_{\boldsymbol{u}_0}\left(\frac{\nabla p}{\rho_0}\right) = \frac{\mathrm{D}_{\boldsymbol{u}_0}(\nabla p)}{\rho_0} + (\nabla\cdot\boldsymbol{u}_0)\frac{\nabla p}{\rho_0} \tag{C.4}$$

From (d), (e) and using (a_0) and (c_0),

$$\mathrm{D}_{\boldsymbol{u}_0}\left(\frac{\nabla p_0}{\rho_0^2}\rho\right) = \frac{\nabla p_0}{\rho_0^2}\mathrm{D}_{\boldsymbol{u}_0}(\rho) - (\nabla \boldsymbol{u}_0)^T \cdot \frac{\nabla p_0}{\rho_0^2}\rho - \frac{a_0^2}{\rho_0}\nabla(\nabla\cdot\boldsymbol{u}_0)\rho + (2-\gamma)(\nabla\cdot\boldsymbol{u}_0)\frac{\nabla p_0}{\rho_0^2}\rho \tag{C.5}$$

And directly from (e):

$$\nabla\left(\mathrm{D}_{\boldsymbol{u}_0}(p)\right) = \mathrm{D}_{\boldsymbol{u}_0}(\nabla p) + (\nabla \boldsymbol{u}_0)^T \cdot \nabla p \tag{C.6}$$

Based on previous calculations $\mathrm{D}_{\boldsymbol{u}_0}(b1)$ writes:

$$\begin{aligned} &D^2_{\boldsymbol{u}_0}(\boldsymbol{u}) + \mathrm{D}_{\boldsymbol{u}_0}((\nabla\boldsymbol{u}_0)\cdot\boldsymbol{u}) + \frac{\mathrm{D}_{\boldsymbol{u}_0}(\nabla p)}{\rho_0} + \frac{\nabla p}{\rho_0}(\nabla\cdot\boldsymbol{u}_0) - \frac{\nabla p_0}{\rho_0^2}\mathrm{D}_{\boldsymbol{u}_0}(\rho) + \frac{a_0^2}{\rho_0}\nabla(\nabla\cdot\boldsymbol{u}_0)\rho \\ &+(\gamma-2)(\nabla\cdot\boldsymbol{u}_0)\frac{\nabla p_0}{\rho_0^2}\rho + (\nabla\boldsymbol{u}_0)^T\cdot\frac{\nabla p_0}{\rho_0^2}\rho = \mathrm{D}_{\boldsymbol{u}_0}(\boldsymbol{S_u}) \end{aligned} \tag{C.7}$$

Whereas $(\nabla\boldsymbol{u}_0)^T\cdot(b_1) - \dfrac{\nabla(c_1)}{\rho_0}$ derives as:

$$\begin{aligned} &(\nabla\boldsymbol{u}_0)^T\cdot\mathrm{D}_{\boldsymbol{u}_0}(\boldsymbol{u}) + (\nabla\boldsymbol{u}_0)^T\cdot(\nabla\boldsymbol{u}_0)\cdot\boldsymbol{u} - (\nabla\boldsymbol{u}_0)^T\cdot\frac{\nabla p_0}{\rho_0^2}\rho - \frac{\mathrm{D}_{\boldsymbol{u}_0}(\nabla p)}{\rho_0} - (\nabla\nabla p_0)\cdot\frac{\boldsymbol{u}}{\rho_0} \\ &-(\nabla\boldsymbol{u})^T\cdot\frac{\nabla p_0}{\rho_0} - \gamma\frac{\nabla p_0}{\rho_0}(\nabla\cdot\boldsymbol{u}) - a_0^2\nabla(\nabla\cdot\boldsymbol{u}) - \gamma(\nabla\cdot\boldsymbol{u}_0)\frac{\nabla p}{\rho_0} - \gamma\frac{\nabla(\nabla\cdot\boldsymbol{u}_0)}{\rho_0}p \\ &= (\nabla\boldsymbol{u}_0)^T\cdot\boldsymbol{S_u} - \frac{\nabla S_p}{\rho_0} \end{aligned} \tag{C.8}$$

Using (a_1) , (d) and (e) are used to reformulate the terms depending on ∇p_0, following exact reformulation of the LEE can be obtained:

$$\begin{aligned} &D^2_{\boldsymbol{u}_0}(\boldsymbol{u}) + \mathrm{D}_{\boldsymbol{u}_0}((\nabla\boldsymbol{u}_0)\cdot\boldsymbol{u}) + (\nabla\boldsymbol{u}_0)^T\cdot\mathrm{D}_{\boldsymbol{u}_0}(\boldsymbol{u}) + (\nabla\boldsymbol{u}_0)^T\cdot(\nabla\boldsymbol{u}_0)\cdot\boldsymbol{u} - a_0^2\nabla(\nabla\cdot\boldsymbol{u}) \\ &+(1-\gamma)\frac{\nabla p_0}{\rho_0}(\nabla\cdot\boldsymbol{u}) + \frac{\nabla p_0}{\rho_0^2}(\nabla\rho_0\cdot\boldsymbol{u}) - \nabla\nabla p_0\cdot\frac{\boldsymbol{u}}{\rho_0} - (\nabla\boldsymbol{u})^T\cdot\frac{\nabla p_0}{\rho_0} \\ &-\gamma\frac{\nabla(\nabla\cdot\boldsymbol{u}_0)}{\rho_0}p + \frac{a_0^2}{\rho_0}\nabla(\nabla\cdot\boldsymbol{u}_0)\rho + (1-\gamma)(\nabla\cdot\boldsymbol{u}_0)\left[\frac{\nabla p}{\rho_0} - \frac{\nabla p_0}{\rho_0^2}\rho\right] \\ &= \mathrm{D}_{\boldsymbol{u}_0}(\boldsymbol{S_u}) + (\nabla\boldsymbol{u}_0)^T\cdot\boldsymbol{S_u} - \frac{\nabla S_p}{\rho_0} + \frac{\nabla p_0}{\rho_0^2}S_\rho \end{aligned} \tag{C.9}$$

The expression involving ∇p are recast with (b_1), while (b_0) enables to reformulate the $\nabla p_0/\rho_0$ terms. Finally, the bellow reformulation of the LEE is obtained:

$$\boxed{\begin{aligned} &D^2_{\boldsymbol{u}_0}(\boldsymbol{u}) + \mathrm{D}_{\boldsymbol{u}_0}((\nabla\boldsymbol{u}_0)\cdot\boldsymbol{u}) + (\nabla\boldsymbol{u}_0)^T\cdot\mathrm{D}_{\boldsymbol{u}_0}(\boldsymbol{u}) + (\nabla\boldsymbol{u}_0)^T\cdot(\nabla\boldsymbol{u}_0)\cdot\boldsymbol{u} - a_0^2\nabla(\nabla\cdot\boldsymbol{u}) \\ &+(\gamma-1)\mathrm{D}_{\boldsymbol{u}_0}(\boldsymbol{u}_0)(\nabla\cdot\boldsymbol{u}) + \nabla\left(\mathrm{D}_{\boldsymbol{u}_0}(\boldsymbol{u}_0)\right)\cdot\boldsymbol{u} + (\nabla\boldsymbol{u})^T\cdot\mathrm{D}_{\boldsymbol{u}_0}(\boldsymbol{u}_0) \\ &+(\gamma-1)(\nabla\cdot\boldsymbol{u}_0)\left[\mathrm{D}_{\boldsymbol{u}_0}(\boldsymbol{u}) + (\nabla\boldsymbol{u}_0)\cdot\boldsymbol{u}\right] + a_0^2\nabla(\nabla\cdot\boldsymbol{u}_0)\left[\frac{\rho}{\rho_0} - \frac{p}{p_0}\right] \\ &= \mathrm{D}_{\boldsymbol{u}_0}(\boldsymbol{S_u}) + (\nabla\boldsymbol{u}_0)^T\cdot\boldsymbol{S_u} + (\gamma-1)(\nabla\cdot\boldsymbol{u}_0)\boldsymbol{S_u} - \frac{\nabla S_p}{\rho_0} - \frac{\mathrm{D}_{\boldsymbol{u}_0}(\boldsymbol{u}_0)}{\rho_0}S_\rho \end{aligned}} \tag{C.10}$$

This equation is very general and apart from the term $\left(\rho/\rho_0 - p/p_0\right)$ is function of the fluctuating velocity

$\boldsymbol{u}$ only. In fact, this term corresponds to fluctuations of the speed of sound a, since,

$$a^2 = \frac{\gamma p}{\rho_0} - \frac{\gamma p_0 \rho}{\rho_0^2} = a_0^2 \left(\frac{p}{p_0} - \frac{\rho}{\rho_0} \right) \tag{C.11}$$

For a parallel base flow, LEWE conveniently simplifies into,

$$\boxed{\begin{aligned} &D^2_{\boldsymbol{u}_0}(\boldsymbol{u}) + \left[(\nabla \boldsymbol{u}_0) + (\nabla \boldsymbol{u}_0)^T \right] \cdot \mathrm{D}_{\boldsymbol{u}_0}(\boldsymbol{u}) + (\nabla \boldsymbol{u}_0)^T \cdot (\nabla \boldsymbol{u}_0) \cdot \boldsymbol{u} - a_0^2 \nabla(\nabla \cdot \boldsymbol{u}) \\ &= \mathrm{D}_{\boldsymbol{u}_0}(\boldsymbol{S_u}) + (\nabla \boldsymbol{u}_0)^T \cdot \boldsymbol{S_u} - \frac{\nabla S_p}{\rho_0} \end{aligned}} \tag{C.12}$$

C.2 Linearised Euler's wave equation for the acoustic potential (LEWE-AP)

LEWE-AP is the the acoustic potential rewriting of LEWE. It is derived for an arbitrary parallel mean flow. For such a specific mean flow some remarkable simplifications will be first given by noting following tensor calculus formula,

$$\begin{aligned} &\nabla(f\boldsymbol{v}) = f \nabla \boldsymbol{v} + \boldsymbol{v} \otimes \nabla f && (f) \\ &(\boldsymbol{a} \otimes \boldsymbol{b})^T = \boldsymbol{b} \otimes \boldsymbol{a} && (g) \end{aligned} \tag{C.13}$$

where by definition of the tensor product $(\boldsymbol{a} \otimes \boldsymbol{b}) \cdot \boldsymbol{x} = \boldsymbol{a}\,(\boldsymbol{b} \cdot \boldsymbol{x})$. Let $\boldsymbol{u}_0 = u_{0,z}\boldsymbol{z}$ be the mean velocity field, where $\boldsymbol{z}$ is a fixed unit vector in the flow direction. Using (f) and (g), then for a parallel mean flow:

$$\begin{cases} (\nabla \boldsymbol{u}_0)^T \cdot \boldsymbol{v} = (\boldsymbol{v} \cdot \boldsymbol{z}) \nabla u_{0,z} \\ (\nabla \boldsymbol{u}_0) \cdot \boldsymbol{v} = (\boldsymbol{v} \cdot \nabla u_{0,z}) \boldsymbol{z} \end{cases} \tag{C.14}$$

And thus for any $\boldsymbol{v}$:

$$\begin{cases} (\nabla \boldsymbol{u}_0)^T \cdot (\nabla \boldsymbol{u}_0)^T \cdot \boldsymbol{v} = \boldsymbol{0} \\ (\nabla \boldsymbol{u}_0) \cdot (\nabla \boldsymbol{u}_0) \cdot \boldsymbol{v} = \boldsymbol{0} \end{cases} \tag{C.15}$$

Based on this observation, it is easy to show that $(\nabla \boldsymbol{u}_0)$ commutes with the material derivative $D_{\boldsymbol{u}_0}$. Moreover for parallel mean flows (a_0) implies $(\boldsymbol{u}_0 \cdot \nabla \rho_0 = 0)$, and (d) proves that ρ_0 also commutes with $D_{\boldsymbol{u}_0}$. Thus LEWE's expression for parallel mean flows, multiplied by ρ_0 is:

$$D^2_{\boldsymbol{u}_0}(\rho_0 \boldsymbol{u}) + \left[(\nabla \boldsymbol{u}_0) + (\nabla \boldsymbol{u}_0)^T \right] \cdot D_{\boldsymbol{u}_0}(\rho_0 \boldsymbol{u}) + (\nabla \boldsymbol{u}_0)^T \cdot (\nabla \boldsymbol{u}_0) \cdot (\rho_0 \boldsymbol{u}) - \gamma p_0 \nabla(\nabla \cdot \boldsymbol{u}) = \boldsymbol{0} \tag{C.16}$$

The acoustic propagation is sought as the solution of a potential scalar field ϕ defined as $\nabla \phi = \rho_0 \boldsymbol{u}$, and LEWE-AP expresses for an arbitrary parallel mean flow as,

$$D^2_{\boldsymbol{u}_0}(\nabla \phi) + \left[(\nabla \boldsymbol{u}_0) + (\nabla \boldsymbol{u}_0)^T \right] \cdot D_{\boldsymbol{u}_0}(\nabla \phi) + (\nabla \boldsymbol{u}_0)^T \cdot (\nabla \boldsymbol{u}_0) \cdot \nabla \phi - \gamma p_0 \nabla \left(\nabla \cdot \left(\frac{\nabla \phi}{\rho_0} \right) \right) = \boldsymbol{0} \tag{C.17}$$

Hereafter equations (C.18) to (C.21) are intermediate results, that are helpful to reformulate in a handy way LEWE-AP. Firstly, the gradient of the material derivative of a scalar f can be computed from (e),

using the symmetry property of the Hessian:

$$\nabla\left(D_{\boldsymbol{u}_0}(f)\right) = D_{\boldsymbol{u}_0}(\nabla f) + (\nabla \boldsymbol{u}_0)^T \cdot \nabla f \tag{C.18}$$

And,

$$D^2_{\boldsymbol{u}_0}(\nabla f) = \nabla\left(D^2_{\boldsymbol{u}_0}(f)\right) - 2(\nabla \boldsymbol{u}_0)^T \cdot \nabla\left(D_{\boldsymbol{u}_0}(f)\right) + \underbrace{(\nabla \boldsymbol{u}_0)^T \cdot (\nabla \boldsymbol{u}_0)^T \cdot \nabla f}_{=\mathbf{0}} \tag{C.19}$$

Similarly,

$$\begin{aligned}\left[(\nabla \boldsymbol{u}_0) + (\nabla \boldsymbol{u}_0)^T\right] \cdot D_{\boldsymbol{u}_0}(\nabla f) = \quad & \left[(\nabla \boldsymbol{u}_0) + (\nabla \boldsymbol{u}_0)^T\right] \cdot \nabla\left(D_{\boldsymbol{u}_0}(f)\right) - (\nabla \boldsymbol{u}_0) \cdot (\nabla \boldsymbol{u}_0)^T \cdot \nabla f \\ & - \underbrace{(\nabla \boldsymbol{u}_0)^T \cdot (\nabla \boldsymbol{u}_0)^T \cdot \nabla f}_{=\mathbf{0}}\end{aligned} \tag{C.20}$$

Using below vector calculus formulas,

$$(\nabla \times \boldsymbol{u}) \times \boldsymbol{v} = \left[(\nabla \boldsymbol{u}) - (\nabla \boldsymbol{u})^T\right] \cdot \boldsymbol{v} \qquad (h) \tag{C.21}$$

LEWE-AP can be written without more assumptions in following attractive form,

$$\boxed{\nabla\left[D^2_{\boldsymbol{u}_0}(\phi) - \nabla \cdot \left(a_0^2 \nabla \phi\right)\right] + (\nabla \times \boldsymbol{u}_0) \times \left[\nabla\left(D_{\boldsymbol{u}_0}(\phi)\right) - \left[(\nabla \boldsymbol{u}_0) + (\nabla \boldsymbol{u}_0)^T\right] \cdot \nabla \phi\right] = \mathbf{0}} \tag{C.22}$$

LEWE-AP is given in its homogeneous form, the corresponding source term is the same as for LEWE but multiplied by ρ_0.

C.3 Compressible generalisation of Pierce's equation

In §2.5 of part I, Pierce's wave equation is derived for a steady and parallel base flow. In the present section, a compressible generalisation of this wave equation is proposed, it is obtained from a change of variable of Blokhintzev's wave equation. Euler's momentum equation in Crocco's form serves as a starting point for this discussion,

$$\frac{\partial \boldsymbol{u}}{\partial t} + \frac{\nabla(\boldsymbol{u} \cdot \boldsymbol{u})}{2} + (\nabla \times \boldsymbol{u}) \times \boldsymbol{u} + \frac{\nabla p}{\rho} = 0 \tag{C.23}$$

The flow is then supposed homentropic and potential, and Gibbs' relation furnishes,

$$\rho\, \delta h = a^2 \delta \rho = \delta p \tag{C.24}$$

where h is the flow enthalpy and expresses for a perfect gas as, $h = a^2/(\gamma - 1)$ with γ the ratio of specific heats. Following Yates (1978), Euler's equation can then be recast in,

$$\begin{cases} \dfrac{\partial \boldsymbol{u}}{\partial t} + \dfrac{\nabla(\boldsymbol{u} \cdot \boldsymbol{u})}{2} + \nabla h = \mathbf{0} \\ \dfrac{\mathrm{D}h}{\mathrm{D}t} + a^2 \nabla \cdot \boldsymbol{u} = 0 \end{cases} \tag{C.25}$$

with $\mathrm{D}/\mathrm{D}t = \partial/\partial t + \boldsymbol{u} \cdot \nabla$ is the material derivative. A linearisation is then performed following a simple Reynolds decomposition of the flow, and $\boldsymbol{u} = \boldsymbol{u}_0 + \boldsymbol{u'}$ and $h = h_0 + h'$. The fluctuations are assumed

potential and Blokhintzev's acoustic potential ψ is introduced, such as $\boldsymbol{u'} = \nabla\psi$. The base flow is steady and is solution of the problem,

$$\begin{cases} \nabla(\boldsymbol{u}_0 \cdot \boldsymbol{u}_0) + 2\nabla h_0 = \boldsymbol{0} \\ \\ \boldsymbol{u}_0 \cdot \nabla h_0 + a^2 \nabla \cdot \boldsymbol{u}_0 = 0 \end{cases} \tag{C.26}$$

As for the first order fluctuations, they are given by

$$\begin{cases} \mathrm{D}_{\boldsymbol{u}_0}(\psi) + h' = 0 \\ \\ \mathrm{D}_{\boldsymbol{u}_0}(h') + \nabla h_0 \cdot \nabla\psi + a_0^2 \Delta\psi + (\gamma - 1)(\nabla \cdot \boldsymbol{u}_0)h' = 0 \end{cases} \tag{C.27}$$

where second order interactions are omitted in this description of sound propagation. Multiplying the second equation by ρ_0/a_0^2, and reformulating following term,

$$\frac{\rho_0}{a_0^2}\mathrm{D}_{\boldsymbol{u}_0}(h') = \mathrm{D}_{\boldsymbol{u}_0}\left(\frac{\rho_0}{a_0^2}h'\right) - h'\nabla\left(\frac{\rho_0}{a_0^2}\right)\cdot\boldsymbol{u}_0 \quad \text{and} \quad \nabla\left(\frac{\rho_0}{a_0^2}\right)\cdot\boldsymbol{u}_0 = (\gamma-2)\frac{\rho_0}{a_0^2}(\nabla\cdot\boldsymbol{u}_0) \tag{C.28}$$

leads to the compressible Blokhintzev equation, defined for $\boldsymbol{u'} = \nabla\psi$

$$\mathrm{D}_{\boldsymbol{u}_0}\left(\frac{\rho_0}{a_0^2}\mathrm{D}_{\boldsymbol{u}_0}(\psi)\right) - \nabla\cdot(\rho_0\nabla\psi) + \frac{\rho_0}{a_0^2}(\nabla\cdot\boldsymbol{u}_0)\mathrm{D}_{\boldsymbol{u}_0}(\psi) = 0 \tag{C.29}$$

That can alternatively be expressed as,

$$\boxed{\mathrm{D}_{\boldsymbol{u}_0}\left(\frac{1}{a_0^2}\mathrm{D}_{\boldsymbol{u}_0}(\psi)\right) - \frac{1}{\rho_0}\nabla\cdot(\rho_0\nabla\psi) = 0} \tag{C.30}$$

Assuming following change of variable,

$$\delta\psi = \frac{\rho_0}{a_0^2}\delta\phi \tag{C.31}$$

The variant of Blokhintzev's wave equation given in equation (C.29) is used to propose a compressible generalisation for Pierce's wave equation,

$$\boxed{\mathrm{D}^2_{\boldsymbol{u}_0}(\phi) - \nabla\cdot(a_0^2\nabla\phi) + (\nabla\cdot\boldsymbol{u}_0)\mathrm{D}_{\boldsymbol{u}_0}(\phi) = 0} \tag{C.32}$$

C.4 Recovering the pressure p from the acoustic potential ϕ

Many acoustic problems involve propagation on a vortical mean-flow, and one may be interested to use, though abusively, the simple formalism of acoustic potential in such cases. In §2.5.2 of part I, it is addressed how the acoustic potential framework can be employed outside of its domain of validity to tackle sound propagation on arbitrary mean flows. Because the propagation problem is approximated it is overdetermined, and different non-equivalent ways to recover the pressure field p from the acoustic potential ϕ exist. It is shown in this paragraph, that with the different approaches, similar results are obtained. By no means, the differences obtained in the post-processings can explain the aberrant results obtained for the pressure field p computed with LEWE-AP and presented in §3.3 of part I. LEWE-AP considers a simplification of the linearised Euler's equation valid for a parallel mean flow and assumes the

fluctuating momentum $\rho_0 \boldsymbol{u}$ be potential, such as $\rho_0 \boldsymbol{u} = \nabla\phi$. Therefore, LEWE-AP is equivalent to,

$$\begin{cases} \mathrm{D}_{\boldsymbol{u}_0}(\nabla\phi) + (\nabla \boldsymbol{u}_0)\cdot\nabla\phi + \nabla p = \rho_0 \boldsymbol{S}_{\boldsymbol{u}} \\ \mathrm{D}_{\boldsymbol{u}_0}(p) + \gamma p_0 \nabla\cdot\left(\dfrac{\nabla\phi}{\rho_0}\right) = S_p \end{cases} \tag{C.33}$$

Different ways to recover the pressure field p are now reviewed.

1. It is seen, that the linearised energy equation can straightly be used to post-process the pressure field p from the acoustic potential ϕ. The momentum fluctuations $\rho_0 \boldsymbol{u}$ are directly rebuilt from the acoustic potential ϕ, and the energy equation does not directly rely on the gradients of the mean flow. This expression is then valid regardless of the considered mean flow, whether it is potential or not. This strategy is a general one, and has already been validated for the wave equations based on the fluctuating velocity $\boldsymbol{u}$, see the validation performed figure 3.8 in §3.2 of part I.

2. Without more assumptions, the linearised momentum equation can be rearranged into,

$$\nabla\left(\mathrm{D}_{\boldsymbol{u}_0}(\phi) + p\right) + (\nabla\times\boldsymbol{u}_0)\times\nabla\phi = \rho_0\boldsymbol{S}_{\boldsymbol{u}} \tag{C.34}$$

   Notice that the term $(\nabla\times\boldsymbol{u}_0)\times\nabla\phi$ that appears here, has been identified in the literature to be responsible for the mode conversion (Yates, 1978; Perez Bergliaffa et al., 2004). It is questionable whether this term should be kept or not in an acoustic potential theory. The latter has not been neglected in the derivations of LEWE-AP, and the above expression is investigated as an attempt to consistently recover p.

3. By neglecting the flow mean vorticity, the linearised momentum equation LHS becomes potential, so must be also the RHS. As in §2.5.2 of part I, a potential momentum source term S_m is introduced such that $\Delta S_m = \nabla\cdot(\rho_0\boldsymbol{S}_{\boldsymbol{u}})$. The linearised momentum equation can then be recast in,

$$p = -\mathrm{D}_{\boldsymbol{u}_0}(\phi) + S_m \tag{C.35}$$

   A similar expression is derived by Pierce (1990, eq. (16)), and this relation is referred to in the following as asymptotic expression.

These three post-processings formulae are tested and compared, so to estimate their influence on the pressure field p. The recovering of the solution obtained with LEWE-AP on the benchmark for a Strouhal number of $St = 0.2$, presented in figure 3.15 in §3.3, is investigated. Figure C.1 presents the real part of the pressure field p obtained from the acoustic potential ϕ computed with LEWE-AP and rebuilt with three different presented methods.
Extracts for these three solutions are compared in C.2. Note that because the reconstruction procedure involving the mean-flow vorticity, equation (C.34), is defined within a constant, the pressure field p computed in that way needs to be recalibrated. The calibration constant is defined so that in the outer-edge of the PML zone p vanishes as illustrated in figure C.2.

The striae in the pressure field p computed with help of the linearised energy equation, visible in figures C.1 and C.2, are a result of the numerical inversion of the material derivative $\mathrm{D}_{\boldsymbol{u}_0}(p)$. Such a behaviour has not been observed for the pressure field p computed for the wave equations based on $\boldsymbol{u}$ and presented in §3.3. Differences are observed in the computed field p, yet qualitatively the solutions are alike. The reconstruction procedure is believed not to play a predominant role, and in the present study, when the

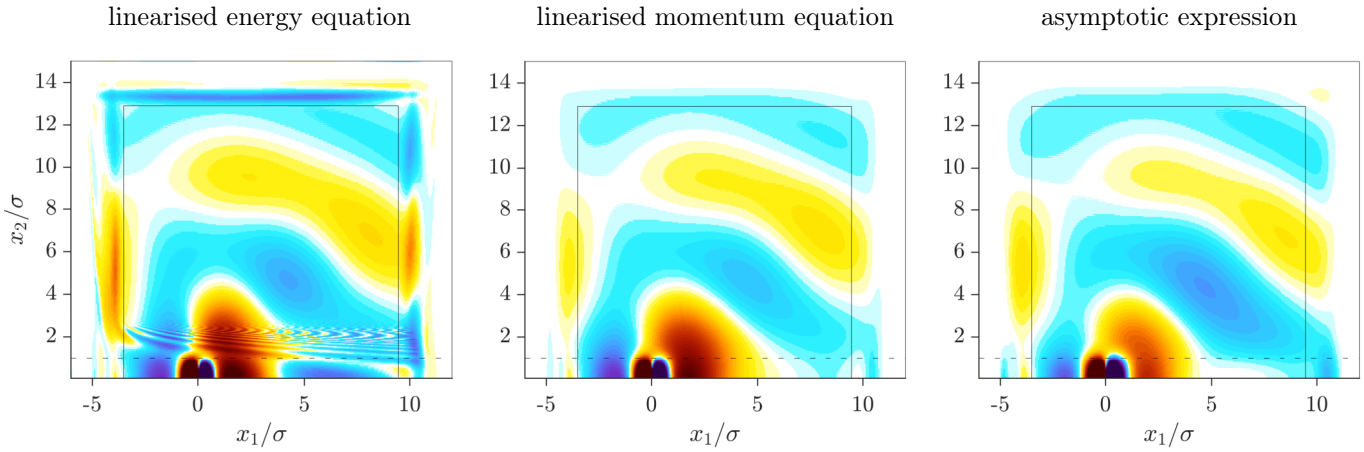

Figure C.1: Real part of the fluctuating pressure p obtained with LEWE-AP and recovered from the acoustic potential ϕ with the different methods. Colour scales are identical, the fifty-cells wide PML region is shown and delimited with solid lines.

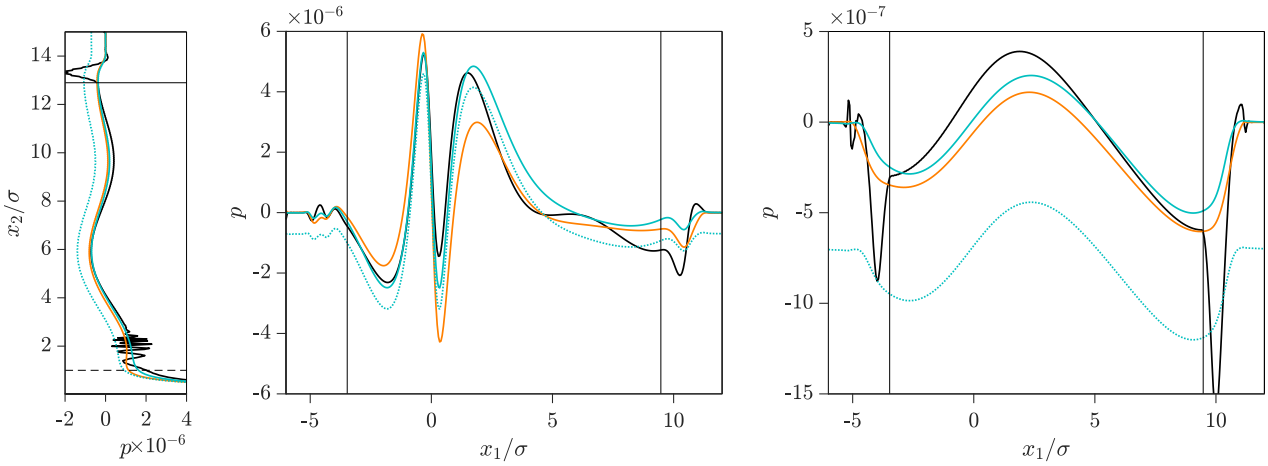

Figure C.2: Extraction along $x_1/\sigma = 0.0$ (left), $x_2/\sigma = 1.0$ (center) and $x_2/\sigma = 12.0$ (right) of the fluctuating pressure p obtained from the acoustic potential ϕ computed with PEWE with different reconstruction procedures. ——linearised energy equation, —— asymptotic expression, ····· expression including mean-flow vorticity, —— expression including mean-flow vorticity with recalibration.

acoustic potential ϕ is computed with LEWE-AP, the linearised momentum equation is used (involves a recalibration of ϕ). When the acoustic potential ϕ is computed with Pierce's wave equation, the asymptotic expression is used to rebuilt the pressure field p.

The surprising acoustic predictions obtained with LEWE-AP, seem consequently not to be caused by the procedure used to recover the pressure p. Figure C.3 presents for the studied case, the acoustic potential field ϕ obtained for LEWE-AP and for Pierce's wave equation. Significant differences in the real part of the acoustic potential field ϕ presented are observed. When the root mean square of the acoustic potential ϕ is computed, an abnormal decrease of the acoustic intensity is seen, and LEWE-AP clearly is ill-posed.

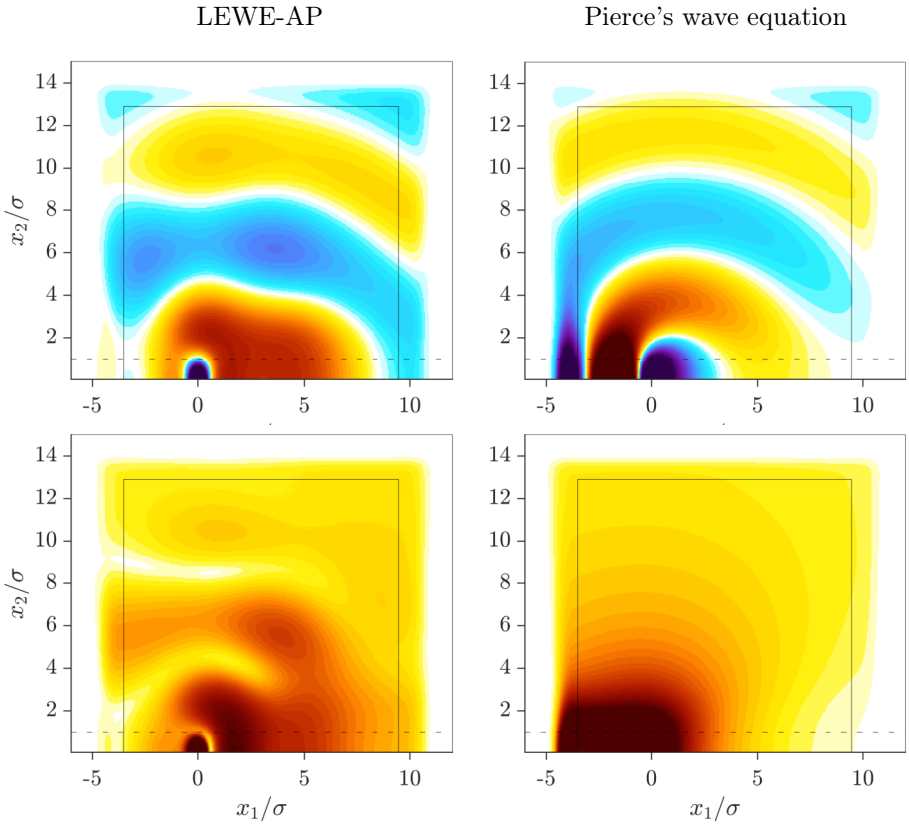

Figure C.3: Acoustic potential fields ϕ computed with LEWE-AP (left) and Pierce's wave equation (right) corresponding to the benchmark configuration for a Strouhal number of $St = 0.2$. The real part (top) and the absolute part (bottom) of the acoustic potential ϕ are presented. Colour scales are identical, the fifty-cells wide PML region is delimited with solid lines.

D Eigenvalue analysis of Euler's equations

The different families of solutions of Euler's equation are recalled here. Effort to recast these results in vector form is made, and the flow velocity $\boldsymbol{u}$, the speed of sound a and the entropy s are considered as the dependence variables. So that for a perfect gas Euler's equations reads,

$$\begin{cases} \dfrac{\mathrm{D}\boldsymbol{u}}{\mathrm{D}t} + \dfrac{2a}{\gamma-1}\nabla a - \dfrac{a^2}{\gamma r}\nabla s = \boldsymbol{0} \\ \dfrac{\mathrm{D}a}{\mathrm{D}t} + \dfrac{\gamma-1}{2}a\nabla\cdot\boldsymbol{u} = 0 \\ \dfrac{\mathrm{D}s}{\mathrm{D}t} = 0 \end{cases} \tag{D.1}$$

Euler's wave equation (EWE) that is a reformulation of Euler's equation with the flow velocity $\boldsymbol{u}$ and speed of sound a only. Some insights in the structure of the solution of EWE is sought.

D.1 Classification of the linearised operator

Euler's equations form a system of quasilinear first order partial differential equations. To provide a classification of this system of differential equations, these equations are linearised with a Reynolds decomposition of the flow variables $\boldsymbol{u} = \boldsymbol{u}_0 + \boldsymbol{u'}$, $a = a_0 + a'$ and $s = s_0 + s'$,

$$\begin{cases} \mathrm{D}_{\boldsymbol{u}_0}(\boldsymbol{u'}) + (\nabla\boldsymbol{u}_0)\cdot\boldsymbol{u'} + \dfrac{2a_0}{\gamma-1}\nabla a' + \left[\dfrac{2\nabla a_0}{\gamma-1} - \dfrac{2a_0\nabla s_0}{\gamma r}\right]a' - \dfrac{a_0^2}{\gamma r}\nabla s' = \boldsymbol{0} \\ \mathrm{D}_{\boldsymbol{u}_0}(a') + \boldsymbol{u'}\cdot\nabla a_0 + \dfrac{\gamma-1}{2}a_0(\nabla\cdot\boldsymbol{u'}) + \dfrac{\gamma-1}{2}(\nabla\cdot\boldsymbol{u_0})a' = 0 \\ \mathrm{D}_{\boldsymbol{u}_0}(s') + \boldsymbol{u'}\cdot\nabla s_0 = 0 \end{cases} \tag{D.2}$$

where $\mathrm{D}_{\boldsymbol{u}_0} = \partial/\partial t + \boldsymbol{u}_0\cdot\nabla$ is the material derivative along the mean flow $\boldsymbol{u}_0$. In this analysis a three dimension space is considered, so that $\boldsymbol{u}_0 = (u_{0,1}, u_{0,2}, u_{0,3})^T$, and the state vector is $\boldsymbol{q} = (u_1', u_2', u_3', a', s')^T$ so that these equations rewrite in matrix form as,

$$\frac{\partial\boldsymbol{q}}{\partial t} + \boldsymbol{A}_1\cdot\frac{\partial\boldsymbol{q}}{\partial x_1} + \boldsymbol{A}_2\cdot\frac{\partial\boldsymbol{q}}{\partial x_2} + \boldsymbol{A}_3\cdot\frac{\partial\boldsymbol{q}}{\partial x_3} + B\cdot q = \boldsymbol{0} \tag{D.3}$$

with,

$$\boldsymbol{A}_1 = \begin{pmatrix} u_{0,1} & & & \frac{2a_0}{\gamma-1} & -\frac{a_0^2}{\gamma r} \\ & u_{0,1} & & & \\ & & u_{0,1} & & \\ \frac{\gamma-1}{2}a_0 & & & u_{0,1} & \\ & & & & u_{0,1} \end{pmatrix} \quad \boldsymbol{A}_2 = \begin{pmatrix} u_{0,2} & & & & \\ & u_{0,2} & & \frac{2a_0}{\gamma-1} & -\frac{a_0^2}{\gamma r} \\ & & u_{0,2} & & \\ & \frac{\gamma-1}{2}a_0 & & u_{0,2} & \\ & & & & u_{0,2} \end{pmatrix} \tag{D.4}$$

$$\boldsymbol{A}_3 = \begin{pmatrix} u_{0,3} & & & & \\ & u_{0,3} & & & \\ & & u_{0,3} & \frac{2a_0}{\gamma-1} & -\frac{a_0^2}{\gamma r} \\ & & \frac{\gamma-1}{2}a_0 & u_{0,3} & \\ & & & & u_{0,3} \end{pmatrix}$$

The nature of the solution is determined by the higher order fluxes in black. The system is hyperbolic if each matrix $\boldsymbol{A}_i$ is diagonalisable with real eigenvalues. From their expression, it is seen that the matrices $\boldsymbol{A}_i$ can be individually diagonalised considering the decomposition,

$$\boldsymbol{A}_i = \boldsymbol{V}_i \cdot \boldsymbol{D}_i \cdot \boldsymbol{V}_i^{-1} \qquad \text{with } i = 1, 2, 3 \tag{D.5}$$

The eigenvalues of $\boldsymbol{A}_i$ are the non-zeros terms of the diagonal matrix $\boldsymbol{D}_i$ and write,

$$\boldsymbol{D}_i = \text{diag}(u_{0,i},\ u_{0,i},\ u_{0,i},\ u_{0,i} + a_0,\ u_{0,i} - a_0) \tag{D.6}$$

they are real and linearised Euler's equations are therefore hyperbolic. The eigenvectors $\boldsymbol{V}_i$ for which each flux is diagonal are however different in each direction, so that a simultaneous diagonalisation of the fluxes is not possible. These eigenvalues correspond to the characteristic speeds of the fluxes, the invariants that are transported by this hyperbolic system are now sought. The fluxes for the quantity $\boldsymbol{Q}_i = \boldsymbol{V}_i^{-1} \cdot \boldsymbol{q}$ are independently computed in each directions,

$$\boldsymbol{V}_i^{-1} \cdot \frac{\partial \boldsymbol{q}}{\partial t} + \boldsymbol{D}_i \cdot \boldsymbol{V}_i^{-1} \cdot \frac{\partial \boldsymbol{q}}{\partial x_i} + \boldsymbol{V}_i^{-1} \cdot \boldsymbol{B} = \boldsymbol{0} \tag{D.7}$$

$$\frac{\partial \boldsymbol{V}_i^{-1} \cdot \boldsymbol{q}}{\partial t} + \boldsymbol{D}_i \cdot \frac{\partial \boldsymbol{V}_i^{-1} \cdot \boldsymbol{q}}{\partial x_i} - \frac{\partial \boldsymbol{V}_i^{-1}}{\partial x_i} \cdot \boldsymbol{q} - \frac{\partial \boldsymbol{V}_i^{-1}}{\partial t} \cdot \boldsymbol{q} + \boldsymbol{V}_i^{-1} \cdot \boldsymbol{B} = \boldsymbol{0} \tag{D.8}$$

and $\widetilde{\boldsymbol{S}} = \frac{\partial \boldsymbol{V}_i^{-1}}{\partial x_i} \cdot \boldsymbol{q} + \frac{\partial \boldsymbol{V}_i^{-1}}{\partial t} \cdot \boldsymbol{q} - \boldsymbol{V}_i^{-1} \cdot \boldsymbol{B}$ is introduced, so that in each directions the characteristic form of Euler's linearised equations is obtained,

$$\frac{\partial \boldsymbol{Q}_i}{\partial t} + \boldsymbol{D}_i \cdot \frac{\partial \boldsymbol{Q}_i}{\partial x_i} = \widetilde{\boldsymbol{S}} \tag{D.9}$$

where,

$$\boldsymbol{Q}_1 = \begin{pmatrix} u_2' \\ u_3' \\ s' \\ \dfrac{2}{\gamma-1}a' + u_1' - \dfrac{a_0}{\gamma r}s' \\ \dfrac{2}{\gamma-1}a' - u_1' - \dfrac{a_0}{\gamma r}s' \end{pmatrix} \quad \boldsymbol{Q}_2 = \begin{pmatrix} u_1' \\ u_3' \\ s' \\ \dfrac{2}{\gamma-1}a' + u_2' - \dfrac{a_0}{\gamma r}s' \\ \dfrac{2}{\gamma-1}a' - u_2' - \dfrac{a_0}{\gamma r}s' \end{pmatrix} \quad \boldsymbol{Q}_3 = \begin{pmatrix} u_1' \\ u_2' \\ s' \\ \dfrac{2}{\gamma-1}a' + u_3' - \dfrac{a_0}{\gamma r}s' \\ \dfrac{2}{\gamma-1}a' - u_3' - \dfrac{a_0}{\gamma r}s' \end{pmatrix} \tag{D.10}$$

The entropy mode s' is convected at the characteristic speed $\boldsymbol{u}_0$. The transverse fluctuating velocities u_i' are transported at the same speed, however the components of the fluctuating vector are twisted so that it does not seem possible to derive a conservation equation for this variable (note that the modified transport equation $\partial \boldsymbol{u'}/\partial t + (\nabla \times \boldsymbol{u'}) \times \boldsymbol{u}_0 = 0$ also fails). In addition the quantity $u_i' \pm \left(\dfrac{2}{\gamma-1}a' - \dfrac{a_0}{\gamma r}s' \right)$ propagates in each direction with the local acoustic group velocity $u_{0,i} \pm a_0$ and corresponds to the acoustic mode.

D.2 Computation of the nonlinear fluxes

The characteristic writing of Euler's equations was first achieved by Riemann (1860) who thereby built the first valid model for nonlinear sound propagation. Drawing inspiration from (Lappas et al., 1999), a generalisation of Riemann's invariants is computed from Euler's equation. Introducing $\boldsymbol{n}$, an arbitrary but constant vector, the two first equations of (D.1) are combined to form,

$$\frac{\mathrm{D}\boldsymbol{u}}{\mathrm{D}t} + a(\nabla \boldsymbol{u}) \cdot \boldsymbol{n} + \frac{2}{\gamma-1}\frac{\mathrm{D}a}{\mathrm{D}t}\boldsymbol{n} + \frac{2a}{\gamma-1}\nabla a = a(\nabla \boldsymbol{u}) \cdot \boldsymbol{n} - a(\nabla \cdot \boldsymbol{u})\boldsymbol{n} + \frac{a^2}{\gamma r}\nabla s \tag{D.11}$$

By defining,

$$\boldsymbol{G_n} = a(\nabla \boldsymbol{u}) \cdot \boldsymbol{n} - a(\nabla \cdot \boldsymbol{u})\boldsymbol{n} + \frac{a^2}{\gamma r}\nabla s \tag{D.12}$$

and introducing the quantity,

$$\boldsymbol{R} = \boldsymbol{u} + \frac{2a}{\gamma-1}\boldsymbol{n} \tag{D.13}$$

A vectorial writing of Riemann's invariants is obtained,

$$\frac{\partial \boldsymbol{R}}{\partial t} + (\nabla \boldsymbol{R}) \cdot (\boldsymbol{u} + a\boldsymbol{n}) = \boldsymbol{G_n} \tag{D.14}$$

where it is seen that the quantity $\boldsymbol{R}$ is conserved in the direction $\boldsymbol{u} + a\boldsymbol{n}$ provided $\boldsymbol{G_n}$ vanishes. Note that the RHS is exactly zero in a mono-dimensional isentropic configuration, as studied by Riemann, but non-zero in general. Moreover, the invariant (D.13) corresponds to a nonlinear recast of the two last invariants given in (D.10). To be closer to the linearised expression found in (D.10), the nonlinear flux $as/(\gamma r)\boldsymbol{n}$ can be added to the invariant $\boldsymbol{R}$ given in equation (D.13), but at the cost of a more complex secular term $\boldsymbol{G_n}$.

The nonlinear flux associated with the entropy variable is directly obtained from the conservation equation,

$$\frac{\partial s}{\partial t} + (\nabla s) \cdot \boldsymbol{u} = 0 \tag{D.15}$$

It is seen that entropy is conserved along the flow.

From previous linear analysis, it is seen that the fluctuations of the transverse velocity are also convected with the flow movement. However, as for the linearised case a conservation equation for the transverse velocity components is tedious to derive. Simply note, that a transport equation for the vorticity $\boldsymbol{\omega} = \nabla \times \boldsymbol{u}$ can be derived from Crocco's form of Euler's equation,

$$\frac{\partial \boldsymbol{u}}{\partial t} + \frac{\nabla(\boldsymbol{u} \cdot \boldsymbol{u})}{2} + (\nabla \times \boldsymbol{u}) \times \boldsymbol{u} + \frac{\nabla a^2}{\gamma - 1} - \frac{a^2 \nabla s}{\gamma r} = \boldsymbol{0} \tag{D.16}$$

By considering its curl, following transport equation is obtained,

$$\frac{\partial \boldsymbol{\omega}}{\partial t} + (\nabla \boldsymbol{\omega}) \cdot \boldsymbol{u} = \boldsymbol{H_\omega} \tag{D.17}$$

where,

$$\boldsymbol{H_\omega} = (\nabla \boldsymbol{u}) \cdot \omega - (\nabla \cdot \boldsymbol{u}) \boldsymbol{\omega} + \frac{\nabla a^2 \times \nabla s}{\gamma r} \tag{D.18}$$

One remarks that the RHS $\boldsymbol{H_\omega}$ possesses a structure comparable to $\boldsymbol{G_n}$.

E The normalised Möhring equation

In this appendix, all considered quantities are non-linear. Möhring's equation is obtained as an exact reformulation of the Navier Stokes equations written in Crocco's form[1],

$$\begin{cases} \dfrac{\partial \rho}{\partial t} + \nabla \cdot (\rho \boldsymbol{u}) = S_\rho \\ \dfrac{\partial \boldsymbol{u}}{\partial t} + \nabla B = \nabla \cdot \boldsymbol{\Sigma} + T \nabla s - \boldsymbol{\omega} \times \boldsymbol{u} + \boldsymbol{S_u} \\ \rho \dfrac{\mathrm{D}B}{\mathrm{D}t} = \dfrac{\partial p}{\partial t} + \nabla \cdot (\boldsymbol{\Sigma} \cdot \boldsymbol{u}) - \nabla \cdot \boldsymbol{q} + \rho \boldsymbol{u} \cdot \boldsymbol{S_u} + \dfrac{1}{\gamma - 1} S_p - \dfrac{a^2}{\gamma} S_\rho \end{cases} \tag{E.1}$$

where, $\mathrm{D}/\mathrm{D}t = \partial/\partial t + \boldsymbol{u} \cdot \nabla$ is the material derivative, $\boldsymbol{\Sigma}$ denotes the friction-related stress tensor, $\boldsymbol{q} = -\lambda \nabla T$ is the heat flux, $\boldsymbol{\omega} = \nabla \times \boldsymbol{u}$ is the vorticity, and S_ρ, $\boldsymbol{S_u}$, S_p are generic forcing terms for the Navier-Stokes equation when written for the principal variables ρ, $\boldsymbol{u}$ and p. To simplify the derivations, let $\boldsymbol{S}_1 = \nabla \cdot \boldsymbol{\Sigma} + T \nabla s - \boldsymbol{\omega} \times \boldsymbol{u} + \boldsymbol{S_u}$ and $S_2 = \nabla \cdot (\boldsymbol{\Sigma} \cdot \boldsymbol{u}) - \nabla \cdot \boldsymbol{q} + \rho \boldsymbol{u} \cdot \boldsymbol{S_u} + \frac{1}{\gamma - 1} S_p - \frac{a^2}{\gamma} S_\rho$. Since $\rho = \rho(p, s)$, the continuity equation can be recast into,

$$\frac{\partial \rho}{\partial t} = \left.\frac{\partial \rho}{\partial p}\right|_s \frac{\partial p}{\partial t} + \left.\frac{\partial \rho}{\partial s}\right|_p \frac{\partial s}{\partial t} = \frac{\rho}{a^2} \frac{\mathrm{D}B}{\mathrm{D}t} - \frac{S_2}{a^2} + \rho_s \frac{\partial s}{\partial t} \tag{E.2}$$

where $a = \sqrt{\left.\frac{\partial p}{\partial \rho}\right|_s}$ is the speed of sound, and $\rho_s = \left.\frac{\partial \rho}{\partial s}\right|_p$. Through integration by part, previous expression can be related to $\rho \partial \boldsymbol{u}/\partial t$ with,

$$\rho \frac{\partial \boldsymbol{u}}{\partial t} = \frac{\partial \rho \boldsymbol{u}}{\partial t} - \boldsymbol{u} \frac{\partial \rho}{\partial t} = \frac{\partial \rho \boldsymbol{u}}{\partial t} - \frac{\rho \boldsymbol{u}}{a^2} \frac{\mathrm{D}B}{\mathrm{D}t} + \frac{\boldsymbol{u}}{a^2} S_2 - \rho_s \boldsymbol{u} \frac{\partial s}{\partial t} \tag{E.3}$$

Additionally the LHS can be recast with the momentum equation leading to,

$$\frac{\partial \rho \boldsymbol{u}}{\partial t} - \frac{\rho \boldsymbol{u}}{a^2} \frac{\mathrm{D}B}{\mathrm{D}t} + \rho \nabla B = \rho \boldsymbol{S}_1 - \frac{\boldsymbol{u}}{a^2} S_2 + \rho_s \boldsymbol{u} \frac{\partial s}{\partial t} \tag{E.4}$$

By dividing previous expression by $-\rho_T$, the normalisation factor, and adding $-\rho \boldsymbol{u} \frac{\partial}{\partial t} \left(\frac{1}{\rho_T} \right)$ on each side

[1] With $B = h + \boldsymbol{v}^2/2$ the momentum equation is recast with $T \delta s = \delta h - \frac{\delta p}{\rho}$ and $(\nabla \times \boldsymbol{v}) \times \boldsymbol{w} = (\nabla \boldsymbol{v}) \cdot \boldsymbol{w} - (\nabla \boldsymbol{v})^T \cdot \boldsymbol{w}$, the energy equation $\rho \frac{\mathrm{D}e}{\mathrm{D}t} + p \nabla \cdot \boldsymbol{v} + \nabla \cdot \boldsymbol{q} = \frac{S_p}{\gamma - 1}$ (e.g. (Delfs, 2016, eq. 37 & eq. 43)) is reformulated with $\delta e = \delta h + \frac{p}{\rho^2} \delta \rho - \frac{\delta p}{\rho}$. The use of the continuity equation and the momentum equation projection along $\boldsymbol{u}$ with $\boldsymbol{u} \cdot \frac{\mathrm{D}\boldsymbol{u}}{\mathrm{D}t} = \frac{1}{2} \frac{\mathrm{D}\boldsymbol{u}^2}{\mathrm{D}t}$ leads to the energy equation for B.

of the equation, the normalised momentum equation is obtained,

$$-\frac{\partial}{\partial t}\left(\frac{\rho \boldsymbol{u}}{\rho_T}\right)+\frac{\rho \boldsymbol{u}}{\rho_T a^2}\frac{\mathrm{D}B}{\mathrm{D}t}-\frac{\rho}{\rho_T}\nabla B=-\frac{\rho}{\rho_T}\boldsymbol{S}_1+\frac{\boldsymbol{u}}{\rho_T a^2}S_2-\frac{\rho_s \boldsymbol{u}}{\rho_T}\frac{\partial s}{\partial t}-\rho \boldsymbol{u}\frac{\partial}{\partial t}\left(\frac{1}{\rho_T}\right) \tag{E.5}$$

The final step leading to Möhring's equation is to take the divergence of previous expression. Beforehand the divergence of the first term is considered separately,

$$\nabla\cdot\left[\frac{\partial}{\partial t}\left(\frac{-\rho \boldsymbol{u}}{\rho_T}\right)\right]=\frac{\partial}{\partial t}\left[\frac{-\nabla\cdot(\rho \boldsymbol{u})}{\rho_T}+\frac{\rho}{\rho_T^2}\boldsymbol{u}\cdot\nabla\rho_T\right]=\frac{\partial}{\partial t}\left[\frac{1}{\rho_T}\frac{\partial \rho}{\partial t}-\frac{S_\rho}{\rho_T}+\frac{\rho}{\rho_T^2}\boldsymbol{u}\cdot\nabla\rho_T\right] \tag{E.6}$$

Making use of the expression of $\partial\rho/\partial t$ gives,

$$\nabla\cdot\left[\frac{\partial}{\partial t}\left(\frac{-\rho \boldsymbol{u}}{\rho_T}\right)\right]=\frac{\partial}{\partial t}\left[\frac{\rho}{\rho_T a^2}\frac{\mathrm{D}B}{\mathrm{D}t}-\frac{S_2}{\rho_T a^2}-\frac{S_\rho}{\rho_T}+\frac{\rho_s}{\rho_T}\frac{\partial s}{\partial t}+\frac{\rho}{\rho_T^2}\boldsymbol{u}\cdot\nabla\rho_T\right] \tag{E.7}$$

enabling a straight calculation of the divergence of the above expression,

$$\begin{aligned}\frac{\partial}{\partial t}\left[\frac{\rho}{\rho_T a^2}\frac{\mathrm{D}B}{\mathrm{D}t}\right]+\nabla\cdot\left[\frac{\rho \boldsymbol{u}}{\rho_T a^2}\frac{\mathrm{D}B}{\mathrm{D}t}-\frac{\rho}{\rho_T}\nabla B\right]= &\ \frac{\partial}{\partial t}\left[\frac{S_2}{\rho_T a^2}+\frac{S_\rho}{\rho_T}-\frac{\rho_s}{\rho_T}\frac{\partial s}{\partial t}+\rho \boldsymbol{u}\cdot\nabla\left(\frac{1}{\rho_T}\right)\right]\\ &+\nabla\cdot\left[-\frac{\rho}{\rho_T}\boldsymbol{S}_1+\frac{\boldsymbol{u}}{\rho_T a^2}S_2-\frac{\rho_s \boldsymbol{u}}{\rho_T}\frac{\partial s}{\partial t}-\rho \boldsymbol{u}\frac{\partial}{\partial t}\left(\frac{1}{\rho_T}\right)\right]\end{aligned} \tag{E.8}$$

Replacing $\boldsymbol{S}_1$ and S_2 by their expression give the normalised Möhring equation,

$$\begin{aligned}\frac{\partial}{\partial t}\left[\frac{\rho}{\rho_T a^2}\frac{\mathrm{D}B}{\mathrm{D}t}\right]+\nabla\cdot\left[\frac{\rho \boldsymbol{u}}{\rho_T a^2}\frac{\mathrm{D}B}{\mathrm{D}t}-\frac{\rho}{\rho_T}\nabla B\right]= &\ \nabla\cdot\left[-\frac{\rho}{\rho_T}\boldsymbol{S}_{\boldsymbol{u}}+\frac{\rho \boldsymbol{u}}{\rho_T a^2}(\boldsymbol{u}\cdot\boldsymbol{S}_{\boldsymbol{u}})+\frac{\boldsymbol{u}}{\rho_T a^2(\gamma-1)}S_p-\frac{\boldsymbol{u}}{\gamma\rho_T}S_\rho\right]\\ &+\frac{\partial}{\partial t}\left[\frac{\rho}{\rho_T a^2}(\boldsymbol{u}\cdot\boldsymbol{S}_{\boldsymbol{u}})+\frac{1}{(\gamma-1)\rho_T a^2}S_p+\frac{\gamma-1}{\gamma\rho_T}S_\rho\right]+\mathcal{R}\end{aligned}$$

$$\begin{aligned}\text{with}\quad \mathcal{R}= &\ \nabla\cdot\left[\frac{\rho}{\rho_T}\boldsymbol{\omega}\times\boldsymbol{u}-\frac{\rho}{\rho_T}T\nabla s-\frac{\rho_s \boldsymbol{u}}{\rho_T}\frac{\partial s}{\partial t}-\frac{\boldsymbol{u}}{\rho_T a^2}\nabla\cdot\boldsymbol{q}-\frac{\rho}{\rho_T}\nabla\cdot\boldsymbol{\Sigma}+\frac{\boldsymbol{u}}{\rho_T a^2}\nabla\cdot(\boldsymbol{\Sigma}\cdot\boldsymbol{u})-\rho \boldsymbol{u}\frac{\partial}{\partial t}\left(\frac{1}{\rho_T}\right)\right]\\ &+\frac{\partial}{\partial t}\left[-\frac{\rho_s}{\rho_T}\frac{\partial s}{\partial t}-\frac{\nabla\cdot\boldsymbol{q}}{\rho_T a^2}+\frac{\nabla\cdot(\boldsymbol{\Sigma}\cdot\boldsymbol{u})}{\rho_T a^2}+\rho \boldsymbol{u}\cdot\nabla\left(\frac{1}{\rho_T}\right)\right]\end{aligned}$$

One verifies that in absence of viscous stresses, heat fluxes and for unitary ρ_T the source term $\mathcal{R}$ given by Möhring (1999) is retrieved and complies with the derivations done by Delfs (2016, § 3.2.2) and Legendre (2014, § 6.2).

F A template for *Actran TM*

In the following section a template to parametrise a simple *Actran TM* analysis is provided. It relies on the extensive use of `actranpy` that is a python-based environment enabling the parametrisation and the run of *Actran TM* analyses. As is, the script requires less than 2 GB of RAM and needs few minutes to run. It has been set-up with *Actran TM* 20.0 (compatible with 19.0) and python 2.7.5 on a CentOS linux distribution. To generate and launch the analysis, save this script in a python file, `ActranAnalysis.py`, and simply enter following command line in a terminal,

```
actranpy -u VI -x ActranAnalysis.py -n
```

This analysis computes the bidimensional solution of a point/planar source over a typical jet mean flow. The script is build up so to enable the acoustic computation of sound source located in or out of the computational domain. The variable '`WhichFlowField`', enables to run a classical *Actran TM* analysis based on Möhring's equation, but also to compute the solution of Pierce's equation with or without flow reversal (FRT). Some development of *Actran TM* are on-going, and it will soon be possible in the future to compute acoustic solution for sources set outside of a computational domain that presents flow heterogeneities. For now, it is recommended the Infinite Elements (IE) are used and that the mean flow is uniform at the Non Reflecting Boundary Condition (NRBC). The design of this script would not have been possible without the invaluable support of César Legendre from *Free Field Technologies*.

```
import numpy as np
import os

def step(x): # numpy.heaviside is defined from version 1.13.0 of numpy only
    return 1 * (x > 0) + 0.5 * (x == 0)

#------------------------------------------------------------
#    PARAMETRISATION OF THE ANALYSIS
#------------------------------------------------------------

output_folder = 'PandaSeasholtz_2Danalysis'

#    DEFINITION OF THE SOURCE

freq_sample = [10, 50, 100] # list of frequency considered
source_type = 'cylindrical' # 'planar','cylindrical': sound source type
R = 50 # polar definition of the sound source position
incommingWaveAngle = 25.0 # planar/cylindrical source angle wrt. the flow (X axis)
source_pos = [R*np.cos(incommingWaveAngle*np.pi/180.0), R*np.sin(incommingWaveAngle*np.pi
    /180.0)]

```

```
#   DEFINITION OF THE MEAN FLOW

M0j = 0.7
M0inf = 0.3
T0j = 500.0 # K
T0inf = 300 # K
p0 = 103330.0 # Pa

#   CHOICE OF THE BASE FLOW TO PERFORM THE ANALYSIS

WhichFlowField = 'rhoT_corrected_FRT_flow' # 'physical_flow', 'rhoT_corrected_flow', '
    rhoT_corrected_FRT_flow'

#   DEFINITION OF THE MESH (jet diameter is unitary)
x_min = -15.0
x_max = 70.0
y_min = -10
y_max = 35.0

elemSizeFluid = 0.15
elemSizeFF = 0.2
elemSizeDuct = 0.1

interpOrder = 1 # 1 or 2: interpolation order of the solution

FF_type = 'IE' # 'PML' or 'IE': choice of the Non-Radiating Boundary-Condition (use 'IE'
    by default)

if FF_type=='IE':
  InfiniteElemInterpOrder = 50 # Increase up to 100 when source is close to a corner
elif FF_type=='PML':
  PML_width = 2*np.sqrt(1.4*287*T0inf)/freq_sample[0] # 2xlambda PML width based on the
    largest frequency

UniformFlowInPML = True # Developments to account for heterogeneous flow in PML when
    source is out of the domain are on-going at FFT (june 2020). When using PML and
    sources out of the domain, the flow must be everywhere uniform.

memoryReguirement_MB = 16000 # maximum RAM memory in MB available to Actran

#-----------------------------------------------------------
#   START OF THE ACTRANVI ANALYSIS
#-----------------------------------------------------------

try:
  os.mkdir(output_folder)
except OSError:
  print ("Creation of the directory failed")
else:
  print ("Successfully created the directory")

current_path = os.getcwd()
res_path = os.path.join(current_path,output_folder)
os.chdir(res_path)

actranvi = ActranVI()
```

```
72
73 #   GENERATION/LOADING OF THE MESH
74
75 if interpOrder==1:
76   MeshInterp = 'LINEAR'
77   FieldInterp = 'linear'
78 elif interpOrder==2:
79   MeshInterp = 'QUADRATIC'
80   FieldInterp = 'quadratic'
81
82 if os.path.isdir(os.path.join( os.path.dirname(os.getcwd()), '2D_'+FieldInterp+'
     Mesh_unflangedDuct_'+FF_type+'.nff')): # .nff are considered as directories and not
     files
83   [topology] = actranvi.read_mesh(file=os.path.join( os.path.dirname(os.getcwd()), '2D_'+
     FieldInterp+'Mesh_unflangedDuct_'+FF_type+'.nff'), load_topology=True)
84 else:
85   [pid_domain_1] = actranvi.create_points_mesh(method='custom',coordinates=[[0.0, 0.5,
     0.0], [0.0, 0.55, 0.0], [x_min, 0.55, 0.0], [x_min, y_max, 0.0], [x_max, y_max, 0.0],
      [x_max, y_min, 0.0], [x_min, y_min, 0.0], [x_min, -0.55, 0.0], [0.0, -0.55, 0.0],
     [0.0, -0.5, 0.0], [x_min, -0.5, 0.0], [x_min, 0.5, 0.0]],topology=None)
86   [pid_domain_2] = actranvi.link_edges_mesh(element_size=elemSizeDuct,input={'topologies'
     : {actranvi.get_topology( id=1 ): {'external_nodes_ids': zipped_list(11, 12)}}},
     replace_input=False,sort_by_node_ID=False)
87   [pid_domain_3] = actranvi.link_edges_mesh(element_size=elemSizeDuct,input={'topologies'
     : {actranvi.get_topology( id=1 ): {'external_nodes_ids': zipped_list(10, 11)}}},
     replace_input=False,sort_by_node_ID=False)
88   [pid_domain_4] = actranvi.link_edges_mesh(element_size=elemSizeDuct,input={'topologies'
     : {actranvi.get_topology( id=1 ): {'external_nodes_ids': zipped_list(9, 10)}}},
     replace_input=False,sort_by_node_ID=False)
89   [pid_domain_5] = actranvi.link_edges_mesh(element_size=elemSizeDuct,input={'topologies'
     : {actranvi.get_topology( id=1 ): {'external_nodes_ids': zipped_list(8, 9)}}},
     replace_input=False,sort_by_node_ID=False)
90   [pid_domain_6] = actranvi.link_edges_mesh(element_size=elemSizeFF,input={'topologies':
     {actranvi.get_topology( id=1 ): {'external_nodes_ids': zipped_list(7, 8)}}},
     replace_input=False,sort_by_node_ID=False)
91   [pid_domain_7] = actranvi.link_edges_mesh(element_size=elemSizeFF,input={'topologies':
     {actranvi.get_topology( id=1 ): {'external_nodes_ids': zipped_list(6, 7)}}},
     replace_input=False,sort_by_node_ID=False)
92   [pid_domain_8] = actranvi.link_edges_mesh(element_size=elemSizeFF,input={'topologies':
     {actranvi.get_topology( id=1 ): {'external_nodes_ids': zipped_list(5, 6)}}},
     replace_input=False,sort_by_node_ID=False)
93   [pid_domain_9] = actranvi.link_edges_mesh(element_size=elemSizeFF,input={'topologies':
     {actranvi.get_topology( id=1 ): {'external_nodes_ids': zipped_list(4, 5)}}},
     replace_input=False,sort_by_node_ID=False)
94   [pid_domain_10] = actranvi.link_edges_mesh(element_size=elemSizeFF,input={'topologies':
      {actranvi.get_topology( id=1 ): {'external_nodes_ids': zipped_list(3, 4)}}},
     replace_input=False,sort_by_node_ID=False)
95   [pid_domain_11] = actranvi.link_edges_mesh(element_size=elemSizeDuct,input={'topologies
     ': {actranvi.get_topology( id=1 ): {'external_nodes_ids': zipped_list(2, 3)}}},
     replace_input=False,sort_by_node_ID=False)
96   [pid_domain_12] = actranvi.link_edges_mesh(element_size=elemSizeDuct,input={'topologies
     ': {actranvi.get_topology( id=1 ): {'external_nodes_ids': zipped_list(1, 2)}}},
     replace_input=False,sort_by_node_ID=False)
97   [pid_domain_13] = actranvi.link_edges_mesh(element_size=elemSizeDuct,input={'topologies
     ': {actranvi.get_topology( id=1 ): {'external_nodes_ids': zipped_list(1, 12)}}},
     replace_input=False,sort_by_node_ID=False)
```

```
98   actranvi.set_prop( actranvi.get_topology( id=1 ), model_dimension=2 )
99   [pid_domain_14] = actranvi.surface_mesh(fill_method='planar',element_type='tria',
       element_size=elemSizeFluid,gradation_factor=2,group_by_loops=False,input=[
       pid_domain_2, pid_domain_3, pid_domain_4, pid_domain_5, pid_domain_6, pid_domain_7,
       pid_domain_8, pid_domain_9, pid_domain_10, pid_domain_11, pid_domain_12,
       pid_domain_13])
100  [pid_domain_6] = actranvi.move_elements(renumbering=True,new_pid_name=u'FreeField',
       input=[pid_domain_6, pid_domain_7, pid_domain_8, pid_domain_9, pid_domain_10],
       new_topology=False,copy=False)
101  [pid_domain_7] = actranvi.move_elements(renumbering=True,new_pid_name=u'InfiniteDuct',
       input=[pid_domain_2],new_topology=False,copy=False)
102  [pid_domain_3] = actranvi.move_elements(renumbering=True,new_pid_name=u'DuctWall',input
       =[pid_domain_3, pid_domain_4, pid_domain_5, pid_domain_11, pid_domain_12,
       pid_domain_13],new_topology=False,copy=False)
103
104  if FF_type=='IE':
105      #   CREATION OF THE TRANSITION LAYER TO TACKLE OUT OF THE DOMAIN SOURCES
106    [pid_domain_15, pid_domain_16, pid_domain_17] = actranvi.extrude_mesh(
       layers_thickness=[elemSizeFF],normal_method='vertex',baffle_planes=[None, None, None
       ],input=[actranvi.get_pid_domain( actranvi.get_topology(id  = 1) , pid=15 )])
107    actranvi.set_prop( actranvi.get_pid_domain( actranvi.get_topology(id  = 1) , pid=18 )
       , basename='NRBC_TransitionLayer' )
108    actranvi.set_prop( actranvi.get_pid_domain( actranvi.get_topology(id  = 1) , pid=19 )
       , basename='FreeField_WithTransitionLayer' )
109
110  elif FF_type=='PML':
111    #   CREATION OF THE PML LAYER
112    [pid_domain_18] = actranvi.create_points_mesh(method='custom',coordinates=[[x_min,
       0.55], [x_min-PML_width, 0.55], [x_min-PML_width, y_max+PML_width], [x_max+PML_width,
        y_max+PML_width], [x_max+PML_width, y_min-PML_width], [x_min-PML_width, y_min-
       PML_width,], [x_min-PML_width, -0.55], [x_min, -0.55]],topology=actranvi.get_topology
       ( id=1 ))
113    [pid_domain_19] = actranvi.link_edges_mesh(element_size=elemSizeFF,input=[
       pid_domain_18],replace_input=False,sort_by_node_ID=True)
114    [pid_domain_2, pid_domain_6, pid_domain_8] = actranvi.merge_nodes_mesh(distance=1e
       -06,replace_input=True,input=[pid_domain_6, pid_domain_19])
115    [pid_domain_9] = actranvi.move_elements(renumbering=True,new_pid_name=u'
       PML_outerLayer',input=[pid_domain_6],new_topology=False,copy=False)
116    [pid_domain_6] = actranvi.surface_mesh(fill_method='planar',element_type='quad',
       element_size=elemSizeFF,gradation_factor=2,group_by_loops=False,input=[pid_domain_2,
       pid_domain_9])
117
118  actranvi.reinterpolate( topology=actranvi.get_topology( id=1 ), interpolation=
       MeshInterp )
119
120  actranvi.write_mesh(source=actranvi.get_topology( id=1 ), format='nff', file=os.path.
       join( os.path.dirname(os.getcwd()), '2D_'+FieldInterp+'Mesh_unflangedDuct_'+FF_type+'
       .nff'), check_duplicated_nodes=True, export_fields=True, fields=[])
121
122 #   DEFINITION AND MAPPING OF THE MEAN FLOW FIELD
123
124 First_MeanFlowBuffer_ratio=0.7 # normalised extent in X where the mean flow is not
       modified
125 Second_MeanFlowBuffer_ratio = 0.8 # normalised extent in X where the flow in the buffer
       reaches ambient value
126 BufferPow = 1 # quickness of the damping
```

```
127
128 # Default ActranTM value for Cp and Cv are 1004.0 and 716.0, they are modified to tune
      gamma
129 fluid_cp = 1004.
130 fluid_cv = fluid_cp/1.4
131 gamma = fluid_cp/fluid_cv
132 R_gaz = 287.0
133
134 a0j = np.sqrt(gamma*R_gaz*T0j)
135 a0inf = np.sqrt(gamma*R_gaz*T0inf)
136
137 u0j = M0j*a0j
138 u0inf = M0inf*a0inf
139
140 u0j_eff = u0j-u0inf # out of the blue flow modification to simulate flight effects,
      u0j_eff is the relative jet velocity
141 M0j_eff = u0j_eff/a0j
142
143 rho0j = gamma*p0/a0j**2
144 rho0inf = gamma*p0/a0inf**2
145
146 if FF_type=='IE':
147   domains_involved = [14,15,16,17,18]
148 elif FF_type=='PML':
149   if UniformFlowInPML:
150     domains_involved = [14,16,17,20]
151   else:
152     domains_involved = [14,16,17,18,20,23,24]
153
154 for dom_id in domains_involved:
155   print("Mean flow is computed on the domain with id=%s"%(dom_id))
156   pid_domain = actranvi.get_pid_domain( actranvi.get_topology( id=1 ) , pid=dom_id )
157   coo_field  = actranvi.get_coordinate_field(pid_domain)
158   x_vec = coo_field.array()[0,:,0];
159   y_vec = coo_field.array()[0,:,1];
160
161   [velocity_field] = actranvi.add_field(field=coo_field,
162                                         name ='Mean_Velocity',
163                                         quantity='MEAN_VELOCITY',
164                                         continuous=True,
165                                         interpolation=FieldInterp,
166                                         vtype='float',
167                                         num_comp=coo_field.num_comp,
168                                         num_realisations=1,
169                                         default_value='0.0')
170
171   x_c = 4.2 + 1.1*M0j_eff**2
172   h = (1-x_vec/x_c)/2
173   b = 1.2658*(elemSizeDuct+abs(x_vec))/10.7*(1-0.273*M0j_eff**2)
174   u_c = (step(x_c-x_vec) + step(x_vec-x_c)*(1-np.exp(-1.35/(elemSizeDuct+abs(1-x_vec/x_c)
      ))))*u0j_eff # expression of the mean axial velocity given in Panda & Seasholtz (
      Physics of Fluid, 1999), thank you Bertrand M.
175
176   velocity_field.array()[0,:,0] = ( step(h-abs(y_vec))*u_c + step(abs(y_vec)-h)*u_c*np.
      exp(-np.log(2)*((abs(y_vec)-h)/b)**2) )*step(x_vec) + u0j_eff*step(-x_vec)*step(0.53-
      abs(y_vec)) + u0inf # value of 0.53 in [0.5,0.55] is to delimit the volume inside the
```

```
    duct

#   CREATION OF A BUFFER ZONE FOR THE MEAN FLOW, TO ENSURE UNIFORM FLOW AT NRBC

x_buffer = First_MeanFlowBuffer_ratio*x_max
x_maxBuffer = Second_MeanFlowBuffer_ratio*(x_max-x_buffer) + x_buffer
L_buffer = x_maxBuffer-x_buffer
velocity_field.array()[0,:,0] = step(x_buffer-x_vec)*velocity_field.array()[0,:,0]   +
    step(x_vec-x_buffer)*step(x_maxBuffer-x_vec)*(   ((x_vec-x_buffer)/L_buffer)**
  BufferPow  *  u0inf   +   (1 - ((x_vec-x_buffer)/L_buffer)**BufferPow)  *
  velocity_field.array()[0,:,0]   )   +   step(x_vec-x_maxBuffer)*u0inf

[density_field] = actranvi.add_field(field=coo_field,
                                     name ='Mean_Density',
                                     quantity='MEAN_DENSITY',
                                     continuous=True,
                                     interpolation=FieldInterp,
                                     vtype='float',
                                     num_comp=1,
                                     num_realisations=1,
                                     default_value= '0.0' )

density_field.array()[0,:,0] = 1/(   -0.5*(gamma-1)/(gamma*p0)*((velocity_field.array()
  [0,:,0]-u0inf)-(u0j-u0inf))*(velocity_field.array()[0,:,0]-u0inf) + 1/rho0j*(
  velocity_field.array()[0,:,0]-u0inf)/(u0j-u0inf) + 1/rho0inf*((u0j-u0inf)-(
  velocity_field.array()[0,:,0]-u0inf))/(u0j-u0inf)   ) # modification of u0j <- u0j-
  u0inf and velocity_field <- velocity_field - u0inf with respect to original
  formulation to tinker some flight effects

if M0j==M0inf:
  print ('WARNING !!! T0j is not taken into account in the definition of the mean flow
  field !!! WARNING !!!')
  density_field.array()[0,:,0] = p0/(R_gaz*T0inf)

[pressure_field] = actranvi.add_field(field=coo_field,
                                      name ='Mean_Pressure',
                                      quantity='MEAN_PRESSURE',
                                      continuous=True,
                                      interpolation=FieldInterp,
                                      vtype='float',
                                      num_comp=1,
                                      num_realisations=1,
                                      default_value= p0 )

[speedOfSound_field] = actranvi.add_field(field=coo_field,
                                      name ='Speed_Of_Sound',
                                      quantity='SPEED_OF_SOUND',
                                      continuous=True,
                                      interpolation=FieldInterp,
                                      vtype='float',
                                      num_comp=1,
                                      num_realisations=1,
                                      default_value= '0.0' )

speedOfSound_field.array()[0,:,0] = np.sqrt(gamma*p0/density_field.array()[0,:,0])

```

```
223   [Mach_field] = actranvi.add_field(field=coo_field,
224                                     name ='Mach_number',
225                                     quantity='MACH_NUMBER',
226                                     continuous=True,
227                                     interpolation=FieldInterp,
228                                     vtype='float',
229                                     num_comp=1,
230                                     num_realisations=1,
231                                     default_value= '0.0' ) # a0 = np.sqrt(gamma*p0/
      rho0)
232
233   Mach_field.array()[0,:,0] = velocity_field.array()[0,:,0]/speedOfSound_field.array()
      [0,:,0]
234
235   if np.amax( (Mach_field.array()[0,:,0]).reshape(-1) )>=1 :
236     print ('WARNING !!! SUPERSONIC REGION DETECTED !!! WARNING !!!')
237
238 actranvi.write_mesh(source=actranvi.get_topology( id=1 ), format='nff', file='
      PandaSeasholtz_2DFlow_'+FieldInterp+'Mesh_'+FF_type+'_physical_flow.nff',
      check_duplicated_nodes=True, export_fields=True, fields=[])
239
240 #    ACTRAN TM'S HIJACKING: MODIFY P_0 AND RHO_0 TO TURN MOHRING'S EQ. INTO PIERCE'S EQ.
241
242 if ~(WhichFlowField=='physical_flow'):
243   rho_T_corr_inf = (1+(gamma-1)/2*(M0inf)**2)**(-2/(gamma-1))
244   rho0inf = rho0inf*rho_T_corr_inf
245   p0 = p0*rho_T_corr_inf # the 'hijacked' mean-pressure is non-uniform. From here on, p0
      reffers to p0inf and is used in the NRBC (IE + transition layer)
246
247   rho_T_corr_j = (1+(gamma-1)/2*(M0j)**2)**(-2/(gamma-1))
248   rho0j = rho0j*rho_T_corr_j
249
250   for dom_id in domains_involved:
251     print("Flow is modified in PID %s to change Mohring's eq. into Pierce's eq."%(dom_id)
      )
252     velocity_field = actranvi.get_field( actranvi.get_pid_domain( actranvi.get_topology(
      id=1 ) , pid=dom_id ) , quantity='MEAN_VELOCITY' )
253     speedOfSound_field = actranvi.get_field( actranvi.get_pid_domain( actranvi.
      get_topology( id=1 ) , pid=dom_id ) , quantity='SPEED_OF_SOUND' )
254     density_field = actranvi.get_field( actranvi.get_pid_domain( actranvi.get_topology(
      id=1 ) , pid=dom_id ) , quantity='MEAN_DENSITY' )
255     pressure_field = actranvi.get_field( actranvi.get_pid_domain( actranvi.get_topology(
      id=1 ) , pid=dom_id ) , quantity='MEAN_PRESSURE' )
256
257     rho_T_corr = (1+(gamma-1)/2*(    np.sqrt(  np.array(velocity_field.array()[0,:,0])**2
       + np.array(velocity_field.array()[0,:,1])**2 )/np.array(speedOfSound_field.array()
      [0,:,0])    )**2)**(-2/(gamma-1))
258
259     density_field.array()[0,:,0] = np.array(density_field.array()[0,:,0])*np.array(
      rho_T_corr)
260     pressure_field.array()[0,:,0] = np.array(pressure_field.array()[0,:,0])*np.array(
      rho_T_corr)
261
262   actranvi.write_mesh(source=actranvi.get_topology( id=1 ), format='nff', file=os.path.
      join(res_path,'PandaSeasholtz_2DFlow_'+FieldInterp+'Mesh_'+FF_type+'
      _rhoT_corrected_flow.nff'), check_duplicated_nodes=True, export_fields=True, fields
```

```
    =[])
263
264   if WhichFlowField=='rhoT_corrected_FRT_flow':
265     u0inf = -u0inf
266     u0j = -u0j
267     for dom_id in domains_involved:
268       print("Flow is reversed for PID number:%s"%(dom_id))
269       velocity_field = actranvi.get_field( actranvi.get_pid_domain( actranvi.get_topology
      ( id=1 ) , pid=dom_id ) , quantity='MEAN_VELOCITY' )
270       speedOfSound_field = actranvi.get_field( actranvi.get_pid_domain( actranvi.
      get_topology( id=1 ) , pid=dom_id ) , quantity='SPEED_OF_SOUND' )
271       density_field = actranvi.get_field( actranvi.get_pid_domain( actranvi.get_topology(
       id=1 ) , pid=dom_id ) , quantity='MEAN_DENSITY' )
272       pressure_field = actranvi.get_field( actranvi.get_pid_domain( actranvi.get_topology
      ( id=1 ) , pid=dom_id ) , quantity='MEAN_PRESSURE' )
273
274       velocity_field.array()[0,:,0] = -np.array(velocity_field.array()[0,:,0])
275       velocity_field.array()[0,:,1] = -np.array(velocity_field.array()[0,:,1])
276
277     actranvi.write_mesh(source=actranvi.get_topology( id=1 ), format='nff', file=os.path.
      join(res_path,'PandaSeasholtz_2DFlow_'+FieldInterp+'Mesh_'+FF_type+'
      _rhoT_corrected_FRT_flow.nff'), check_duplicated_nodes=True, export_fields=True,
      fields=[])
278
279   #   CORRECTION OF THE SOURCE AMPLITUDE
280
281   if (WhichFlowField=='physical_flow'):
282     SourceAmplitude=1.0
283   else:
284     # check if the source point is located in this PID. Calculate distance of the source
      position to the nearest point of the mesh
285     ThisPID_sourceDist = np.amin(np.sqrt((np.array(source_pos)[0]-x_vec)**2 + (np.array(
      source_pos)[1]-y_vec)**2))
286     LargestCellMeasure = np.sqrt(elemSizeFluid**2+elemSizeFF**2+elemSizeDuct**2)
287     if (ThisPID_sourceDist<=LargestCellMeasure):
288       sourceIndex = np.argmin(np.sqrt((np.array(source_pos)[0]-x_vec)**2 + (np.array(
      source_pos)[1]-y_vec)**2))
289       sourceMach = np.sqrt(velocity_field.array()[0,sourceIndex,0]**2+velocity_field.
      array()[0,sourceIndex,1]**2)/speedOfSound_field.array()[0,sourceIndex,0]
290
291     if ~(WhichFlowField=='physical_flow'):
292         if ~('sourceMach' in locals()): # if the variable sourceMach was not created
293         sourceMach = M0inf
294
295     SourceAmplitude = -1j/4*(1+(gamma-1)/2*sourceMach**2)**(-1/(gamma-1))
296
297     '''
298     IMPORTANT: In post-processing, this amplitude correction needs still to be multiplied
       with the source pulsation. The computed velocity potential then represents the
      complex conjuguate of Pierce's wave equation solution, normalised by the sound speed
      at the observer location. Please compare the formula coded here, with the one
      provided in the chapter "Solving adjoint Pierce's equation with Actran TM".
      '''
299
300
301 #-------------------------------------------------------
302 #   SET-UP OF THE DIRECT FREQUENCY RESPONSE (.EDAT)
```

```
303 #-------------------------------------------------------
304
305 #   CREATION OF THE DOMAINS
306
307 domain_0 = actranvi.auto_create_domain( pid_domain=actranvi.get_pid_domain( actranvi.
        get_topology( id=1 ) , pid=17 ) )
308 actranvi.set_prop( domain_0, name='DuctWall' )
309 domain_1 = actranvi.auto_create_domain( pid_domain=actranvi.get_pid_domain( actranvi.
        get_topology( id=1 ) , pid=14 ) )
310 actranvi.set_prop( domain_1, name='MovingFluid' )
311 domain_2 = actranvi.auto_create_domain( pid_domain=actranvi.get_pid_domain( actranvi.
        get_topology( id=1 ) , pid=16 ) )
312 actranvi.set_prop( domain_2, name='InfiniteDuct' )
313
314 if FF_type=='IE':
315   domain_3_trans = actranvi.auto_create_domain( pid_domain=actranvi.get_pid_domain(
        actranvi.get_topology( id=1 ) , pid=18 ) ) # moving fluid domain
316   domain_3 = actranvi.auto_create_domain( pid_domain=actranvi.get_pid_domain( actranvi.
        get_topology( id=1 ) , pid=19 ) ) # free-field radiation condition
317   actranvi.set_prop( domain_3, name='FreeField' )
318
319 elif FF_type=='PML':
320   domain_3 = actranvi.auto_create_domain( pid_domain=actranvi.get_pid_domain( actranvi.
        get_topology( id=1 ) , pid=24 ) )
321   actranvi.set_prop( domain_3, name='PML_layer' )
322   domain_4 = actranvi.auto_create_domain( pid_domain=actranvi.get_pid_domain( actranvi.
        get_topology( id=1 ) , pid=23 )) # free-field radiation condition
323   actranvi.set_prop( domain_4, name='PML_outer_skin' )
324
325 #   INITIATE THE ANALYSIS
326
327 analysis_1 = actranvi.add_analysis(type='Direct Frequency Response')
328
329 N_freq = np.size(freq_sample)
330 this_freq_sample = np.zeros([N_freq,1]) # change freq_sample into a column array
331 this_freq_sample[:] = np.array(freq_sample).reshape(-1,1)
332 actranvi.set_prop( analysis_1, freq=this_freq_sample.tolist() ) # change array into list
        again to have correct formatting...
333
334 #   CREATE THE FIELD DATA FROM THE .NFF FILES
335
336 field_data_1 = actranvi.add_field_data(analysis=analysis_1,type='File Field Data')
337 actranvi.set_prop( field_data_1, field_ndim=2 )
338 actranvi.set_prop( field_data_1, name='U0' )
339 actranvi.set_prop( field_data_1, file_format='NFF' )
340 actranvi.set_prop( field_data_1, file='PandaSeasholtz_2DFlow_'+FieldInterp+'Mesh_'+
        FF_type+'_'+WhichFlowField+'.nff')
341
342 field_data_2 = actranvi.add_field_data(analysis=analysis_1,type='File Field Data',
        field_ndim=1)
343 actranvi.set_prop( field_data_2, name='P0' )
344 actranvi.set_prop( field_data_2, file_format='NFF' )
345 actranvi.set_prop( field_data_2, file='PandaSeasholtz_2DFlow_'+FieldInterp+'Mesh_'+
        FF_type+'_'+WhichFlowField+'.nff')
346
347 field_data_3 = actranvi.add_field_data(analysis=analysis_1,type='File Field Data',
```

```
    field_ndim=1)
actranvi.set_prop( field_data_3, name='rho0' )
actranvi.set_prop( field_data_3, file_format='NFF' )
actranvi.set_prop( field_data_3, file='PandaSeasholtz_2DFlow_'+FieldInterp+'Mesh_'+
    FF_type+'_'+WhichFlowField+'.nff')

field_data_4 = actranvi.add_field_data(analysis=analysis_1,type='File Field Data',
    field_ndim=1)
actranvi.set_prop( field_data_4, name='a0' )
actranvi.set_prop( field_data_4, file_format='NFF' )
actranvi.set_prop( field_data_4, file='PandaSeasholtz_2DFlow_'+FieldInterp+'Mesh_'+
    FF_type+'_'+WhichFlowField+'.nff')

#   PARAMETRISATION OF THE FLUID DOMAIN (acoustic_1)

acoustic_1 = actranvi.add_component(type='Finite Fluid', analysis=analysis_1)
actranvi.add( where=acoustic_1, what=domain_1 )

actranvi.set_prop( acoustic_1, mean_velocity=field_data_1 )
actranvi.set_prop( acoustic_1, mean_pressure=field_data_2 )
actranvi.set_prop( acoustic_1, mean_density=field_data_3 )
# actranvi.set_prop( acoustic_1, mean_sos=field_data_4 ) # avoid redundancy for
    robustness

fluid_material_1 = actranvi.add_material('Fluid Material')
actranvi.set_prop( fluid_material_1, cp=fluid_cp )
actranvi.set_prop( fluid_material_1, cv=fluid_cv )
actranvi.set_prop( acoustic_1, material=fluid_material_1 )

#   PARAMETRISATION OF THE INFINITE DUCT BC (numerical_duct_1)

numerical_duct_1 = actranvi.add_component(type='Modal Duct (numerical)', analysis=
    analysis_1)
actranvi.add( where=numerical_duct_1, what=domain_2 )
actranvi.set_prop( numerical_duct_1, material=fluid_material_1 )
actranvi.compute_duct_center( node=numerical_duct_1 )
actranvi.compute_duct_axes( node=numerical_duct_1 )
actranvi.set_prop( numerical_duct_1, visible=True )
actranvi.compute_duct_reverse_propagation_axis( node=numerical_duct_1 )
actranvi.compute_duct_geometrical_parameters( node=numerical_duct_1 )

propagating_mode = actranvi.add_propagating_mode( duct=numerical_duct_1)
actranvi.set_prop( propagating_mode, direction=-1 )
actranvi.set_prop( propagating_mode, frange=True )
actranvi.set_prop( propagating_mode, min_freq=0.0 )
actranvi.set_prop( propagating_mode, max_freq=10*np.amax(np.array(freq_sample)).tolist()
    ) # set maximum frequency at least 1.5 times the maximal frequency of analysis
actranvi.set_prop( propagating_mode, format='Free' )
actranvi.set_prop( propagating_mode, offset=0.0 )
actranvi.set_prop( numerical_duct_1, mean_velocity=u0j )

if FF_type=='IE':

  #   CREATION OF A TRANSITION DOMAIN PARAMETRISED WITHOUT FIELD DATA (acoustic_2) TO
    ENABLE OUT OF THE SOURCE COMPUTATION (Cesar's 'divide et impera' - 17/06/20)

```

```
396   acoustic_2 = actranvi.add_component(type='Finite Fluid', analysis=analysis_1)
397   actranvi.add( where=acoustic_2, what=domain_3_trans )
398
399   actranvi.set_prop( acoustic_2,
400                   mean_velocity=[u0inf, 0],
401                   mean_pressure=p0,
402                   mean_density = rho0inf,
403                   material = fluid_material_1,
404                   power_evaluation=0,
405                   incident_scattered_evaluation=1 )
406
407
408   #   PARAMETRISATION OF THE INFINITE ELEMENT BC (infinite_acoustic_1)
409
410   infinite_acoustic_1 = actranvi.add_component(type='Infinite Fluid', analysis=analysis_1
      )
411   actranvi.add( where=infinite_acoustic_1, what=domain_3 )
412   actranvi.set_prop( infinite_acoustic_1, material=fluid_material_1 )
413   # actranvi.set_prop( infinite_acoustic_1, center=np.array(source_pos).tolist() ) #
      precise here the center for the chosen source
414   actranvi.compute_infinite_fluid_center( node=infinite_acoustic_1 ) # let Actran compute
       the source position
415   actranvi.set_prop( infinite_acoustic_1, axes=[[np.sign(u0inf+ np.finfo(float).eps )
      *1.0, 0.0], [0.0, 1.0]] ) # add epsilon so that the axis is always well-defined. Axes
       must be oriented in the flow direction, so that the flow velocity is always positive
       wrt. the axis.
416   actranvi.set_prop( infinite_acoustic_1, mean_velocity= np.abs(u0inf) ) # AMBIENT MEAN-
      FLOW (working)
417   # actranvi.set_prop( infinite_acoustic_1, mean_velocity= 'AUTO' ) # AMBIENT MEAN-FLOW (
      working)
418   actranvi.set_prop( infinite_acoustic_1, interp_order=InfiniteElemInterpOrder ) #
      increase the order (<100) may reduce the reflection at the BC
419
420 elif FF_type=='PML':
421
422   #   CREATION OF THE PML BOUNDARY CONDITION (pml_1)
423
424   pml_1 = actranvi.add_component(type='PML', analysis=analysis_1)
425   actranvi.set_prop( pml_1, material=fluid_material_1 )
426   actranvi.add( where=pml_1, what=domain_3 )
427   # actranvi.set_prop( pml_1, center=np.array(source_pos).tolist() ) # let Actran compute
       the source position
428
429   if UniformFlowInPML:
430     # UNIFORM MEAN FLOW IN PML
431     ### auto velocity definition:
432     # actranvi.set_prop( pml_1, mean_velocity="AUTO" )
433     # actranvi.set_prop( pml_1, auto_direction=[1.0, 0.0] )
434     ### manual velocity definition:
435     actranvi.set_prop( pml_1, mean_velocity=[u0inf, 0] )
436     #
437     actranvi.set_prop( pml_1, mean_pressure=p0)
438     actranvi.set_prop( pml_1, mean_density=rho0inf )
439     # actranvi.set_prop( pml_1, mean_sos=a0inf ) # avoid redundancy for robustness
440   else:
441     print ("THIS IS NOT SUPPORTED BY ACTRAN YET - 05/06/20")
```

```
442     # FLOW FROM FIELD DATA
443     actranvi.set_prop( pml_1, mean_velocity=field_data_1 )
444     actranvi.set_prop( pml_1, mean_pressure=field_data_2 )
445     actranvi.set_prop( pml_1, mean_density=field_data_3 )
446     # actranvi.set_prop( pml_1, mean_sos=field_data_4 ) # avoid redundancy for robustness
447
448   #   CREATION OF THE NRBC AT THE PML OUTER-SKIN (non_reflecting_bc_1)
449
450   non_reflecting_bc_1 = actranvi.add_bc(type='Non Reflecting Boundary', analysis=
        analysis_1)
451   actranvi.add( where=non_reflecting_bc_1, what=domain_4 )
452
453 #   CREATION OF THE ACOUSTIC SOURCE
454
455 if source_type=='planar':
456   # PLANAR SOURCE
457   source_1 = actranvi.add_bc(type='Source (planar)', analysis=analysis_1)
458   actranvi.set_prop( source_1, direction=(-np.array(source_pos)/R).tolist() ) # unitary
        inward propagation direction
459 elif source_type=='cylindrical':
460   # CYLINDRICAL SOURCE
461   source_1 = actranvi.add_bc(type='Source (cylindrical)', analysis=analysis_1)
462   actranvi.set_prop( source_1, name='AcousticMonopole' )
463   actranvi.set_prop( source_1, amplitude_type='P' )
464
465 actranvi.set_prop( source_1, origin=np.array(source_pos).tolist() )
466 actranvi.set_prop( source_1, amplitude=SourceAmplitude )
467
468
469 #   DEFINITION OF THE SOLVER
470
471 mumps = actranvi.add_solver(analysis=analysis_1,type='Mumps')
472
473 #   ADD FIELD MAP
474
475 field_map_1 = actranvi.add_field_map(analysis=analysis_1)
476 actranvi.add( where=field_map_1, what=domain_0 )
477 actranvi.add( where=field_map_1, what=domain_1 )
478 actranvi.add( where=field_map_1, what=domain_2 )
479 actranvi.add( where=field_map_1, what=domain_3 )
480 if FF_type=='IE':
481   actranvi.add( where=field_map_1, what=domain_3_trans )
482 elif FF_type=='PML':
483   actranvi.add( where=field_map_1, what=domain_4 )
484 actranvi.set_prop( field_map_1, format='NFF' )
485 actranvi.set_prop( field_map_1, result_name='Acoustic_MovingFluid_'+FieldInterp+'Elem_'+
      WhichFlowField+'_'+source_type+'Source_'+str(int(incommingWaveAngle))+'deg_R='+str(
      int(R)))
486 actranvi.set_prop( field_map_1, step=1 )
487
488 #   EXPORT THE ANALYSIS
489
490 actranvi.write_analysis( analysis=analysis_1, file='PandaSeasholtz2D_'+FieldInterp+'Elem_
      '+WhichFlowField+'_'+source_type+'Source_'+FF_type+'_'+str(int(incommingWaveAngle))+'
      deg_R='+str(int(R))+'.edat', format='edat' )
491
```

```
#-----------------------------------------------------------
#    LAUNCH THE ANALYSIS
#-----------------------------------------------------------

analysis_1 = actranvi.read_analysis(file='PandaSeasholtz2D_'+FieldInterp+'Elem_'+
    WhichFlowField+'_'+source_type+'Source_'+FF_type+'_'+str(int(incommingWaveAngle))+'
    deg_R='+str(int(R))+'.edat',  type='ACTRAN' )

if FF_type=='IE':
  actranvi.run_analysis(analysis=analysis_1, memory=memoryReguirement_MB, working_dir=
    res_path)
elif FF_type=='PML':
  actranvi.run_analysis(analysis=analysis_1, memory=memoryReguirement_MB , options=u'-e
    distance', working_dir=res_path) # prior computations with '-e distance' when PML are
     jointly considered with mixed BC
  edat2run = os.path.join(res_path,'PandaSeasholtz2D_'+FieldInterp+'Elem_'+WhichFlowField
    +'_'+source_type+'Source_'+FF_type+'_'+str(int(incommingWaveAngle))+'deg_R='+str(int(
    R))+'.edat')
  os.system('cd '+res_path+'&& actranpy -i '+edat2run+' -e distance && actranpy -i '+
    edat2run+' -m '+str(memoryReguirement_MB ))

#-----------------------------------------------------------
#    GO BACK TO INITIAL PATH AND CLEAR ANALYSIS
#-----------------------------------------------------------

actranvi.clear_all() # clear analysis to enable another analysis to start afterward
os.chdir(current_path) # go back to initial directory
```

G Two congresses held at E.C.L.

"*If I have seen further it is by standing on the shoulders of Giants.*" (Newton, 1675)

Flow acoustics 1994

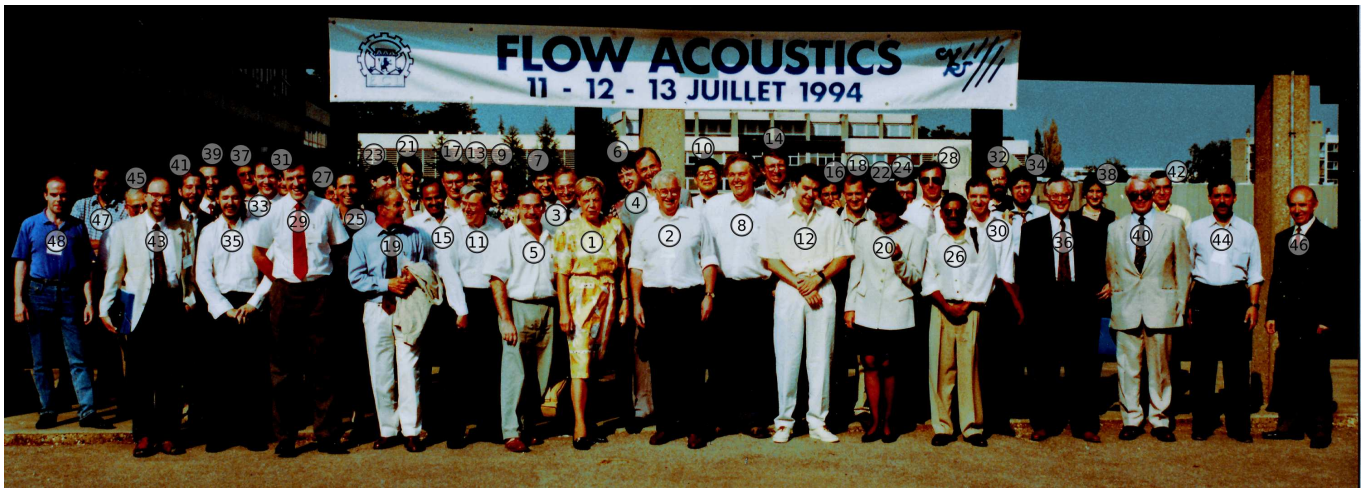

1. Geneviève Comte-Bellot (E.C.L.)
2. John E. Ffowcs-Williams (Univ. Cambridge)
3. Geoffrey M. Lilley (Univ. Southampton)
4. F. R. Grosche (D.L.R.)
5. Giles Robert (E.C.L.)
6. P. Sijtsma
7.
8. Willi Möhring
9. A. Witkowska (E.C.L.)
10.
11. W. G. Richarz (Univ. Carleton)
12.
13.
14. R. L. Panton (Univ. Texas)
15. Sanjiva K. Lele (Stanford Univ.)
16.
17. Christophe Bailly (E.D.F.-E.C.P.)
18.
19.
20. Ann P. Dowling (Univ. Cambridge)
21. François Bastin (E.D.F.-D.E.R.)
22.
23. S. Guerrand
24. Philippe Blanc-Benon (E.C.L.)
25. Ricardo E. Musafir
26. A. Krothapalli (Univ. Florida)
27.
28. Edmond Bennarous
29. Philip A. Nelson (I.S.V.R.)
30.
31.
32. V. F. Kopier (TsAgi)
33.
34. Michel Sunyach (E.C.L.)
35.
36.
37.
38.
39.
40.
41. B. E. Mitchell (Stanford Univ.) (?)
42. Th. Faure
43.
44. O. Knio
45.
46.
47.
48.


FLOW ACOUSTICS
11 - 12 - 13 JUILLET 1994

IUTAM 1985

1. Geneviève Comte-Bellot (E.C.L.)
2. John E. Ffowcs-Williams (Univ. Cambridge)
3.
4. Daniel Juvé (E.C.L.)
5. A. R. George (Cornell University, New-York)
6. R. Perret (Alsthom - Grenoble)
7. Giles Robert (E.C.L)
8.
9. F. N. D'Ambra (Aérospatiale - Marignane)
10. Sjoerd W. Rienstra (National Aerospace Lab - Amsterdam)
11.
12. E. Luzzato (E.D.F. - Clamart)
13. Michel Roger (E.C.L.)
14. P. J. T. Filippi (L.M.A. - Marseille)
15. F. Farassat (N.A.S.A. Langley Research Center)
16. Michel Sunyach (E.C.L.)
17.
18. C. Ross (Topexpress - Cambridge)
19. Ann Patricia Dowling (Univ. Cambridge)
20. E. Acton (Topexpress - Cambridge)
21. K. Schaaf (Physikalisches Instit. - Göttingen)
22. Philippe Esparcieux (DCAN - Toulon)
23. E. J. Kerschen (Univ. Arizona - Tucson)
24.
25. F. R. Grosche (D.F.V.L.R. Gottinger & V.K.I.)
26. S. Narayanan (T.U. Berlin – R.F.A.)
27. R. J. Hansen (Naval Research Lab. - Washington D.C.)
28. S. H. Ko (Dept. Navy – New London)
29. E. Benarrous (Metraflu - Écully)
30. D. Bechert (D.F.V.L.R. Berliner – R.F.A.)
31. J. Delcambre (E.D.F. - Clamart)
32. M. Chosson (Brüel et Kjaer - Bron)
33. M. C. Welsh (C.S.I.R.O. - Highett)
34. A. Laake (Max-Planck Instit. - Göttingen)
35. M. Sevik (David Taylor Naval Ship - Maryland)
36.
37. Julian Scott (Topexpress - Cambridge)
38. Frank Obermeier (Max-Planck Instit. - Göttingen)
39. W. Richarz (Univ. Ottawa)
40.
41.
42. J. A. Fitzpatrick (Trinity College - Dublin)
43. J. Hardin (N.A.S.A. Langley Research Center)
44. P. Leehey (Office of Naval Research - London)
45.
46.
47.
48. D. C. Hill (Univ. Cambridge)
49. Ernst-August Müller (Max-Planck Instit. - Göttingen)
50. Alan Powell (David Taylor Naval Ship - Maryland)
51. Willi Möhring (Max-Planck Instit. - Göttingen)
52.
53. M. Bruneau (L.A.U.M.)
54.
55. G. E. A. Meier (Max-Planck Instit. - Göttingen)
56. E. Brocher (I.M.F.M - Marseille)
57.
58.
59. Ph. A. Nelson (I.S.V.R. - Southampton)
60. C. M. Ho (Univ. Southern California)
61. J. C. Rebillat (C.E.A.T. - Poitiers)
62.
63.
64.
65. J. R. Mahan (Virginia Polytechnic Inst.)
66.
67. Sébastien Candel (O.N.E.R.A. - Chatillon)
68. Harold Lévine (Univ. Stanford)
69. A. Michalke (T.U. Berlin – R.F.A.)
70.
71. A. Garcia (Thomson C.S.F. - Cagnes sur mer)
72. Jadi (?)
73. Jacques Haertig (I.S.L. - Saint-Louis)
74. A. Petitjean (E.D.F. - Clamart)
75. Mohammed Sidki (E.C.L.)
76. Donald B. Hanson (Hamilton standard - Connecticut)
77.
78. Patrick Huerre (Univ. Southern California)
79.
80. J. Piraux (L.M.A. - Marseille)
81. David George Crighton (Univ. Leeds)
82.
83.
84. P. Esposito (E. D. F. - Clamart)
85. J. M. Auger (U. T. C. - Compiègne)
86. J. M. Ville (U. T. C. - Compiègne)
87. Véronique Villouvier (E.D.F. - Clamart)
88. M. A. Hamdi (U. T. C. - Compiègne)
89. G. Borrello (C. N. E. S. - Evry)
90. J. Daniel Reber (TechnicAtome - Cadarache)
91. William K. Blake (David Taylor Naval Ship - Maryland)

Bibliography

Afsar, M. Z. (2009). Solution of the parallel shear layer Green's function using conservation equations. *International Journal of Aeroacoustics*, 8(6):585–602.

Afsar, M. Z. (2010). Asymptotic properties of the overall sound pressure level of subsonic jet flows using isotropy as a paradigm. *Journal of Fluid Mechanics*, 664:510–539.

Afsar, M. Z. (2012). Insight into the two-source structure of the jet noise spectrum using a generalized shell model of turbulence. *European Journal of Mechanics-B/Fluids*, 31:129–139.

Afsar, M. Z., Dowling, A. P., and Karabasov, S. A. (2006). Comparison of jet noise models. In *12th AIAA/CEAS Aeroacoustics Conference*, Cambridge, Massachusetts. AIAA Paper 2006-2593.

Afsar, M. Z., Dowling, A. P., and Karabasov, S. A. (2007). Jet noise in the 'zone of silence'. In *13th AIAA/CEAS Aeroacoustics Conference*, Rome. AIAA Paper 2007-3606.

Afsar, M. Z., Leib, S. J., and Bozak, R. F. (2017a). Effect of de-correlating turbulence on the low frequency decay of jet-surface interaction noise in sub-sonic unheated air jets using a CFD-based approach. *Journal of Sound and Vibration*, 386:177–207.

Afsar, M. Z., Sescu, A., and Leib, S. J. (2016a). Predictive capability of low frequency jet noise using an asymptotic theory for the adjoint vector Green's function in non-parallel flow. In *22nd AIAA/CEAS Aeroacoustics Conference*, Lyon. AIAA Paper 2016-2804.

Afsar, M. Z., Sescu, A., Sassanis, V., and Lele, S. K. (2017b). Supersonic jet noise predictions using a unified asymptotic approximation for the adjoint vector Green's function and LES data. In *23rd AIAA/CEAS Aeroacoustics Conference*, Denver, Colorado. AIAA Paper 2017-3030.

Afsar, M. Z., Sescu, A., Sassanis, V., Towne, A., Bres, G. A., and Lele, S. K. (2016b). Prediction of supersonic jet noise using non-parallel flow asymptotics and LES data within Goldstein's acoustic analogy. In *Proceedings of the Summer Program*, Center for Turbulence Research, pages 253–262.

Agarwal, A., Morris, P. J., and Mani, R. (2004). Calculation of sound propagation in nonuniform flows: Suppression of instability waves. *AIAA Journal*, 42(1):80–88.

Almeida, O. (2009). *Aeroacoustics of dual-stream jets with application to turbofan engines*. PhD thesis, Aeronautics Institute of Technology.

Alonso, J. S. and Burdisso, R. A. (2007). Green's functions for the acoustic field in lined ducts with uniform flow. *AIAA Journal*, 45(11):2677–2687.

Anderson Jr., J. D. (1997). *A history of aerodynamics*. Cambridge University Press, Cambridge Aerospace Series 8.

Andrews, D. G. and McIntyre, M. E. (1978). On wave-action and its relatives. *Journal of Fluid Mechanics*, 89(4):647–664.

Angeloski, A., Discacciati, M., Legendre, C., Lielens, G., and Huerta, A. (2014). Challenges for time and frequency domain aeroacoustic solvers. In *11th World Congress on Computational Mechanics (WCCM XI); 5th European Conference on Computational Mechanics (ECCM V); 6th European Conference on Computational Fluid Dynamics (ECFD VI): July 20-25, 2014, Barcelona, Spain*, pages 1–12.

Astley, R. J., Macaulay, G. J., Coyette, J.-P., and Cremers, L. (1998). Three-dimensional wave-envelope elements of variable order for acoustic radiation and scattering. Part I. Formulation in the frequency domain. *The Journal of the Acoustical Society of America*, 103(1):49–63.

Atvars, J., Schubert, L. K., and Ribner, H. S. (1965). Refraction of sound from a point source placed in an air jet. *The Journal of the Acoustical Society of America*, 37(1):168–170.

Azarpeyvand, M. (2008). *Some Aspects of RANS based jet noise prediction*. PhD thesis, University of Southampton, Institute of Sound and Vibration Research (ISVR).

Azarpeyvand, M. and Self, R. H. (2009). Improved jet noise modeling using a new time-scale. *The Journal of the Acoustical Society of America*, 126(3):1015–1025.

Bailly, C. and Bogey, C. (2003). Radiation and refraction of sound waves through a two-dimensional shear layer. In *Fourth computational aeroacoustics (CAA) workshop on benchmark problems. NASA/CP2004-212954*. Citeseer.

Bailly, C., Bogey, C., and Candel, S. (2010). Modelling of Sound Generation by Turbulent Reacting Flows. *International Journal of Aeroacoustics*, 9(4-5):461–489.

Bailly, C., Candel, S. M., and Lafon, P. (1996). Prediction of supersonic jet noise from a statistical acoustic model and a compressible turbulence closure. *Journal of Sound and Vibration*, 194(2):219–242.

Bailly, C. and Comte-Bellot, G. (2015). *Turbulence*. Experimental Fluid Mechanics. Springer, Switzerland.

Bailly, C., Lafon, P., and Candel, S. M. (1997). Subsonic and supersonic jet noise predictions from statistical source models. *AIAA Journal*, 35(11):1688–1696.

Bailly, C., Lafon, P., and Gandel, S. (1995). A stochastic approach to compute noise generation and radiation of free turbulent flows. In *1st AIAA/CEAS Aeroacoustics Conference*, pages 669–674, Munich. AIAA Paper 95-092.

Barber, T. J., Neudungadi, A., and Khavaran, A. (2001). Predicting the jet noise from high-speed round jets. In *39th AIAA Aerospace Sciences Meeting and Exhibit*, Reno, Nevada. AIAA Paper 2001-819.

Barcelo, C., Liberati, S., and Visser, M. (2011). Analogue gravity. *Living Reviews in Relativity*, 14(1):3.

Barone, M. F., Kalashnikova, I., Segalman, D. J., and Thornquist, H. K. (2009). Stable Galerkin reduced order models for linearized compressible flow. *Journal of Computational Physics*, 228(6):1932–1946.

Barone, M. F. and Lele, S. K. (2005). Receptivity of the compressible mixing layer. *Journal of Fluid Mechanics*, 540:301–335.

Bassetti, A. (2009). *A statistical jet-noise model based on the acoustic analogy and a RANS solution*. PhD thesis, University of Southampton, Institute of Sound and Vibration Research (ISVR).

Béchara, W., Bailly, C., Lafon, P., and Candel, S. M. (1994). Stochastic approach to noise modeling for free turbulent flows. *AIAA Journal*, 32(3):455–463.

Béchara, W., Lafon, P., Bailly, C., and Candel, S. M. (1995). Application of a κ-ε turbulence model to the prediction of noise for simple and coaxial free jets. *The Journal of the Acoustical Society of America*, 97(6):3518–3531.

Berenger, J.-P. (1994). A perfectly matched layer for the absorption of electromagnetic waves. *Journal of Computational Physics*, 114:185–200.

Berland, J., Bogey, C., Marsden, O., and Bailly, C. (2007). High-order, low dispersive and low dissipative explicit schemes for multiple-scale and boundary problems. *Journal of Computational Physics*, 224(2):637–662.

Berry, M. V. (1980). Some geometric aspects of wave motion: wavefront dislocations, diffraction catastrophes, diffractals. In *Proceedings of symposia in pure mathematics*, volume 36, pages 13–28. American Mathematical Society.

Berton, J. J. (2016). System noise prediction of the DGEN 380 turbofan engine. *Journal of Aircraft*, 53(6):1779–1786.

Bertschinger, E. (1999). *Hamiltonian dynamics of particle motion*. Massachusetts Institute of Technology - Physics 8.962. `http://web.mit.edu/edbert/GR/gr3.pdf`.

Bertschinger, E. (2002). *Symmetry Transformations, the Einstein-Hilbert Action, and Gauge Invariance*. Massachusetts Institute of Technology - Physics 8.962. `http://web.mit.edu/edbert/GR/gr5.pdf`.

Biondi, B. (1992). Solving the frequency-dependent eikonal equation. In *Technical Program Expanded Abstracts, Annual Meeting*, pages 1315–1319. Society of Exploration Geophysicists. `http://sepwww.stanford.edu/data/media/public/docs/sep73/biondo.ps.gz`.

Biot, M. A. and Tolstoy, I. (1957). Formulation of wave propagation in infinite media by normal coordinates with an application to diffraction. *The Journal of the Acoustical Society of America*, 29(3):381–391.

Blanchet, D. and Golota, A. (2014). Validation of a wind noise source characterization method for vehicle interior noise prediction. In *Proceedings of ISMA 2014 International Conference on Noise and Vibration Engineering, USD 2014 International Conference on Uncertainty in Structural Dynamics, Leuven*, pages 241–256.

Blokhintzev, D. I. (1946). The propagation of sound in an inhomogeneous and moving medium I. *The Journal of the Acoustical Society of America*, 18(2):322–328.

Blokhintzev, D. I. (1956). *Acoustics of a Nonhomogeneous Moving Medium*. National Advisory Committee for Aeronautics (NACA) Washington, D. C.

Bodard, G., Bailly, C., and Vuillot, F. (2009). Matched hybrid approaches to predict jet noise by using large eddy simulation. In *15th AIAA/CEAS Aeroacoustics Conference*, Miami, Florida. AIAA Paper 2009-3316.

Bogey, C. and Bailly, C. (2002). Three-dimensional non-reflective boundary conditions for acoustic simulations: far field formulation and validation test cases. *Acta Acoustica United with Acoustica*, 88:463–471.

Bogey, C. and Bailly, C. (2004). A family of low dispersive and low dissipative explicit schemes for flow and noise computations. *Journal of Computational Physics*, 194(1):194–214.

Bogey, C., Bailly, C., and Juvé, D. (2002). Computation of flow noise using source terms in linearized Euler's equations. *AIAA Journal*, 40(2):235–243.

Bojarski, N. N. (1983). Generalized reaction principles and reciprocity theorems for the wave equations, and the relationship between the time-advanced and time-retarded fields. *The Journal of the Acoustical Society of America*, 74(1):281–285.

Bonnet, A. and Luneau, J. (1989). *Théorie de la dynamique des fluides*. Cépaduès Éditions.

Brès, G. A. and Lele, S. K. (2019). Modelling of jet noise: a perspective from large-eddy simulations. *Philosophical Transactions of the Royal Society A*, 377(2159):20190081.

Bretherton, F. P. and Garrett, C. J. R. (1968). Wavetrains in inhomogeneous moving media. *Proceedings of the Royal Society of London. Series A. Mathematical and Physical Sciences*, 302(1471):529–554.

Brouwer, H. H. and Nijboer, R. J. (2005). Computation of fine-scale turbulence jet noise. Technical Report 053, Nationaal Lucht- en Rulmtevaartlaboratorlum (NLR).

Campos, L. M. B. C. (1988). On the generalizations of the Doppler factor, local frequency, wave invariant and group velocity. *Wave Motion*, 10(3):193–207.

Campos, L. M. B. C. and Serrão, P. G. T. A. (2013). On the discrete and continuous spectrum of acoustic-vortical waves. *International Journal of Aeroacoustics*, 12(7-8):743–781.

Candel, S. M. (1972). *Analytical studies of some acoustic problems of jet engines*. PhD thesis, California Institute of Technology.

Candel, S. M. (1975). Acoustic conservation principles and an application to plane and modal propagation in nozzles and diffusers. *Journal of Sound and Vibration*, 41(2):207–232.

Candel, S. M. (1977). Numerical solution of conservation equations arising in linear wave theory: application to aeroacoustics. *Journal of Fluid Mechanics*, 83(3):465–493.

Cantrell, R. H. and Hart, R. W. (1964). Interaction between sound and flow in acoustic cavities: Mass, momentum, and energy considerations. *The Journal of the Acoustical Society of America*, 36(4):697–706.

Casalino, D. (2012). Finite element solutions of a wave equation for sound propagation in sheared flows. *AIAA Journal*, 50(1):37–45.

Chapman, C. J. (2000). *High speed flow*, volume 23. Cambridge University Press.

Cheung, L. C., Pastouchenko, N. N., Mani, R., and Paliath, U. (2015). Fine-scale turbulent noise predictions from non-axisymmetric jets. *International Journal of Aeroacoustics*, 14(3-4):457–487.

Cho, Y. C. (1980). Reciprocity principle in duct acoustics. *The Journal of the Acoustical Society of America*, 67(5):1421–1426.

Chong, Y. D. (2016). Mh2801: Complex methods for the sciences. Technical report, Nanyang Technological University, Singapore. `http://www1.spms.ntu.edu.sg/~ydchong/teaching/10_greens_function.pdf`.

Chu, B.-T. and Kovásznay, L. S. G. (1958). Non-linear interactions in a viscous heat-conducting compressible gas. *Journal of Fluid Mechanics*, 3(5):494–514.

Clebsch, A. (1859). Über die Integration der hydrodynamischen Gleichungen. *Journal für die reine und angewandte Mathematik*, 56:1–10.

Crighton, D. G. and Leppington, F. G. (1970). Scattering of aerodynamic noise by a semi-infinite compliant plate. *Journal of Fluid Mechanics*, 43(4):721–736.

Crighton, D. G. and Leppington, F. G. (1971). On the scattering of aerodynamic noise. *Journal of Fluid Mechanics*, 46(3):577–597.

Crighton, D. G. and Leppington, F. G. (1973). Singular perturbation methods in acoustics: diffraction by a plate of finite thickness. *Proceedings of the Royal Society of London. Series A. Mathematical and Physical Sciences*, 335(1602):313–339.

Dahl, M. D. (2004). Fourth CAA workshop on benchmark problems. Technical Report 2004-212954, NASA.

Das, I. S., Khavaran, A., and Krejsa, E. A. (1997). A computational study of contoured plug-nozzle jet noise. *Journal of Sound and Vibration*, 206(2):169–194.

Davis, T. A. (2004). Algorithm 832: UMFPACK v4.3 an unsymmetric-pattern multifrontal method. *ACM Transactions on Mathematical Software (TOMS)*, 30(2):196–199.

Delfs, J. (2016). *Grundlagen der Aeroakustik (Basics of Aeroacoustics)*. WS 2016/2017 at Technische Universität Braunschweig. `https://dlr.de/as/Portaldata/5/Resources/dokumente/abteilungen/abt_ta/Notes_Basics_of_Aeroacoustics_Delfs.pdf`.

Depuru Mohan, N. K., Dowling, A. P., Karabasov, S. A., Xia, H., Graham, O., Hynes, T. P., and Tucker, P. G. (2015). Acoustic sources and far-field noise of chevron and round jets. *AIAA Journal*, 53(9):2421–2436.

Dezitter, F., Bezard, H., De Saint Victor, X., Zeggai, K., Britchford, K., Joubert, G., and Puigt, G. (2009). Installation effects characterization of VHBR engines part III: CFD assessment for jet mixing. In *15th AIAA/CEAS Aeroacoustics Conference*, Miami, Florida. AIAA Paper 2009-3370.

Di Francescantonio, P., Hirsch, C., Ferrante, P., and Isono, K. (2015). Side mirror noise with adaptive spectral reconstruction. Technical report, SAE Technical Paper.

Doak, P. E. (1954). Vorticity generated by sound. *Proceedings of the Royal Society of London. Series A. Mathematical and Physical Sciences*, 226(1164):7–16.

Doak, P. E. (1998). Fluctuating total enthalpy as the basic generalized acoustic field. *Theoretical and Computational Fluid Dynamics*, 10(1-4):115–133.

Dowling, A. P. (1983). Flow-acoustic interaction near a flexible wall. *Journal of Fluid Mechanics*, 128:181–198.

Dowling, A. P., Ffowcs Williams, J. E., and Goldstein, M. E. (1978). Sound production in a moving stream. *Philosophical Transactions of the Royal Society of London A: Mathematical, Physical and Engineering Sciences*, 288(1353):321–349.

Eastwood, S. J. and Tucker, P. G. (2011). Hybrid LES—RANS of complex geometry jets. *International Journal of Aeroacoustics*, 10(5-6):659–684.

ECAC (2016). Doc 29, 4th ed. "Report on standard method of computing noise contours around civil airports", volume 1: Applications guide. Technical report, DGCA/147.

Ehrenfried, K. (2004). *Strömungsakustik - Skript zur Vorlesung*. Mensch & Buch Verlag.

Eisler, T. J. (1969). An introduction to Green's functions. Technical report, Catholic University of America Washington DC Institute of Ocean Science and Engineering.

Engel, R. C., Silva, C. R. I., and Deschamps, C. J. (2014). Application of RANS-based method to predict acoustic noise of chevron nozzles. *Applied Acoustics*, 79:153–163.

Engquist, B. and Runborg, O. (2003). Computational high frequency wave propagation. *Acta numerica*, 12:181–266.

Euler, L. (1757). Principes généraux du mouvement des fluides. *Mémoires de l'Académie des Sciences de Berlin*, pages 274–315.

Euler, L. (1767). Éclaircissemens plus détaillés sur la génération et la propagation du son, et sur la formation de l'écho. *Mémoires de l'académie des sciences de Berlin*, pages 335–363.

Eversman, W. (1976). A reciprocity relationship for transmission in non-uniform hard walled ducts without flow. *Journal of Sound and Vibration*, 47(4):515–521.

Eversman, W. (2001). The boundary condition at an impedance wall in a non-uniform duct with potential mean flow. *Journal of Sound and Vibration*, 246(1):63–69.

Ewert, R. (2007). RPM - the fast Random Particle-Mesh method to realize unsteady turbulent sound sources and velocity fields for CAA applications. In *13th AIAA/CEAS Aeroacoustics Conference*, Rome. AIAA Paper 2007-3506.

Ewert, R. (2008). Broadband slat noise prediction based on CAA and stochastic sound sources from a fast random particle-mesh (RPM) method. *Computers & Fluids*, 37(4):369–387.

Ewert, R., Dierke, J., Siebert, J., Neifeld, A., Appel, C., Siefert, M., and Kornow, O. (2011). CAA broadband noise prediction for aeroacoustic design. *Journal of sound and vibration*, 330(17):4139–4160.

Ewert, R. and Schröder, W. (2003). Acoustic perturbation equations based on flow decomposition via source filtering. *Journal of Computational Physics*, 188(2):365–398.

Fedorchenko, A. T. (1997). A model of unsteady subsonic flow with acoustics excluded. *Journal of Fluid Mechanics*, 334:135–155.

Fedorchenko, A. T. (2000). On some fundamental flaws in present aeroacoustic theory. *Journal of Sound and Vibration*, 232(4):719–782.

Fernandez-Grande, E. and Jacobsen, F. (2014). Conservation of power of the supersonic acoustic intensity. *The Journal of the Acoustical Society of America*, 136(2):461–465.

Fernandez-Grande, E., Jacobsen, F., and Leclère, Q. (2012). Direct formulation of the supersonic acoustic intensity in space domain. *The Journal of the Acoustical Society of America*, 131(1):186–193.

Ffowcs Williams, J. E. and Hawkings, D. L. (1969). Sound generation by turbulence and surfaces in arbitrary motion. *Proceedings of the Royal Society of London. Series A. Mathematical and Physical Sciences*, 264(1151):321–342.

Fleury, V., Bailly, C., Jondeau, E., Michard, M., and Juvé, D. (2008). Space-time correlations in two subsonic jets using dual particle image velocimetry measurements. *AIAA Journal*, 46(10):2498–2509.

Floyd, E. R. (1990). Comments on "an exact ray theoretical formulation of the Helmholtz equation" [J. Acoust. Soc. Am. 86, 234–246 (1989)]. *The Journal of the Acoustical Society of America*, 88(5):2483–2483.

Foreman, T. L. (1989). An exact ray theoretical formulation of the Helmholtz equation. *The Journal of the Acoustical Society of America*, 86(1):234–246.

Fornberg, B. (1988). Generation of finite difference formulas on arbitrarily spaced grids. *Mathematics of computation*, 51(184):699–706.

Free Field Technologies, S. A. (2018a). *Actran 19.0 User's Guide Unified Graphical User Interface for Pre and Post-Processing*. MSC Software Company.

Free Field Technologies, S. A. (2018b). *Actran 19.0 User's Guide Volume 1 Installation, Operations, Theory and Utilities*. MSC Software Company.

Free Field Technologies, S. A. (2018c). *Actran 19.0 User's Guide Volume 2 Extended DAT (EDAT) Input File Syntax*. MSC Software Company.

Fuchs, L. (1873). Über Relationen, welche für die zwischen je zwei singulären Punkten erstreckten Integrale der Lösungen linearer Differentialgleichungen stattfinden. *Journal für die reine und angewandte Mathematik*, 76:177–213.

Gabard, G., Lefrancois, E., and Ben Tahar, M. (2004a). Aeroacoustic noise source simulations based on Galbrun's equation. In *10th AIAA/CEAS Aeroacoustics Conference*, Manchester. AIAA Paper 2004-2892.

Gabard, G., Treyssède, F., and Tahar, M. B. (2004b). A numerical method for vibro-acoustic problems with sheared mean flows. *Journal of Sound and Vibration*, 272(3-5):991–1011.

Gainville, O. (2008). *Modélisation de la propagation atmosphérique des ondes infrasonores par une méthode de tracé de rayons non linéaire*. PhD thesis, École centrale de Lyon, Laboratoire de Mécanique des Fluides et d'Acoustique (LMFA).

Galbrun, H. (1931). *Propagation d'une onde sonore dans l'atmosphère et théorie des zones de silence*. Gauthier-Villars et Cie., Éditeurs, Libraires du Bureau des longitudes, de l'École polytechnique.

Garrett, C. J. R. (1967). Discussion: the adiabatic invariant for wave propagation in a nonuniform moving medium. *Proceedings of the Royal Society of London. Series A. Mathematical and Physical Sciences*, 299(1456):26–27.

Giles, M. B. and Pierce, N. A. (1997). Adjoint equations in CFD: duality, boundary conditions and solution behaviour. In *13th Computational Fluid Dynamics Conference*, Snowmass Village, Colorado. AIAA Paper 1997-1850.

Godin, O. A. (1997). Reciprocity and energy theorems for waves in a compressible inhomogeneous moving fluid. *Wave Motion*, 25:143–167.

Godin, O. A. and Voronovich, A. G. (2004). Fermat's principle for non–dispersive waves in non–stationary media. *Proceedings of the Royal Society of London. Series A: Mathematical, Physical and Engineering Sciences*, 460(2046):1631–1647.

Goldstein, M. E. (1976). *Aeroacoustics*. New York, McGraw-Hill International Book Co.

Goldstein, M. E. (1978). Unsteady vortical and entropic distortions of potential flows round arbitrary obstacles. *Journal of Fluid Mechanics*, 89(3):433–468.

Goldstein, M. E. (1982). High frequency sound emission from a moving point multipole sources embedded in arbitrary transversely sheared mean flows. *Journal of Sound and Vibration*, 80(4):499–522.

Goldstein, M. E. (2002). A unified approach to some recent developments in jet noise theory. *International Journal of aeroacoustics*, 1(1):1–16.

Goldstein, M. E. (2003). A generalized acoustic analogy. *Journal of Fluid Mechanics*, 488:315–333.

Goldstein, M. E. (2005a). Ninety-degree acoustic spectrum of a high speed air jet. *AIAA Journal*, 43(1):96–102.

Goldstein, M. E. (2005b). On identifying the true sources of aerodynamic sound. *Journal of Fluid Mechanics*, 526:337.

Goldstein, M. E. (2006). Hybrid Reynolds-averaged Navier-Stokes/large eddy simulation approach for predicting jet noise. *AIAA Journal*, 44(12):3136–3142.

Goldstein, M. E. (2010). Relation between the generalized acoustic analogy and Lilley's contributions to aeroacoustics. *International Journal of Aeroacoustics*, 9(4-5):401–418.

Goldstein, M. E. and Khavaran, A. (2005). Acoustic source modeling for high speed air jets. In *39th AIAA Aerospace Sciences Meeting and Exhibit*, Reno, Nevada. AIAA Paper 2001-415.

Goldstein, M. E., Khavaran, A., and Musafir, R. E. (2005a). Jet noise predictions based on two different forms of Lilley's equation, Part 1: Basic theory. In *INTER-NOISE and NOISE-CON Congress and Conference Proceedings*, number 8 in 2005, pages 278–287. Institute of Noise Control Engineering.

Goldstein, M. E., Khavaran, A., and Musafir, R. E. (2005b). Jet noise predictions based on two different forms of Lilley's equation, Part 2: Acoustic predictions and comparison with data. In *INTER-NOISE and NOISE-CON Congress and Conference Proceedings*, number 8 in 2005, pages 269–277. Institute of Noise Control Engineering.

Goldstein, M. E. and Leib, S. J. (2008). The aeroacoustics of slowly diverging supersonic jets. *Journal of Fluid Mechanics*, 600:291–337.

Goldstein, M. E. and Leib, S. J. (2018). Azimuthal source noncompactness and mode coupling in sound radiation from high-speed axisymmetric jets. *AIAA Journal*, 56(10):3915–3925.

Goldstein, M. E., Sescu, A., and Afsar, M. Z. (2012). Effect of non-parallel mean flow on the Green's function for predicting the low-frequency sound from turbulent air jets. *Journal of Fluid Mechanics*, 695:199–234.

Golubev, V. V. and Atassi, H. M. (1998). Acoustic-vorticity waves in swirling flows. *Journal of Sound and Vibration*, 209(2):203–222.

Gottlieb, P. (1959). *Acoustics in moving media*. PhD thesis, Massachusetts Institute of Technology.

Gradshteyn, I. S. and Ryzhik, I. M. (1963). *Table of integrals, series, and products (in Russian)*. [sn].

Grande, E. (1965). Refraction of injected sound by a very cold nitrogen jet. *The Journal of the Acoustical Society of America*, 38(6):1063–1064.

Gréverie, L. and Bailly, C. (1998). Construction d'un opérateur de propagation à partir des équations d'euler linéarisées. *Comptes Rendus de l'Académie des Sciences-Series IIB-Mechanics-Physics-Astronomy*, 326(11):741–746.

Gryazev, V. and Karabasov, S. A. (2018). Comparison of two Goldstein acoustic analogy implementations with the Tam&Auriault model for heated and unheated jet noise prediction. In *24th AIAA/CEAS Aeroacoustics Conference*, Atlanta, Georgia. AIAA Paper 2018-2828.

Gryazev, V., Markesteijn, A. P., and Karabasov, S. A. (2018). Temperature effect on the apparent position of effective noise sources in a hot jet. In *24th AIAA/CEAS Aeroacoustics Conference*, Atlanta, Georgia. AIAA Paper 2018-2827.

Hardin, J. C. and Pope, D. S. (1994). An acoustic/viscous splitting technique for computational aeroacoustics. *Theoretical and computational fluid dynamics*, 6(5-6):323–340.

Hascher, X. and Papadopoulos, A. (2015). *Leonhard Euler: Mathématicien, physicien et théoricien de la musique*. CNRS Éditions.

Hayes, W. D. (1968). Energy invariant for geometric acoustics in a moving medium. *The Physics of Fluids*, 11(8):1654–1656.

Hayes, W. D. (1970a). Conservation of action and modal wave action. *Proceedings of the Royal Society of London. Series A. Mathematical and Physical Sciences*, 320:187–208.

Hayes, W. D. (1970b). Kinematic wave theory. *Proceedings of the Royal Society of London. Series A. Mathematical and Physical Sciences*, 320:209–226.

Hecht, F. (2012). New development in FreeFem++. *Journal of Numerical Mathematics*, 20(3-4):251–265. `https://freefem.org/`.

Helmholtz, H. (1858). Über Integrale der hydrodynamischen Gleichungen, welche den Wirbelbewegung entsprechen. *Journal für die reine und angewandte Mathematik*, 55:25–55.

Helmholtz, H. (1860). Theorie der Luftschwingungen in Röhren mit offenen Enden. *Journal für die reine und angewandte Mathematik*, 57:1–72.

Henry, C., Bailly, C., and Bodard, G. (2012). Statistical modeling of BBSAN including refraction effects. In *18th AIAA/CEAS Aeroacoustics Conference*, Colorado Springs, Colorado. AIAA Paper 2012-2163.

Hill, D. C. (1995). Adjoint systems and their role in the receptivity problem for boundary layers. *Journal of Fluid Mechanics*, 292:183–204.

Hirschberg, A. (2009). *Introduction to aero-acoustics of internal flow*. Lecture series - von Karman Institute for fluid dynamics.

Hirschberg, A., Aurégan, Y., and Pelorson, X. (2018). Contributions of bram wijnands to experimental aeroacoustics, part I: from supersonic jet screech to human voiced soundsproduction. In *14ème Congrès Français d'Acoustique (CFA)*.

Howe, M. S. (1975a). Contributions to the theory of aerodynamic sound, with application to excess jet noise and the theory of the flute. *Journal of Fluid Mechanics*, 71(4):625–673.

Howe, M. S. (1975b). The generation of sound by aerodynamic sources in an inhomogeneous steady flow. *Journal of Fluid Mechanics*, 67(3):597–610.

Hu, F. Q. (2005). A Perfectly Matched Layer absorbing boundary condition for linearized Euler equations with a non-uniform mean flow. *Journal of Computational Physics*, 208(2):469–492.

Hu, F. Q. (2008). Development of PML absorbing boundary conditions for computational aeroacoustics: A progress review. *Computers & Fluids*, 37(4):336–348.

Huber, J., Drochon, C., Pintado-Peno, A., Cléro, F., and Bodard, G. (2014). Large-scale jet noise testing, reduction and methods validation "EXEJET": 1. project overview and focus on installation. In *20th AIAA/CEAS Aeroacoustics Conference*, Atlanta, Georgia. AIAA Paper 2014-3032.

Ilário, C. R. S., Azarpeyvand, M., Rosa, V., Self, R. H., and Meneghini, J. R. (2017). Prediction of jet mixing noise with Lighthill's acoustic analogy and geometrical acoustics. *The Journal of the Acoustical Society of America*, 141(2):1203–1213.

Jameson, A. (1988). Aerodynamic design via control theory. *Journal of Scientific Computing*, 3(3):233–260.

Johnson, S. G. (2010). Notes on perfectly matched layers (PMLs). Technical report, Massachusetts Institute of Technology. http://math.mit.edu/~stevenj/18.369/pml.pdf.

Kaltenbacher, M., Hüppe, A., Reppenhagen, A., and Kühnel, W. (2015). Coupled CFD-CAA approach for rotating systems. In *COUPLED VI: proceedings of the VI International Conference on Computational Methods for Coupled Problems in Science and Engineering*, pages 524–531. CIMNE.

Kaltenbacher, M., Hüppe, A., Wohlmuth, B., and Kühnelt, H. (2013). Coupling acoustic perturbation equations and Pierce wave equation for computational aeroacoustics. In *19th AIAA/CEAS Aeroacoustics Conference*, Berlin. AIAA Paper 2013-2169.

Kalyan, A. and Karabasov, S. A. (2017). Broad band shock associated noise predictions in axisymmetric and asymmetric jets using an improved turbulence scale model. *Journal of Sound and Vibration*, 394:392–417.

Karabasov, S. A., Afsar, M. Z., Hynes, T. P., Dowling, A. P., McMullan, W. A., Pokora, C. D., Page, G. J., and McGuirk, J. J. (2010). Jet noise: acoustic analogy informed by large eddy simulation. *AIAA Journal*, 48(7):1312–1325.

Karabasov, S. A., Bogey, C., and Hynes, T. P. (2013). An investigation of the mechanisms of sound generation in initially laminar subsonic jets using the Goldstein acoustic analogy. *Journal of Fluid Mechanics*, 714:24–57.

Karabasov, S. A. and Hynes, T. P. (2005). An efficient frequency-domain algorithm for wave scattering problems in application to jet noise. In *11th AIAA/CEAS Aeroacoustics Conference*, Monterey, California. AIAA Paper 2005-2827.

Karabasov, S. A., Hynes, T. P., and Dowling, A. P. (2007). Effect of mean-flow evolution on sound propagation through non-uniform jet flows. In *13th AIAA/CEAS Aeroacoustics Conference*, Rome. AIAA Paper 2007-3655.

Karabasov, S. A. and Sandberg, R. D. (2015). Influence of free stream effects on jet noise generation and propagation within the Goldstein acoustic analogy approach for fully turbulent jet inflow boundary conditions. *International Journal of Aeroacoustics*, 14(3-4):413–429.

Khalighi, Y., Mani, A., Ham, F., and Moin, P. (2010). Prediction of sound generated by complex flows at low mach numbers. *AIAA Journal*, 48(2):306–316.

Khavaran, A. (1999). Role of anisotropy in turbulent mixing noise. *AIAA Journal*, 37(7):832–841.

Khavaran, A. and Bridges, J. (2005). Modelling of fine-scale turbulence mixing noise. *Journal of Sound and Vibration*, 279(3-5):1131–1154.

Khavaran, A., Georgiadis, N. J., Bridges, J., and Dippold, V. F. (2005). Effect of free jet on refraction and noise. In *11th AIAA/CEAS Aeroacoustics Conference*, Monterey, California. AIAA Paper 2005-2941.

Khavaran, A. and Kenzakowski, D. C. (2007). Progress toward improving jet noise predictions in hot jets. In *45th AIAA Aerospace Sciences Meeting and Exhibit*, Reno, Nevada. AIAA Paper 2007-12.

Khavaran, A., Krejsa, E. A., and Kim, C. M. (1994). Computation of supersonic jet mixing noise for an axisymmetric convergent-divergent nozzle. *Journal of Aircraft*, 31(3):603–609.

Klainerman, S. and Majda, A. (1982). Compressible and incompressible fluids. *Communications on Pure and Applied Mathematics*, 35:629–651.

Kline, M. (1990). *Mathematical Thought From Ancient to Modern Times*, volume 2. Oxford University Press.

Lafitte, A., Le Garrec, T., Bailly, C., and Laurendeau, E. (2012). Prediction of subsonic jet noise relying on a sweeping based turbulence generation process. In *18th AIAA/CEAS Aeroacoustics Conference*, Colorado Springs, Colorado. AIAA Paper 2012-2149.

Lagrange, J. L. (1761). Nouvelles recherches sur la nature et la propagation du son. *Oeuvres*, 1:151–332.

Lagrange, J. L. (1781). Mémoire sur la théorie du mouvement des fluides. *Oeuvres*, 4:695–748.

Lamb, H. (1879). *Hydrodynamics*, volume 6th edition, 1st american edition 1945. Dover, New York.

Lamb Jr., G. L. (1995). *Introductory applications of partial differential equations: with emphasis on wave propagation and diffusion*. John Wiley & Sons.

Lanczos, C. (1996). *Linear differential operators*. Society for Industrial and Applied Mathematics (SIAM).

Landau, L. D. and Lifshitz, E. M. (1951). *Course of theoretical physics. vol. 2: The Classical Theory of Fields*. London.

Landau, L. D. and Lifshitz, E. M. (1959). *Course of theoretical physics. vol. 6: Fluid mechanics*. London.

Lappas, T., Leonard, A., and Dimotakis, P. E. (1999). Riemann invariant manifolds for the multidimensional Euler equations. *SIAM Journal on Scientific Computing*, 20(4):1481–1512.

Legendre, C. (17/07/2019). Free Field Technologies, communication via e-mail.

Legendre, C. (2014). *On the interactions of sound waves and vortices*. PhD thesis, Université Libre de Bruxelles.

Legendre, C., de Brye, B., Detandt, Y., Lielens, G., and Van den Nieuwenhof, B. (2018). On the effects of vorticity on the acoustic field through a scalar operator based on total enthalpy terms. In *INTER-NOISE and NOISE-CON Congress and Conference Proceedings*, pages 105–112. Institute of Noise Control Engineering.

Legendre, C., de Brye, B., Subramaniyam, S., Ganty, B., Detandt, Y., and Bailly, C. (2016). Towards large aeroacoustic applications through a hybrid approach based on the linearized euler equations. In *23rd International Congress on Sound and Vibration (ICSV)*.

Legendre, C., Lielens, G., and Coyette, J.-P. (2012). Sound propagation in a sheared flow based on fluctuating total enthalpy as a generalized acoustic variable. In *INTER-NOISE and NOISE-CON Congress and Conference Proceedings*, pages 5557–5562. Institute of Noise Control Engineering.

Leib, S. J. (2013). Noise predictions for rectangular jets using a conformal mapping method. *AIAA Journal*, 51(3):721–737.

Leib, S. J. and Goldstein, M. E. (2011). Hybrid source model for predicting high-speed jet noise. *AIAA Journal*, 49(7):1324–1335.

Lele, S. K. and Nichols, J. W. (2014). A second golden age of aeroacoustics? *Philosophical Transactions of the Royal Society A: Mathematical, Physical and Engineering Sciences*, 372(2022):20130321.

Lempereur, P. (2018). Aviation noise research policy, Airframer view (Airbus). Workshop on EU Aviation Research Policy on Noise, 16-17 January 2018, Covent Garden Building, Brussels.

Levine, H. and Schwinger, J. (1948). On the radiation of sound from an unflanged circular pipe. *Physical Review*, 73(4):383–406.

Li, X. D., Gao, J. H., Eschricht, D., and Thiele, F. (2004). Numerical computation of the radiation and refraction of sound waves through a two dimensional shear layer. In *NASA CP Paper*, 2004-212954.

Lielens, G. (11/09/2019). Free Field Technologies, personnal communication, Mont-Saint-Guibert.

Lighthill, M. J. (1952). On sound generated aerodynamically I. General theory. In *Proceedings of the Royal Society of London. Series A. Mathematical and Physical Sciences*, volume 1107, pages 564–587. The Royal Society London.

Lighthill, M. J. (1954). On sound generated aerodynamically II. Turbulence as a source of sound. In *Proceedings of the Royal Society of London. Series A. Mathematical and Physical Sciences*, volume 1148, pages 1–32. The Royal Society London.

Lighthill, M. J. (1962). The bakerian lecture, 1961 sound generated aerodynamically. *Proceedings of the Royal Society of London. Series A. Mathematical and Physical Sciences*, 267(1329):147–182.

Lighthill, M. J. (1982). Early development of an "acoustic analogy" approach to aeroacoustic theory. *AIAA Journal*, 20(4):449–450.

Lilley, G. M., Plumblee, H. E., Strahle, W. C., Ruo, S. Y., and Doak, P. E. (1972). The generation and radiation of supersonic jet noise. Volume IV. Theory of turbulence generated jet noise, noise radiation from upstream sources, and combustion noise. Technical report, Lockheed-Georgia Co. Marietta.

Luchini, P. and Bottaro, A. (1998). Görtler vortices: a backward-in-time approach to the receptivity problem. *Journal of Fluid Mechanics*, 363:1–23.

Lyamshev, L. M. (1961). On certain integral relations in the acoustics of a moving medium. In *Doklady Akademii Nauk SSSR*, volume 138, pages 575–578. Russian Academy of Sciences.

Maestrello, L., Bayliss, A., and Turkel, E. (1981). On the interaction of a sound pulse with the shear layer of an axisymmetric jet. *Journal of Sound and Vibration*, 74(2):281–301.

Markesteijn, A. P. and Karabasov, S. A. (2020). GPU CABARET flow and noise solutions of an installed jet configuration. In *26th AIAA/CEAS Aeroacoustics Conference*, Virtual envent. AIAA Paper 2020-2563.

Marsh Jr., H. W. (1950). Theory of the anomalous propagation of acoustic waves in the ocean. Technical report, Navy underwater sound lab new London, Connecticut.

Martelet, Y. (2020). *Jet mixing noise model based on geometrical acoustics for the prediction of installation effects*. PhD thesis, École centrale de Lyon, Laboratoire de Mécanique des Fluides et d'Acoustique (LMFA) - CIFRE Airbus Commercial Aircraft.

Martelet, Y., Suratteau, J.-Y., Pont, G., and Bailly, C. (2019). Prediction of fine-scale jet mixing noise using geometrical acoustics. In *25th AIAA/CEAS Aeroacoustics Conference*, Delft. AIAA Paper 2019-2755.

McIntyre, M. E. (1981). On the 'wave momentum' myth. *Journal of Fluid Mechanics*, 106:331–47.

Michalke, A. (1965). On spatially growing disturbances in an inviscid shear layer. *Journal of Fluid Mechanics*, 23(3):521–544.

Miller, S. A. E. (2014a). The prediction of jet noise ground effects using an acoustic analogy and a tailored Green's function. *Journal of Sound and Vibration*, 333(4):1193–1207.

Miller, S. A. E. (2014b). Toward a comprehensive model of jet noise using an acoustic analogy. *AIAA Journal*, 52(10):2143–2164.

Miller, S. A. E. (2015). The scaling of broadband shock-associated noise with increasing temperature. *International Journal of Aeroacoustics*, 14(1-2):305–326.

Miller, S. A. E. and Morris, P. J. (2012). The prediction of broadband shock-associated noise including propagation effects. *International Journal of Aeroacoustics*, 11(7-8):755–781.

Möhring, W. (1978). Acoustic energy flux in nonhomogeneous ducts. *The Journal of the Acoustical Society of America*, 64(4):1186–1189.

Möhring, W. (1979). Modelling low mach number noise. In *IUTAM Symposium on Mechanics of Sound Generation in Flows*, pages 85–96, Göttingen.

Möhring, W. (1999). A well posed acoustic analogy based on a moving acoustic medium. In *Aeroacoustic workshop SWING*, Dresden.

Möhring, W. (2001). Energy conservation, time-reversal invariance and reciprocity in ducts with flow. *Journal of Fluid Mechanics*, 431:223–237.

Möhring, W., Müller, E. A., and Obermeier, F. (1969). Schallerzeugung durch instationäre Strömung als singuläres Störungsproblem. *Acustica*, 21:184–188.

Möhring, W., Müller, E.-A., and Obermeier, F. (1983). Problems in flow acoustics. *Reviews of modern physics*, 55(3):707.

Mohseni, K., Colonius, T., and Freund, J. B. (2002). An evaluation of linear instability waves as sources of sound in a supersonic turbulent jet. *Physics of fluids*, 14(10):3593–3600.

Moon, Y. J., Seo, J. H., Bae, Y. M., Roger, M., and Becker, S. (2010). A hybrid prediction method for low-subsonic turbulent flow noise. *Computers & Fluids*, 39(7):1125–1135.

Moore, C. J. (1977). The role of shear-layer instability waves in jet exhaust noise. *Journal of Fluid Mechanics*, 80(2):321–367.

Morfey, C. L. (1971). Acoustic energy in non-uniform flows. *Journal of Sound and Vibration*, 14(2):159–170.

Morris, P. J. (1981). Stability of a two-dimensional jet. *AIAA Journal*, 19(7):857–862.

Morris, P. J. (2007). Jet noise prediction: past, present and future. *Canadian Acoustics*, 35(3):16–22.

Morris, P. J. (2012). Jet noise: a perspective on recent developments and future directions. In *11ème Congrès Français d'Acoustique (CFA)*.

Morris, P. J. and Boluriaan, S. (2004). The prediction of jet noise from CFD data. In *10th AIAA/CEAS Aeroacoustics Conference*, Manchester. AIAA Paper 2004-2977.

Morris, P. J. and Farassat, F. (2002). Acoustic analogy and alternative theories for jet noise prediction. *AIAA Journal*, 40(4):671–680.

Morris, P. J. and Farassat, F. (2003). Reply by the authors to c. k. w. tam. *AIAA Journal*, 41(9):1845–1847.

Morris, P. J. and Miller, S. A. E. (2010). Prediction of broadband shock-associated noise using reynolds-averaged navier-stokes computational fluid dynamics. *AIAA Journal*, 48(12):2931–2944.

Morris, P. J., Richarz, W., and Ribner, H. S. (1973). Reduction of peak jet noise using jet refraction. *Journal of Sound and Vibration*, 29(4):443–455.

Morse, P. M. and Feshbach, H. (1953). *Methods of theoretical physics - Part I*. New York: McGraw-Hill.

Mosson, A., Binet, D., and Caprile, J. (2014). Simulation of the installation effects of the aircraft engine rear fan noise with ACTRAN/DGM. In *20th AIAA/CEAS Aeroacoustics Conference*, Atlanta, Georgia. AIAA Paper 2014-3188.

Munz, C.-D., Dumbser, M., and Roller, S. (2007). Linearized acoustic perturbation equations for low Mach number flow with variable density and temperature. *Journal of Computational Physics*, 224(1):352–364.

Panda, J. and Seasholtz, R. G. (1999). Measurement of shock structure and shock–vortex interaction in underexpanded jets using rayleigh scattering. *Physics of Fluids*, 11(12):3761–3777.

Pastouchenko, N. N. and Tam, C. K. W. (2007). Installation effects on the flow and noise of wing mounted jets. *AIAA Journal*, 45(12):2851–2860.

Perez Bergliaffa, S. E., Hibberd, K., Stone, M., and Visser, M. (2004). Wave equation for sound in fluids with vorticity. *Physica D: Nonlinear Phenomena*, 191(1-2):121–136.

Petitjean, B. P., Viswanathan, K., and McLaughlin, D. K. (2006). Acoustic pressure waveforms measured in high speed jet noise experiencing nonlinear propagation. *International Journal of Aeroacoustics*, 5(2):193–215.

Peyret, C. and Elias, G. (2001). Finite-element method to study harmonic aeroacoustics problems. *The Journal of the Acoustical Society of America*, 110(2):661–668.

Phillips, O. M. (1960). On the generation of sound by supersonic turbulent shear layers. *Journal of Fluid Mechanics*, 9(1):1–28.

Pierce, A. D. (1981). *Acoustics: An Introduction to Its Physical Principles and Applications*. ASA.

Pierce, A. D. (1990). Wave equation for sound in fluids with unsteady inhomogeneous flow. *The Journal of the Acoustical Society of America*, 87(6):2292–2299.

Plaut, E. (2017). *Le calcul tensoriel et différentiel: outil mathématique pour la physique des milieux continus*. École des Mines de Nancy.

Posson, H. and Peake, N. (2013). The acoustic analogy in an annular duct with swirling mean flow. *Journal of Fluid Mechanics*, 726:439–475.

Powell, A. (1964). Theory of vortex sound. *The Journal of the Acoustical Society of America*, 36(1):177–195.

Prax, C., Golanski, F., and Nadal, L. (2008). Control of the vorticity mode in the linearized euler equations for hybrid aeroacoustic prediction. *Journal of Computational Physics*, 227(12):6044–6057.

Raizada, N. and Morris, P. J. (2006). Prediction of noise from high speed subsonic jets using an acoustic analogy. In *12th AIAA/CEAS Aeroacoustics Conference*, Cambridge, Massachusetts. AIAA Paper 2006-2596.

Rao, P. P. and Morris, P. J. (2006). Use of finite element methods in frequency domain aeroacoustics. *AIAA Journal*, 44(7):1643–1652.

Ray, J. R. and Reid, J. L. (1979). Exact time-dependent invariants for N-dimensional systems. *Physics Letters A*, 74(1-2):23–25.

Revalor, Y. (2007). *Méthodes de rayons en aéroacoustique*. PhD thesis, École centrale de Lyon, Laboratoire de Mécanique des Fluides et d'Acoustique (LMFA).

Ribner, H. S. (1962). Aerodynamic sound from fluid dilitations. A theory of the sound from jets and other flows. Technical report, University of Toronto, Institute of aerophysics. UTIA Report N^o 86, AFOSR TN 3430.

Ribner, H. S. (1964). The generation of sound by turbulent jets. In *Advances in Applied Mechanics*, volume 8, pages 103–182. Elsevier.

Ribner, H. S. (1969). Quadrupole correlations governing the pattern of jet noise. *Journal of Fluid Mechanics*, 38(1):1–24.

Ribner, H. S. (1981). Perspectives on jet noise. *AIAA Journal*, 19(12):1513–1526.

Ribner, H. S. (1996). Effects of jet flow on jet noise via an extension to the Lighthill model. *Journal of Fluid Mechanics*, 321:1–24.

Richter, C. and Thiele, F. (2007). Stability of time explicit impedance models. In *13th AIAA/CEAS Aeroacoustics Conference*, Rome. AIAA Paper 2007-3538.

Riemann, B. (1860). Über die Fortpflanzung ebener Luftwellen von endlicher Schwingungsweite. *Abhandlungen der Königlichen Gesellschaft der Wissenschaften zu Göttingen*, 8.

Rienstra, S. W. and Hirschberg, A. (2004). *An introduction to acoustics*. Eindhoven University of Technology.

Röber, N., Kaminski, U., and Masuch, M. (2007). Ray acoustics using computer graphics technology. In *10th International Conference on Digital Audio Effects (DAFx-07)*, pages 117–124. Citeseer.

Roberts, P. H. (1960). Characteristic value problems posed by differential equations arising in hydrodynamics and hydromagnetics. *Journal of Mathematical Analysis and Applications*, 1(2):195–214.

Rosa, V., Deschamps, C. J., Salazar, J. P. L. C., and Ilário, C. R. S. (2017). Comparison of RANS-based jet noise models and assessment of a ray tracing method. *Journal of the Brazilian Society of Mechanical Sciences and Engineering*, 39(6):1859–1872.

Roy, R. (2011). *Sources in the Development of Mathematics: Series and Products from the Fifteenth to the Twenty-first Century*. Cambridge University Press.

Schoder, S., Roppert, K., and Kaltenbacher, M. (2020). Postprocessing of direct aeroacoustic simulations using Helmholtz decomposition. *AIAA Journal*, pages 1–9.

Schubert, L. K. (1972a). Numerical study of sound refraction by a jet flow. I. Ray acoustics. *The Journal of the Acoustical Society of America*, 51(2A):439–446.

Schubert, L. K. (1972b). Numerical study of sound refraction by a jet flow. II. Wave acoustics. *The Journal of the Acoustical Society of America*, 51(2A):447–463.

Self, R. H. (2005). A RANS CFD coupled model for predicting coaxial jet noise. Technical Report 304, University of Southampton, Institute of Sound and Vibration Research (ISVR), Fluid Dynamics and Acoustics group.

Self, R. H. and Azarpeyvand, M. (2008). Utilization of turbulent energy transfer rate time-scale in aeroacoustics with application to heated jets. *International Journal of Aeroacoustics*, 7(2):83–102.

Semiletov, V. A. and Karabasov, S. A. (2013). A 3D frequency-domain linearised Euler solver based on the Goldstein acoustic analogy equations for the study of nonuniform meanflow propagation effects. In *19th AIAA/CEAS Aeroacoustics Conference*, Berlin. AIAA Paper 2013-2019.

Semiletov, V. A. and Karabasov, S. A. (2016). On the properties of fluctuating turbulent stress sources for high-speed jet noise. In *22nd AIAA/CEAS Aeroacoustics Conference*, Lyon. AIAA Paper 2016-2867.

Semiletov, V. A. and Karabasov, S. A. (2017). Similarity scaling of jet noise sources for low-order jet noise modelling based on the Goldstein generalised acoustic analogy. *International Journal of Aeroacoustics*, 16(6):476–490.

Semiletov, V. A. and Karabasov, S. A. (2018). A volume integral implementation of the Goldstein generalised acoustic analogy for unsteady flow simulations. *Journal of Fluid Mechanics*.

Seo, J. H. and Moon, Y. J. (2006). Linearized perturbed compressible equations for low mach number aeroacoustics. *Journal of Computational Physics*, 218(2):702–719.

Serre, G., Lafon, P., Gloerfelt, X., and Bailly, C. (2012). Reliable reduced-order models for time-dependent linearized Euler equations. *Journal of Computational Physics*, 231(15):5176–5194.

Shen, W. Z. and Sørensen, J. N. (1999a). Aeroacoustic modelling of low-speed flows. *Theoretical and Computational Fluid Dynamics*, 13(4):271–289.

Shen, W. Z. and Sørensen, J. N. (1999b). Comment on the aeroacoustic formulation of Hardin and Pope. *AIAA Journal*, 37(1):141–143.

Shnip, A. I. (1999). Concerning the equations of the acoustics of moving media. *Journal of engineering physics and thermophysics*, 72(5):815–820.

Slimon, S. A., Soteriou, M. C., and Davis, D. W. (2000). Development of computational aeroacoustics equations for subsonic flows using a Mach number expansion approach. *Journal of Computational Physics*, 159(2):377–406.

Spieser, É. and Bailly, C. (2018). Adjoint solution to the linearized euler equations computed from the direct problem. In *14ème Congrès Français d'Acoustique (CFA)*.

Spieser, É. and Bailly, C. (2020). Sound propagation using an adjoint-based method. *Journal of Fluid Mechanics*, 900:A5.

Starobinski, R. and Aurégan, Y. (1998). Fluctuations of vorticity and entropy as sources of acoustical exergy. *Journal of Sound and Vibration*, 216(3):521–527.

Stone, M. (2000). Acoustic energy and momentum in a moving medium. *Physical Review E*, 62(1):1341.

Stone, M. and Goldbart, P. (2009). *Mathematics for physics*. Cambridge University Press. `http://goldbart.gatech.edu/PG_MS_MfP.htm`

Strutt, J. W. (1877). *The theory of sound*, volume 1 of *2nd ed. (1945)*. Dover, New York.

Taira, K., Brunton, S. L., Dawson, S. T. M., Rowley, C. W., Colonius, T., McKeon, B. J., Schmidt, O. T., Gordeyev, S., Theofilis, V., and Ukeiley, L. S. (2017). Modal analysis of fluid flows: An overview. *AIAA Journal*, 55(12):4013–4041.

Tam, C. K. W. (1987). Stochastic model theory of broadband shock associated noise from supersonic jets. *Journal of Sound and Vibration*, 116(2):265–302.

Tam, C. K. W. (2001). On the failure of the acoustic analogy theory to identify the correct noise sources. In *7th AIAA/CEAS Aeroacoustics Conference*, Maastricht. AIAA Paper 2001-2117.

Tam, C. K. W. (2002). Computational aeroacoustics examples showing the failure of the acoustic analogy theory to identify the correct noise sources. *Journal of Computational Acoustics*, 10(04):387–405.

Tam, C. K. W. (2003). Comment on "acoustic analogy and alternative theories for jet noise prediction". *AIAA Journal*, 41(9):1844–1845.

Tam, C. K. W. (2006). Dimensional analysis of jet noise data. *AIAA Journal*, 44(3):512–522.

Tam, C. K. W. and Auriault, L. (1998). Mean flow refraction effects on sound radiated from localized source in a jet. *Journal of Fluid Mechanics*, 370:149–174.

Tam, C. K. W. and Auriault, L. (1999). Jet mixing noise from fine-scale turbulence. *AIAA Journal*, 37(2):145–153.

Tam, C. K. W., Golebiowski, M., and Seiner, J. (1996). On the two components of turbulent mixing noise from supersonic jets. In *2nd AIAA/CEAS Aeroacoustics Conference*, State College, Pennsylvania. AIAA Paper 1996-1716.

Tam, C. K. W. and Pastouchenko, N. N. (2002). Noise from fine-scale turbulence of nonaxisymmetric jets. *AIAA Journal*, 40(3):456–464.

Tam, C. K. W. and Pastouchenko, N. N. (2006). Fine-scale turbulence noise from dual-stream jets. *AIAA Journal*, 44(1):90–101.

Tam, C. K. W., Pastouchenko, N. N., and Auriault, L. (2001). Effects of forward flight on jet mixing noise from fine-scale turbulence. *AIAA Journal*, 39(7):1261–1269.

Tam, C. K. W., Pastouchenko, N. N., and Schlinker, R. H. (2006). Noise source distribution in supersonic jets. *Journal of Sound and Vibration*, 291(1-2):192–201.

Tam, C. K. W., Pastouchenko, N. N., and Viswanathan, K. (2005). Fine-scale turbulence noise from hot jets. *AIAA Journal*, 43(8):1675–1683.

Tam, C. K. W., Pastouchenko, N. N., and Viswanathan, K. (2010). Continuation of near-acoustic fields of jets to the far field. part I: Theory. In *16th AIAA/CEAS Aeroacoustics Conference*, Stockholm. AIAA Paper 2010-3728.

Tam, C. K. W., Viswanathan, K., Ahuja, K. K., and Panda, J. (2008). The sources of jet noise: experimental evidence. *Journal of Fluid Mechanics*, 615:253–292.

Tam, C. K. W. and Webb, J. C. (1993). Dispersion-relation-preserving finite difference schemes for computational acoustics. *Journal of Computational Physics*, 107:262–281.

Tautz, M., Kaltenbacher, M., and Becker, S. (2018). Comparison of Lighthill's analogy and acoustic perturbation equations for the prediction of HVAC blower noise. In *Fan 2018 international conference*.

Thies, A. T. and Tam, C. K. W. (1996). Computation of turbulent axisymmetric and nonaxisymmetric jet flows using the κ-ε model. *AIAA Journal*, 34(2):309–316.

Tyacke, J. C., Mahak, M., and Tucker, P. G. (2016). Large-scale multifidelity, multiphysics, hybrid reynolds-averaged Navier-Stokes/large-eddy simulation of an installed aeroengine. *Journal of Propulsion and Power*, 32(4):997–1008.

Unruh, W. G. (1981). Experimental black-hole evaporation? *Physical Review Letters*, 46(21):1351.

Uosukainen, S. (2011). Foundations of acoustic analogies. Technical Report 757, VTT Technical Research Centre of Finland.

Vasconcelos, I., Snieder, R., and Douma, H. (2009). Representation theorems and Green's function retrieval for scattering in acoustic media. *Physical Review E*, 80(3):036605.

Virieux, J., Garnier, N., Blanc, E., and Dessa, J.-X. (2004). Paraxial ray tracing for atmospheric wave propagation. *Geophysical research letters*, 31(20).

Viswanathan, K. (2006). Scaling laws and a method for identifying components of jet noise. *AIAA Journal*, 44(10):2274–2285.

Voronovich, A. G. and Godin, O. A. (2003). Fermat principle for a nonstationary medium. *Physical review letters*, 91(4):044302.

Wapenaar, C. P. A. (1996). Reciprocity theorems for two-way and one-way wave vectors: A comparison. *The Journal of the Acoustical Society of America*, 100(6):3508–3518.

Wei, M. and Freund, J. B. (2006). A noise-controlled free shear flow. *Journal of Fluid Mechanics*, 546:123–152.

Whitham, G. B. (1965). A general approach to linear and non-linear dispersive waves using a Lagrangian. *Journal of Fluid Mechanics*, 22(2):273–283.

Witze, P. O. (1974). Centerline velocity decay of compressible free jets. *AIAA Journal*, 12(4):417–418.

Wundrow, D. W. and Khavaran, A. (2004). On the applicability of high-frequency approximations to Lilley's equation. *Journal of Sound and Vibration*, 272(3):793–830.

Xia, H., Tucker, P. G., Eastwood, S. J., and Mahak, M. (2012). The influence of geometry on jet plume development. *Progress in Aerospace Sciences*, 52:56–66.

Xu, X., He, J., Li, X., and Hu, F. Q. (2015). 3-D jet noise prediction for separate flow nozzles with pylon interaction. In *53rd AIAA Aerospace Sciences Meeting*, Kissimmee, Florida. AIAA Paper 2015-512.

Yates, J. E. (1978). Application of the Bernoulli enthalpy concept to the study of vortex noise and jet impingement noise. Technical report, NASA Contractor Report 2987.

Zhu, T. (1988). A ray-Kirchhoff method for body-wave calculations in inhomogeneous media: theory. *Geophysical Journal International*, 92(2):181–193.

dernière page de la thèse

AUTORISATION DE SOUTENANCE

Vu les dispositions de l'arrêté du 25 mai 2016,

Vu la demande du directeur de thèse

Monsieur C. BAILLY

et les rapports de

M. S. LELE
Professeur - Stanford University - Department of Aeronautics and Astronautics
Durand RM 253 - Stanford - California 94305-4035 - USA

et de

M. S. KARABASOV
Professeur - Queen Mary University of London - Division of Aerospace Engineering and Fluid Mechanics - 319 Mile End Road - Bethnal Green - London E1 4NS - Royaume-Uni

Monsieur SPIESER Etienne

est autorisé à soutenir une thèse pour l'obtention du grade de **DOCTEUR**

Ecole doctorale MECANIQUE, ENERGETIQUE, GENIE CIVIL ET ACOUSTIQUE

Fait à Ecully, le 2 décembre 2020

P/Le directeur de l'E.C.L.
Le directeur des Etudes

Grégory VIAL